



Research of Aviation PM Technologies, mOdelling and Regulation - RAPTOR

Clean Sky 2 JU under H2020 Grant Agreement number: 863969

Work Package 4: PM Measurements Deliverables Report:

D4.1 Uncertainty of nvPM Standards, D4.2 Improvement in nvPM Standards Uncertainty & D4.3 Future Reduction in Aviation nvPM Impact

Delivery Date:	30/04/2022 (M30)
Date of submission:	30/04/2022

Start date of project:	01/11/2019
Duration:	24 months


**LEAD BENEFICIARY FOR THIS DELIVERABLE**

Name:	Cardiff University – Gas Turbine Research Centre
Contact Person:	Dr Andrew Crayford
Address:	School of Engineering, The Parade, Cardiff, UK CF243AA
Phone:	+44 (0)2920876043
E-mail:	Crayfordap1@cf.ac.uk

## Work Package 4: Deliverables Report

<b>Authors:</b>			
<b>Participants:</b>	Dr's A Crayford, D Delhaye, E Durand, L Durdina, Ismael Ortega & P I Williams		
<b>Work Package:</b>	4		
<b>Dissemination level:</b>		<b>Nature:</b>	
<b>Version:</b>		<b>Number of Pages:</b>	

REVISION HISTORY			
VERSION	DATE	AUTHOR / REVIEWER	NOTES

REVIEWED AND SIGNED OFF BY			
ROLE	DATE	NAME	SIGNATURE
DELIVERABLE LEADER			
WP LEADER	30/04/22	Dr Andrew Crayford	



## EXECUTIVE SUMMARY

The Particulate Matter (PM) Measurement work package (WP4), was undertaken with three aims namely: 1) to understand uncertainty in current CAEP10/11 nvPM regulatory practices (D4.1) 2) to investigate the requirement of potential corrections to be considered towards reduced uncertainty during CAEP/12 (D4.2) and 3) to assess likely benefits future technologies and further regulation will offer in terms of reducing the impact of nvPM beyond CAEP/12 (D4.3).

To achieve the aims of D4.1 & 4.2, aero-engine relevant RQL combustor rig tests were performed at Cardiff University's Gas Turbine Research Centre (GTRC) in Dec 2020, Feb 2021 and Dec 2021 in addition a laboratory scale fuel assessment was performed by ONERA using a liquid-fuel CAST. Towards informing the relevant technical committees (SAE E31 & ICAO WG3) an assessment of currently unquantified uncertainties, namely system variability and drift, limits of detection/quantification (LOD/LOQ) of mass analysers and calibration methodologies was undertaken to understand relative differences in two ICAO Annex 16 compliant systems over a calibration cycle. This assessment was performed by the European (EUR) and Swiss (CH) reference nvPM sampling and measurement systems, which made regulatory compliant measurements in parallel, initially following joint calibration and then after a further 12-month period.

During the campaigns > 250 discrete test-points were performed across various power conditions, using seven fuels of varying hydrogen content (aromatic content), which afforded a wide range of number and mass concentrations and particle size distributions representative of large civil aviation gas turbines. It was seen that on average the two systems agreed within expected uncertainty levels, with mass comparisons exhibiting an 11% offset and number agreeing within 2% on average immediately following calibration. After a 12-month period, without recalibration, a better agreement of 3% for mass and 0.2% for number were observed. It is proposed that these observed reductions likely stem from improved protocols in rig operation, sampling and cleanliness checks for the final campaign, which were adopted as an outcome of lessons learned during the initial tests which highlighted discrepancies significantly increased at low mass concentrations indicating shedding of particles from the cyclone. In both comparison campaigns intra-comparisons within individual systems highlighted good agreement between different instrument types for both mass and number. VPR penetration data collected on aero-engine representative soot was seen to closely match that reported on the ICAO compliant calibration certification, offering confidence that current methodologies employing a diffusion flame calibration source are robust.

In terms of CAEP/12 improvements and corrections, intensive size measurement were performed towards understanding system loss correction. Size instruments observed good agreement between the three analyser types compared (SMPS, DMS-500 & EEPS) with particle size and shape agreeing within 6% and 4% of the mean for GMD and GSD respectively. It was shown that size measurement potentially offers a more rigorous opportunity for loss correction compared to the current ICAO method (also described in ARP 6481), particularly when the measured nvPM mass is near LOD/LOQ and for distributions which are neither lognormal or monomodal. It was demonstrated that with loss correction methodology, correlation could be found between regulatory and size derived number concentrations. In terms of fuel correction, it was observed that changes in sulphur and aromatic content, within the ranges permitted in ASTM, resulted in differences in reported nvPM mass and number, with data generated on the RQL rig supporting the requirement for a CAEP/12 fuel correction methodology based on fuel hydrogen content. Additionally, humidity studies highlighted competing influence dependant on humidity injection location. Reductions in nvPM were observed at elevated primary flame zone humidity but conversely increased nvPM correlated with increased humidity in the secondary zone leading to inconclusive results of the net impact humidity plays in a full Rich burn engine.

Desk based review highlighted that currently unregulated engines (<26.7kN) emit nvPM which is similar in nature to those regulated, with an assessment of future technologies and fuels indicating that future aircraft will likely emit significantly lower nvPM concentrations than those of today. As a result it is proposed that future regulation will likely need to have greater sensitivity and be inclusive of volatile PM emanating from both the exhaust and oil lubrication system in order to ensure protection of LAQ surrounding future airports.



## Contents

EXECUTIVE SUMMARY .....	3
List of figures .....	7
List of tables .....	12
1 Introduction .....	13
2 Experimental Setup .....	14
2.1 GTRC's High Pressure Combustor Rig Design .....	14
2.1.1 High Pressure Optical Chamber (HPOC) .....	14
2.1.2 Rich Quench Lean (RQL) combustor rig .....	15
2.2 Particulate and gaseous sampling and measurement .....	16
2.3 Fuels .....	19
3 Operation and Data processing .....	20
3.1 Rig operating conditions .....	20
3.2 Test matrix .....	20
3.3 Data reporting and processing .....	21
3.4 Particle loss correction .....	21
4 Uncertainty in current CAEP10/11 nvPM regulatory practices (D4.1) .....	22
4.1 nvPM Mass measurement uncertainty RQL 1 test (M4.1) .....	22
4.1.1 EI Mass Intercomparison RQL 1 test (Swiss Vs. EUR) .....	22
4.1.2 EI Mass Intra-comparisons RQL 1 test .....	23
4.1.3 RQL 1: Mass measurement uncertainty discussion .....	25
4.2 nvPM Mass measurement uncertainty RQL 2 tests (M4.2) .....	25
4.2.1 Pre-test mass instrument intercomparison RQL 2 test .....	25
4.2.2 EI mass intercomparison RQL 2 test (Swiss Vs. EUR) .....	27
4.2.3 EI mass intra-comparisons RQL 2 test .....	28
4.2.4 nvPM mass calibration uncertainty RQL 2 test (NIOSH 5040) .....	30
4.2.5 Mass measurement uncertainty discussion .....	34
4.3 nvPM Number measurement uncertainty M4.1 RQL 1 test .....	34
4.3.1 EI Number Intercomparison RQL 1 test .....	34
4.3.2 EI Number Intra-comparison RQL 1 test .....	36
4.3.3 RQL 1: Number measurement uncertainty discussion .....	37
4.4 nvPM Number measurement uncertainty M4.2 RQL 2 test .....	37
4.4.1 EI Number intercomparison RQL 2 test .....	38



## Work Package 4: Deliverables Report

4.4.2	Number measurement uncertainty discussion .....	38
4.5	Line cleanliness, shedding and LOD of mass measurement M4.1 RQL test.....	39
4.5.1	Cleanliness checks RQL 1 (Cyclone cleaning).....	39
4.5.2	Measured Size derived Volume over time RQL 1 .....	40
4.5.3	Comparison nvPM mass raw/diluted near LOD RQL 1 .....	41
4.6	Line cleanliness, shedding and LOD of mass measurement RQL 2 test .....	42
4.6.1	Cleanliness checks RQL 2 (Cyclone cleaning).....	42
4.6.2	Comparison nvPM mass raw/diluted near LOD RQL 2 .....	44
4.6.3	Discussion line cleanliness, shedding and LOD of mass measurement .....	45
4.7	VPR uncertainty.....	46
4.7.1	VPR penetration efficiency measurement RQL 1 .....	46
4.7.2	VPR penetration MC uncertainty analysis (RQL 2) .....	49
4.8	System-to-System MC uncertainty analysis .....	55
4.9	Conclusions – CAEP/11 uncertainties (D4.1) .....	56
5	Corrections to be considered towards reduced uncertainty in CAEP/12 (D4.2) .....	58
5.1	nvPM Size measurements RQL 1 test .....	58
5.1.1	Sizing Instrument Intercomparison RQL 1 test .....	58
5.1.2	SMPS Hardware impact RQL 1 test .....	59
5.1.3	Size derived number concentrations RQL 1 test .....	62
5.1.4	Size measurement uncertainty discussion RQL 1 test .....	63
5.2	nvPM size measurements RQL 2 test .....	65
5.2.1	Pre-test size instrument intercomparison RQL 2 test.....	65
5.2.2	Size-derived number and mass concentrations RQL 2 test .....	67
5.2.3	Size measurement uncertainty discussion RQL 2 test .....	69
5.3	Particle loss correction RQL 1 test.....	69
5.3.1	Number correction factor ( $K_{sl_{num}}$ ) RQL 1 test.....	70
5.3.2	Mass correction factor ( $K_{sl_{mass}}$ ) RQL 1 test .....	70
5.3.3	Loss correction discussion RQL 1 test.....	72
5.4	Particle loss correction RQL 2 test.....	72
5.4.1	Measured Vs predicted loss RQL 2 test .....	72
5.4.2	Comparison of size distribution properties (GMD, GSD) at the combustor-exit RQL 2 test	75
5.4.3	Number correction factor ( $K_{sl_{num}}$ ) RQL 2 test .....	76
5.4.4	Mass correction factor ( $K_{sl_{mass}}$ ) RQL 2 test .....	78
5.4.5	Particle loss correction discussion RQL 2 test .....	79



## Work Package 4: Deliverables Report

5.5	Impact of fuel composition on nvPM emissions.....	80
5.5.1	Small-scale Laboratory Testing.....	80
5.5.2	RQL Combustor Rig Testing.....	80
5.6	Impact of humidity on nvPM emissions (M4.2 RQL test) .....	82
5.7	Conclusions – Improvements and correction requirements CAEP/12 (WP4.2) 84	
6	Benefits of future technologies and regulation in terms of reducing nvPM impact beyond CAEP/12 (D4.3). .....	86
6.1	Introduction .....	86
6.2	Assessment of nvPM emission characteristics of unregulated engines .....	86
6.2.1	Particle size distribution properties and nvPM mass and number .....	87
6.2.2	nvPM mass – smoke number correlation.....	88
6.3	Modern low emissions combustion technologies .....	89
6.3.1	Rich-Burn Quick-Quench Lean Burn (RQL) .....	90
6.3.2	Double Annular Combustor (DAC).....	90
6.3.3	Axial Staged Combustor (ASC).....	91
6.3.4	Twin Annular Premixing Swirler combustor (TAPS).....	91
6.3.5	Lean Direct Injector (LDI).....	92
6.3.6	Lean Premixed Pre-vaporised (LPP).....	92
6.3.7	Variable Geometry Combustor (VGC) .....	93
6.4	Sustainable Aviation Fuels (SAFs).....	93
6.4.1	Drop-in SAFs.....	93
6.4.2	Non-drop-in Hydrogen .....	95
6.5	Electric powered aircraft.....	96
6.5.1	Series configuration .....	96
6.5.2	Parallel configuration .....	96
6.5.3	Series - Parallel configuration.....	97
6.6	Future Total PM Regulation .....	98
6.6.1	Sampling Methodology .....	99
6.6.2	Fuel Effects.....	100
6.6.3	Impacts on communities .....	100
6.6.4	Road map moving forward.....	100
6.6.5	Summary .....	101
7	References.....	102
8	Appendix .....	107
8.1	EUR APC CPC/VPR cal certs .....	107



## Work Package 4: Deliverables Report

8.2	SWISS APC CPC/VPR cal certs .....	109
8.3	ONERA mini-CAST report .....	111
	Glossary .....	115
	Introduction .....	116
8.3.1	CAMPAIGN description .....	116
8.3.2	Experimental set up .....	118
8.3.3	Results.....	122
8.3.4	Conclusions .....	131

## List of figures

Figure 1: Photographs of HPOC during maintenance (left) and installed in the HPCR (right).....	15
Figure 2: Picture of the RQL combustor during assembly and in use .....	15
Figure 3: Combustor Can damaged during RQL 1 Test .....	16
Figure 4 (a&b): Diagram of the experimental setup in RQL 1 Combustor Rig Test (M4.1) and RQL 2 combustor Rig (M4.2) respectively.....	17
Figure 5 (a&b): Photographs of the European and Swiss measurement systems respectively .....	17
Figure 6 (a&b): Photographs of the Swiss system with the MSS2 on the nvPM line and the MSS2 on the raw line (during RQL 2) respectively.....	18
Figure 7: EUR nvPM EI mass Vs. SWISS nvPM EI mass (left) and ratio of SWISS/EUR nvPM EI mass over the average of the two (right) – Error bars represent $\pm 1$ standard deviation.....	22
Figure 8: Ratio of SWISS/EUR nvPM EI mass over the measured GMD (left) and the diluter inlet pressure P1 (right) .....	23
Figure 9: Swiss MSS Vs MSS2 mass concentration (left) and percent difference (MSS-MSS2)/MSS Vs mass concentration (right) – Error bars represent $\pm 1$ standard deviation .....	24
Figure 10: EUR MSS Vs LII-300 mass concentration (left) and ratio of MSS/LII-300 mass over the average of the two (right) – Error bars represent $\pm 1$ standard deviation .....	24
Figure 11: Diagram of the nvPM mass instrument intercomparison.....	26
Figure 12: Measured black carbon (rBC or eBC) mass for the six investigated nvPM mass analysers (left) and ratio to the mean Vs the mean BC mass of the size analysers (right).....	27
Figure 13: EUR nvPM EI mass Vs. SWISS nvPM EI mass (left) and ratio of SWISS/EUR nvPM EI mass over the average of the two (right) for RQL 1 & 2 test .....	28
Figure 14: Measured MSS Vs MSS2 RQL 1 & 2 and measured MSS Vs measured/loss corrected MSS2 for RQL 2.....	29



## Work Package 4: Deliverables Report

Figure 15: EUR MSS Vs LII-300 mass concentration (left) and ratio of MSS/LII-300 mass Vs the MSS mass (right) for RQL 1, RQL 2 and A-pride data .....	30
Figure 16: Fuel-differentiated ratio of MSS/LII-300 mass Vs the MSS mass from RQL TEST 1 and 2 (left) ratio of MSS/LII-300 mass Vs measured GMD for RQL TEST 2 (right) .....	30
Figure 17: Experimental setup for the filter sampling uncertainty investigation during the RQL 2 test.....	31
Figure 18: EC and nvPM mass concentrations determined from TOT analysis and with the MSS 2. The color scale represents the sampling flow rate of the filter sampling systems.....	32
Figure 19: Ratios of EC mass determined using the three filter sampling setups to MSS2-measured nvPM mass for the automatic and manual OC/EC split points. ....	33
Figure 20: EC mass loadings determined using the automatic and manual split for the filter samples obtained with the three sampling systems. ....	33
Figure 21: EUR nvPM EI number Vs. SWISS nvPM EI number(left) and ratio of SWISS/EUR nvPM EI number over the average of the two (right) – Error bars represent $\pm 1$ standard deviation .....	34
Figure 22: ratio of SWISS/EUR nvPM EI number over the CPC count (left) and measured GMD (right).....	35
Figure 23: ratio of SWISS/EUR VPR/CPC loss-corrected nvPM EI number over the measured GMD.....	36
Figure 24: Swiss APC Vs Secondary APC (TSI and AVL CPC) number concentration .....	36
Figure 25: Swiss secondary APC TSI CPC Vs AVL CPC number concentration (left) and percent difference (TSI-AVL)/TSI Vs number concentration (right) – Error bars represent $\pm 1$ standard deviation.....	37
Figure 26: EUR nvPM EI number Vs. SWISS nvPM EI number (left) and ratio of SWISS/EUR nvPM EI number over the average of the two (right) for RQL TEST 1 and 2 .....	38
Figure 27: EUR (left) and SWISS (right) MSS nvPM mass Vs time to highlight the effect of cleanliness (zero) checks and cyclone cleaning on measured data.....	40
Figure 28: Ratio of volume < 150 nm to the total volume measured by the DMS-500 (top) and the SMPS (bottom) over the three-day long test campaign .....	41
Figure 29: EUR (left) and SWISS (right) nvPM mass measured on the raw line Vs measured on the diluted line and DF1-corrected.....	42
Figure 30: Effect of cyclone cleaning on EUR system nvPM mass (left) and number (right) concentration during cleanliness checks in M4.2 RQL 2 .....	43
Figure 31: Difference between the LII and the MSS observed during the cleanliness checks in RQL 1 where the MSS resonance check was performed on diluent, and in RQL test 2 where the MSS resonance check was performed on the combustion exhaust.....	44
Figure 32: diluted Vs raw (corrected) nvPM mass (left) and ratio of the two Vs the diluted mass (right) for the NRC LII (raw) and EUR MSS (dil) .....	45
Figure 33: Diluted Vs raw (corrected) mass during LOD specific experiment in the EUR system (LII NRC raw Vs EUR MSS dil) and in the Swiss system (MSS2 raw Vs MSS Swiss dil).....	45
Figure 34: Diagram of the VPR experiment .....	46





## Work Package 4: Deliverables Report

Figure 35: Measured number concentration from CPC 1 Vs that measured simultaneously with CPC2 .....	47
Figure 36: measured/calibrated VPR penetration efficiency Vs particle size using different classification methods .....	47
Figure 37: AAC (left) and DMA classified (right) particle size distributions measured with an SMPS (DMA-CPC).....	48
Figure 38: Measured aerodynamic diameter (da) Vs measured electrical mobility diameter (dm) for fuel A (100% GTL) .....	48
Figure 39: Results of the CPC intercomparison performed on silver prior to the VPR RQL 2 tests.....	50
Figure 40: VPR penetration efficiency measured during RQL 2 using silver nanoparticles.....	51
Figure 41: VPR penetration measured at ten sizes with silver and fitted using the ARP 6481 method with 4-10 points .....	52
Figure 42: Histogram of the modelled & measured penetration distribution for the 15nm VPR fit .....	53
Figure 43: Example of tri-modality on EI num when running MC uncertainty analysis on a test point with a small Dmg.....	55
Figure 44: Output Dmg, ARP6481 loss-corrected EI num and EI mass calculated using the EU Labview code (MC analysis) on the EUR and Swiss system using a representative sample of RQL 2 .....	56
Figure 45: Examples of measured particle size distributions from the Cambustion DMS-500 (blue) and the TSI SMPS (orange) across a range of particle size, shape and concentration .....	59
Figure 46: Overview of size distributions measured by the SMPS. The blue curves are measurements without the CS. The red are measurements with the CS without loss correction and the green curves are measurements with the CS including size-dependent loss correction for the CS (provided by the manufacturer for the flow rate measured at the CS inlet). .....	60
Figure 47: Comparison of SMPS total number (corrected to APC CPC inlet) CVs APC number. ....	61
Figure 48: SMPS scans with nano DMA at one test point. DMS500 data are shown for comparison. This test point was unstable and the concentration during the measurement with CS increased, resulting in disagreement between the data with CS after loss correction and without CS. ....	61
Figure 49: EUR APC Vs DMS-500-corrected number concentration (left) and ratio of APC/DMS-500 number over the average of the two (right) – Error bars represent $\pm 1$ standard deviation .....	62
Figure 50: Swiss APC Vs SMPS-corrected number concentration (left) and ratio of APC/SMPS number over the average of the two (right) – Error bars represent $\pm 1$ standard deviation .....	63
Figure 51: Comparison of SMPS and DMS500 results (DF1 corrected) highlighting the portions of the size distribution above 230 nm not measured by the SMPS. ....	64
Figure 52: Diagram of the pre-test size instrument intercomparison .....	65
Figure 53: Particle size distributions measured by different size analysers during pre-test size intercomparison.....	66



## Work Package 4: Deliverables Report

Figure 54: Measured GMD (left), GSD (centre) and STP-corrected total number concentration (right) derived from the four particle size instruments assessed during the pre-test size intercomparison.....	66
Figure 55: Ratio to the mean Vs mean GMD (left) and GSD (right) of the four particle size instruments assessed during the pre-test size intercomparison .....	67
Figure 56: APC (EUR or CH) Vs size-instrument-corrected (DMS CU, EEPS, SMPS) number concentration (left) and ratio of APC/size-instrument-number over the average of the two (right) .....	67
Figure 57: MSS (EUR or CH) Vs size-instrument-corrected (DMS CU, EEPS, SMPS) mass concentration (left) and ratio of APC/size-instrument-number over the average of the two (right) using sphericity and unit particle effective density assumptions.....	68
Figure 58: Volume-weighted particle size distributions measured by different size analysers during pre-test size intercomparison .....	69
Figure 59: Particle number correction factor (kslnum) calculated using different methodologies Vs. the measured GMD (left) and Engine-Exit-Plane GMD predicted by method 0 Vs. that derived from the measured particle size distribution (right) .....	70
Figure 60: Particle mass correction factor (kslmass) calculated using different methodologies Vs. the measured GMD (left) and method 2 kslmass when using the whole DMS-500 size distribution Vs when cutting to 240 nm (right) .....	71
Figure 61: Example Mass-weighted size distribution from the DMS-500 along with the penetration efficiency of a regulatory compliant sampling system to highlight the mass fraction > 240 nm. ....	71
Figure 62: Correction functions between the CU DMS and the NRC DMS (left) and the SMPS and the EEPS (right) using the pre-test size intercomparison data .....	73
Figure 63: Comparison of the “measured” (DMS CU Vs DMS NRC) and “modelled” (UTRC) losses in a regulatory compliant sampling system .....	74
Figure 64: Comparison of the “measured” (DMS CU Vs DMS NRC & SMPS Vs EEPS) and “modelled” (UTRC) losses in the 25m line of a regulatory compliant sampling system (the 08/12/21 corresponds to TP 27-33 and the 09/12/21 corresponds to TP 34-40) .....	75
Figure 65: Combustor-exit GMD measured by the four size instruments Vs their average (left) and Combustor-exit GMD predicted by the ARP 6481 loss correction methodology Vs the measured-average (right) .....	76
Figure 66: Combustor-exit GSD measured by the four size instruments Vs their average .....	76
Figure 67: Number loss correction factor (ksl_num) calculated using the ARP 6481 method 0 (left) and the bin-by-bin method 2 (right) plotted against the measured GMD.....	77
Figure 68 : Average number loss correction factor (ksl_num) plotted against the measured GMD for method 0 and method 2 (left) and ratio of the two methods Vs the measured GMD (right) - error bars represent $\pm 1$ standard deviation of the average (i.e., average of 2 data points for method 0 and average of 4 data points for method 2) .....	78
Figure 69: Mass loss correction factor (ksl_mass) calculated using the ARP 6481 method 0 (left) and the bin-by-bin method 2 (right) plotted against the measured GMD .....	79



## Work Package 4: Deliverables Report

Figure 70: Average mass loss correction factor (ksl <sub>mass</sub> ) plotted against the measured GMD for method 0 and method 2 (left) and ratio of the two methods Vs the measured GMD (right) - error bars represent $\pm 1$ standard deviation of the average (i.e., average of 2 data points for method 0 and average of 4 data points for method 2) .....	79
Figure 71 Fuel impact on loss corrected nvPM emissions for alternative fuels in RQL 1 test. ....	81
Figure 72: Normalised nvPM emissions dataset (mass left, number middle and GMD right) across the Mk. 1 (Jetscreen), Mk. II (RQL test 1) and Mk. II-A (RQL test 2).....	82
Figure 73: Timeseries of the EUR system nvPM number and mass when injecting water in the primary air and secondary air in the RQL combustor rig .....	83
Figure 74: EI mass percentage reduction when adding water (% mass) in the RQL combustor primary air (left), secondary air (centre) and both (right).....	83
Figure 75: EI number percentage reduction when adding water (% mass) in the RQL combustor primary air (left), secondary air (centre) and both (right).....	84
Figure 76: Geometric mean diameter (GMD, left) and geometric standard deviation (GSD, right) as a function of engine thrust. The GMD and GSD were obtained from fits of lognormal distributions and the system penetration function to the SMPS measurement data. The thrust was determined either from direct test cell measurements and correction to standard day or from correlations with the low-pressure shaft speed (N1).....	87
Figure 77: Geometric mean diameter (GMD, left) and geometric standard deviation (GSD, right) as a function of the nvPM number to mass ratio measured (i.e. no system loss correction applied). The GMD and GSD were obtained from fits of lognormal distributions and the system penetration function to the SMPS measurement data. ....	88
Figure 78: nvPM mass as a function of smoke number for large (grey) and unregulated turbofan engines (red). The blue curve shows the SCOPE11 correlation implemented in FOA 4.0.....	89
Figure 79 Schematic representation of plume evolution .....	98



## List of tables

Table 1: Summary of fuels chemical properties .....	19
Table 2: Combustor rig operating conditions during RQL 1 Combustor Rig Test (M4.1) .....	20
Table 3: Combustor rig operating conditions during RQL 2 Combustor Rig Test (M4.2) .....	20
Table 4: Test points and flow rates used for the filter sampling uncertainty test. The flow rates are nominal values (STP for the Swiss and NRC system and actual flows for the EUR smoke meter and MSS2). .....	31
Table 5: Data from the Silver VPR penetration tests. The concentrations are averages in $\text{cm}^{-3}$ . The CPC comp model is the fit between the two CPCs to account for the difference. CPC1 has been corrected for dilution factor and using the CPC comp model to account for CPC differences. Note that the 100nm point was not measured but inserted to allow the line loss models to run. The uncertainties are standard deviations. ...	51
Table 6. Effects of using the default 4 and 8 data points VPR fit on simulated engine data. The number and mass ranges are chosen to give a range of theoretical engine exit plane modal diameter of the theoretical size distribution. Data in red is explained in section 4.7.2.5.....	53
Table 7: Standard deviations as a percentage of the mean from the line loss model with different number of points and uncertainties in the measurements. Data in red is explained in section 4.7.2.5 .....	54



## 1 Introduction

This report details experiments and assessments undertaken as part of WP4 of the RAPTOR program. The three aims of the work were to:

- 1.) Understand uncertainty in current CAEP/11 nvPM regulatory practices (D4.1)
- 2.) Explore potential corrections that could be applied CAEP/12 to reduce uncertainty in reported nvPM. (D4.2)
- 3.) Assess likely benefits future technologies and regulation may offer in terms of reducing the impact of nvPM beyond CAEP/12 (D4.3).

To achieve Aim 1, a series of non-volatile PM (nvPM) and gaseous measurements were performed on a small-scale Rich-burn Quick-quench Lean-burn (RQL) combustor rig, at Cardiff University's Gas Turbine Research Centre (GTRC), to empirically quantify the uncertainty associated with the CAEP10/11 nvPM standards. This was achieved by assessing the current specifications as set-out in ICAO Annex 16, Volume II Appendix. 7 with regard to: Unquantified measurement uncertainty associated with system variability and drift; Limits of detection/quantification (LOD/LOQ) and Calibration methodologies and schedule. Whilst performing the above assessments additional size measurements and intercomparisons were undertaken towards improved system loss correction.

The initial experimental campaign was performed in December 2020 & February 2021 (M4.1 RQL Combustor Rig Test 1) and the second campaign undertaken in December 2021 (M4.2 RQL Combustor Rig Test 2). In both test campaigns two compliant nvPM reference systems were used, namely the Swiss (CH) and European (EUR) nvPM reference systems, performing parallel measurement of nvPM number, mass and size distributions across a range of nvPM concentrations representative of modern aircraft turbine engines. Similarly, prescribed gaseous measurements (CO<sub>2</sub>, CO, NO<sub>x</sub>, UHC & SO<sub>2</sub>) were also undertaken; they are not reported here but are available in the publicly available data files. Prior to the initial test campaign, the respective nvPM number (AVL APC) and mass (AVL MSS) analysers were simultaneously calibrated in parallel (on the same source, at the same time) by the instrument manufacturer, in compliance with ICAO Annex 16 volume II. This joint calibration was undertaken to limit calibration uncertainty in the first intercomparison. The second test campaign, performed after a 12-month period in which both nvPM reference systems were extensively used for other projects, permitted an assessment of system drift across the CAEP/11 specified calibration schedule. The second test campaign was also tasked with assessing the performance of different size analysers for aviation nvPM measurement and particle loss correction. As a result of data observed in the first test, a thorough assessment of the impact of cleanliness on nvPM mass measurements was undertaken. Also, towards better sensitivity of mass measurement, quantification of the uncertainty of collection protocols of NIOSH5040 were undertaken and the feasibility of measuring nvPM mass on the raw line assessed. Towards determining the requirement of future corrections fuel impact was assessed using data from the numerous test programmes and the impact of humidity on nvPM characterising by injecting steam into the combustor primary and secondary zones.

As highlighted above, it is noted that additional particle size measurements, not specified by ICAO Annex 16, Vol II, were undertaken deemed necessary to fully assess size dependant particle loss calculation and correction. Due to differences in the size of emitted nvPM, correction is required to understand observed differences in reported nvPM concentrations across engine powers and technologies, along with allowing an assessment of the impact of SAF, which is acknowledged to cause a reduction in nvPM size and required to inform the outcomes of both D2.2 & 2.3. A Combustion DMS-500 (EUR system) and TSI SMPS (Swiss system with different DMAs and chargers) were permanently used alongside the nvPM number and mass



## Work Package 4: Deliverables Report

analysers with an additional loaned TSI EEPS and a second DMS-500 from NRC, both newly calibrated by their manufacturer also included in RQL Combustor Rig Test 2.

To provide further understanding size instruments were used at different locations of the sampling system during the RQL 2 campaign, namely by the nvPM number and mass analysers, in the diluter 1 vent and on the raw line, to experimentally assess the penetration of particle size in an ICAO regulatory compliant sampling system.

To further investigate measurement uncertainties, additional parallel nvPM number intercomparisons (second APC with 2-off CPCs) was performed on the Swiss system in the RQL 1 campaign, with additional nvPM mass intercomparisons performed on both the Swiss (AVL MSS vs MSS2) and EUR (AVL MSS vs. Artium LII 300) sampling and measurement systems in both test campaigns.

Experiments concerned with determination of VPR penetration efficiency were also performed by Cardiff University and University of Manchester in February 2021 and December 2022, with filters also collected for various conventional and SAF's in order to supply data for health assessment in WP6.

## 2 Experimental Setup

As discussed, testing was performed during experimental campaigns performed at Cardiff University's Gas Turbine Research Centre (GTRC) located in Port Talbot, South Wales, UK. The setup consisted of a small-scale RQL combustor rig (previously used to investigate alternative fuels in the EU Jetscreen Programme) from which aeronautical relevant emissions were extracted, using a 9-point equal area emissions probe, to the two ICAO compliant nvPM reference sampling and measurement systems.

### 2.1 GTRC's High Pressure Combustor Rig Design

#### 2.1.1 High Pressure Optical Chamber (HPOC)

The HPOC is the central pressure-containing apparatus of the GTRC's High Pressure Combustor Rigs. The HPOC allows both axial and radial visual access to the burners and operational flames within it. Designed for pressures and preheat air temperatures of 16bara and 573K respectively, the HPOC is 0.716 meters in length with an inside diameter (ID) of 0.315 m. A thermal barrier coating (TBC) has been applied along the entire ID of the HPOC to protect the stainless-steel casing from excessive temperatures during combustion experiments.

Photographs of the HPOC are shown in **Figure 1**, with the HPOC removed for maintenance (left) and installed in the HPCR (right). During combustion experimentation, the flame/ combustion can is monitored remotely via HD cameras through radial windows, and aids in the visual confirmation of flame phenomena such as flame stability and combustion can thermal distribution.





Figure 1: Photographs of HPOC during maintenance (left) and installed in the HPCR (right)

### 2.1.2 Rich Quench Lean (RQL) combustor rig

A Rich Quench Lean (RQL) combustor rig was developed for use in the RAPTOR programme based on recommendations presented in the literature [1,2] which was mounted within the HPOC. A pre-filming airblast atomiser designed using the Parker Hannifin Corporation concept [1], demonstrated as capable of producing a representative combustion source at low power conditions (125kW) by Makida et al. [2], was manufactured using AM techniques to introduce the fuel to the combustor as discussed by Crayford et al. [3]. A photograph of the RQL combustor mounted in the HPOC during testing is presented below in **Figure 2**.

For this study, the RQL was configured for high repeatability and precise control over fuel and air flows. This was achieved using three high precision Emerson Coriolis MFCs, controlling three independent air lines and using a high precision Bronkhorst coriflow, magnetically coupled variable speed gear pump, to deliver set fuel flows. Fuel and airflow preheat temperatures were also independently maintained using water and electric heating systems.

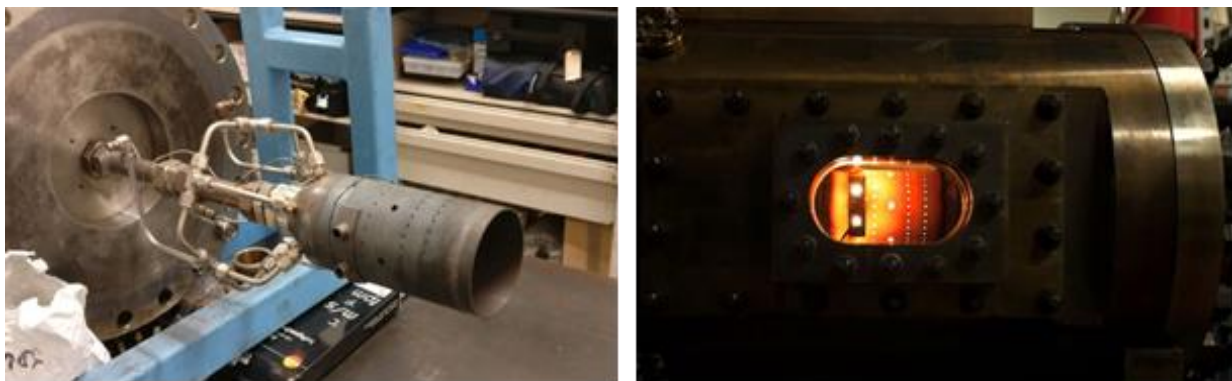


Figure 2: Picture of the RQL combustor during assembly and in use

It is noted that due to damage sustained during the RQL 1 test, which resulted in a total burnout of the combustor can as shown in **Figure 3**, a nominally identical combustor Can was manufactured for use in the February 2021 and December 2021 tests. To reduce the likelihood of similar damage a new fuel injector was also designed and manufactured, which displayed a narrower fuel cone-angle for use in the RQL 2 test, performed in December 2021.





Figure 3: Combustor Can damaged during RQL 1 Test

## 2.2 Particulate and gaseous sampling and measurement

As discussed previously, the nvPM and gaseous emission measurements were obtained in accordance with both the ICAO standards and SAE ARP 6320 [4] using both the European (EUR) and Swiss (CH) nvPM reference systems in parallel. The exhaust aerosol was extracted in the combustor exhaust stream using a water cooled (160°C) 9-point, equal area piccolo emissions probe, coupled with a 2.8 m long 160°C water-cooled heat exchanger (3/8" ID) before being split between the two nvPM reference systems via a 160°C heated splitter box (30° angle). The EUR nvPM reference system was run with additional particle sizing instrumentation (Cambustion DMS-500) on an ancillary sampling port behind the prescribed sharp-cut cyclone. The Swiss nvPM reference system was also equipped with additional particle sizing instrumentation (TSI SMPS Model 3938). During the RQL 1 test campaign, the SMPS ran with/without a catalytic stripper (Catalytic Instruments CS08) with different DMAs (long DMA Model 3081A and nano DMA Model 3085) and with different aerosol chargers (<sup>85</sup>Kr Model 3077A and soft x-ray Model 3088). In addition to the SMPS and nvPM instruments, an AVL MSS 2 and a customized AVL APC with two CPCs was connected and operated in parallel. During the RQL 2 test campaign, an additional DMS-500 (NRC M125) measured particle size from either the EUR diluter vent or from a raw line close to the sampling probe. Similarly, in the Swiss system an additional TSI EEPS (Model 3090, built in 2020) measured in parallel with the nvPM instruments and the SMPS was positioned either in parallel with the EEPS or in the Swiss diluter vent. Additionally, an Aerodyne CAPS PMssa (LED wavelength 660 nm) was positioned in the Swiss system but unfortunately was not functional for the majority of test points. The instrument in its current version has been found to be impractical, poorly built and insufficiently robust for nvPM testing. The instrument suffers continuous increase of the mirror contamination when sudden pressure changes occur in the system (e.g. as a result of valves switching or cyclone cleaning). The contamination increases the measurement noise. Several cleaning attempts were performed during the campaign, but eventually the instrument was disconnected.

A schematic representation of the experimental set-ups used in RQL 1 and RQL 2 comparison testing is given in

**Figure 4 (a&b)**;, with a photograph of the Swiss and EUR nvPM reference systems set-up during coparison testing at the GTRC given in **Figure 5**.





Work Package 4: Deliverables Report

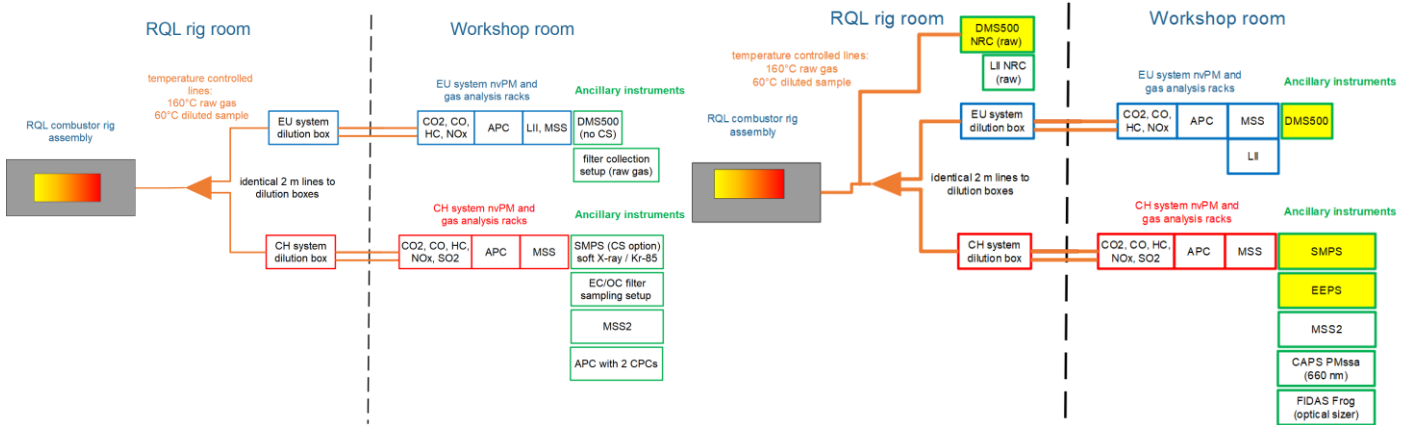


Figure 4 (a&b): Diagram of the experimental setup in RQL 1 Combustor Rig Test (M4.1) and RQL 2 combustor Rig (M4.2) respectively

It is noted that cleanliness, leak and ambient background system checks were regularly performed in accordance with the ARP 6320 to ensure the measured aerosol was representative of the combustion exhaust and not compromised from sample line contamination or leaks.

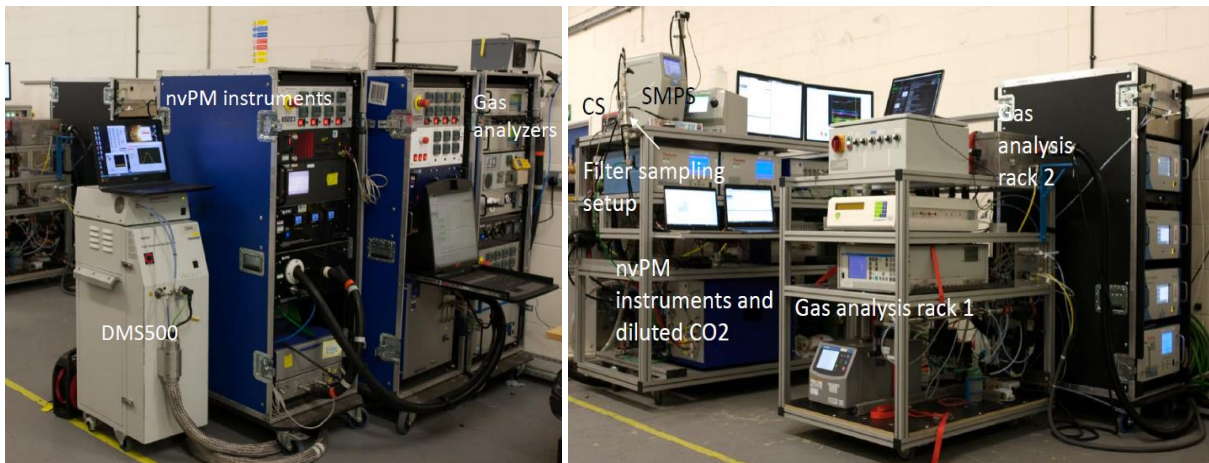


Figure 5 (a&b): Photographs of the European and Swiss measurement systems respectively





Figure 6 (a&b): Photographs of the Swiss system with the MSS2 on the nvPM line and the MSS2 on the raw line (during RQL 2) respectively



## 2.3 Fuels

To afford a large variation in nvPM mass, number and size emitted from the RQL combustor rig testing, a total of seven fuels, were used in the delivery of RQL 1 (M4.1) and RQL 2 (M4.2) combustor tests, with the data also then processed to inform the impact of fuel composition on nvPM mass emissions. Brief details of each fuels feedstock and composition are presented below with more detailed chemical properties, as derived using GCxGC analysis, listed in **Table 1**:

(1) Low aromatic Fischer Tropsch (FT) Gas-To-Liquid (GTL) fuel derived from natural gas

(2) GTL (75 %) (1) and 25% Jet-A fuel (3).

(3) High aromatic Jet-A fuel

(4) Catalytic Hydrothermal Conversion Jet (CHCJ) fuel

(5) Low sulphur Jet-A fuel (70%) mixed with HEFA fuel (30%)

(6) High Di-aromatic Jet-A fuel

(7) Low sulphur Jet-A fuel (as used in 5)

As can be seen, in **Table 1**, the fuel hydrogen content ranged from ~13.4 to ~15.5%, while the total aromatic content ranged from 0 to ~25%. Generally the fuels displayed low Sulphur contents with variations from 0 to ~100 ppm. The Mono/Di aromatics percentages correspond to the sum of mono/di and Naphthenic content within the fuel. It is noted that the fuel analysis for fuels 1-3 was performed by Shell in 2010 (Middle-distillate exhaustive analysis report) whilst the fuel analysis for fuels 4-7 was performed in 2021 by DLR-Germany with more detailed physicochemical properties found in [5].

Table 1: Summary of fuels chemical properties

Fuel	Test Campaign	Hydrogen Content (%)	H/C ratio	Specific Energy (MJ/kg)	Mono-Aromatics (MA%)	Di-Aromatics (DA%)	Total Aromatics (%)
1- 100% GTL	RQL 1 & 2	15.47	2.181	44.25	0.06	0	0.06
2- 75% GTL	RQL 1 & 2	14.895	2.086	43.864	6.33	0.38	6.71
3- Jet-A (J-FHA)	RQL 1 & 2	13.427	1.848	43.013	23.18	1.07	24.24
4- B3 (A-HA)	RQL 1 & 2	13.51	1.848	43.30	24.91	0.28	25.18
5- F4 (B-HE2)	RQL 1 & 2	14.514	1.861	44.16	12.68	0.14	12.82
6- F1 (J-HA)	RQL 1	13.649	1.884	42.85	20.57	2.18	22.75
7- E5 (B-REF)	RQL 2	14.405	2.005	43.62	12.89	1.28	14.16



### 3 Operation and Data processing

#### 3.1 Rig operating conditions

A total of eight rig operating conditions were investigated during RQL 1 Combustor Rig Test (A1-H1 **Table 2**), where combustor pressures ranged from 2 to 5 bara, primary AFRs from 5.9 to 8.4 and global AFRs from 40.0 to 56.7. To protect the combustor can and avoid damage whilst offering a range on nvPM concentrations, during RQL 2 testing, four rig operating conditions were investigated (A2-D2 **Table 3**) at a combustor pressure of 3 bara and with conditions B2 and D2 corresponding to reduced atomisation conditions when compared with A2 and C2.

Table 2: Combustor rig operating conditions during RQL 1 Combustor Rig Test (M4.1)

Condition	Combustor Pressure [bara]	Condition	Fuel Mass Flowrate (g/s)	Primary Air Mass Flowrate (g/s)	Secondary Air Mass Flowrate (g/s)	Primary Cooling Air Mass flowrate (g/s)
A1	2.0	dirty	1.1	3.9	41.9	3.5
B1	2.0	clean	1.1	4.5	41.0	3.5
C1	3.0	dirty	1.6	5.8	64.4	5.3
D1	3.0	clean	1.6	6.9	61.2	5.3
E1	4.0	dirty	2.2	7.9	86.1	7
F1	4.0	clean	2.2	9.0	81.6	7
G1	5.0	dirty	2.7	9.8	107.2	8.9
H1	5.0	clean	2.7	11.1	102.2	8.9

Table 3: Combustor rig operating conditions during RQL 2 Combustor Rig Test (M4.2)

Condition	Combustor Pressure [bara]	Condition	Fuel Mass Flowrate (g/s)	Primary Air Mass Flowrate (g/s)	Secondary Air Mass Flowrate (g/s)	Primary Cooling Air Mass flowrate (g/s)
A2	3.0	Dirty 1	2.1	5.9	64.6	5.3
B2	3.0	Clean 1	2.0	6.9	61.4	5.3
C2	3.0	Dirty 2	2.1	5.4	64.6	5.9
D2	3.0	Clean 2	2.0	6.3	61.4	5.9

#### 3.2 Test matrix

During RQL 1 Combustor Rig Testing, at each rig operating condition (**Table 2**), three consecutive test points were taken at a stable rig and sampling condition (i.e., raw CO<sub>2</sub> fluctuation of  $\pm 0.1\%$ ):



#### Work Package 4: Deliverables Report

- (1) a 1-minute test point with a SMPS scan without CS (diluting exhaust with clean house air)
- (2) a 1-minute test point with a SMPS scan with CS (dilution with clean house air)
- (3) a 30-seconds test point as per nvPM regulation (dilution with zero grade synthetic air)

Additional long (30 minute) test points were also obtained at some conditions to assess low mass conditions.

During RQL 2 testing, a 1-minute average corresponding to two SMPS scans was taken at each rig operating condition (**Table 3**) at stable rig and sampling condition while diluting with particle-free house air.

### 3.3 Data reporting and processing

The nvPM emissions indices (EIs) reported in the results were calculated using the simplified equations below, as prescribed in SAE ARP 6320 (ambient CO<sub>2</sub> correction not applied – absolute difference <1%). It is noted that this calculation was deemed appropriate as the measured UHC was ~0 ppm with CO ranging from 11-160 ppm and NO<sub>x</sub> from 50-71 ppm across all test conditions during RQL 1, and UHC, CO, and NO<sub>x</sub> ranging from 0-18 ppm, 126-712 ppm and 46-55 ppm respectively during RQL 2 testing.

$$EI_{\text{mass}} \approx \frac{22.4 \times \text{nvPM}_{\text{mass}} \text{ -STP} \times 10^{-6}}{([\text{CO}_2]_{\text{dil1}} - [\text{CO}_2]_{\text{b}}) / \text{DF}_1 \times (M_{\text{C}} + \alpha M_{\text{H}})} \times k_{\text{thermo}}$$

$$EI_{\text{num}} \approx \frac{22.4 \times \text{nvPM}_{\text{num}} \text{ -STP} \times \text{DF}_2 \times 10^6}{([\text{CO}_2]_{\text{dil1}} - [\text{CO}_2]_{\text{b}}) / \text{DF}_1 \times (M_{\text{C}} + \alpha M_{\text{H}})} \times k_{\text{thermo}}$$

### 3.4 Particle loss correction

The nvPM EIs were corrected for size-dependent particle loss to derive EIs representative of the combustor exit (probe inlet) and independent of any loss in the sampling systems. Two size-dependent system loss correction factors (i.e., kSL<sub>mass</sub> and kSL<sub>num</sub>) calculations were performed and compared:

- (1) as per SAE ARP 6481/Annex 16 Vol. II Appendix 8, requiring only measured nvPM number and mass inputs along with assumptions of lognormality & GSD (also referred to as method 0)
- (2) Using additional particle size distribution measurements and correcting for losses for each discrete size bin (also referred to as bin-by-bin method or method 2)

For both calculation methods, the size-dependent penetration functions were calculated similarly using the UTRC model utilised in ARP6481, theoretically predicting particle loss at any given size in terms of diffusional, thermophoretic, bend and inertial loss mechanisms. Losses in the APC (VPR and CPC loss) and cyclone were also accounted for as prescribed in ARP6481.

It is noted that additional particle loss correction was performed using method 2 to allow a more representative comparison between the nvPM mass and number measurements performed at different locations and on different sampling lines (e.g. raw vs diluted).



## 4 Uncertainty in current CAEP10/11 nvPM regulatory practices (D4.1)

### 4.1 nvPM Mass measurement uncertainty RQL 1 test (M4.1)

As part of RQL 1 test, EI mass intercomparison was performed both across the two compliant systems (AVL MSS Swiss vs AVL MSS EUR) and within respective systems (AVL MSS vs AVL MSS2 Swiss & AVL MSS vs. Artium LII-300 EUR) as discussed below.

#### 4.1.1 EI Mass Intercomparison RQL 1 test (Swiss Vs. EUR)

Simplified EI mass from RQL 1 test, as defined in Section 3.3, for both the EUR and Swiss AVL MSS units are shown in **Figure 7**. As can be observed the average difference between the EUR and Swiss nvPM EI was ~11% with lower values reported by the EUR system (**Figure 7 (a)**). The 11% difference appears consistent across the range of number/mass/GMD investigated as highlighted by the high  $R^2$  (**Figure 7 (b) & Figure 8 (a)**), with larger scatter observed towards the LOD < 5 mg/kg<sub>fuel</sub> (i.e., 15 µg/m<sup>3</sup> measured) which may likely be attributed to shedding interference (see section 4.5). The larger error bars witnessed on some of the data points > 100 mg/kg<sub>fuel</sub> are symptomatic of rig instability and longer averaging times (30 minutes Vs 1 minute and 30 seconds for most of the test points).

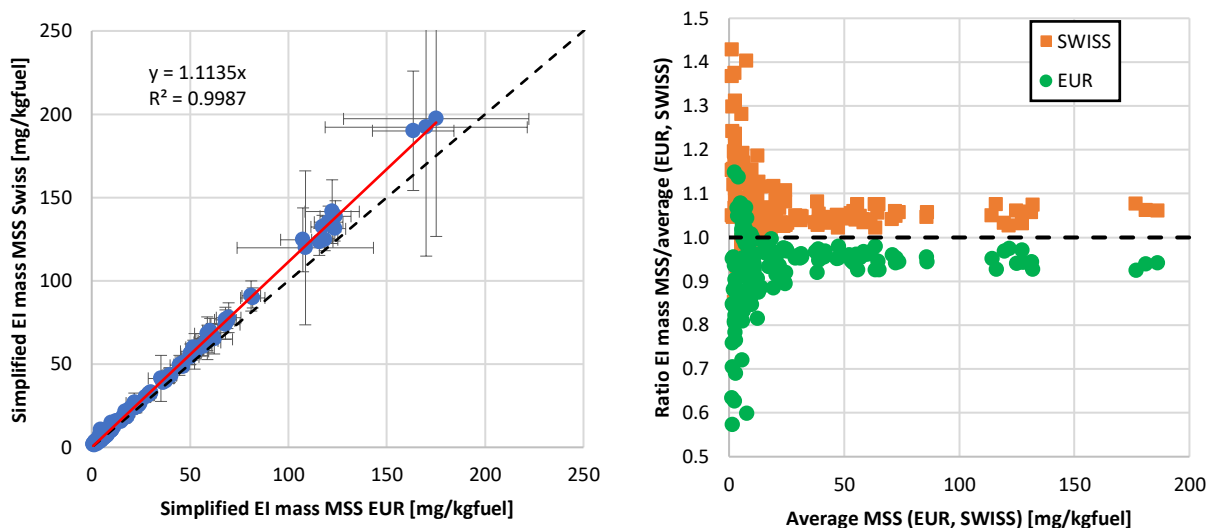


Figure 7: EUR nvPM EI mass Vs. SWISS nvPM EI mass (left) and ratio of SWISS/EUR nvPM EI mass over the average of the two (right) – Error bars represent  $\pm 1$  standard deviation



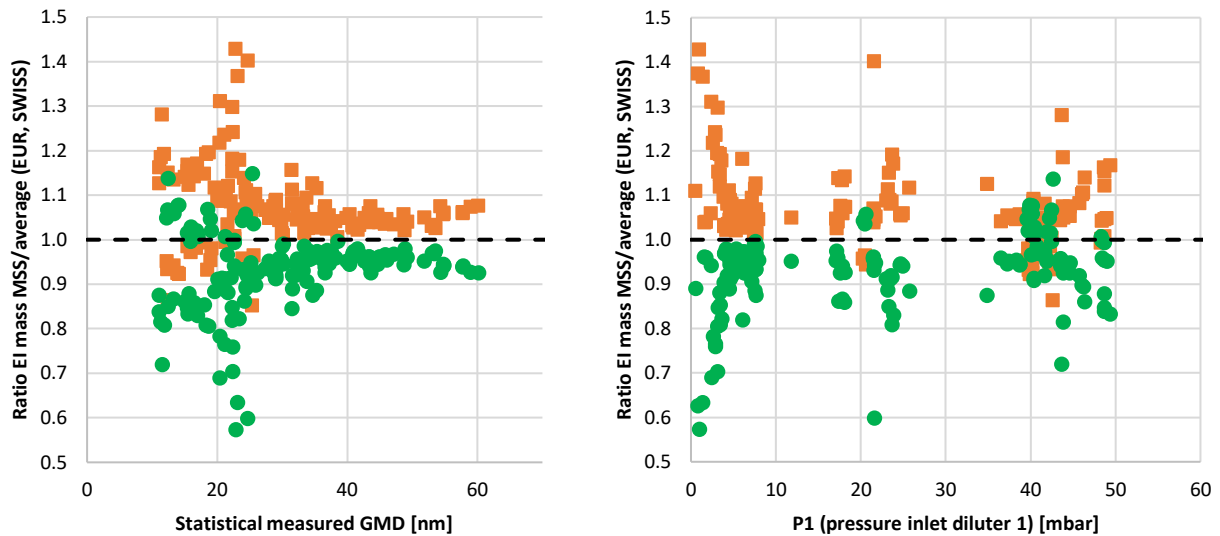


Figure 8: Ratio of SWISS/EUR nvPM EI mass over the measured GMD (left) and the diluter inlet pressure P1 (right)

Further interrogation of the larger than expected uncertainty witnessed around 20 nm highlighted that this data is predominantly from a one-off high pressure (6 bar) case. It is noted that to regulate the excessive pressure in the sample lines an additional smoke measurement analyser, sampling at 20slpm, was used on the EUR raw sample line. This additional flow may have significantly impacted the flow split ratio in the system splitters impacting loss and hence uncertainty between the two lines.

It is noted that the diluter inlet pressure (P1) controlled by the spill in each system was relatively similar but the exact spill dimensions are different and flowrates at a given P1 were unknown. Differences in flowrates in splitters could cause preferential paths and additional particle loss. However as observed in **Figure 8 (b)**, no clear trend is observable. As such system control data from RQL 1, was examined retrospectively which suggested during testing both systems had their spill systems open fully when above ambient pressure. Similarly, data generated in another program was consulted which highlighted changes to Splitter 1 flow caused no discernible change in measured concentrations, therefore as discussed previously in RQL 2 the splitter systems exhausts were decoupled from one and other to reduce potential feedback issues. It should also be noted that the EUR system typically sampled at slightly higher flowrates in the raw segment (~13 slpm vs. ~9 slpm for the Swiss system).

## 4.1.2 EI Mass Intra-comparisons RQL 1 test

### 4.1.2.1 Swiss System (AVL MSS Vs. AVL MSS 2)

Comparison of the two different mass analyser types on the Swiss system during RQL 1 (AVL MSS and an AVL MSS2) are given in **Figure 9 (a)**. As can be seen on the same sampling system the two analysers agree within 2%, on average, with the AVL MSS generally reporting higher values than the AVL MSS2. It is seen that this difference increases at smaller mass (i.e., size) in **Figure 9 (b)**. It is thought that this trend can be attributed to the additional 1m unheated Tygon tubing which was required to connect to the MSS2 inlet to the splitter on the Swiss sampling system, which caused additional thermophoretic and diffusional losses.



## Work Package 4: Deliverables Report

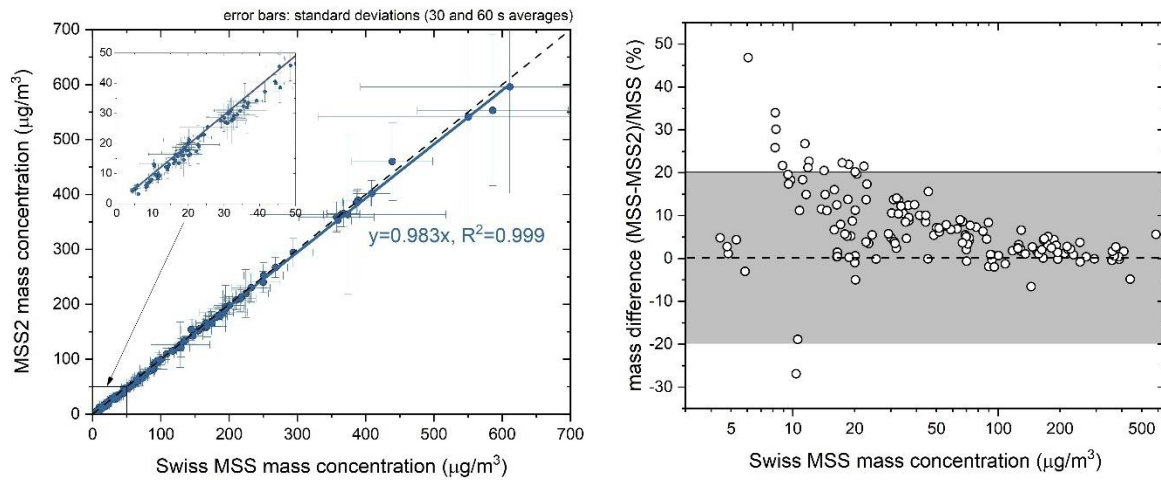


Figure 9: Swiss MSS Vs MSS2 mass concentration (left) and percent difference  $(MSS-MSS2)/MSS$  Vs mass concentration (right) – Error bars represent  $\pm 1$  standard deviation

#### 4.1.2.2 European system (AVL MSS VS Artium LII-300)

Comparisons of the EUR mass analysers (AVL MSS and Artium LII-300) during RQL 1 testing are presented in **Figure 10**. Both instruments are seen to agree on a 1:1 line on average across the mass loadings tested (**Figure 10 (a)**), indicating that any differences in fuel physiochemical properties had no impact (or impacted similarly) on both measurement techniques. However, as seen in **Figure 10 (b)**, at concentrations  $< 10 \mu\text{g}/\text{m}^3$ , differences exceeding 40% are observed. It is thought this increase in data spread is caused by increased measurement uncertainty towards the LOD and shedding interference as one analyser does not consistently read higher than the other at these low concentration conditions.

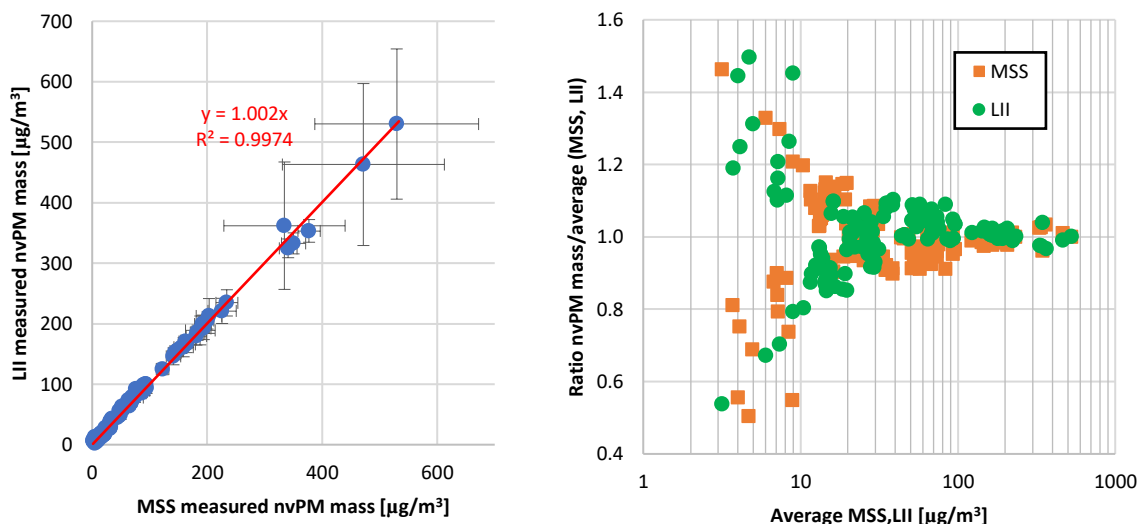


Figure 10: EUR MSS Vs LII-300 mass concentration (left) and ratio of MSS/LII-300 mass over the average of the two (right) – Error bars represent  $\pm 1$  standard deviation





### 4.1.3 RQL 1: Mass measurement uncertainty discussion

Given that immediately prior to RQL 1 testing, both the EUR and Swiss AVL MSS's were calibrated simultaneously by the instrument manufacturer (on the same source at same time) and agreed with the other nvPM mass instruments within their respective sampling systems (i.e., AVL MSS2 in SWISS system [Figure 9] and Artium LII-300 in EUR system [Figure 10]) it is thought that the 11% difference observed across the two reference systems in their quoted EI Mass concentrations may not be attributed to the analyser calibration uncertainty but rather caused by differences in sampling and transport of the nvPM mass to the analysers. Potential explanations explaining the 11% bias witnessed in RQL 1 testing are presented below and were used to develop tighter sampling and cleanliness protocols used in the RQL 2 testing (Section 4.2):

- 1) Differences in conversion to EI because of diluted CO<sub>2</sub> measurement uncertainty - as discussed later this is potentially unsupported due to agreement observed in reported EI number
- 2) Leak in EUR sampling system – unsupported given relevant leak checks and zero checks were passed during the test week. Similarly, as discussed later there are good nvPM EI number, size and gas agreements across systems
- 3) Additional loss of larger particles (>100 nm) in EUR system which would significantly impact the mass measurement (additional loss in splitter 1 or diluter 1?) – most likely scenario and supported by larger uncertainty witnessed around 20nm in Figure 8 (a), but not proven hence will be reconsidered during the second RQL test.

## 4.2 nvPM Mass measurement uncertainty RQL 2 tests (M4.2)

Similar to experiments performed in RQL 1, the measured nvPM mass was again compared across the two reference nvPM systems (simplified EI mass AVL MSS Swiss vs AVL MSS EUR) and within the respective systems (AVL MSS vs AVL MSS2 Swiss & AVL MSS vs. Artium LII-300 EUR) during RQL 2 test. Furthermore, to validate the aforementioned average difference of 11% witnessed during RQL test 1 (section 4.1.1), a pre-test mass instrument intercomparison was performed to assess whether this difference originated from the analysers or from the sampling system. Additionally, it was found in RQL 1 that line cleanliness and shedding from the cyclone was leading larger uncertainties < 5 mg/kg<sub>fuel</sub> (i.e., 15 µg/m<sup>3</sup> measured) as discussed in sections 4.1.1 and 4.5, therefore more regular cleanliness checks and cyclone pot cleaning was performed and it was ensured the MSSs resonance checks were performed on combustion exhaust as discussed in more details in section 4.6.

### 4.2.1 Pre-test mass instrument intercomparison RQL 2 test

Prior to the main nvPM system intercomparison, a mass instrument intercomparison experiment was performed, as shown in Figure 11, with all mass instruments sampling from the same source (i.e., combustor rig exhaust) diluted using a PALAS VKL-10ED to ensure mass loadings in the same range as would be witnessed at the end of sampling systems, suppressed water condensation, homogenous aerosol mixing, and sufficient flow for all mass analysers. The aerosol was split using a Grimm flow splitter 5483 (without the critical orifice to minimise the pressure drop) with each leg of the splitter sampling at a similar flowrate to ensure similar loss.



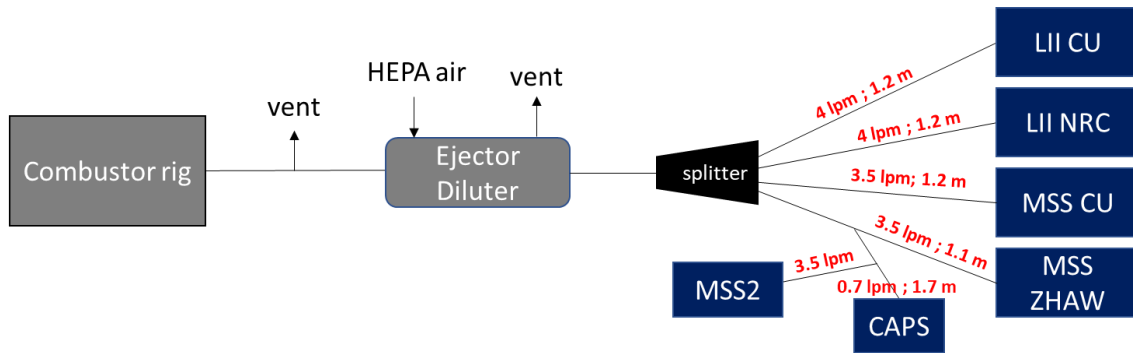


Figure 11: Diagram of the nvPM mass instrument intercomparison

All data was corrected to STP (correction required for the CAPS) with the regulatory analysers (MSS & LII) calibrated as per ICAO standards (described in ARP6320) as detailed below.

- The EUR and Swiss MSS were calibrated next to each other on the same source (mini-CAST) by AVL in September 2020
- The EUR LII was calibrated on a Rolls-Royce GNOME engine in November 2020
- The NRC LII was calibrated on a Rolls-Royce GNOME engine in March 2020
- The MSS 2 was calibrated just before RQL 2 (November 2021) by AVL (same calibration line as used for the MSS)

Furthermore, in line with suggestions in the literature, CAPS had applied a mass absorption cross-section (MAC) of  $6.3\text{m}^2/\text{g}$  to calculate nvPM mass from the absorption (extinction minus scattering measured) to allow comparison on combustion soot [7].

The mass instrument intercomparison was performed on the four test points (A2-D2 **Table 3**) using two fuels (2 and 3 in **Table 1**), with the measured nvPM mass ranging from 15 to  $120\ \mu\text{g}/\text{m}^3$ , and the results displayed in **Figure 12**. Firstly, it can be seen that the Swiss and EUR MSS agree within  $1\ \mu\text{g}/\text{m}^3$  twelve months after calibration (**Figure 12 (a)**). Given their relative absorber window checks were still in compliance, this supports that the 11% difference observed during RQL 1, likely did not originate from measurement uncertainty between the instruments. Secondly the MSS2, which as discussed above was recalibrated immediately prior to this intercomparison, was seen to correlate well with both the Swiss and EUR MSSs. Comparing both LIIs, which were calibrated on the same source but at different times, a  $\sim 15\%$  bias is observed, with the NRC LII reading consistently higher than the EUR LII and both reporting higher concentrations than the MSSs, and the CAPS appearing to agree better with MSS at low concentration and LII at higher loadings. These observations suggest that the current calibration methodology may be a source of systematic bias, particularly when applied to different analyser technologies. Comparing all analysers against the mean value recorded, as can be seen in **Figure 12 (b)**, highlights that generally all mass analysers agree within  $\pm 15\%$ , with the exception of the NRC LII which typically reports 20 to 30% above the mean.



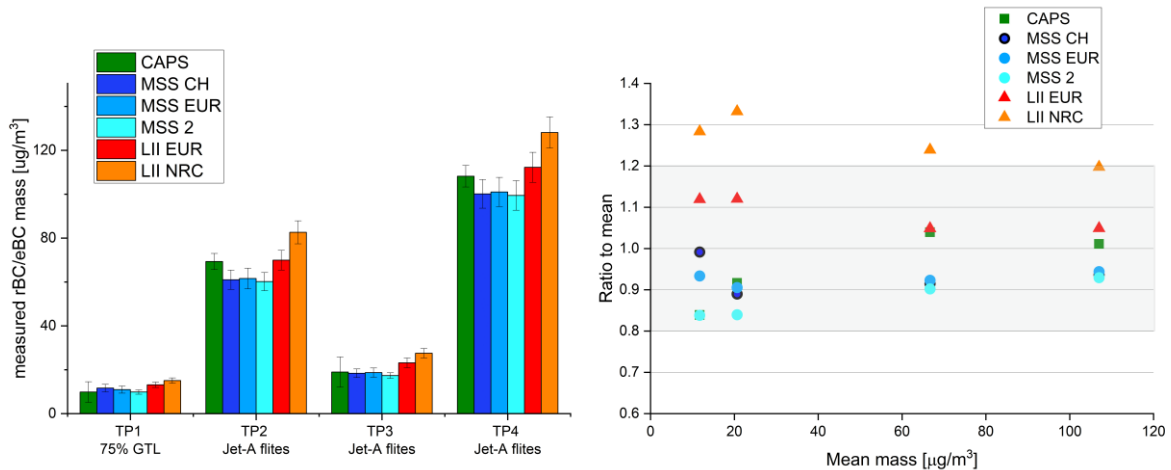


Figure 12: Measured black carbon (rBC or eBC) mass for the six investigated nvPM mass analysers (left) and ratio to the mean Vs the mean BC mass of the size analysers (right)

#### 4.2.2 EI mass intercomparison RQL 2 test (Swiss Vs. EUR)

Simplified EI mass, as defined in Section 3.3, for both the EUR and Swiss (CH) AVL MSS units are shown in **Figure 13** for RQL 1 (previously discussed in section 4.1.1) and RQL 2 tests. As can be observed, the average difference between the EUR and Swiss nvPM EI is  $\sim 3\%$  for RQL 2 across all concentration tested with lower values reported by the EUR system (**Figure 13 (a)**). It is noted that this difference is lower than the 11% average difference witnessed in RQL test 1, and in-line with the results of the pre-test intercomparison (section 4.2.1). As an outcome of lessons learned in RQL 1 testing, the Swiss and EUR diluter boxes spill exhaust connections, which were interconnected during RQL test 1 were decoupled for RQL 2 in order to try and limit any feedback and bias in the spill rates. Similarly, more regular cleanliness checks and cyclone pot cleaning were performed during RQL 2, in a bid to reduce the uncertainty near LOD. In **Figure 13 (b)**, it can be seen that less scatter is observed during RQL 2 towards the LOD  $< 5 \text{ mg}/\text{kg}_{\text{fuel}}$  (i.e.,  $15 \mu\text{g}/\text{m}^3$  measured). Therefore, it is supported that as speculated in RQL 1 the 11% difference witnessed was caused by sampling impacts rather than measurement uncertainty.



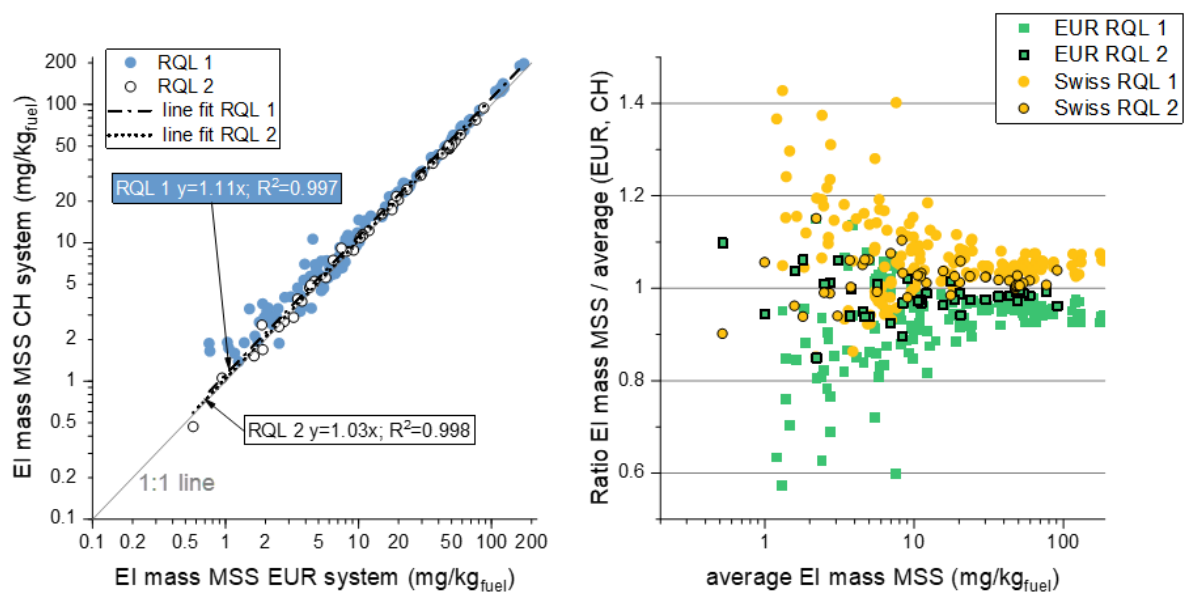


Figure 13: EUR nvPM EI mass Vs. SWISS nvPM EI mass (left) and ratio of SWISS/EUR nvPM EI mass over the average of the two (right) for RQL 1 & 2 test

## 4.2.3 EI mass intra-comparisons RQL 2 test

### 4.2.3.1 Swiss System (MSS Vs. MSS2)

Comparison of two different MSS mass analyser models (AVL MSS and an AVL MSS2) located near each other in the Swiss reference system are given in **Figure 14 (a)** for RQL 1 (as previously discussed in section 4.1.2.1) and RQL 2 testing. As can be seen on the same sampling system the two analysers agree within ~2% on average for RQL 1 and ~4% during RQL 2, with the Swiss MSS generally reporting higher values than the AVL MSS2 in agreement with the results witnessed in the pre-test intercomparison (**Figure 12**). The difference between agreement between RQL 1 and RQL 2 may partially at least, be attributed to the MSS2 being re-calibrated immediately before RQL 2, with this additional difference of ~2% representing the calibration uncertainty for a given laboratory and methodology.

It was previously hypothesised that the increasing difference witnessed at smaller mass (i.e., size) in **Figure 14 (a)** was attributed to additional losses in the unheated line required to connect the MSS2 to the splitter in the Swiss nvPM system. To confirm this hypothesis, particle loss correction between the MSS2 and the MSS was performed using the bin-by-bin method (described in section 3.4) using the Swiss SMPS data and correcting the MSS2 for losses by multiplying its measured mass by the ratio  $k_{sl_{mass}}(MSS2)/k_{sl_{mass}}(MSS)$ . The loss-corrected MSS2 data is presented in **Figure 14 (b)** where it can be seen that the overall agreement is improved from ~4% to ~1%, however it is noted that the discrepancy observed at smaller mass (i.e. Size) is still present.



## Work Package 4: Deliverables Report

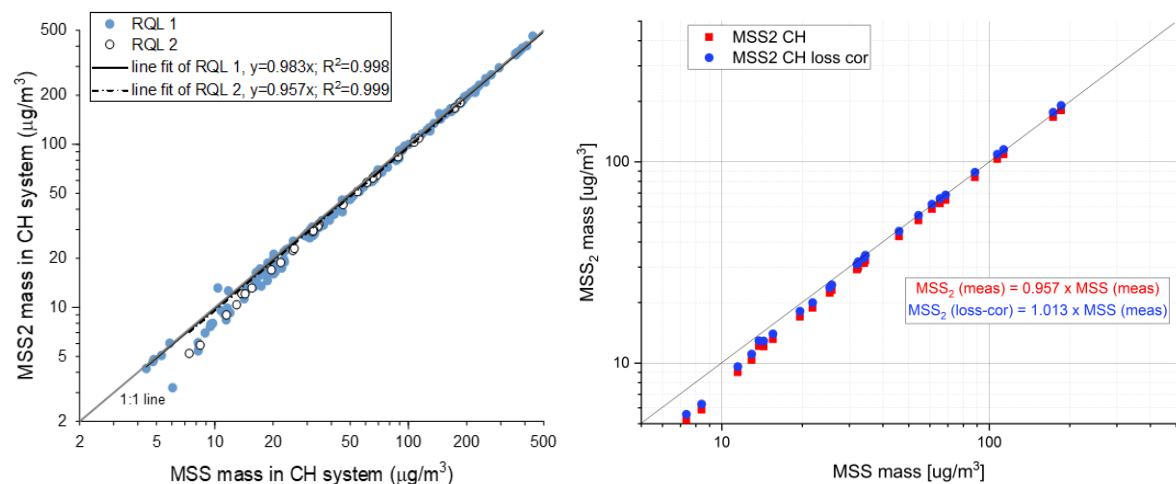


Figure 14: Measured MSS Vs MSS2 RQL 1 & 2 and measured MSS Vs measured/loss corrected MSS2 for RQL 2

#### 4.2.3.2 EUR system (MSS Vs. LII)

Comparison of the EUR MSS and LII-300 when located near each-other is presented in **Figure 15 (a)** for RQL 1 (as previously discussed in section 4.1.2.2), RQL 2 and the published A-pride 5 data which was collected on a full-engine in 2013 [8]. While the LII to MSS agreement is generally near 1:1 across all concentrations in RQL, further analysis highlighted that this agreement appears non-linear against concentration, as can be seen in **Figure 15 (b)**. It was confirmed that the non-linearity between the EUR MSS and LII-300 was not driven by differences in fuel properties (**Figure 16 (a)**) but was correlating with GMD (**Figure 16 (b)**). Given the non-linearity observed between 20-500  $\mu\text{g}/\text{m}^3$  in **Figure 15 (b)** appears apparent in datasets as old as APRIDE 5, is thought the issue is specific to this analyser and not from calibration potentially resulting from an imperfect black body calibration conducted on the analyser when new (other MSSs and LII-300 were reported to be linear in the 1-500  $\mu\text{g}/\text{m}^3$  range).

Furthermore, differences in scatter observed at concentrations  $< 20 \mu\text{g}/\text{m}^3$  between RQL 1 & 2 tests may be attributed to the fact that the MSS resonance check was performed on zero air during RQL 1, which could result in MSS over-reporting near LOD, while it was performed on representative exhaust in RQL 2. Cleanliness checks and cyclone pot cleaning were also more regularly performed during RQL 2.



## Work Package 4: Deliverables Report

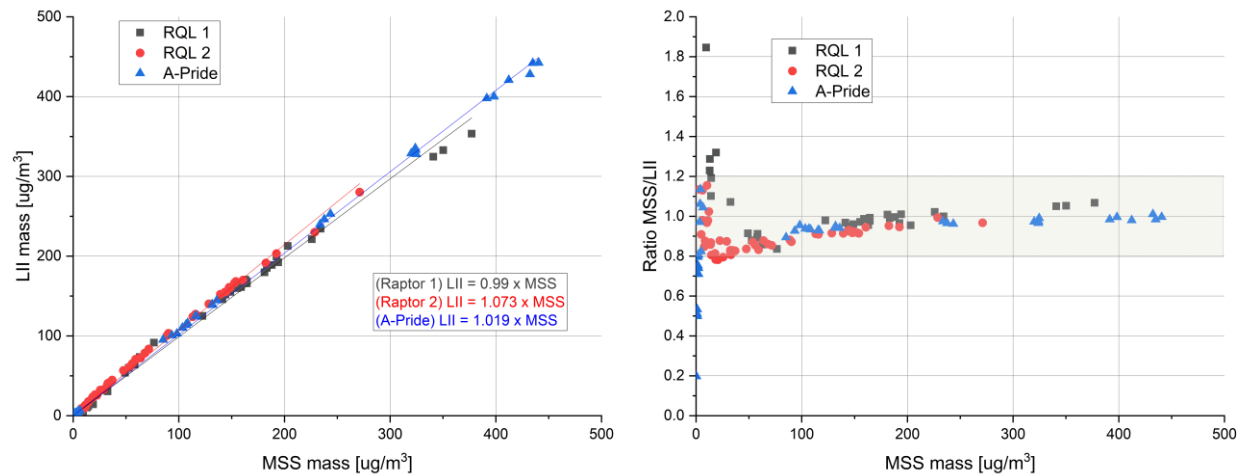


Figure 15: EUR MSS Vs LII-300 mass concentration (left) and ratio of MSS/LII-300 mass Vs the MSS mass (right) for RQL 1, RQL 2 and A-pride data

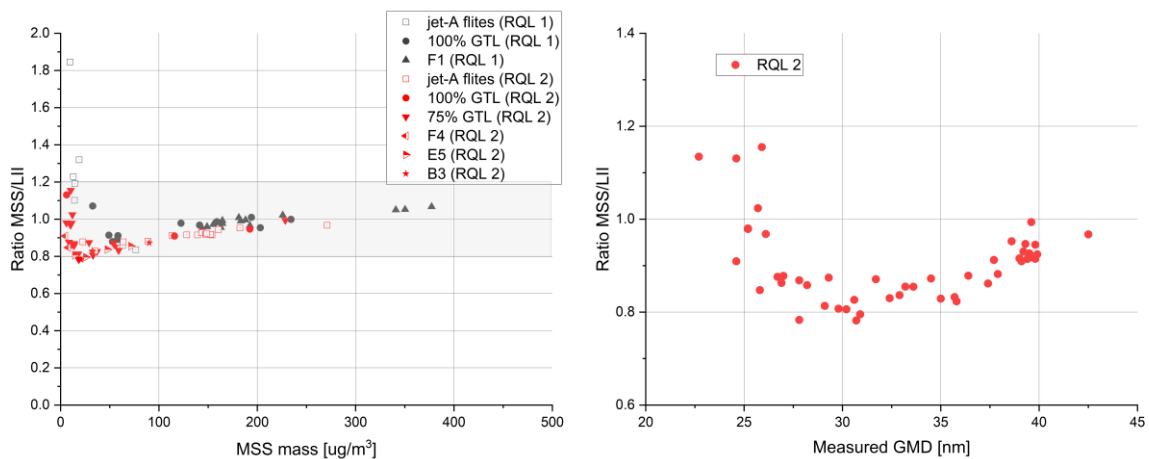


Figure 16: Fuel-differentiated ratio of MSS/LII-300 mass Vs the MSS mass from RQL TEST 1 and 2 (left) ratio of MSS/LII-300 mass Vs measured GMD for RQL TEST 2 (right)

#### 4.2.4 nvPM mass calibration uncertainty RQL 2 test (NIOSH 5040)

The reference method for the calibration of nvPM mass instruments is the ASTM D6877-13 method, which uses a diffusion flame source of nvPM and a thermal/optical transmittance (TOT) carbon analyser for the measurement of Elemental Carbon (EC) from an aerosol sample collected on a pre-baked quartz filter. The method provides Total Carbon (TC) loading on the filter. A laser is used to measure the transmittance of the filter and the instrument software calculates the split between Organic Carbon (OC) and EC. The quoted precision of this method for EC is  $\sim 10\%$ . However, this precision applies for the TOT analysis and does not include the filter sampling uncertainty. The filter sampling uncertainty includes the flow measurement uncertainty (mass flow controller uncertainty) and potentially additional uncertainties due to uneven flow splitting ratios in a flow splitter between the quartz filter collection setup and the nvPM instrument being calibrated.



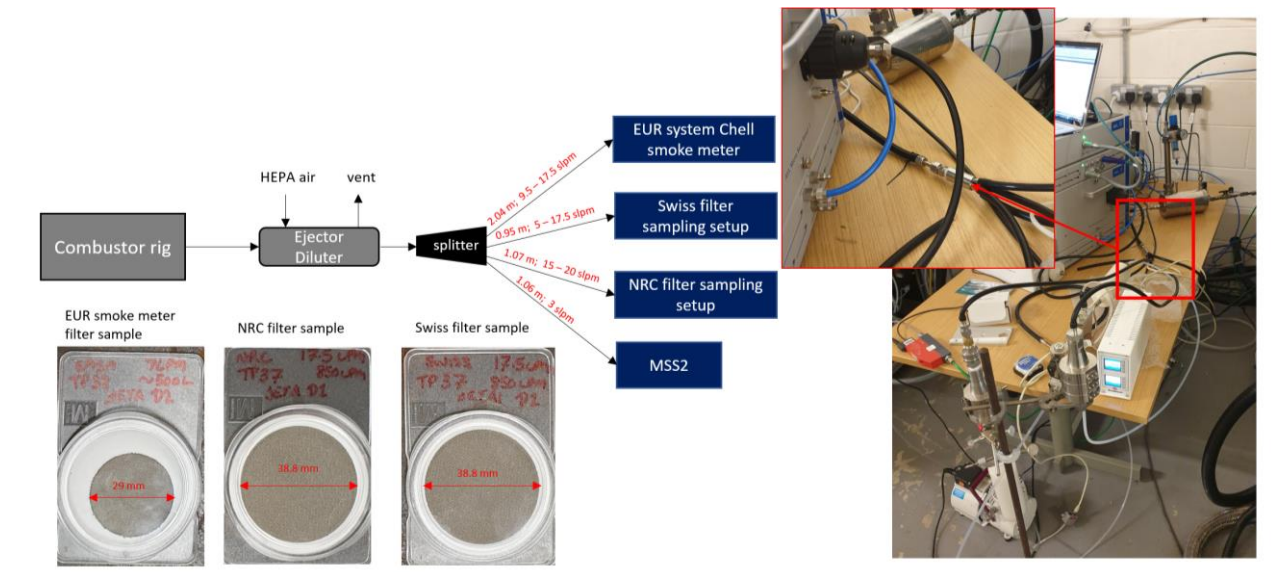


Figure 17: Experimental setup for the filter sampling uncertainty investigation during the RQL 2 test.

As a part of the RQL 2 test, filter sampling uncertainty was investigated using three filter sampling setups operated in parallel with a freshly calibrated MSS2 (**Figure 21**). The combustor rig sample was diluted using an ejector diluter and split to the instruments using a Grimm four-way flow splitter. The Swiss and NRC sampling setups consisted of a two-stage stainless steel filter holder (URG Corp., USA) for 47 mm filters using identical filter cartridges. The flow rate was controlled by MFCs, Voegtlin red-y in the Swiss setup and a Bronkhorst F-111BI in the setup operated by NRC. The Bronkhorst MFC was loaned for the test by Rolls-Royce. The MFC flow rates were verified using a reference flow meter Gilibrator 3 with slope within 1% of the reference. A small HEPA filter was installed downstream of the filter holder to protect the MFCs. A correction factor of 0.9115 was applied to the flows measured by the Chell smoke meter (Gilibrator-determined correction to STP). The nominal flow rates for the sampling setups and the MSS2 are shown in **Table 4**.

Table 4: Test points and flow rates used for the filter sampling uncertainty test. The flow rates are nominal values (STP for the Swiss and NRC system and actual flows for the EUR smoke meter and MSS2).

Test Point	EUR smoke meter	Swiss system	NRC system	MSS2
36	15	15	15	3.5
37	17.5	17.5	17.5	3.5
38	7	5	20	3.5
39	9.5	17.5	17.5	3.5

The filter samples were analysed offline by NRC Canada using a Sunset TOT analyser using both automatic OC/EC split and a manual split, which was chosen by the experienced operator. Typically, EC content determined using the automatic split is used for nvPM mass instrument calibration. The EC/TC ratio without gaseous OC correction and blank correction ranged from 0.55 to 0.75. The mass concentrations determined during the four test points with the three filter sampling systems and the MSS2 are shown in **Figure 18** and the ratios of EC to MSS 2 are shown in **Figure 23**.



## Work Package 4: Deliverables Report

Overall the EC determined with the manual split resulted in a better agreement with the MSS2 and the filter (on average within 10%). The Swiss and NRC filter samplers operated at the same flow rate during test points 36, 37 and 39 resulted in an agreement with each other and the MSS2 within 2% with the manual split and within ~5% using the automatic split. The largest spread was observed at TP 38, with the Swiss system operating at 5 slpm and the NRC system at 20 slpm and at TP39 with the smoke meter operating at lower flow rate than the Swiss and NRC systems. However, it is unclear to which extent this spread is caused by the flow split ratios and by the OC/EC split points. As seen at TP 38 for the Swiss system, the OC/EC split choice causes ~30% difference in the EC mass concentration and the EC/MSS 2 ratio. A similar observation can be made for the smoke filter sample at TP 39. Due to the differences in spot size between the smoke meter and the URG filter holder, the different flow rates used at TP39 resulted in nearly identical surface loadings (**Figure 20**). Thus, the differences seen at TP39 are likely driven by the flow splits and the differences between the filter sampling systems.

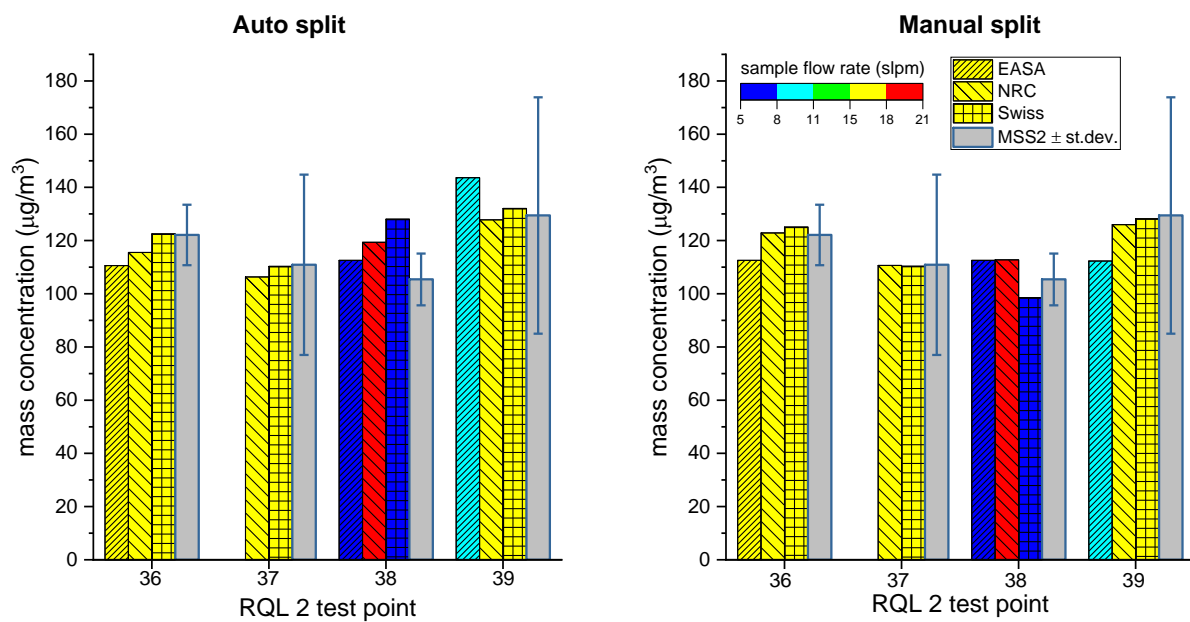


Figure 18: EC and nvPM mass concentrations determined from TOT analysis and with the MSS 2. The color scale represents the sampling flow rate of the filter sampling systems.





## Work Package 4: Deliverables Report

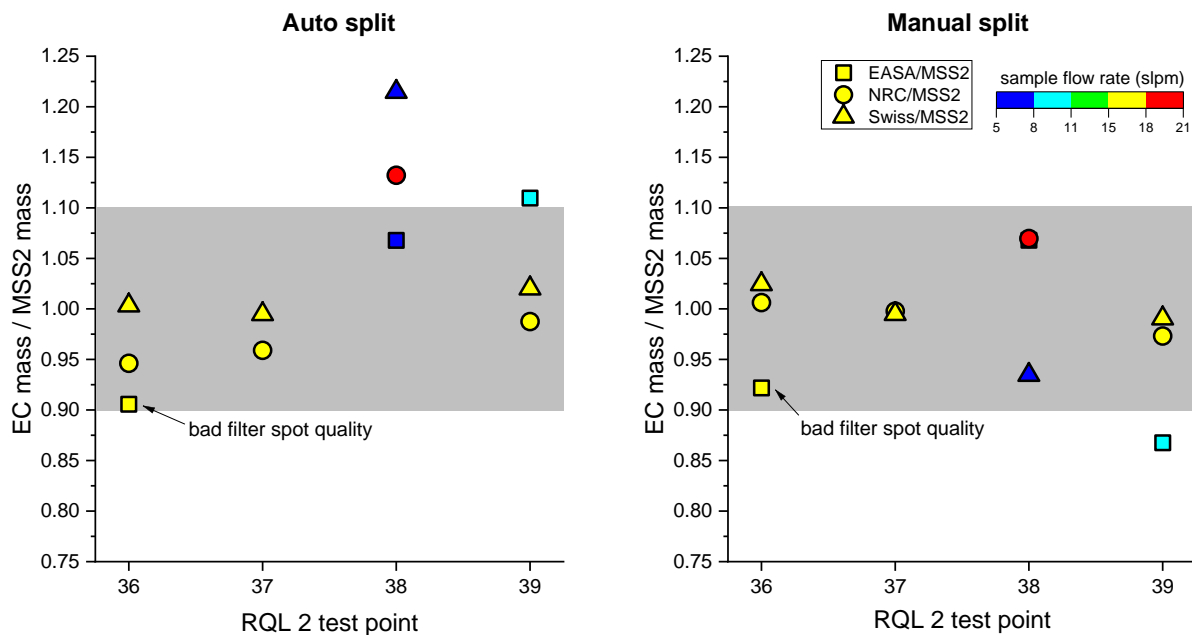


Figure 19: Ratios of EC mass determined using the three filter sampling setups to MSS2-measured nvPM mass for the automatic and manual OC/EC split points.

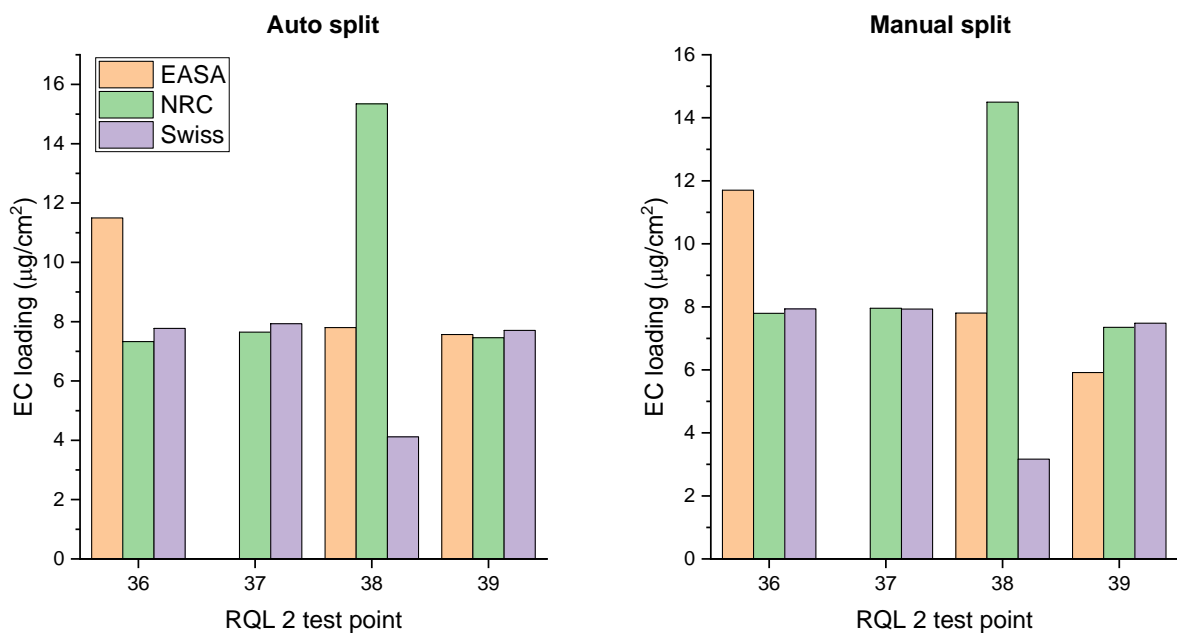


Figure 20: EC mass loadings determined using the automatic and manual split for the filter samples obtained with the three sampling systems.

These results indicate that filter samples obtained with two filter sampling setups operated at the same flow rate and using nearly identical filter holder geometry result in minimal differences in the EC content determined (<~5% with the automatic split). However, filter samples obtained with these two nominally identical systems operated at different flow rates (here flow split ratio of 1:4 at TP 38) result in a wider spread. Nevertheless, the differences seen due to different sampling setups and different flow rates and surface loadings were smaller than the differences seen between the automatic and manual split points,



which resulted in up to 30% differences in the EC content determined, highlighting that this is a protocol that warrants further investigation.

### 4.2.5 Mass measurement uncertainty discussion

It was shown during RQL 2 that an average EI mass agreement of 3% could be reached across all concentrations tested (all data within  $\pm 15\%$  of the average) when using two reference systems in parallel with the same nvPM mass analyser type (AVL MSS) > 12-months after simultaneous calibration by the instrument manufacturer, when taking additional care of sampling and cleanliness practices (i.e., regular cleanliness check and cyclone pot cleaning). The fact that better EI mass agreement was reached after 12-months post calibration ( $\sim 3\%$  Vs  $\sim 11\%$ ), with intra-comparison uncertainty within the individual systems remaining roughly constant, suggests that instrument drift was negligible compared to sampling uncertainties with the 11% bias observed during RQL 1 seemingly reduced by tighter cleaning protocols (particularly at low mass concentrations) and decoupling of the two systems spill exhausts.

## 4.3 nvPM Number measurement uncertainty M4.1 RQL 1 test

Similarly, to the mass nvPM uncertainty assessment, the nvPM EI number was intercompared during RQL 1 test firstly across reference systems (AVL APC vs. AVL APC) and intra-compared within the Swiss reference system (AVL APC vs. AVL APC – 2 CPC).

### 4.3.1 EI Number Intercomparison RQL 1 test

A intercomparison of the two number counters across all relevant test-points collected during RQL 1 (Swiss AVL APC vs EUR AVL APC) is shown in **Figure 21 (a)**. As can be seen an average difference of  $\sim 2\%$  was witnessed between the EUR and Swiss reported EI number across all concentrations tested, with lower values typically reported by the Swiss system. However, as witnessed in **Figure 21 (b)**, as in the case of mass, the difference is seen to increase significantly, up to 20%, at the lowest concentrations measured.

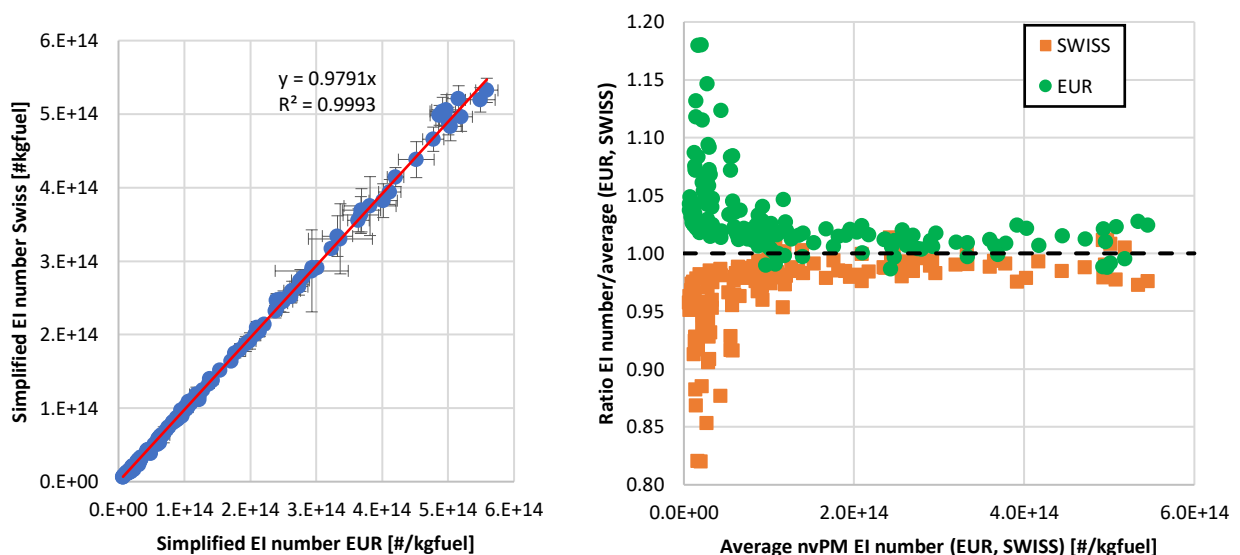


Figure 21: EUR nvPM EI number Vs. SWISS nvPM EI number(left) and ratio of SWISS/EUR nvPM EI number over the average of the two (right) – Error bars represent  $\pm 1$  standard deviation



## Work Package 4: Deliverables Report

It is noted that due to variable dilution ratio control afforded by the AVL APC, lower EI concentrations do not necessarily correspond to low CPC number counts and EI is dependent on fuel burn in addition to particle concentration. Therefore, to assess if the uncertainty is associated with low CPC count, the average difference is also given against CPC count in **Figure 22 (a)**. Finally, it is noted that low number concentrations were often witnessed when testing with the cleanest (GTL) fuels, which also exhibited the smallest particles. As such to assess if particle size impacted the uncertainty the average difference was plotted against GMD and is given in **Figure 22 (b)**. As can be seen, when plotted against size it appears that there is a clear divergence of the instruments at the lowest sizes (<20nm). This result may suggest that the Swiss system experiences higher loss of smaller particles (diffusional losses in sampling system or catalytic stripper) or that the Swiss systems CPC has a lower counting efficiency at the smaller sizes compared to the nominally identical CPC found in the EUR system, although calibration data suggest they have similar counting efficiencies (see **Appendix**).

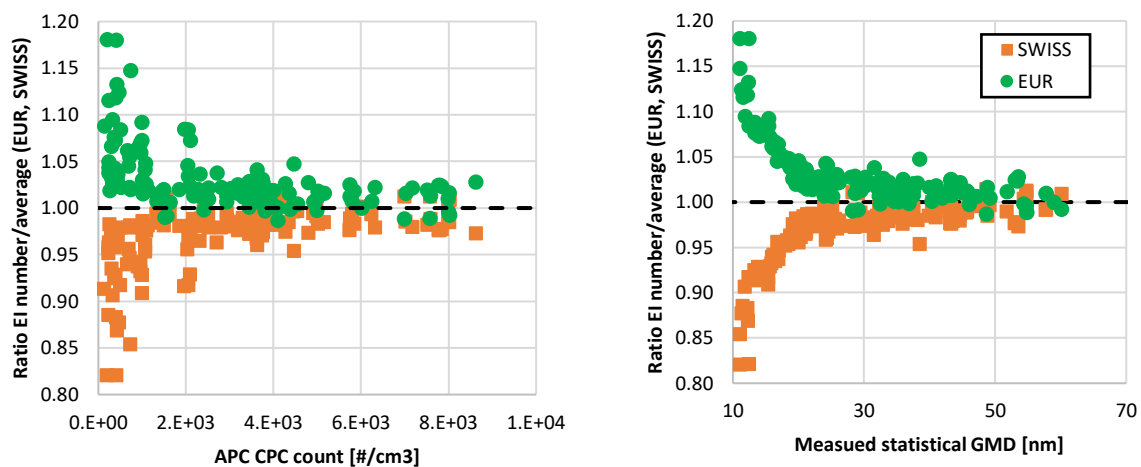


Figure 22: ratio of SWISS/EUR nvPM EI number over the CPC count (left) and measured GMD (right)

To assess whether the difference in nvPM EI number was caused by differences in quoted VPR penetration efficiencies and CPC cut-off efficiencies, the simplified nvPM EI numbers were corrected for VPR loss and CPC counting efficiencies using the quoted penetration efficiencies given in their respective calibration certificates (see **Appendix**). Corrected data at different particle sizes is presented in **Figure 23**. It is seen that the difference in VPR/CPC loss-corrected nvPM EI number between the Swiss and EU system still increases at decreasing GMD, suggesting that the observed difference doesn't originate from differences in VPR penetration efficiencies and CPC cut-off efficiencies.



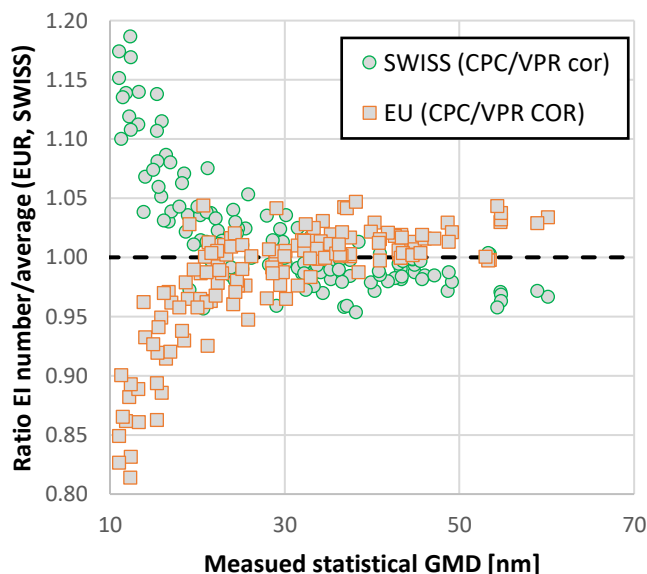


Figure 23: ratio of SWISS/EUR VPR/CPC loss-corrected nvPM EI number over the measured GMD

### 4.3.2 EI Number Intra-comparison RQL 1 test

As discussed earlier an additional prototype AVL APC equipped with both a TSI CPC and AVL CPC was added to the Swiss reference system to assess uncertainties associated with calibration, VPR and CPC count efficiency.

#### 4.3.2.1 Swiss System (AVL APC Vs. AVL APC – 2 CPC's)

The comparison of results on the Swiss system comparing the standard AVL APC to a secondary AVL APC equipped with two CPCs can be seen in **Figure 24**. It is observed that the EI number for both CPCs in the secondary APC under-report the standard AVL APC by 11% on average. It is thought this offset is likely attributed to additional loss in the Tygon line required to connect the secondary APC to the system. However, there is the potential that the offset is impacted by potential differences in VPR losses, which is yet to be investigated.

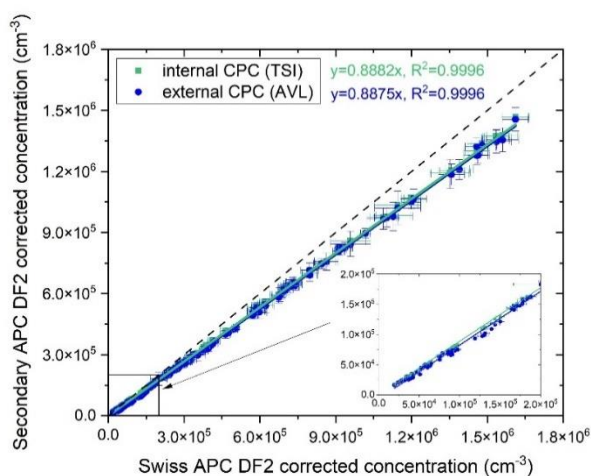


Figure 24: Swiss APC Vs Secondary APC (TSI and AVL CPC) number concentration



## Work Package 4: Deliverables Report

When looking at the relative response of the two CPCs in the secondary APC (internal TSI Vs external AVL), as seen in **Figure 25 (a)** they agree very well,  $\sim 2\%$ , across all number concentrations investigated. It is however noted that at lower concentrations (which also corresponds to small size) higher discrepancy was observed, likely caused by differences in CPC counting efficiency and/or loss in the sampling lines to the individual counters.

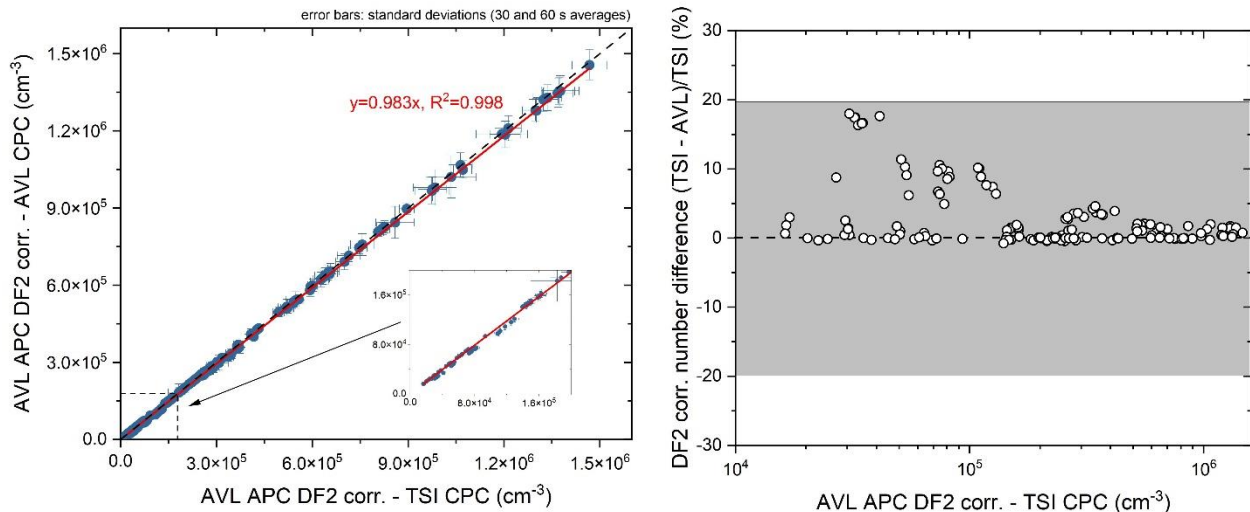


Figure 25: Swiss secondary APC TSI CPC Vs AVL CPC number concentration (left) and percent difference (TSI-AVL)/TSI Vs number concentration (right) – Error bars represent  $\pm 1$  standard deviation

### 4.3.3 RQL 1: Number measurement uncertainty discussion

As discussed above, a very good agreement in average response was observed across the two reference systems ( $\sim 2\%$  (**Figure 21 (a)**)). As would be expected given the types of VPR and CPC in both systems, both AVL APC with TSI CPC, are nominally identical and they were simultaneously calibrated at the instrument manufacturers. However, deeper analysis highlighted that there may be a size dependant bias witnessed between the two systems which is not accounted for when correcting for known differences in VPR penetration and CPC count efficiency as given in the ICAO compliant calibration certificates (**Figure 23**).

It was also observed that two similarly specified and calibrated CPCs from different manufacturers, if sampling behind the same VPR offer good average agreement across a range of number concentrations (**Figure 24**). However, again on closer analysis it appears this agreement may be impacted by particle size. Finally, it is noted that changes to the specified sampling system should be done in a cautionary manner and may account for the relatively large  $\sim 11\%$  offset witnessed between the two AVL APCs sampling on the Swiss system.

## 4.4 nvPM Number measurement uncertainty M4.2 RQL 2 test

Similarly to the mass nvPM uncertainty assessment performed in RQL 1 & 2, the nvPM EI number was again compared across reference systems (AVL EUR APC vs. AVL Swiss APC) as part of RQL 2 after a 12-month period in which both analysers were used extensively for offsite testing. It is noted that unlike nvPM mass instruments, no pre-test nvPM number instrument intercomparison was performed on combustor rig exhaust. However, a thorough nvPM number instrument intercomparison was undertaken using different particle types (gold, silver & graphite) as part of a SAMPLE IV SC01 test campaign occurring at a similar time.



### 4.4.1 EI Number intercomparison RQL 2 test

EI number comparison of the two number counters (EUR AVL APC vs Swiss AVL APC) is shown in **Figure 26** for both RQL 1 (as previously discussed in section 4.3.1) and RQL 2. While an average difference of  $\sim 2\%$  was witnessed between the EUR and Swiss EI number during RQL 1 across all concentrations tested, better agreement was witnessed during RQL 2 a year later (average difference  $\sim 0.2\%$ ), as displayed in **Figure 26 (a)**. It can also be seen in **Figure 26 (b)** that all data agree within  $\pm 5\%$  of the average for RQL 2, and that the larger difference observed at smaller sizes during RQL 1 is not seen in RQL 2. It was hypothesised that the increasing difference witnessed  $< 20$  nm during RQL 1 (red dashed circle in **Figure 26 (b)**) was caused by differences in material properties of the aerosol, whereby condensed metallic particles, generated during combustor can damage at high thermal powers (see **Figure 3**) were dominating the sampled aerosol and differently impacting loss in the VPRs and/or counting efficiency in the CPCs of the two systems. Indeed, it was found as part of SAMPLE IV SC01 that different particle types and morphologies (silver, gold & graphite) were affecting the relative APC nvPM number counting differently.

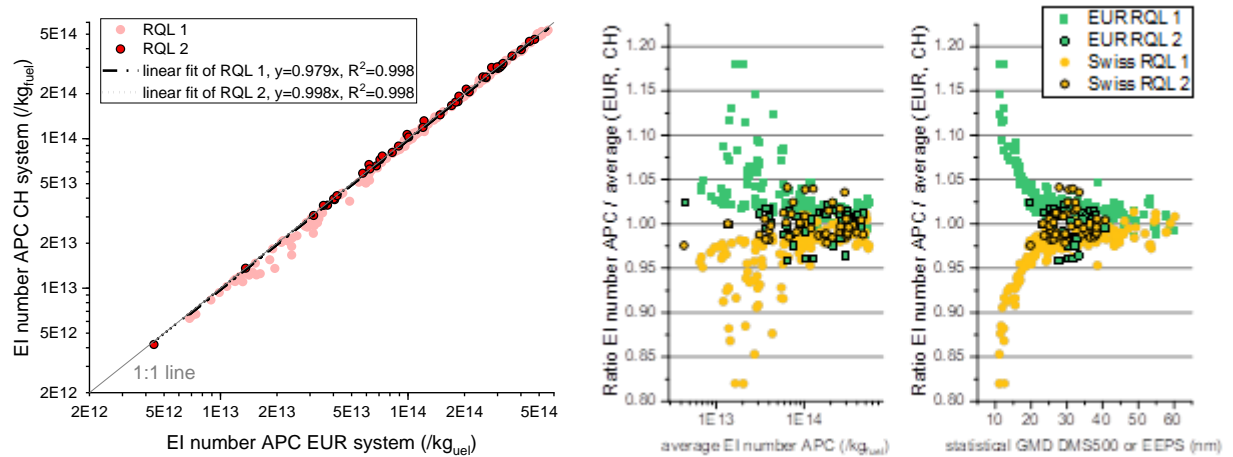


Figure 26: EUR nvPM EI number Vs. SWISS nvPM EI number (left) and ratio of SWISS/EUR nvPM EI number over the average of the two (right) for RQL TEST 1 and 2

### 4.4.2 Number measurement uncertainty discussion

Both RQL test 1 & 2 test campaigns demonstrated that an excellent agreement could be reached for EI number when using two reference systems in parallel with the same nvPM number analyser type (AVL APC) calibrated simultaneously by the instrument manufacturer and with good operating practices. Average EI number agreement within 2% was observed during RQL 1 testing and 0.2% during RQL 2 tests, with all data agreeing within  $\pm 5\%$  of the average across the concentrations tested. A size-dependent uncertainty was witnessed between the two systems  $< 20$  nm GMD during RQL 1, however it is suggested that it originated from a metallic peak  $\sim 10$ nm, resulting during combustor damage, differently impacting both the EUR and Swiss APCs. This size dependency was not observed during RQL 2.



## 4.5 Line cleanliness, shedding and LOD of mass measurement

### M4.1 RQL test

It is noted that artifacts shed from the sampling system and cyclone can seriously impact the mass measured particularly in the case of very low mass concentrations. As such several experiments were conducted to assess the impact on sample line/ cyclone cleanliness at and near the Mass instruments LOD.

#### 4.5.1 Cleanliness checks RQL 1 (Cyclone cleaning)

The ICAO nvPM standard [6] states that prior to an engine test, the sampling and measurement system must pass a prescribed cleanliness/leakage check, whereby a 30-seconds averaged nvPM mass concentration  $< 1 \mu\text{g}/\text{m}^3$  and a 30-seconds averaged nvPM number concentration less than  $< 2.0$  particles/ $\text{cm}^3$  must be demonstrated. During RQL 1 testing, cleanliness checks were regularly done, at the beginning of each day, but also throughout the day to highlight issues with line cleanliness.

Using previous experience, when the check failed, the cyclone collection pot and inner walls near the cyclone were cleaned thoroughly with IPA, which was generally shown to resolve the cleanliness issue. This phenomenon is clearly shown in **Figure 27 (a)** whereby it is seen that a cleanliness check is failed in terms of nvPM mass and subsequently passed after cyclone cleaning. In the case of this example **Figure 27 (a)**, which was in the middle of a test run, it is demonstrated that shedding from the cyclone may lead to a highly inaccurate nvPM mass reading (zero is 6 times higher before cleaning) in the case of test points where the nvPM mass is low. Currently as defined in the ICAO Annex 16 nvPM standard the cleanliness check conducted prior to this test point, would be viewed as a pass as was demonstrated at the beginning of the test run (at 10:08am the cleanliness check passed and at 11:29am it failed). Indeed, the test point recorded before the cyclone cleaning in **Figure 27 (a)** shows a value of  $6 \mu\text{g}/\text{m}^3$  vs.  $3 \mu\text{g}/\text{m}^3$  after cyclone cleaning. This demonstrates that it should be considered whether cleanliness checks should be prescribed more regularly (than only prior to an engine test) to ensure the integrity of low concentration cases, particularly if they are following high mass conditions.

**Figure 27 (b)** shows the difference in measured mass concentrations of the Swiss system AVL MSS on the diluted line compared to the AVL MSS2 which was temporarily moved to the raw line (without a cyclone). As can be seen, before cyclone cleaning there was a significant difference in measured mass with the dilution corrected AVL MSS overpredicting the raw mass concentration measured by the AVL MSS2 by 1.5 times ( $80 \mu\text{g}/\text{m}^3$  vs  $50 \mu\text{g}/\text{m}^3$ ). As can be seen excellent agreement between the two analysers is witnessed immediately after cyclone cleaning again demonstrating the requirement for regular cyclone cleaning – particularly at mass levels close to the LOD.



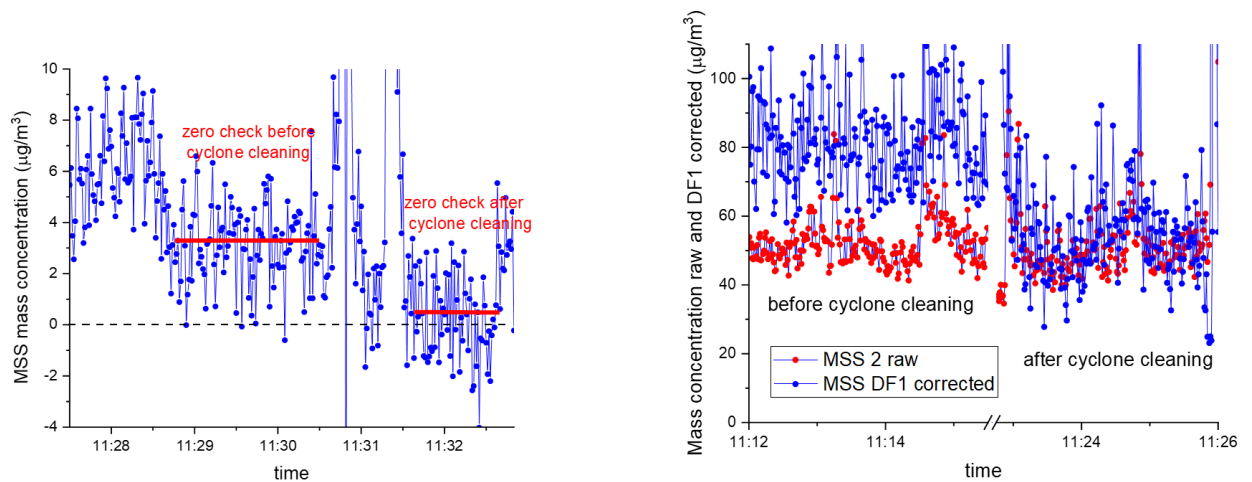


Figure 27: EUR (left) and SWISS (right) MSS nvPM mass Vs time to highlight the effect of cleanliness (zero) checks and cyclone cleaning on measured data

#### 4.5.2 Measured Size derived Volume over time RQL 1

As discussed above, it was hypothesised that the cause for a cleanliness check fail is shedding of a few large particles ( $\sim 300$  nm) from the cyclone. To highlight this, the total volume (directly proportional to the mass) was derived from the measured particle size distributions by assuming sphericity. The ratio of volume  $< 150$  nm to the total volume ( $< 1000$  nm (DMS-500) or  $< 240$  nm (SMPS)) was then subsequently investigated over time. As seen in **Figure 28**, where the dashed red lines correspond to the cleaning times of the cyclones, the volume ratio keeps decreasing over time, potentially suggesting shedding from the cyclone increases over time, generally until the cyclone is cleaned which is particularly evident in both plots midway through day 2.

However, further analysis is required to ascertain that this isn't a secondary artifact caused by the increasing rig pressures typically investigated as the day progressed. It is noted that only datapoints with a volume  $> 10 \mu\text{m}^3$  ( $\sim \text{mass} > 15 \mu\text{g}/\text{m}^3$ ) were used to derive **Figure 28**, given the relatively higher uncertainty below that volume (i.e., conversion of very low number count into a volume) and that the DMS-500 has an additional cyclone at its inlet, hence potentially sees shedding from two cyclones.





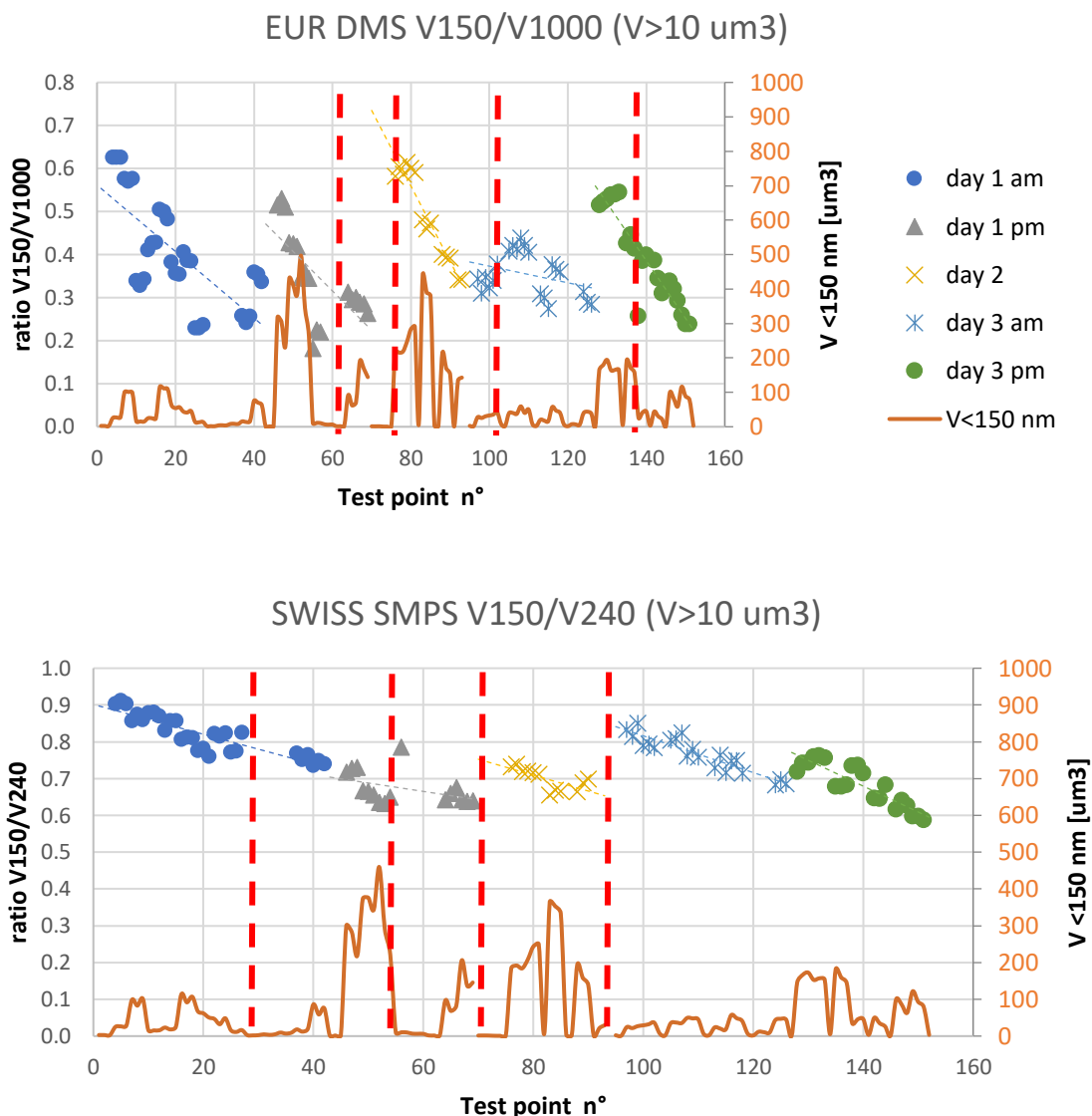


Figure 28: Ratio of volume < 150 nm to the total volume measured by the DMS-500 (top) and the SMPS (bottom) over the three-day long test campaign

### 4.5.3 Comparison nvPM mass raw/diluted near LOD RQL 1

As briefly discussed in the explanation of **Figure 27 (b)**, as both the Swiss and EUR systems had two nvPM mass analysers, it was attempted to measure the nvPM mass simultaneously from the diluted nvPM line and the undiluted raw (gas & smoke) sample line. These measurements were attempted when the nvPM mass was near LOD ( $< 10 \mu\text{g}/\text{m}^3$ ). The results, shown in **Figure 29**, highlight relatively poor agreement for the EUR system, whether before or after the cyclone cleaning. The agreement is better for the Swiss system although the scatter is large. It is thought that significant shedding can occur in the raw line since it is normally used for gases and is relatively dirtier than the diluted line and has no cyclone, which would support the higher readings on the EUR LII-300 instrument. It is also noted that although nvPM mass analysers were shown to agree well within their own sampling system, the scatter significantly increased



near the LOD (see sections 4.1.2.1 and 4.1.2.2). This finding has indicated that more work investigating the mass LOD during the second RQL test campaign.

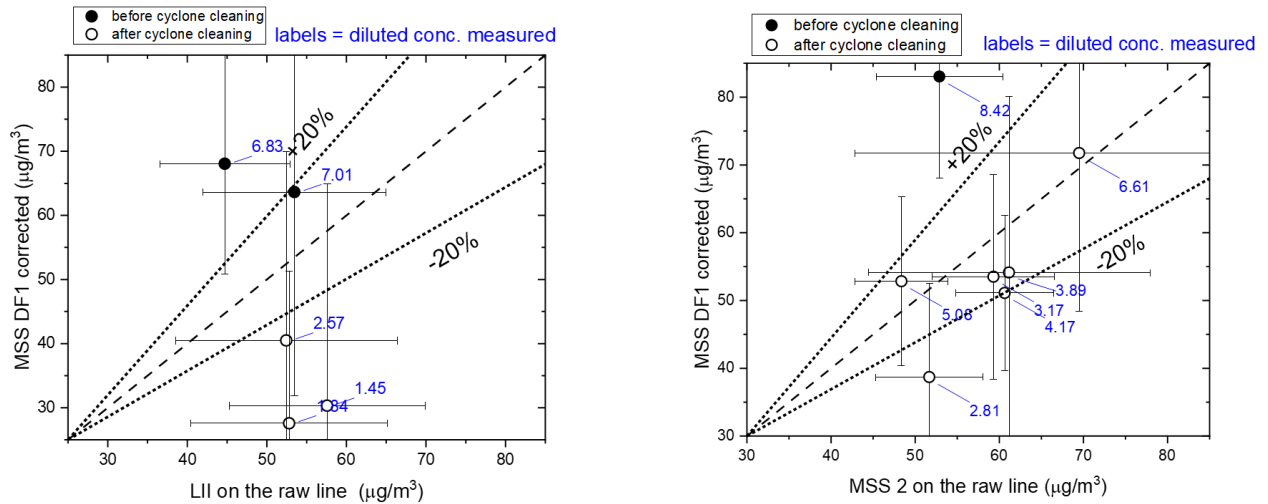


Figure 29: EUR (left) and SWISS (right) nvPM mass measured on the raw line Vs measured on the diluted line and DF1-corrected

## 4.6 Line cleanliness, shedding and LOD of mass measurement RQL 2 test

It was discussed during RQL 1 that artifacts shed from the sampling system and cyclone can seriously impact the mass measured particularly in the case of very low mass concentrations ( $<10 \mu\text{g}/\text{m}^3$ ). As such, additional experiments were performed as part of RQL 2 where more regular and consistent cleanliness checks were performed on both the Swiss and EUR sampling systems. The cyclone pot was also more regularly cleaned to quantify its impact on nvPM mass measurement uncertainty.

### 4.6.1 Cleanliness checks RQL 2 (Cyclone cleaning)

Following RQL 1 results (section 4.5.1), the impact of cyclone pot cleaning on measured nvPM mass was assessed in more detail by performing more regular cleanliness checks, before and after cyclone cleaning, whether cleanliness checks passed ( $<1 \mu\text{g}/\text{m}^3$ ) or failed. The nvPM mass and number reduction observed during RQL 2 testing after cyclone cleaning is presented in **Figure 30** for the EUR system. In **Figure 30 (a)**, it can be seen that cyclone cleaning generally brings a reduction in measured nvPM mass, and that this reduction from cleaning is generally higher when the measured mass concentrations before cyclone cleaning were higher. It also shows that although cleanliness and cyclone cleaning were performed several times a day, shedding from the cyclones was often above the  $1 \mu\text{g}/\text{m}^3$  limit, suggesting that cleanliness checks should be performed more regularly than once prior to an engine test as prescribed by ICAO [6]. In **Figure 30 (b)**, it can be seen that cyclone pot cleaning doesn't significantly impact nvPM number, as the reduction is randomly scattered around the zero mark. This finding supported the earlier hypothesis that the cyclone pot sheds large particles  $\sim 300 \text{ nm}$  which mostly affects nvPM mass measurement  $< 10 \mu\text{g}/\text{m}^3$ .



## Work Package 4: Deliverables Report

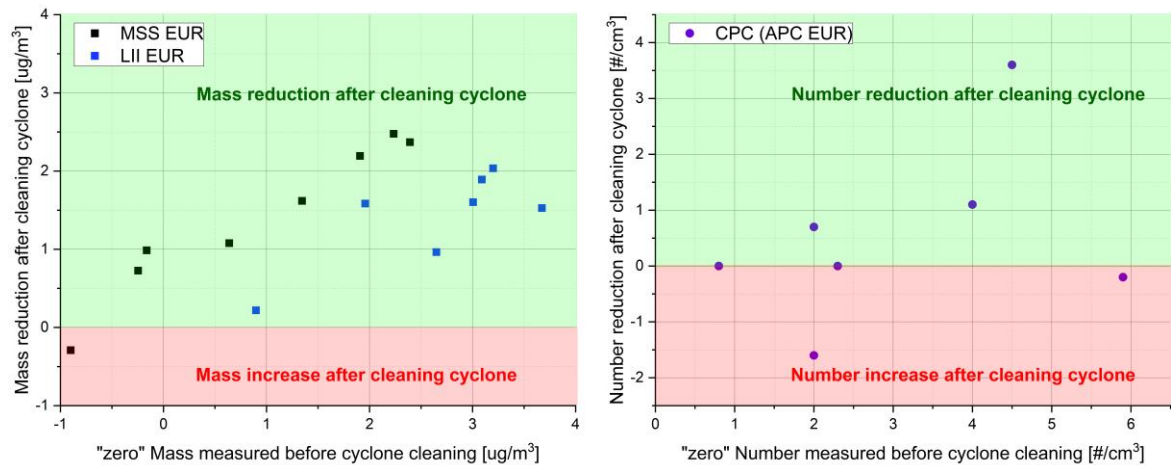


Figure 30: Effect of cyclone cleaning on EUR system nvPM mass (left) and number (right) concentration during cleanliness checks in M4.2 RQL 2

It was found that after cleaning the cyclone pot, the MSS could sometimes be observed to report negative values during a cleanliness check (e.g., **Figure 30 (a)** three points  $< 0 \mu\text{g}/\text{m}^3$  measured [x-axis]). It was discovered that this was caused by the MSS resonance check (i.e., noise correction) being performed on the exhaust aerosol, while the cleanliness checks are performed on diluent having a different gas composition. This highlights that with incorrectly defined resonance check protocols, the MSS could inadvertently underreport during cleanliness checks. This is also shown in **Figure 31**, where the EUR LII to MSS difference is plotted for RQL 1 when the MSS resonance checks were performed on the diluent, and for RQL 2 when the MSS resonance checks were performed on the rig exhaust aerosol. As can be seen, the MSS reports significantly higher values than the LII during RQL 1 when compared with RQL 2 (shift of  $\sim 4 \mu\text{g}/\text{m}^3$ ) which shows that the gas source on which the resonance check is performed can result in an impact of up to  $4 \mu\text{g}/\text{m}^3$  on the nvPM mass value reported during cleanliness check when using an MSS (that is assuming the EUR LII hasn't drifted at low mass in comparison to the MSS between RQL 1 and 2).

The correct procedure to accurately report cleanliness with the MSS would be to perform a resonance check on the diluent before doing a cleanliness check, and then perform another resonance check back on the combustion exhaust before starting exhaust measurements again, however given a resonance check takes 2-3 minutes, this may pose practicality issues during certification testing, particularly at higher powers.



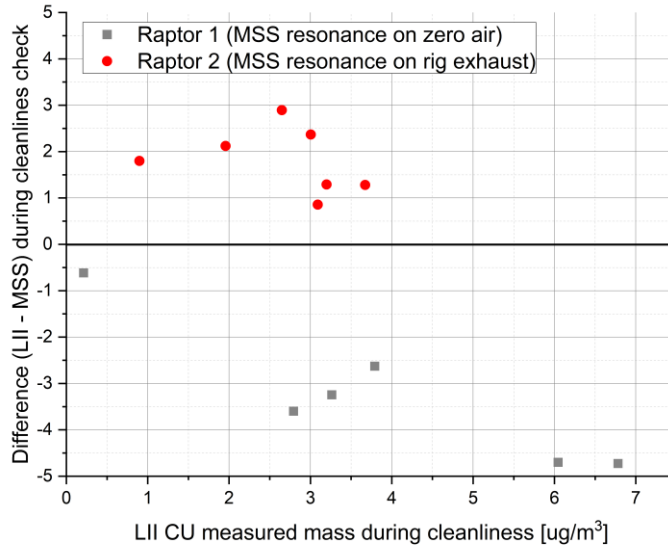


Figure 31: Difference between the LII and the MSS observed during the cleanliness checks in RQL 1 where the MSS resonance check was performed on diluent, and in RQL test 2 where the MSS resonance check was performed on the combustion exhaust

#### 4.6.2 Comparison nvPM mass raw/diluted near LOD RQL 2

Building on the lessons of RQL 1 testing (section 4.5.3), a more complete and dedicated experiment was performed measuring nvPM mass simultaneously on both the raw and diluted lines of the Swiss and EUR systems. This was achieved using the additional NRC LII (EUR system) and MSS2 (Swiss system) on the raw lines, with the measured nvPM mass purposely driven down towards the LOD, using the AFR and Fuel type. It is noted that the NRC LII was fitted with a 1-µm cyclone at its inlet whilst the MSS2 was not.

The results are presented in **Figure 32** and **Figure 33** in which the raw nvPM mass measurement (from either the NRC LII or the MSS2) was corrected for  $DF_1$  and differences in system loss using method 2 ( $loss\ correction = ksl_{mass}(nvPM\ raw)/ksl_{mass}(nvPM\ dil)$ ) as described earlier. Firstly for the EUR system, the raw (corrected) vs diluted nvPM mass is plotted for the whole test campaign, with diluted mass ranging from 1-200 µg/m<sup>3</sup> (**Figure 32 (a)**). It can be seen that the nvPM mass agree within ~3% on average with a line of best fit of 0.969, and that the raw-corrected and diluted nvPM mass generally agrees within ±10% (**Figure 32 (b)**). It is noted that this agreement is significantly better than the differences reported between the NRC LII and the EUR MSS during the pre-test mass intercomparison (section 4.2.1).

**Figure 33** displays the results of the LOD-specific experiment (subset of **Figure 32**) in which the MSS2 measuring on the raw Swiss line was compared to the diluted Swiss MSS, in addition to the NRC LII being compared to the EUR MSS in the EUR system. Again, for diluted nvPM mass between 3 – 18 µg/m<sup>3</sup>, the raw-corrected nvPM mass is seen to be in excellent agreement with the diluted nvPM mass (line of best fit of 1.018 and 0.981 in **Figure 33**).



## Work Package 4: Deliverables Report

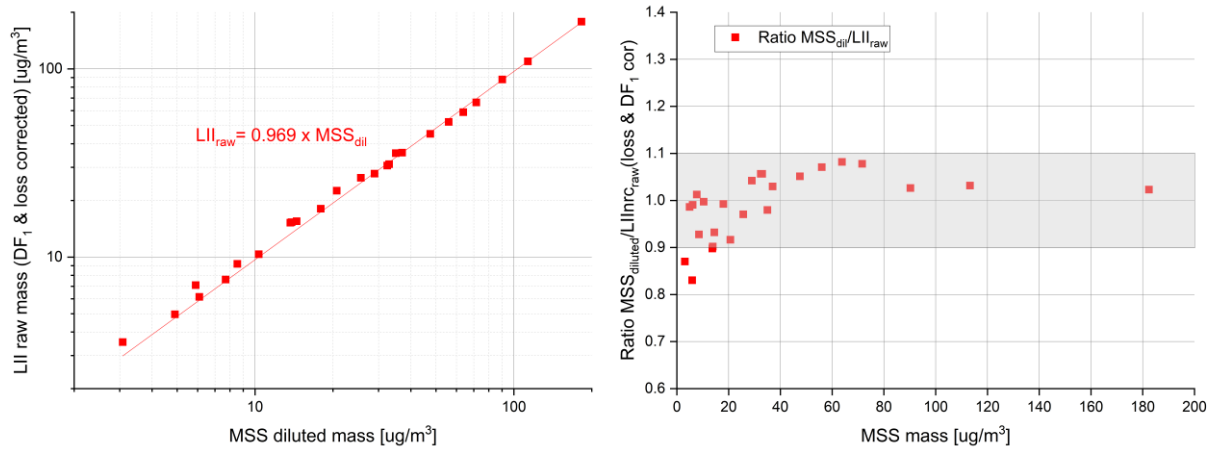


Figure 32: diluted Vs raw (corrected) nvPM mass (left) and ratio of the two Vs the diluted mass (right) for the NRC LII (raw) and EUR MSS (dil)

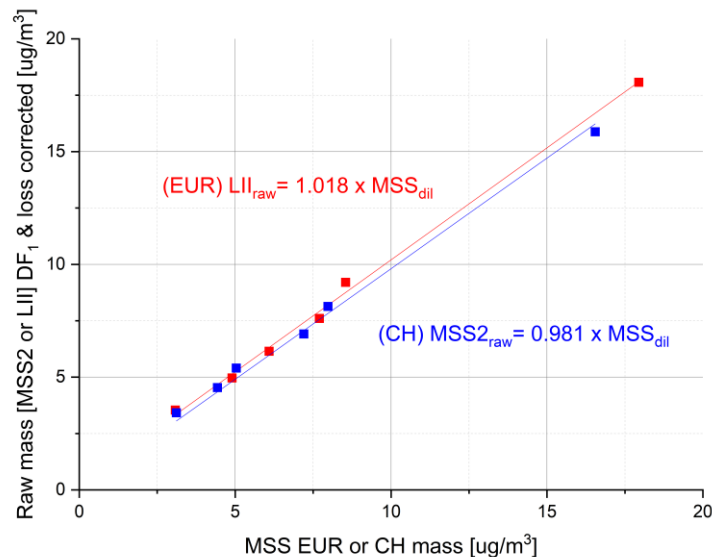


Figure 33: Diluted Vs raw (corrected) mass during LOD specific experiment in the EUR system (LII NRC raw Vs EUR MSS dil) and in the Swiss system (MSS2 raw Vs MSS Swiss dil)

#### 4.6.3 Discussion line cleanliness, shedding and LOD of mass measurement

The results of the LOD experiment demonstrated that it is possible to take a raw nvPM mass measurement, either close to the inlet probe (LII-300 at 160°C) or by the gas analysers (MSS2 at 60°C), with excellent agreement to diluted nvPM mass observed in both cases, following dilution and size dependant loss correction. The agreement was similar regardless of whether a cyclone was used at the inlet of the raw nvPM mass measurement. This experiment also demonstrated that it is possible to take an accurate diluted nvPM mass measurement down to  $\sim 3 \mu\text{g}/\text{m}^3$  when performing regular cleanliness checks, cyclone cleaning and MSS resonance checks on the correct gas source.



## 4.7 VPR uncertainty

### 4.7.1 VPR penetration efficiency measurement RQL 1

Particle loss through the VPR is an area of uncertainty for nvPM number reporting and for system loss correction. As part of RQL 1 tests, the losses (dilution and particle loss) through the EUR reference systems VPR was empirically derived using soot particles generated from the RQL combustor.

#### 4.7.1.1 Experimental setup

The experimental setup is depicted in **Figure 34**, with particle size selected using either a Cambustion AAC (aerodynamic size selection) or a TSI nano-DMA (electrical mobility size selection). The VPR penetration efficiency was measured by simultaneously using two TSI-3776 CPCs at the inlet and outlet of the VPR. It is noted that when the AAC was being used, a Cambustion CS was added at its inlet to ensure any potential volatile material was removed. However, because of additional PM loss experienced in a DMA a CS wasn't used during DMA because of low concentrations at the inlet of the VPR setup. However, given the results highlighted in the size measurements with and without CS on an SMPS (Section 5.1.2.1) on the same rig source it was deemed to still be scientifically robust.

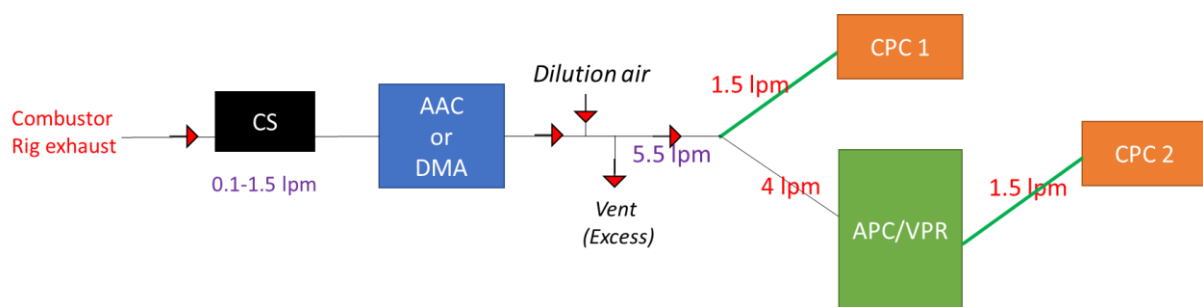


Figure 34: Diagram of the VPR experiment

#### 4.7.1.2 CPC intercomparison

Prior to the VPR experiment, the difference in response from both CPCs was characterised using soot particles generated using different fuels across a range of sizes. The results are shown in **Figure 35**, where CPC 1 measured on average  $4.7 \pm 1.5\%$  a higher concentration than CPC 2. No clear correlations were found between the relative difference and particle size (i.e., counting efficiency) or concentration (i.e., linearity). The line of best fit ( $CPC_{blue} = 1.0375 \times CPC_{red}$ ) was subsequently used to correct CPC data for VPR penetration efficiency.



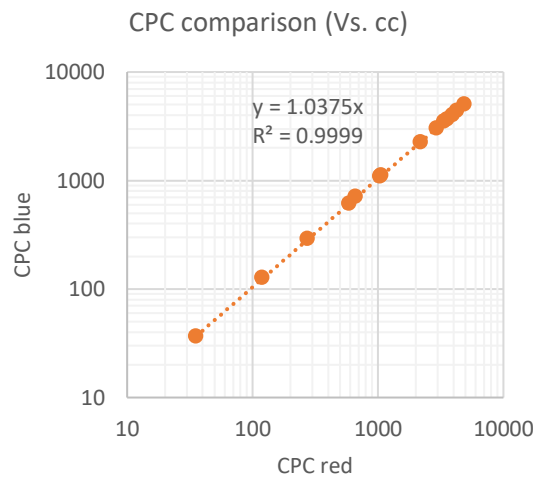


Figure 35: Measured number concentration from CPC 1 Vs that measured simultaneously with CPC2

#### 4.7.1.3 VPR penetration efficiency Results

The VPR penetration efficiency experiment results are shown in **Figure 36**. As seen, there is good correlation between the penetration measured on the RQL combustor exhaust (burning fuel 6) and those determined by AVL on a propane diffusion burner (CAST 5210C). It is observed that independent of size selection methodology the differences in penetration curves appear to be within the expected uncertainty (e.g., CPC standard deviations, classifier, DMA Sheath/sample flow and charging, etc.). This supports that in both cases the soot has a similar enough morphology and organic content to exhibit similar loss.

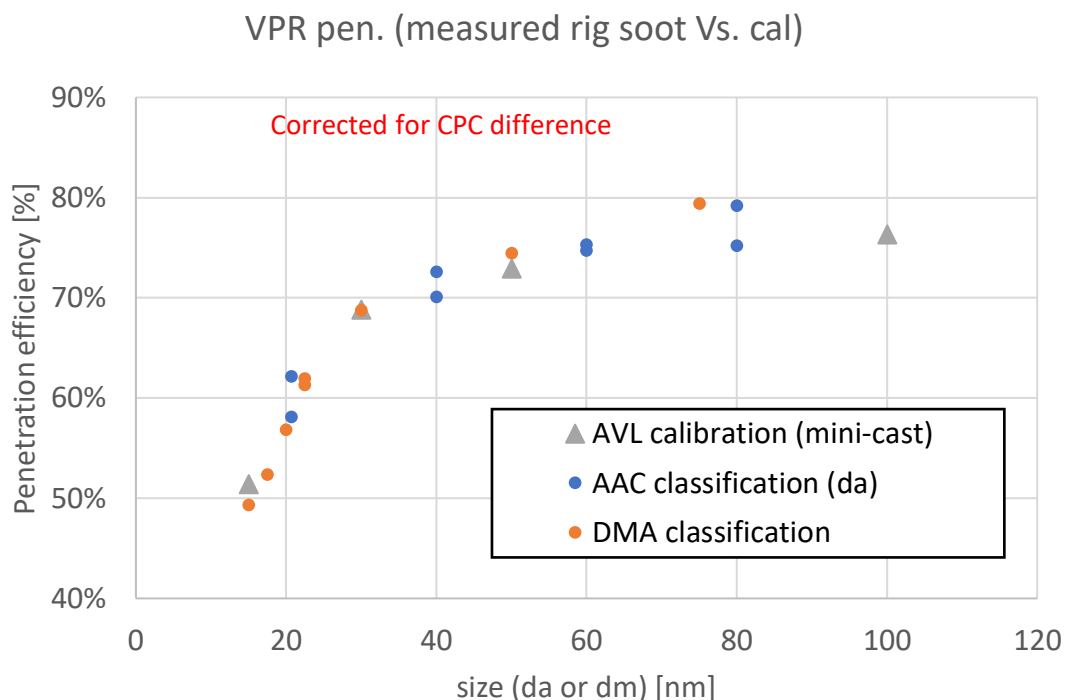


Figure 36: measured/calibrated VPR penetration efficiency Vs particle size using different classification methods



## Work Package 4: Deliverables Report

## 4.7.1.4 AAC classification results

In addition to the VPR experiment, the AAC classification capabilities were assessed and compared with DMA classification. It was found that the AAC could classify combustion exhaust soot down to  $\sim 25$  nm equivalent mobility diameter, with differently classified particle size distributions shown in **Figure 37**.

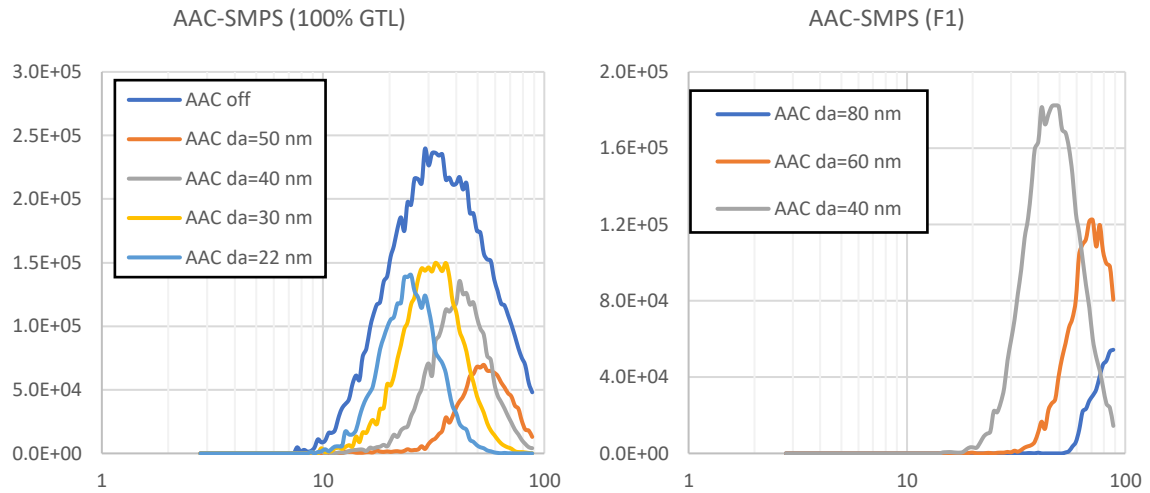


Figure 37: AAC (left) and DMA classified (right) particle size distributions measured with an SMPS (DMA-CPC)

Comparing AAC classified (aerodynamic diameter) and DMA classified (mobility diameter) GMD can also provide information about the density of the measured particles. For example, in **Figure 38**, the line of best fit is near 1:1, suggesting that particles produced by 100% GTL fuel (fuel 1) have an average effective density of  $\sim 1$  g/cm<sup>3</sup>, in agreement with particles emitted from large commercial engines at Particle Size distributions of  $<200$  nm.

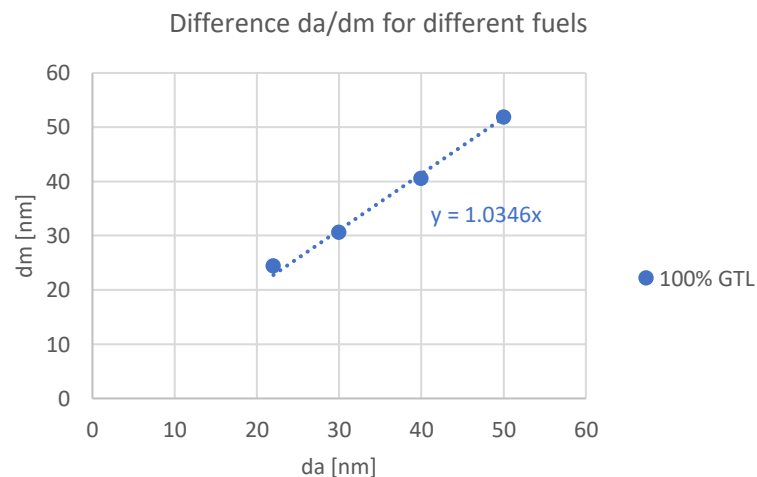


Figure 38: Measured aerodynamic diameter (da) Vs measured electrical mobility diameter (dm) for fuel A (100% GTL)





## 4.7.2 VPR penetration MC uncertainty analysis (RQL 2)

As specified in the ARP 6241, there are four points required for a VPR calibration, namely 15 nm, 30 nm, 50 nm and 100 nm, with concentrations at these four points upstream of the CPC required to be at least 5,000 #/cm<sup>3</sup>. Historically, it has been challenging to decrease the size of the calibrants below 15nm and still produce a) high enough concentrations and b) stable conditions.

Furthermore, a suite of tools were developed to take nvPM measurement system parameters and data products, and calculate the Engine-exit representative (i.e., loss-corrected) Emission Indices for nvPM number and mass (E<sub>num</sub> and E<sub>mass</sub> respectively). These were based on the sampling system, the fuel properties, the measured engine CO<sub>2</sub> concentrations and number and mass of the nvPM. This included calculations of the losses in the system (which includes the VPR) as prescribed in the ARP 6481, producing what is known as the number and mass loss correction factors (K<sub>sl\_num</sub> and K<sub>sl\_mass</sub>). In effect, by knowing the concentrations as measured by the sampling system, the engine exit plane concentrations can be estimated by multiplying by those factors using the loss correction methodology described in ARP 6481. There are currently three main tools in operation: two USA written codes in Matlab and Excel (ARP 6481) and a EUR written in LabView. The LabView code also uses a modelling approach called Monte Carlo simulation (MC) to estimate the uncertainty in the models, rather than numerical error propagation using the general error model approach.

In parallel with the RQL 2 test, several novel methods of particle generation were tested to determine suitability for looking at VPR penetrations on sources other than gas turbine engines as part of the SAMPLE IV SC01 project. These new methods included a prototype Silver Particle Generator (SPG) from Catalytic instruments which is based on heating, evaporation and then nucleation of nanoparticles. SAMPLE IV work showed that it was possible to generate particles down to 5 nm with relatively stable concentrations and at concentrations close to the required value for ARP 6241 CPC/VPR penetration testing (i.e., minimum 5000 #/cm<sup>3</sup>).

The following section looks at the effect of increasing the number of points in the VPR penetration calibration requirements on the penetration efficiency fit, loss-corrected EI number and mass, and ARP 6481 predicted D<sub>mg</sub> (i.e. probe inlet GMD) using experimental data as described below and the EUR written LabView code with MC simulation.

### 4.7.2.1 Experimental data

This VPR uncertainty analysis used experimental VPR penetration efficiency data taken using silver particles during SAMPLE IV testing as discussed below.

As with all penetration tests, the goal is to calculate the loss of particles through a system as a function of size. This is achieved by size selecting particles and passing them through the system of interest, whilst simultaneously recording the particle concentration upstream and downstream of the system under test (as described in section 4.7.1). For these tests, the size selection was done using a TSI 3082 Scanning Mobility Particle Spectrometer (SMPS) with a TSI 3085 nano DMA and two Ultrafine Condensation Particle Counters (CPC), TSI models 3776 and 3756. Both CPCs had a D<sub>50</sub> of 2.5nm.

The first step is to compare the two CPCs to ensure they agree as a function of size and as a function of particle composition. This is done by sampling polydisperse aerosol from the SPG into the SMPS and selecting a single size and recording the response of the CPCs. The length of pipes to the CPCs was matched so the residence time in the tubes was the same for both CPCs, removing any bias due to diffusion. The ratio of CPC1:CPC2 was then plotted against diameter and, where necessary, a fit function is applied.



Data from the intercomparison is shown in **Figure 39**. The error bars are the standard deviation and the colours are the concentration as recorded by CPC1. The data presented was fitted with an exponential function (not shown for clarity) and was used to adjust CPC1 concentration to account for the reported differences when calculating the VPR penetration.

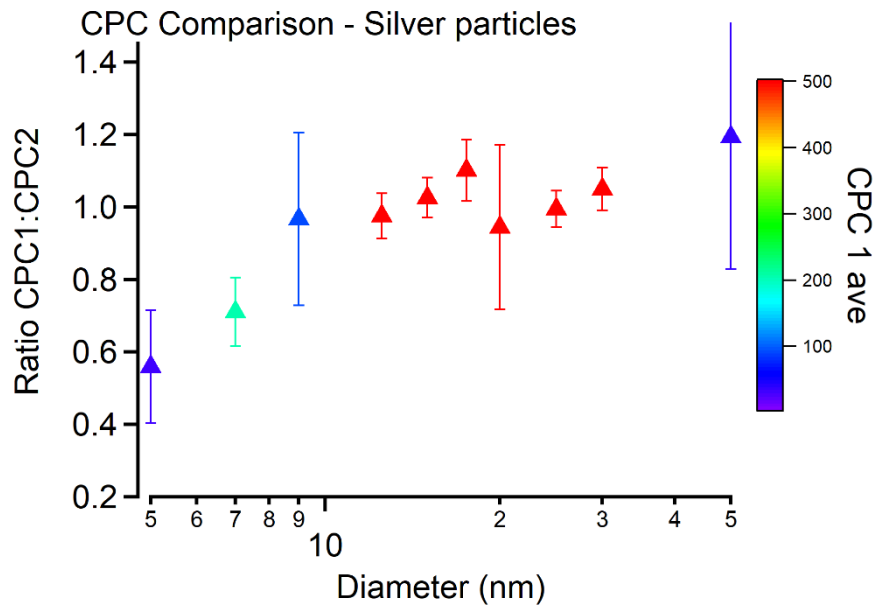


Figure 39: Results of the CPC intercomparison performed on silver prior to the VPR RQL 2 tests

After completing the CPC comparison, the next stage was to measure the VPR loss and to increase the number of points below 15 nm. For these tests, CPC1 was used as the downstream CPC, and was corrected for differences between the two CPCs and for the VPR dilution factor.

**Table 5** and **Figure 40** show all the penetration data and uncertainties from the silver VPR penetration for the EUR VPR, subsequently used in the MC uncertainty analysis. The penetrations reported here are well below those typically reported by AVL. For example, at 50 -100 nm the VPR is normally plateauing around 0.8, whereas here it is 0.57. Given the many years of VPR calibrations from AVL, and that similar penetrations were reported during RQL 1 (section 4.7.1), it is extremely unlikely this difference was due to a reduced penetration efficiency of the VPR. During the tests, there was an incident of low pressure in the lines which may have temporarily contaminated the optics of CPC1. However, tests of the CPCs back at Manchester showed they agreed well, so the source of the difference cannot be determined. However, for the subsequent sections, only the relative change in number of points and errors is required. In addition to the reduced penetration, it was not possible to get data at 100 nm from the SPG. To allow the penetration fit functions to be applied, a point at 100 nm was inserted, based on a plateauing function, with a relatively small uncertainty.



## Work Package 4: Deliverables Report

Table 5: Data from the Silver VPR penetration tests. The concentrations are averages in  $\text{cm}^{-3}$ . The CPC comp model is the fit between the two CPCs to account for the difference. CPC1 has been corrected for dilution factor and using the CPC comp model to account for CPC differences. Note that the 100nm point was not measured but inserted to allow the line loss models to run. The uncertainties are standard deviations.

Dp	CPC comp Model	CPC2 Ave	CPC2 STDEV	CPC1 Ave	CPC1 STDEV	Penetration	Penetration STDEV	Penetration STDEV (%)
5	0.5165	4537	144.1	349	227	0.0769	0.0502	65.3%
7	0.7521	5146	160.9	674	301	0.1309	0.0586	44.8%
9	0.8810	6506	149.0	1261	353	0.1939	0.0545	28.1%
12.5	0.9826	5929	278.3	1574	386	0.2654	0.0663	25.0%
15	1.0113	7359	168.0	2353	472	0.3198	0.0645	20.2%
30	1.0365	9160	539.9	4403	578	0.4807	0.0691	14.4%
50	1.0368	9455	257.3	5156	691	0.5453	0.0746	13.7%
65	1.0368	5786	191.0	3256	530	0.5627	0.0935	16.6%
75	1.0368	2664	92.2	1535	349	0.5761	0.1325	23.0%
100						0.57	0.07	12.3%

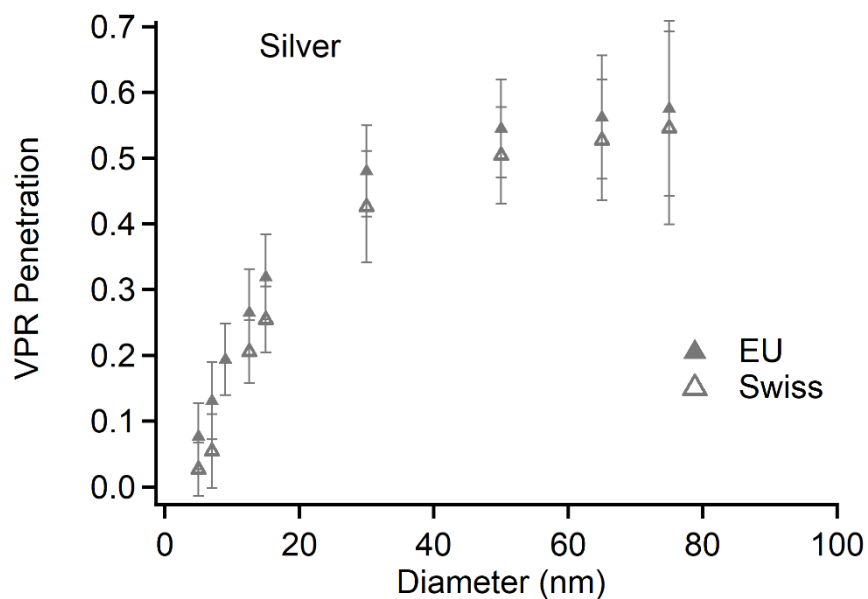


Figure 40: VPR penetration efficiency measured during RQL 2 using silver nanoparticles

#### 4.7.2.2 Effects of increasing the number of VPR penetration data points on the VPR penetration efficiency fit

In this section, the effect of adding points to the VPR fitting function was investigated. The results of this are shown in **Figure 41**. Data points were first added less than 15 nm, namely (in order): 12.5 nm, 9 nm, 7 nm and 5 nm. It can be seen that for five data points (12.5nm plus the default), the fits are similar to the default points and the fits pass through the measured penetrations, as previously reported. As the number of points increases to eight, the fitting attempts to force the fit at the smaller sizes and as a consequence, reduces the quality of the fit at larger sizes. This can be seen by the decreasing value in the fit at 100 nm.



## Work Package 4: Deliverables Report

As data points 65 nm and 75 nm are added, this has a small effect increasing the asymptotic value at large sizes.

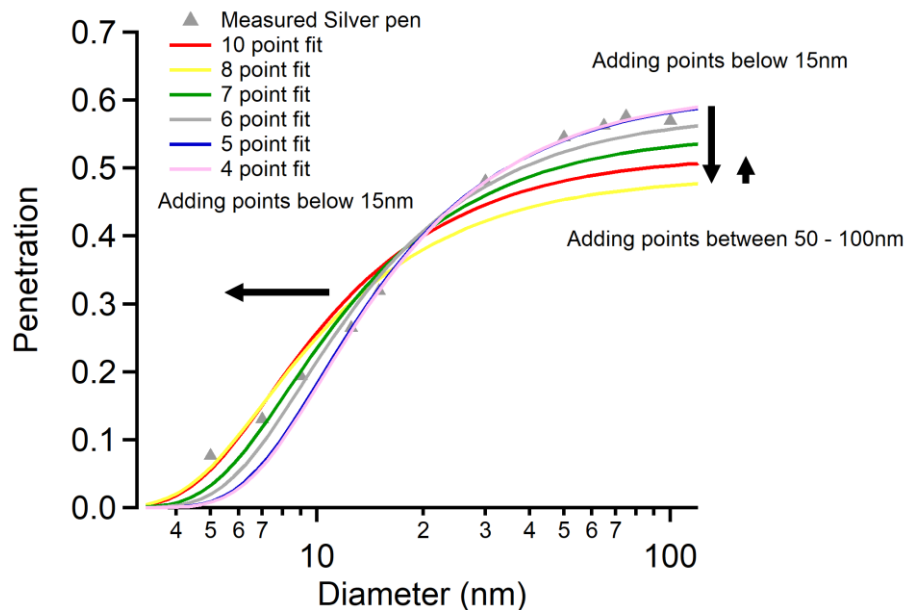


Figure 41: VPR penetration measured at ten sizes with silver and fitted using the ARP 6481 method with 4-10 points

The cause of the problem is that the fitting model used is not adequately describing the data. It is based on a simple size dependant particle diffusion model multiplied by a thermophoretic loss, which is approximately size independent. This is not capturing the measured data. There are some important conclusions from this which should be addressed in future work looking to improve VPR penetration measurements:

- 1) Notwithstanding the reduced penetrations reported here, adding more data points to the VPR fit at smaller sizes may cause improper fitting at larger sizes and additional points may be required to ensure the fit is properly weighted across all sizes. All fits should be inspected.
- 2) There is a need to understand the penetrations at small sizes to see if the diffusion-thermophoretic loss model is appropriate.
- 3) Future models may need to consider fitting functions based on modified loss theory or numerical fits that are not based on a theoretical model (free form fitting).

#### 4.7.2.3 Effects of increasing the number of VPR penetration data points on EI number and mass

**Table 3** shows the results of the LabView code running on simulated engine data. The data produces a range of theoretical engine exit plane size distributions and the associated loss corrected EInum and Elmass, and uses a standardised sampling system, which is used to validate model development.  $D_{mg}$  is the diameter of the theoretical engine exit plane size distribution predicted by the ARP 6481 line loss tool based on the measured nvPM number and mass and other system parameters.

The data shows that as the number of points changes, the  $D_{mg}$  and EInum are the most effected by the changing VRP fit function, with the biggest effect on the EInum. The Elmass is not impacted by the VPR fit change given no VPR corrections are required for Elmass.



## Work Package 4: Deliverables Report

Table 6. Effects of using the default 4 and 8 data points VPR fit on simulated engine data. The number and mass ranges are chosen to give a range of theoretical engine exit plane modal diameter of the theoretical size distribution. Data in red is explained in section 4.7.2.5

Inputs		[outputs] Default 4 points				[outputs] 8 points (5 – 12.5nm added)				
Number	Mass	EI		D <sub>mg</sub>	EI		D <sub>mg</sub> diff %	EI		Mass diff %
		Dmg	Num		Mass	Num		Mass	Num diff %	
8.1E+06	1.0E+02	5.18	7.1E+15	1.2E+01	5.6E+00	6.1E+15	1.2E+01	-7.5	14.2	1.5
3.2E+06	1.1E+02	12.36	1.4E+15	1.0E+01	1.2E+01	1.5E+15	1.0E+01	2.7	-6.5	-0.9
6.4E+03	1.3E+00	29.37	1.4E+12	9.0E-02	2.8E+01	1.7E+12	9.2E-02	5.5	-18.4	-2.0
4.6E+03	6.8E+00	66.15	6.5E+11	4.6E-01	6.2E+01	8.0E+11	4.6E-01	6.7	-23.2	0.0
1.0E+07	5.5E+04	107.15	1.3E+15	3.8E+03	9.9E+01	1.6E+15	3.8E+03	7.2	-24.2	0.0

#### 4.7.2.4 Effects of increasing the number of VPR penetration data points on uncertainty

The effects on the uncertainty are not so clear. **Figure 42** shows a histogram of the modelled penetration distribution for the 15nm VPR fit, applying the default values to the silver data as measured by AVL (~3%) and the measured standard deviations. Similar distributions are used for the other VPR data points. The ARP6481 line loss model was run with the standard 4 data points, with default STDEV and measured, and a subset of the data was run with 10 VPR points with the measured uncertainty. The results are shown in **Table 7**, which reports the calculated standard deviation in the D<sub>mg</sub>, and loss-corrected Elnum and Elmass, based on the MC outputs.

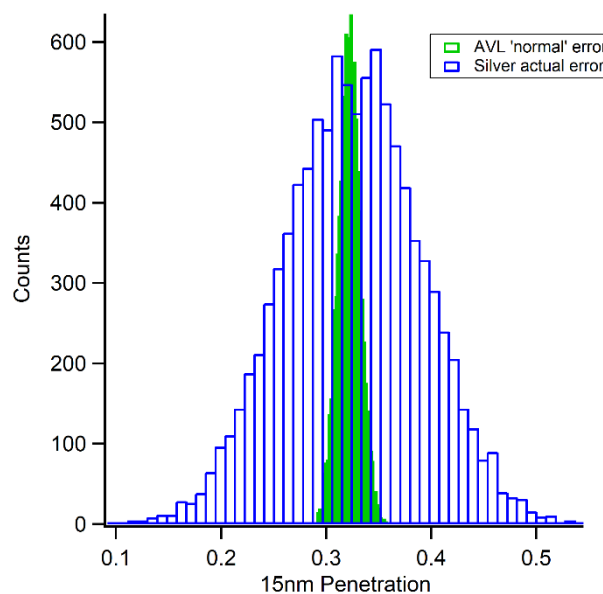


Figure 42: Histogram of the modelled & measured penetration distribution for the 15nm VPR fit

**Table 7** shows that using measured STDEV has little to no impact on the overall uncertainty calculated by the tool (with the exception of the first point which is in red and explained later). This means that whilst the VPR fit function does impact the absolute results, the increased uncertainties measured here are having little effect on the overall uncertainty in the ARP 6481-line loss model. The reason for this is discussed in section 4.8 below.



## Work Package 4: Deliverables Report

However, one point to note is the run time and errors produced when fitting ten data points. The model uses a default value of 10,000 iterations for the MC simulation. This will normally take less than one minute to run and produce few or no errors. Errors in this context are when the model cannot converge on a solution for the input parameters. With increasing numbers of points at smaller size, the model is running between 1.5-2.5 hours and not converging on a solution approximately 20% of the time.

Table 7: Standard deviations as a percentage of the mean from the line loss model with different number of points and uncertainties in the measurements. Data in red is explained in section 4.7.2.5

4 points							
Input	Input	Default STDEV (~3%)			Measured STDEV		
Number	Mass	D <sub>mg</sub> STDEV	EINum STDEV	Elmass STDEV	D <sub>mg</sub> STDEV	EINum STDEV	Elmass STDEV
<b>8.1E+06</b>	<b>1.0E+02</b>	<b>93.55%</b>	<b>22.16%</b>	<b>14.70%</b>	<b>54.02%</b>	<b>24.07%</b>	<b>16.37%</b>
<b>3.2E+06</b>	1.1E+02	36.74%	18.71%	7.32%	38.20%	21.91%	9.06%
<b>6.4E+03</b>	1.3E+00	27.07%	18.79%	7.62%	27.35%	19.01%	7.52%
<b>4.6E+03</b>	6.8E+00	21.54%	11.62%	7.76%	22.27%	12.05%	7.74%
<b>1.0E+07</b>	5.5E+04	18.88%	8.52%	8.19%	19.32%	8.53%	8.25%
10 points							
Input	Input	Measured STDEV			Run time	Number of errors	
Number	Mass	D <sub>mg</sub> STDEV	EINum STDEV	Elmass STDEV			
<b>3.2E+06</b>	1.1E+02	36.45%	18.70%	8.32%	01:40	1827	
<b>1.0E+07</b>	5.5E+04	19.99%	22.73%	9.11%	01:37	1821	

#### 4.7.2.5 Effects of small D<sub>mg</sub> on loss-corrected EIs

When the ARP 6481 line loss tools were being developed, the RAPTOR team members funded by EASA (along with American colleagues), reported deficiencies in the models as the theoretical D<sub>mg</sub> approached small sizes. Specifically, the outputs D<sub>mg</sub>, EI num and EI mass were reporting bi- and tri-modal distributions when performing an MC uncertainty analysis and were also failing to converge for some input parameters. With the addition of the extra points below 12.5nm (and fit functions not tending to zero), this non, mono-modal behaviour is appearing at small D<sub>mg</sub> and increasing the frequency of non-convergence. An example of the effects of small D<sub>mg</sub> and the output of the modelled EI num is shown in **Figure 43**. In **Table 3** and **Table 7**, the values highlighted in red are points which produce these non, mono-modal results. It is apparent that further work is needed to understand what the actual penetration at small sizes is and to invest time into understanding what the limiting factor is that is causing the models to produce these results.



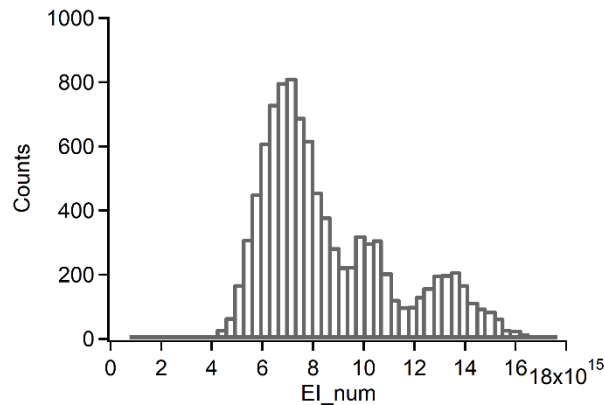


Figure 43: Example of tri-modality on EI num when running MC uncertainty analysis on a test point with a small Dmg

## 4.8 System-to-System MC uncertainty analysis

One of the objectives of RAPTOR was to assess how two regulatory compliant sampling systems compared when measuring the same source. Some of the data (measured nvPM number, mass and diluted CO<sub>2</sub>) from the RQL 2 test was used to calculate the loss-corrected EI num and EI mass of the Swiss and EU systems, using the EU LabView code. The inputs/assumptions to the setup is as follows:

- The exact sampling set up (line lengths, flows, temperatures etc) for each system was used.
- The last VPR penetration data from AVL for each VPR was used, however the default uncertainties for the penetrations were used
- The last reported DF factor from AVL for each VPR was used
- The measured standard deviations of nvPM number and mass were used; the systematic errors were the default (~10%)
- The measured CO<sub>2</sub> values were used for each system, and this defined DF1
- The standard deviations for CO<sub>2</sub> were not available for the Swiss system, so the values reported by the EU system were applied
- Only the uncertainty in the number, mass, VPR penetrations, total line loss, Ksl\_num and Ksl\_mass and the dilution factors were used.
- Fuel properties and other gas species were set to default

The sub-dataset used included the max and min number and mass, the maximum and minimum difference between number and mass, and the maximum, mean and minimum difference in the dilution factor from RQL 2 test. This ensured tested points examined the complete range of the data.

The results are given in **Figure 44**, showing the scatter plots of (EU vs Swiss): D<sub>mg</sub>, Elnum and Elmass and the STDEV of D<sub>mg</sub>, Elnum and Elmass. The data shows that the predicted parameters from the tools agree within 5% with one exception (7%). The R<sup>2</sup> (not shown) are noted to have been 0.92 -0.99. Upon examination of the data, the recorded values by both systems (nvPM and system parameters) are very similar and the sampling architecture is almost identical. This should mean that the reported values are the same, and the model confirms this.

In addition, the differences in the STDEV are not driving major differences in the EI values. This is to be expected. In the line loss model, the final uncertainty in EI is determined by the combination of the



## Work Package 4: Deliverables Report

systematic errors and standard error. The standard error is the standard deviation divided by the square root of the number of data points, which for each test was 60 (60s sampling).

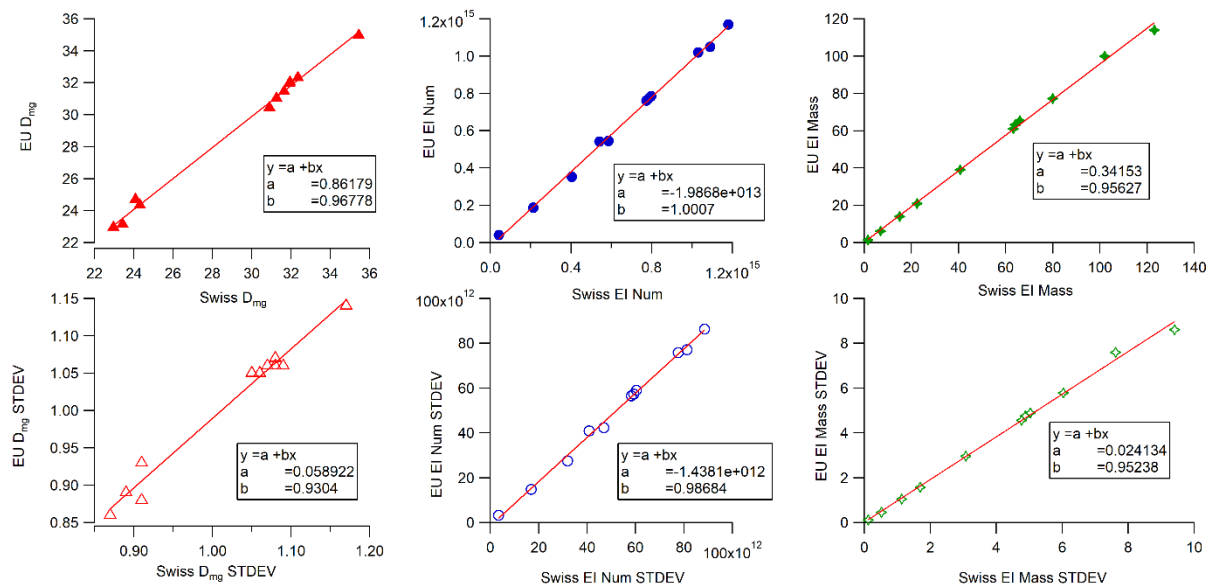


Figure 44: Output Dmg, ARP6481 loss-corrected EI num and EI mass calculated using the EU Labview code (MC analysis) on the EUR and Swiss system using a representative sample of RQL 2

## 4.9 Conclusions – CAEP/11 uncertainties (D4.1)

The outcomes of the RAPTOR RQL experimental programme highlight current levels of uncertainty in the CAEP10/11 nvPM standards are within anticipated bounds. The compliant system intercomparison testing highlighted that low levels of uncertainty across the total range of concentrations, for both EI mass and EI number, was observed between two reference systems. It is however noted that calibration uncertainty was largely removed from the analysis by ensuring that the instruments were simultaneously calibrated immediately prior to RQL 1 experimentation. The following uncertainties and findings for mass and number noted:

- Average differences in reported nvPM EI mass from the EUR and SWISS systems (both AVL MSSs) were ~11% across the average of all mass concentrations tested during RQL test 1 (immediately following calibration) and ~2% during RQL test 2 (after a 12-month period). It is proposed that the better agreement during RQL 2 likely stem from improved protocols in rig operation, sampling and cleanliness checks for the final campaign, which were adopted as an outcome of lessons learned during the initial tests which highlighted discrepancies significantly increased at low mass concentrations indicating shedding of particles from the cyclone.
- The nvPM mass analysers sampling from the same sampling system, namely the AVL MSS and Artium LII on the EUR system and AVL MSS and AVL MSS2 on the Swiss system generally agreed well with each-other, within ~1% for the Swiss MSS Vs MSS2 when loss correction is applied, and within ~7% for the EUR LII Vs MSS. It was found that the EUR LII displayed a non-linear behavior specific to this analyser and thought to result from the initial blackbody calibration performed when new, given a rework of data from 2013 displays a similar trend.





## Work Package 4: Deliverables Report

- It was observed during RQL 1, where cleanliness checks and cyclone pot cleaning were only performed on a daily basis, that mass uncertainties significantly increased at low mass concentrations with differences of up to 40% observed at concentrations  $< 10\mu\text{g}/\text{m}^3$ . During RQL 2, where cleanliness checks and cyclone cleaning was performed more regularly, mass uncertainty remained low at concentrations  $< 10\mu\text{g}/\text{m}^3$  (within  $\pm 10\%$  of the mean).
- nvPM EI number agreement between the EUR and SWISS reference system was within  $\sim 2\%$  on average across the number concentrations tested during RQL 1 tests and within  $\sim 0.2\%$  during RQL 2. Larger discrepancies at lower sizes witnessed during RQL 1 suggest a potential condensed metallic peak as a result of combustor damage, impacting losses and counting efficiency within the EUR and Swiss APC differently. No discrepancies were observed during RQL 2, with all data agreeing within  $\pm 5\%$  of the average across all concentrations tested.
- System-to-system comparison data analysed with the LabView/Monte Carlo model highlighted system agree within 5% or better in terms of Dmg and EI\_num&mass for the majority of cases, with changes in (or difference between) standard deviations reported in RAPTOR having limited effect on the EI\_num and EI\_mass uncertainty, which it was seen was driven by the systematic errors prescribed in the model.
- NIOSH 5040 filter sampling uncertainty for two nominally similar filter sampling setups resulted in an agreement in EC mass within 2% when the OC/EC split point was chosen manually and within 5% for an automatic split point determined by the TOT analyzer software. A flow split ratio of 1:4 between two filter sampling setups with the same nominal filter holder geometry led to  $\sim 15\%$  difference in EC mass. However, the differences found due to uneven splits were inconsistent as a function of the OC/EC split point chosen. It is noted that sampling methodology is currently not factored into the overall uncertainty of the reference method.

Additional observations from the RAPTOR RQL campaign highlight a number of observations and potential opportunities for improvements including:

- Particle shedding from the  $1\mu\text{m}$  cyclone can significantly impact the reported EI mass measurements at low mass concentrations  $< 10\mu\text{g}/\text{m}^3$ . It was observed that the prescribed scheduling of cleanliness checks is not sufficient to ensure accurate mass measurement at low mass loadings.
- It is suggested that cleanliness checks and cyclone cleaning should be performed more often, particularly when measuring nvPM mass near LOD particularly after comparatively higher mass loadings.
- The VPR penetration efficiency provided by the AVL calibration using mini-CAST soot was found to match the penetrations measured using RQL rig combustion soot. Empirical assessment extending the calibration range down to 5nm showed that simple diffusion - thermophoretic modelling may not capture the true loss, resulting in significant difference in reported Dmg and EI\_num.
- When using an MSS for nvPM mass cleanliness checks, a resonance check on the zero gas should be performed prior to the cleanliness checks to ensure accurate reporting.



- It was demonstrated that nvPM mass measurement on the raw line is achievable with an average agreement within 2% when compared with the diluted nvPM mass (between 3 – 18  $\mu\text{g}/\text{m}^3$  diluted) after dilution and loss corrections. This experiment demonstrated that it is possible to take an accurate diluted nvPM mass measurement down to  $\sim 3 \mu\text{g}/\text{m}^3$  when performing regular cleanliness checks, cyclone cleaning and MSS resonance checks on the correct gas source. Therefore, a diluted nvPM mass Limit Of Quantification (LOQ) of 3  $\mu\text{g}/\text{m}^3$  is suggested for a regulatory compliant sampling system.
- Choice of the automatic or manual OC/EC split point in the TOT analysis noticeably affected the relative agreement of the EC mass determined using the three sampling systems. Up to a 30% difference in the EC mass was found for the same filter samples depending on the split point choice. This result confirms previous findings that highlighted differences in EC mass determined for the same filter sample using different split points and software versions. The nvPM mass calibration protocol shall further clarify this issue.

## 5 Corrections to be considered towards reduced uncertainty in CAEP/12 (D4.2)

### 5.1 nvPM Size measurements RQL 1 test

Numerous assessments of size were undertaken during RQL 1 testing with intercomparisons of different analysers (Cambustion DMS-500 vs TSI SMPS) made by the two reference systems in addition to the impact of different SMPS hardware options (DMA and Chargers) and a Catalytic Stripper being investigated.

Finally, an assessment of size derived number concentration was made in comparison to the ICAO regulatory prescribed CS-CPC measure, towards assessment of improved (simplified) regulatory nvPM sampling and measurement systems of the future.

#### 5.1.1 Sizing Instrument Intercomparison RQL 1 test

Particle size distributions as measured simultaneously on both the EUR reference system (Cambustion DMS-500) and Swiss reference system (TSI SMPS) were compared. Example comparative size distributions, representative of the entire test campaign, are plotted in **Figure 45**. As can be seen the two size distributions generally correlated with each other on all the modes seen. It is noted that minor differences could be caused by: (1) different DF1 in each sampling system, (2) rig instabilities during the 30 seconds SMPS scan (when compared with the 1Hz DMS data), (3) different losses occurring in the SWISS/EUR sampling systems, (4) DMS-500 inversion matrix uncertainty.



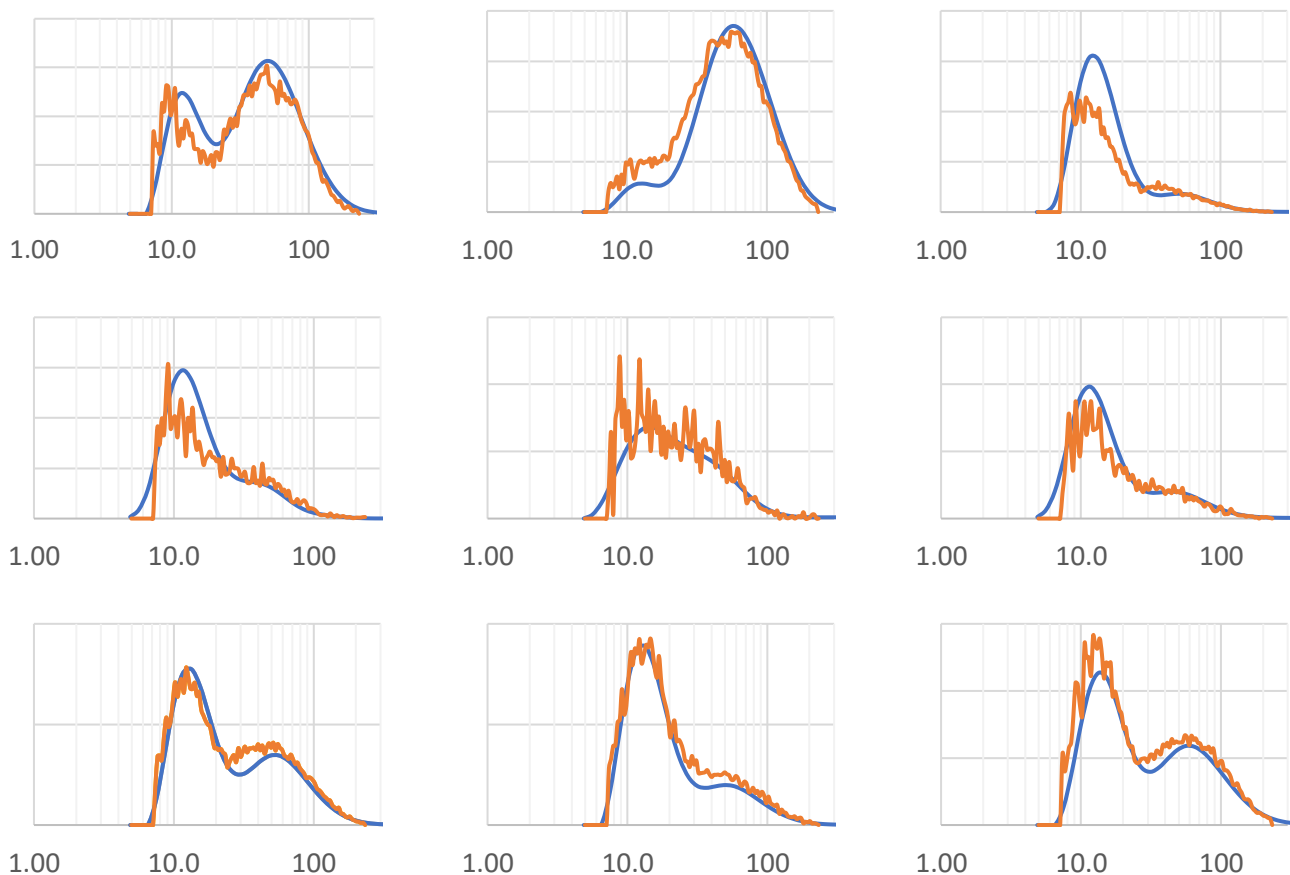


Figure 45: Examples of measured particle size distributions from the Cambustion DMS-500 (blue) and the TSI SMPS (orange) across a range of particle size, shape and concentration

### 5.1.2 SMPS Hardware impact RQL 1 test

It is noted that there are many options available when setting up an SMPS for a size measurement with regards to the DMA selected and the type of charging employed. More recently, additional volatile particle removal hardware in the form of catalytic strippers have become commercially available. As such, numerous experiments were performed to investigate the impact of these different setups on the measured size distribution.

It is also noted that the SMPS scan settings (aerosol flow rate, sheath flow rate, scan time, purge time, diffusional loss correction) affect the results. The sheath-to-aerosol flow ratio impacts resolution and size range. As such all settings were kept constant during the campaign. The CPC was operated in the high flow mode (1.5 lpm nominal flow rate). The aerosol flow rate measured at the inlet of the classifier was 1.37 – 1.39 lpm, the sheath flow was 13 lpm, and the scan time was 30 seconds (with 2 seconds retrace and 10 seconds purge period after each scan). The resulting size range was 8 nm – 233 nm.

#### 5.1.2.1 Impact of Catalytic Stripper on observed size distributions

As discussed, for each investigated combustor rig condition, SMPS scans were performed with and without a catalytic stripper (CS, Catalytic Instruments CS08) fitted at its inlet. The measured size distributions with the CS on were subsequently corrected for particle loss within the CS to allow direct comparison with the



## Work Package 4: Deliverables Report

respective unstripped size distributions. As can be seen in **Figure 46**, the size distributions without CS (blue) are significantly higher than the relative CS cases (red). However, it is noted that the unstripped distribution correlates well with that of the loss corrected CS measurement (green) for all the test points, indicating that all the modes measured by the size analysers are non-volatile, irrespective of whether the distribution was monomodal or bimodal. This finding was supported by the near zero measurement of UHCs across all test conditions.

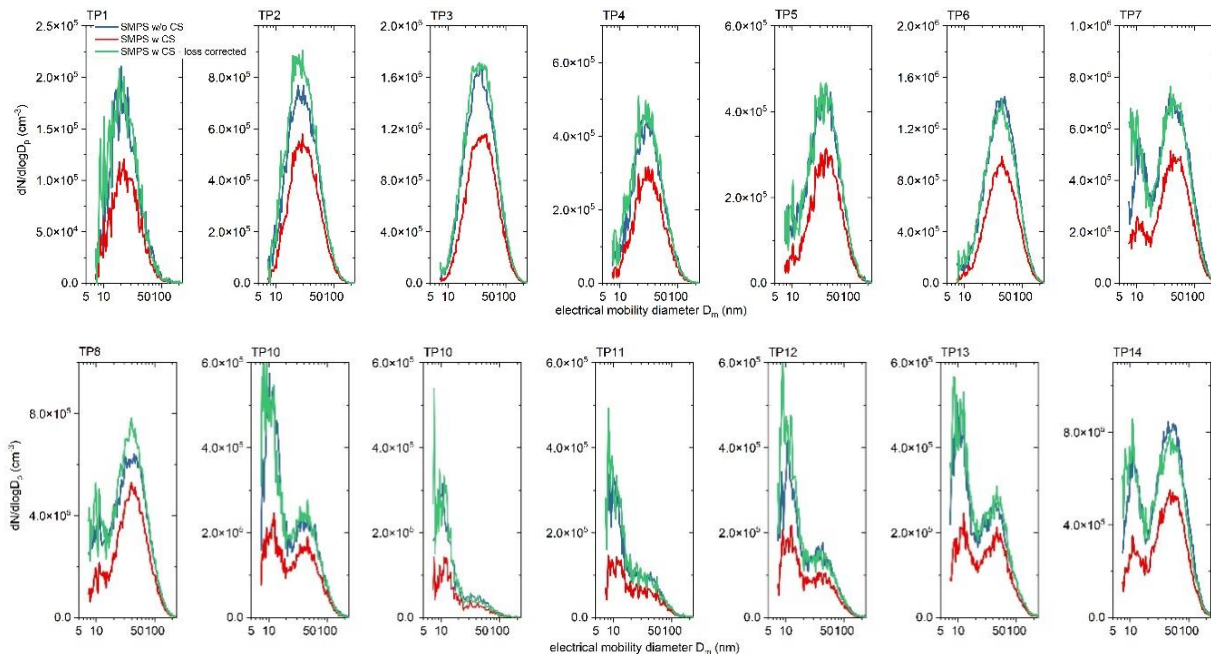


Figure 46: Overview of size distributions measured by the SMPS. The blue curves are measurements without the CS. The red are measurements with the CS without loss correction and the green curves are measurements with the CS including size-dependent loss correction for the CS (provided by the manufacturer for the flow rate measured at the CS inlet).

### 5.1.2.2 SMPS particle charger

In the specifications<sup>1</sup> of the soft x-ray neutralizer Model 3088, the manufacturer TSI mentions differences to be expected in the sizing performance and concentration reported in comparison to the Model 3077A <sup>85</sup>Kr neutralizer. TSI notes that “this difference is likely due to the fact that air ions from soft X-ray neutralizers have similar, but not exactly the same electrical mobilities as air ions generated from radioactive neutralizers. This difference is likely not due to incomplete charge neutralization, e.g., due to ion depletion. Whatever the cause, typically there will be a small concentration difference (commonly on the order of 10-20%) between SMPS systems using the different neutralizers.” In terms of sizing, TSI expects two SMPS systems equipped with the two different neutralizers to measure GMD within 5%.

The impact of the different chargers were investigated on total concentration from the SMPS measurements by comparing the SMPS total number concentration with the concentration measured by the AVL APC (**Figure 47**). The ratio of the SMPS total concentration corrected for VPR losses to APC number

<sup>1</sup>[https://tsi.com/getmedia/85d6abad-a56a-4a1f-a61d-1c73983c7e7a/Aerosol%20Neutralizers%203088\\_A4\\_5001321\\_RevE\\_Web?ext=.pdf](https://tsi.com/getmedia/85d6abad-a56a-4a1f-a61d-1c73983c7e7a/Aerosol%20Neutralizers%203088_A4_5001321_RevE_Web?ext=.pdf)



## Work Package 4: Deliverables Report

was on average only 3% higher with the soft X-ray neutralizer than with the  $^{85}\text{Kr}$ , which is within the expected uncertainty of these measurements. Note that the soft X-ray neutralizer was used during only one test day. This agreement is much better than predicted by TSI. TSI obtained their data using emery oil and NaCl aerosol. No results are reported with soot. This result is encouraging, in terms of the practicality of certification measurements, as the soft X-ray neutralizer does not require special permits for shipping and operation, unlike its radioactive counterpart.

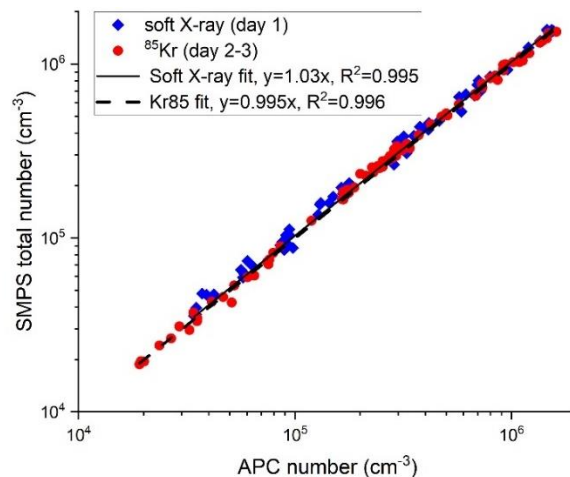


Figure 47: Comparison of SMPS total number (corrected to APC CPC inlet) CVs APC number.

### 5.1.2.3 DMAs (long and nano)

During the majority of the RQL 1 test campaign, a long DMA was used (8-233 nm range). However, on one rig condition, a nano-DMA (5-74 nm range) was used. **Figure 48** shows the results of the nano DMA test with and without CS. This test point was unstable and the two modes' peak concentrations varied rapidly, which the SMPS could not capture. In terms of sizing, the nano DMA results agree well with the DMS500 results over the same size range. The DMS500 reported zero concentrations below 7.5 nm and the concentration of sub-8 nm particles reported by the SMPS (without CS) represents 1.6% of the total SMPS concentration (< 75 nm).

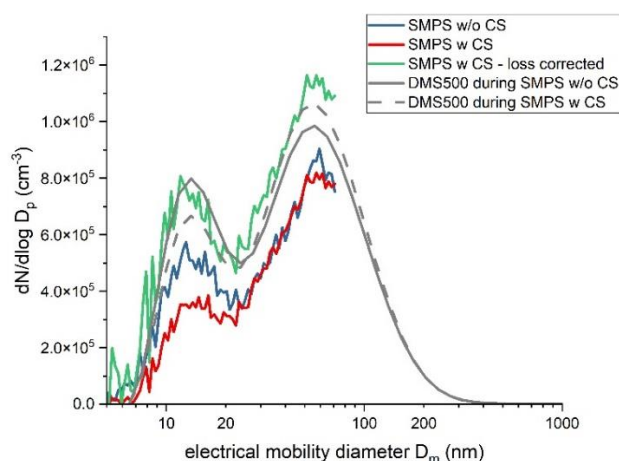


Figure 48: SMPS scans with nano DMA at one test point. DMS500 data are shown for comparison. This test point was unstable and the concentration during the measurement with CS increased, resulting in disagreement between the data with CS after loss correction and without CS.



### 5.1.3 Size derived number concentrations RQL 1 test

To afford a direct comparison of the number concentrations measured using the compliant number counting systems (AVL APC) and respective sizing instruments (Cambustion DMS-500 & TSI SMPS), it was first necessary to correct the total number concentration from the SMPS and DMS-500 for differences in particle losses (sample line difference & VPR) and relative size dependant counting efficiencies. As seen in **Figure 49 & Figure 50**, suitably corrected number concentrations from both the Cambustion DMS-500 and TSI SMPS offer agreements of ~2% and 1% respectively, with their corresponding AVL APC. As was the case of earlier mass and number intercomparisons, again the difference is seen to increase at lower number concentrations (corresponding with generally smaller sizes), particularly for the DMS, likely due to larger measurement uncertainty at low concentration.

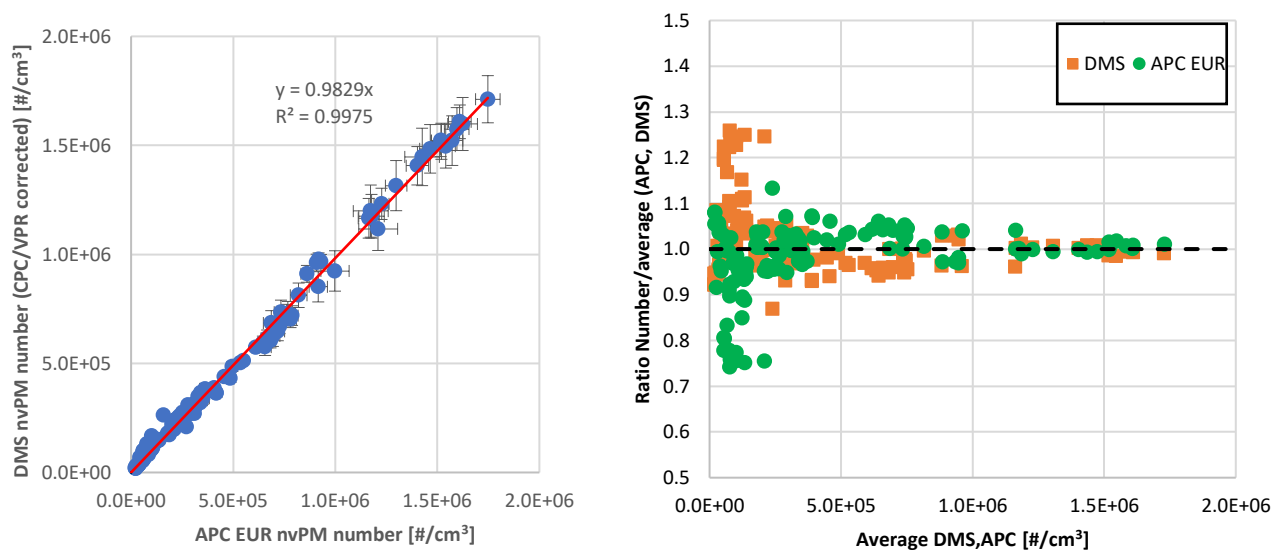


Figure 49: EUR APC Vs DMS-500-corrected number concentration (left) and ratio of APC/DMS-500 number over the average of the two (right) – Error bars represent  $\pm 1$  standard deviation



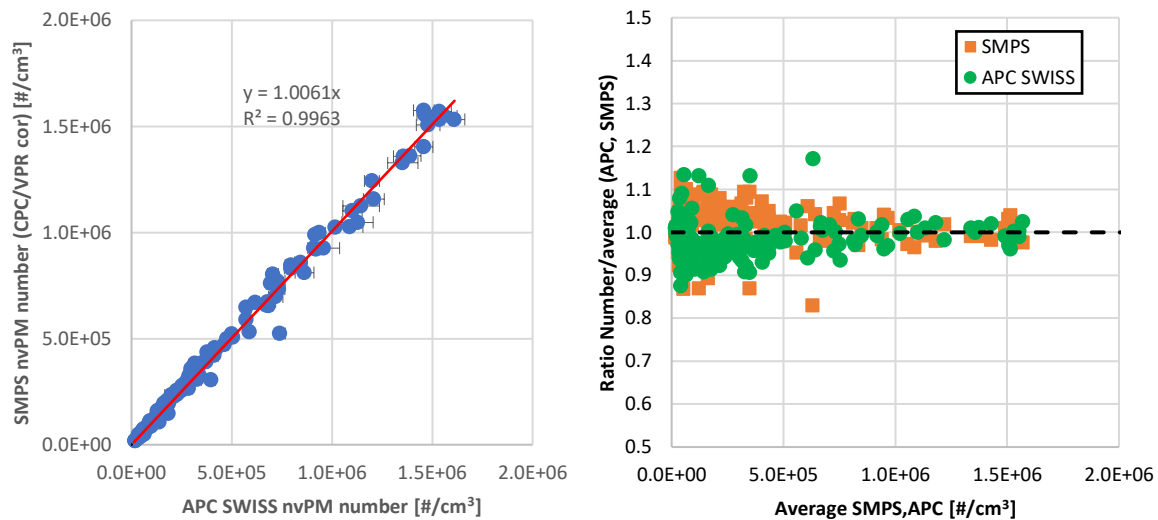


Figure 50: Swiss APC Vs SMPS-corrected number concentration (left) and ratio of APC/SMPS number over the average of the two (right) – Error bars represent  $\pm 1$  standard deviation

### 5.1.4 Size measurement uncertainty discussion RQL 1 test

The SMPS and DMS-500 correlated well on both monomodal and bimodal distributions. Further detailed analysis evaluated lognormality of the modes measured, and the determination of GMD and GSD. The SMPS scans with CS after loss correction agreed well with scans without CS, which suggests no measurable volatile PM fraction in the diluted exhaust samples. These findings imply that a CS may not be needed for nvPM size distribution measurement in ARP6320 compliant systems. If this result is confirmed consistently in other tests involving full-scale gas turbine engines, the loss correction uncertainty could be reduced (removing requirement for correction of diffusion and thermophoretic loss of CS). The total number concentrations reported by both instruments (after loss correction in the VPR and CPC cut-off) agreed well with the nvPM number reported by the APCs. The effects of the different aerosol neutralisers on total SMPS number concentrations were found negligible. However, it is noted that the SMPS data were not corrected to STP (0°C, 1 101.325 kPa). A correction of the order of 25% is expected and further investigation is required. Since the primary use of the size measurement is the correction for size-dependent losses, the different size ranges of the two instruments could lead to discrepancies in mass-based loss correction factors if a significant mass fraction is reported above  $\sim 200$  nm (section 5.3.2). As shown in **Figure 51**, the DMS-500 reported particle concentrations up to 1000 nm. It is unclear whether these large particles originated from the source or resulted from shedding from the sampling system lines and the cyclone. The DMS-500 inversion matrix may also affect the results and more intercomparisons with the SMPS configured for larger particles are desired.



## Work Package 4: Deliverables Report

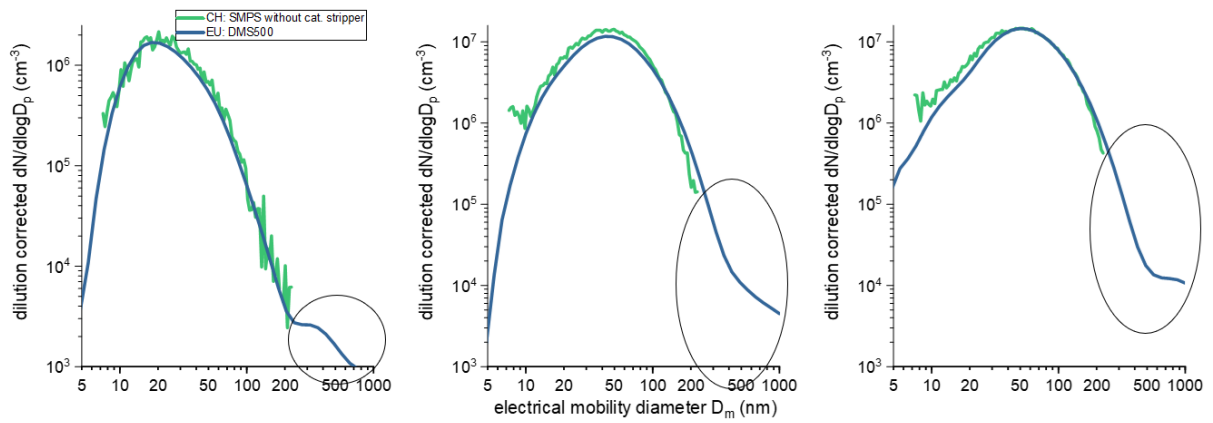


Figure 51: Comparison of SMPS and DMS500 results (DF1 corrected) highlighting the portions of the size distribution above 230 nm not measured by the SMPS.





## 5.2 nvPM size measurements RQL 2 test

In addition to the size measurement assessment performed in RQL 1 tests (section 5.1), the particle size measurement capabilities of the three main commercially available instrument technologies (i.e., fast-response differential mobility spectrometers and scanning mobility particle sizer) used for aviation PM size measurements were further assessed during RQL 2 testing. The four sizing instruments (1 x TSI EEPS, 1 x TSI SMPS, 2 x Cambustion DMS-500s) were first intercompared prior to the RQL 2 campaign and then subsequently used at different locations on both the Swiss and EUR sampling systems to investigate measurement and loss correction uncertainties associated with different size analyser technologies.

An assessment of size-derived number and mass concentration was also made in comparison to the ICAO regulatory prescribed measure of EI number and mass, towards assessment of improved (simplified) regulatory nvPM sampling and measurement systems of the future.

### 5.2.1 Pre-test size instrument intercomparison RQL 2 test

As discussed, a size instrument intercomparison experiment was performed during RQL 2 testing as presented in **Figure 52**, with all size instruments sampling from the same source (i.e., combustor rig exhaust) diluted using a PALAS VKL 10 ED to ensure satisfactory aerosol mixing and enough flow for all size analysers.

The two DMS-500s were processed using the monomodal aggregate inversion matrix (generated using mini-CAST soot) as advised by Cambustion. The EEPS was processed using the compact inversion matrix (generated from spherical particles); a “soot” inversion matrix, produced using diesel soot, was also available but is thought to be less representative of aviation nvPM than spherical particles given diesel soot is relatively larger and more aggregated than aviation PM (as advised by SAE E-31 members who have extensive knowledge of the TSI EEPS). The SMPS doesn’t require an inversion matrix, but was corrected to STP, as was the EEPS, to permit direct comparison of the total number concentrations derived by the four size instruments. It is noted that the NRC DMS-500 was freshly serviced and calibrated while the CU DMS-500 was outside of a 12-month calibration schedule (cal. September 2020). Both the EEPS and SMPS were also recently serviced/calibrated.

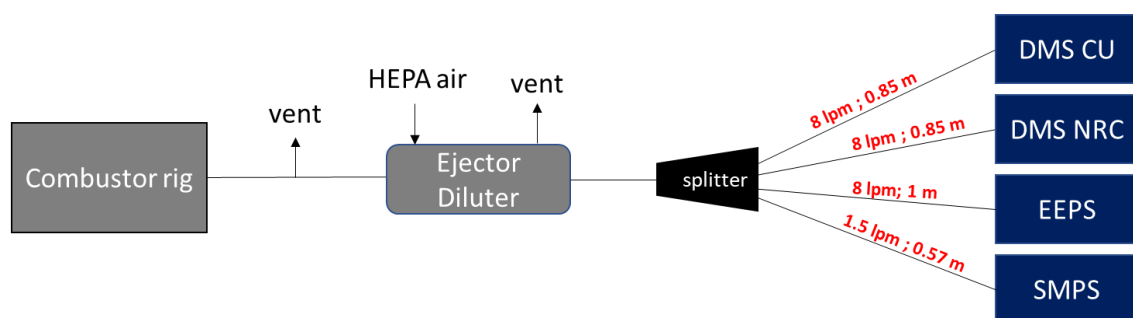


Figure 52: Diagram of the pre-test size instrument intercomparison

The results of the pre-test size instrument intercomparison are presented in **Figure 53**, **Figure 54** and **Figure 55** for the five test points investigated on rig soot. The size distributions, shown in **Figure 53**, are seen to be in general agreement. It is noted that for TP3-5, an inflection  $\sim 30$  nm is observed for the DMS NRC, which is thought to be the result of calibration uncertainty. Indeed, 30nm is roughly the size at which particles start gaining two charges rather than one within the DMS-500 and although the inversion matrix generally takes out this charging effect, it isn’t always perfect at doing so (from discussion with Cambustion support).



Work Package 4: Deliverables Report

The size distribution properties (GMD, GSD and total number) are displayed in **Figure 54** and **Figure 55**, where it can be seen that the DMS NRC generally predicts the largest GMD and GSD and the EEPS generally predicts the smallest GMD and GSD. It can also be seen that the GMDs agree within  $\pm 6\%$  of the mean and the GSD within  $\pm 4\%$ , demonstrating again that the four instruments agree relatively well with each other. Finally, it was observed that the SMPS total number is under-reporting when comparing with the three other size instruments (**Figure 54 (c)**).

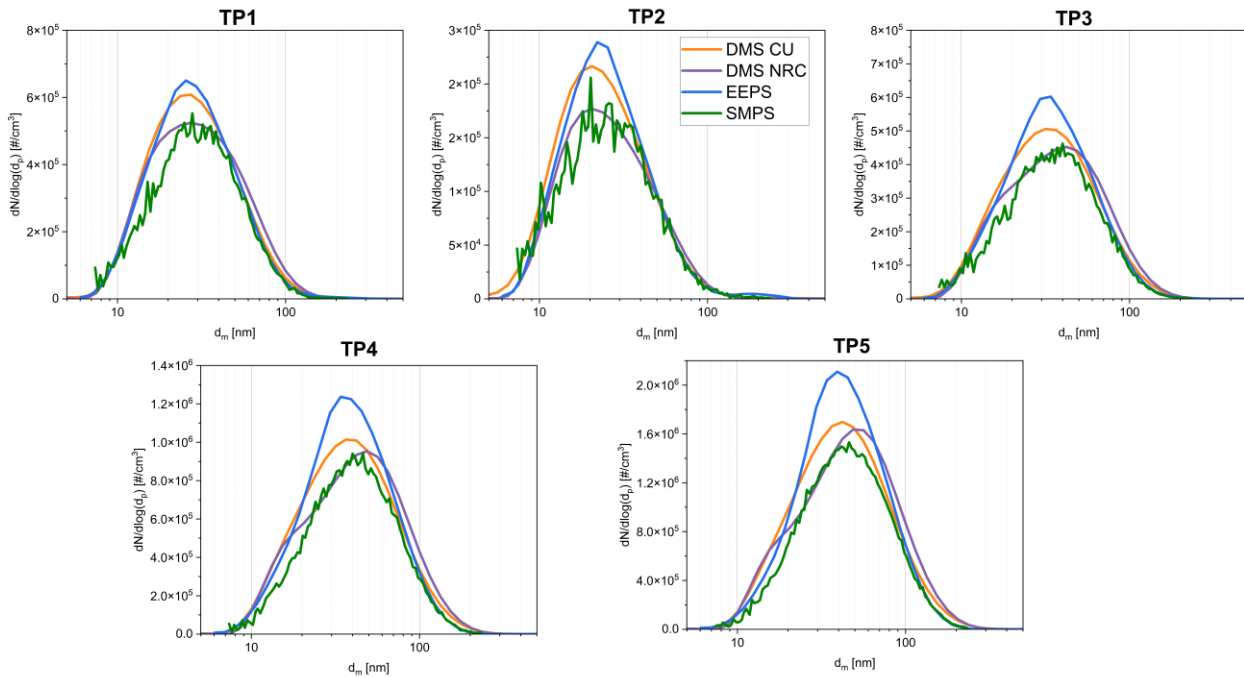


Figure 53: Particle size distributions measured by different size analysers during pre-test size intercomparison

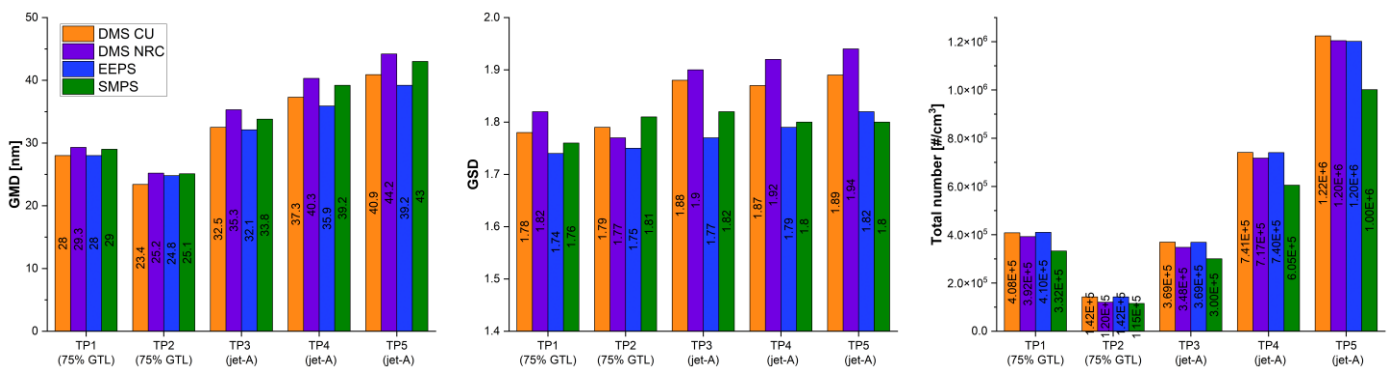


Figure 54: Measured GMD (left), GSD (centre) and STP-corrected total number concentration (right) derived from the four particle size instruments assessed during the pre-test size intercomparison



## Work Package 4: Deliverables Report

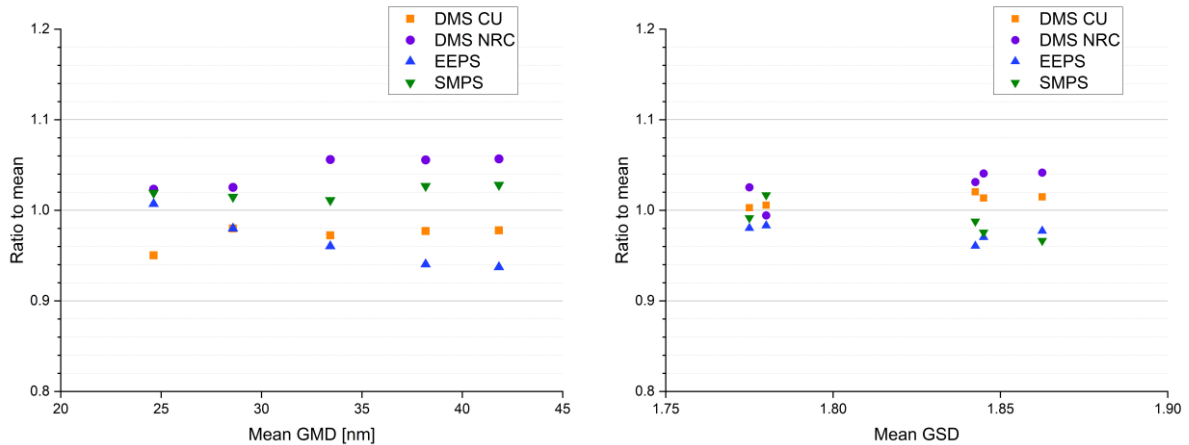


Figure 55: Ratio to the mean Vs mean GMD (left) and GSD (right) of the four particle size instruments assessed during the pre-test size intercomparison

## 5.2.2 Size-derived number and mass concentrations RQL 2 test

Similarly to the analysis performed in the RQL 1 test (section 5.1.3), the size-instrument-derived total numbers from the CU DMS-500, EEPS and SMPS were compared to the corresponding compliant number measurement (from either EUR or Swiss AVL APC). To afford a direct comparison, the size-instrument-derived total number was corrected for the additional VPR and CPC losses in the APC as well as the small differences in sampling, with the results displayed in **Figure 56**. It can be seen that size-derived number overpredicts the APC number for all three analysers (1.16 – 1.36). When comparing with RQL 1 test, the agreement between the SMPS and the APC is not as good (1.01 RQL 1 Vs 1.16 RQL 2), however the SMPS-derived number was only corrected to STP for RQL 2 test, hence it is noted that if corrected the RQL 1 data would also overpredict the APC. Concerning the CU DMS, it is noted that the number agreement drifted from 0.98 to 1.26 over the 12-month interval.

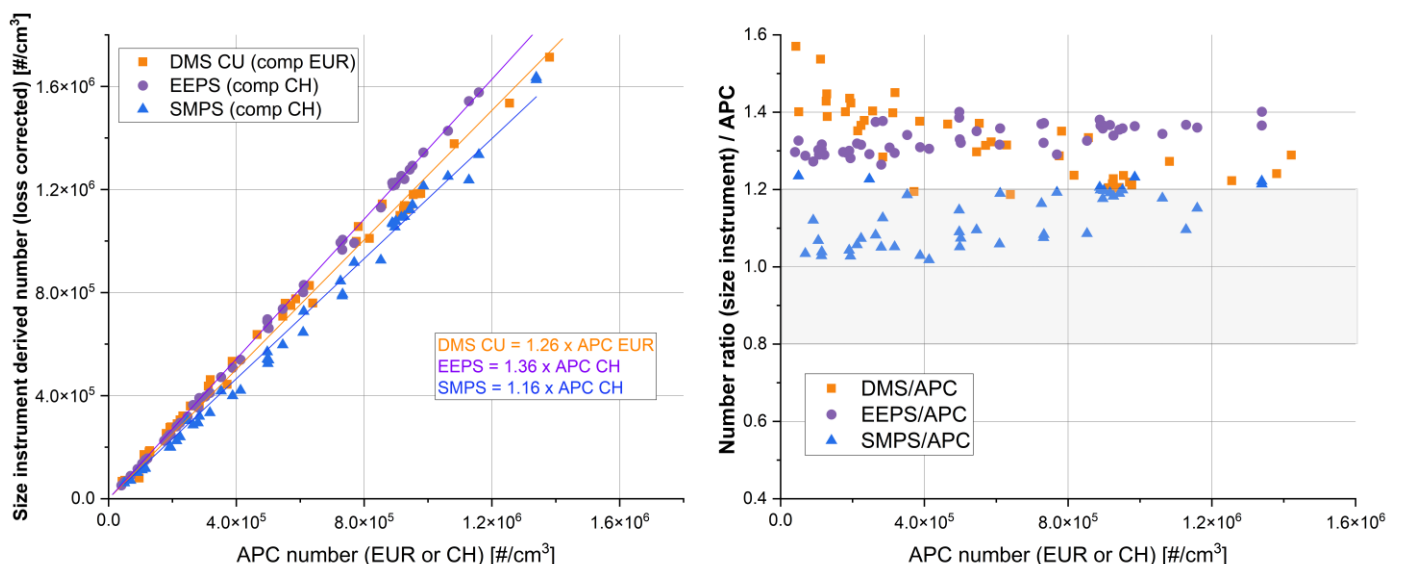


Figure 56: APC (EUR or CH) Vs size-instrument-corrected (DMS CU, EEPS, SMPS) number concentration (left) and ratio of APC/size-instrument-number over the average of the two (right)



## Work Package 4: Deliverables Report

As part of RQL 2 testing, similar analysis was performed for mass, in which the loss-corrected total mass derived from the size instruments was compared to that measured by the MSSs, as displayed in **Figure 57**. It is noted that there are significant uncertainties associated with deriving mass from size instruments, namely: (1) It requires a particle effective density assumption which is directly proportional to the output mass; (2) Most of the mass resides in the larger size bins at the right tail of the distribution where the count is low and the measurement uncertainty is higher, particularly for the fast-scanning instruments (i.e., EEPS & DMS-500); (3) the MSS only measured BC mass while the size instruments report total PM mass. It is also noted that the size distributions for the EEPS and DMS-500 were cut at 240 nm to allow representative comparison with the SMPS which only counted up to that size, as the DMS-500 and EEPS can measure larger sizes as highlighted in **Figure 58**.

In **Figure 57**, all size analysers are seen to overpredict the MSS mass (1.8 - 2.16), suggesting that the unit density assumption is inaccurate and that the measured particles had an average particle effective density  $\sim 0.5 \text{ g/cm}^3$ . The difference between MSS and mass derived by the size analysers decreases  $< 50 \text{ } \mu\text{g/m}^3$ , which could be explained by the fact that as the measured mass reduces, the particles are smaller and less aggregated and their effective density increases.

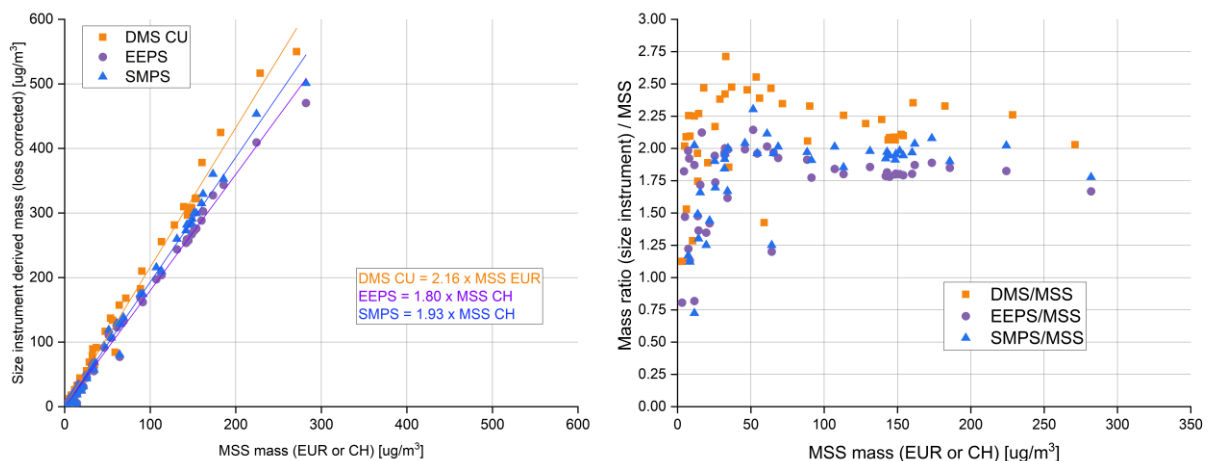


Figure 57: MSS (EUR or CH) Vs size-instrument-corrected (DMS CU, EEPS, SMPS) mass concentration (left) and ratio of APC/size-instrument-number over the average of the two (right) using sphericity and unit particle effective density assumptions



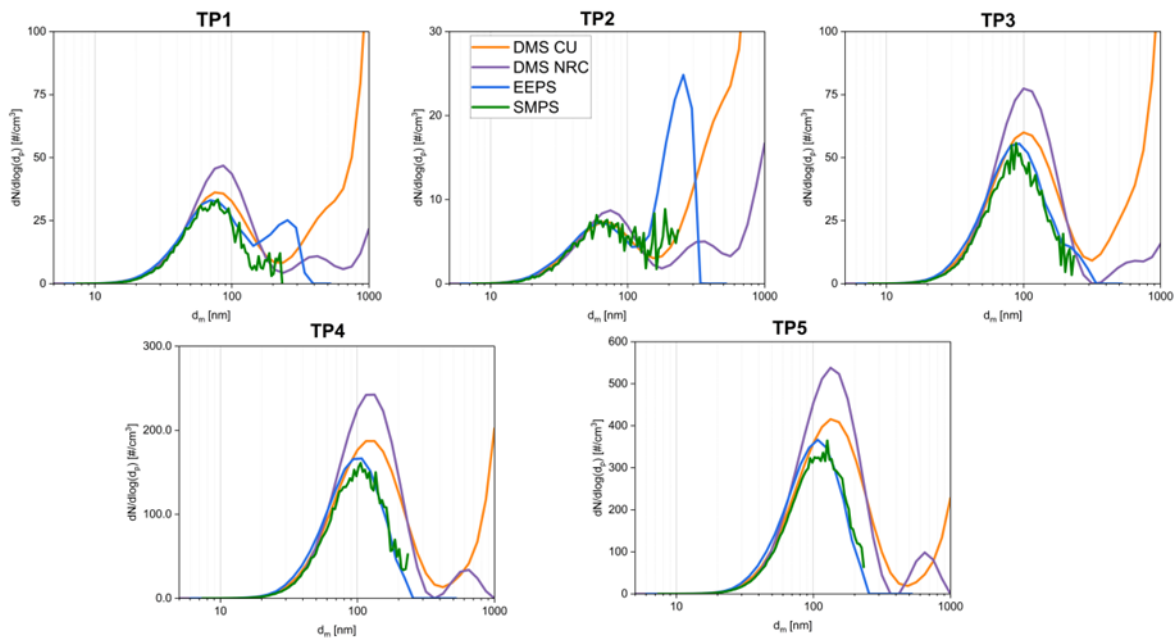


Figure 58: Volume-weighted particle size distributions measured by different size analysers during pre-test size intercomparison

### 5.2.3 Size measurement uncertainty discussion RQL 2 test

During the size intercomparison experiment, the SMPS, EEPS and DMS-500 were seen to correlate well with each-other in terms of GMD and GSD (within  $\pm 6\%$  of the mean), although some small differences in reported shape were observed, particularly with the NRC DMS-500. A combustor-exit GMD comparison of the different size instruments during the main RQL 2 tests is provided in section 5.4.2.

The total number and mass derived from the size-analysers were also compared to regulatory compliant nvPM number and mass. Size-derived number was between 0-60% of the APC number, suggesting that while size-instruments can give a good estimate of total number, they may not be as precise as a dedicated number analyser given the large uncertainties associated with loss and charging efficiency corrections in a size instrument. Size-derived mass was around double that of the MSS, which can be attributed to the fact that a unit particle effective density assumption was made, but also highlight the large uncertainty of deriving a mass from a size instrument.

## 5.3 Particle loss correction RQL 1 test

Due to the length and complexity of a regulatory compliant sampling and measurement system, significant particle losses are unavoidable. Particle loss therefore need to be corrected in order to obtain nvPM emission concentrations representative of the engine/combustor exit. Two particle loss correction methodologies were assessed to predict combustor-exit representative nvPM EI number and mass namely:

- 1) the regulatory method, as described in SAE ARP 6481, which uses a ratio of measured nvPM number and mass (with assumptions regarding lognormality, GSD and particle density) to predict a size distribution at the probe inlet which using the UTRC model is used to generate loss correction factors.



## Work Package 4: Deliverables Report

- 2) A bin-by-bin measured size method, which uses the directly measured particle size distributions (using SMPS, DMS-500) along with the UTRC model (along with VPR, CPC and cyclone losses) to predict loss correction factors.

### 5.3.1 Number correction factor ( $K_{sl_{num}}$ ) RQL 1 test

Number correction factors calculated using both the regulatory loss method (ratio nvPM number and mass) and measured particle size method (bin-by-bin) are presented in **Figure 59 (a)**. It is seen that there is a significant difference between the two methods, particularly at smaller particle sizes,  $GMD < 30$  nm, where the regulatory method significantly underpredicts  $ksl_{num}$  values when compared with the measured size method. The reasons for this divergence are:

- The regulatory method predicts a size distribution from the nvPM number and mass and assumes a lognormal monomodal distribution, however the size distributions in this study were found to sometimes be bimodal (**Figure 45**).
- The regulatory method assumes a fixed GSD of 1.8 when the measured GSD ranged from 1.5 to 2.4.

These assumptions for the regulatory method, along with the uncertainty in the reported nvPM mass values  $< 10 \mu\text{g}/\text{m}^3$  (see section 4.5) lead to an over-prediction of the EEP GMD (**Figure 59 (b)**) and therefore an under-prediction of the number loss correction factor. It is noted that as was observed with the measured particle size distributions (**Figure 45**), the  $ksl_{num}$  derived from both the DMS-500 and SMPS appear to correlate well with each other.

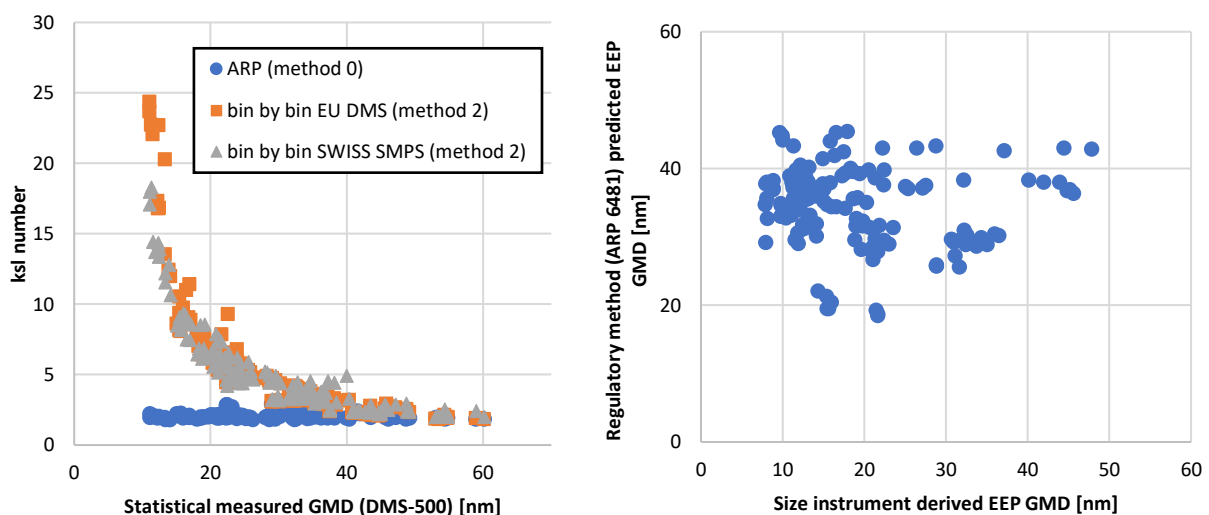


Figure 59: Particle number correction factor ( $ksl_{num}$ ) calculated using different methodologies Vs. the measured GMD (left) and Engine-Exit-Plane GMD predicted by method 0 Vs. that derived from the measured particle size distribution (right)

### 5.3.2 Mass correction factor ( $K_{sl_{mass}}$ ) RQL 1 test

The mass correction factors calculated using the regulatory method (ratio nvPM number and mass) and measured size method (bin-by-bin) are presented in **Figure 60 (a)**. There appears to be a good agreement



## Work Package 4: Deliverables Report

between both loss correction methods derived from the SMPS data for  $ksl_{mass}$ . However, it is observed that  $ksl_{mass}$  derived from the DMS-500 diverges at particle sizes below a GMD of 15 nm. It is noted that to allow for direct comparison with the SMPS, only the DMS-500 data up to 240 nm was used for the mass correction factor calculation. Indeed, the DMS-500 measures up to 1000 nm and because the DMS-500 consistently measured a signal  $> 300$  nm for which additional correction would be applied from the 1 $\mu$ m cyclone loss (see **Figure 61**Figure 61), the  $ksl_{mass}$  derived from the full DMS-500 size distribution was found to be significantly higher, as shown in **Figure 60 (b)**. It is noted that the signal  $> 300$  nm is believed to be shedding from the sampling system and not a combustion by-product, hence this issue may likely be resolved should more stringent sampling and operability protocols be found and adopted.

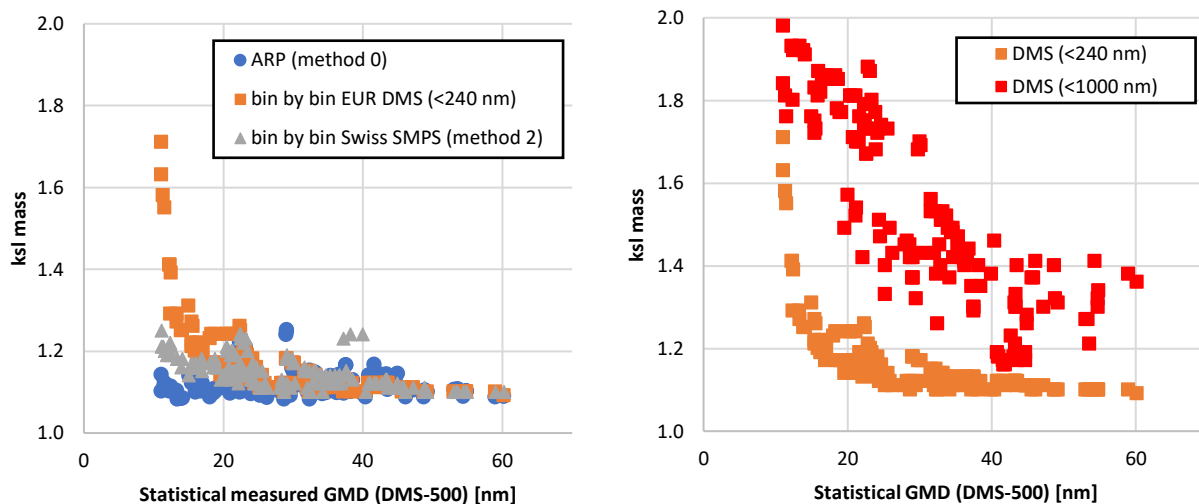


Figure 60: Particle mass correction factor ( $ksl_{mass}$ ) calculated using different methodologies Vs. the measured GMD (left) and method 2  $ksl_{mass}$  when using the whole DMS-500 size distribution Vs when cutting to 240 nm (right)

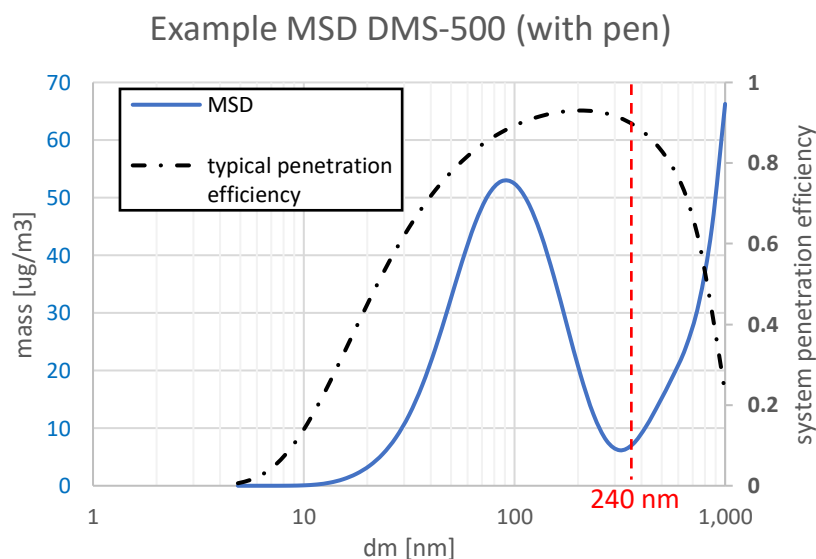


Figure 61: Example Mass-weighted size distribution from the DMS-500 along with the penetration efficiency of a regulatory compliant sampling system to highlight the mass fraction  $> 240$  nm.



### 5.3.3 Loss correction discussion RQL 1 test

It is observed that there are significant losses within the regulatory nvPM sampling and measurement system, which require predicted correction factors ( $K_{sl_{num}}$ ) of 25 times in the case of number for the smallest particles. It is also observed that in the case of very small particles with an observed bimodal distribution (and associated low mass – and increased measurement uncertainty) that the regulatory loss correction method which is based on a ratio of measured mass and number, with limited assumptions, appears to massively underpredict the actual losses witnessed.

It is observed that although the required correction factors are much lower in the case of mass, that caution is required when using the measured size method. As discussed, the upper- limit of measured size will directly impact the predicted loss given the specified cyclone is designed to effectively remove the larger particles. Hence, within the loss model significant loss of mass is predicted in the case of a few large particles entering the cyclone. However, it is noted that some of the larger particles measured by the sizing instruments are potentially shed from the sampling system/ cyclone, hence should not be included in predicting loss as these in reality are not necessarily representative of particles witnessed at the combustor/ engine exit and have already been accounted for in the cyclone loss.

## 5.4 Particle loss correction RQL 2 test

The presence of four size instruments during the RQL test 2 test campaign afforded two particle loss correction experiments to be undertaken, namely:

- (1) Real-time measurement of particle loss in different sections of a regulatory compliant sampling system by moving size instruments to the diluter vent and raw line.
- (2) A more detailed assessment of the two loss correction methodologies presented in section 3.4 and preliminary assessed in RQL test 1 section 5.3 (SAE ARP 6481 Vs bin-by bin method) in which the uncertainty associated with instrument location and using different size instruments/technologies as inputs can be quantified.

### 5.4.1 Measured Vs predicted loss RQL 2 test

Measuring particle loss in a regulatory compliant system is complicated and requires lengthy dedicated experiments which cannot be afforded during aircraft engine certification. Therefore, to correct for particle loss and predict nvPM concentration at the exhaust of an aircraft engine, losses can be predicted at a given size using the UTRC model described in the SAE ARP 6481 and used in the regulatory loss correction methodology (method 0). Experimental validation of the UTRC model on a regulatory compliant system has been published in the literature ([7] & [9]), but only for specific sections of the system and loss mechanisms. As part of RQL 2 tests, penetration efficiencies were experimentally characterised real-time in the 25 m line and in the entire sampling system using two size instruments in parallel. The measured losses were compared to the UTRC model as presented below.

#### 5.4.1.1 Correction function between different size analysers

The measured losses were derived by comparing the measurement of two sizing instruments (either EEPS Vs SMPS in Swiss system or NRC DMS-500 Vs CU DMS-500 in EUR system). To afford greater precision in the reported losses, a correction function was first defined to correct for any systematic bias between the instruments. This was done using pre-test size intercomparison data (section 5.2.1).





## Work Package 4: Deliverables Report

The two correction functions, as presented in **Figure 62**, correspond to the average of  $(Size\ instrument\ 1)/(Size\ instrument\ 2)$  for each size bin. The error bars represent  $\pm 1$  standard deviation from the average of the five pre-test size intercomparison data points. It is noted that for the DMS-500 data (CU Vs NRC), only size bins where the number concentration was above  $1E4\ \#/cm^3$  were included in this analysis as the data was assumed to be noise below that threshold. It is also noted that given the SMPS and EEPS don't measure in the same size range using the same size bins, their correction factor was derived by lognormally fitting the measured data from the pre-test size intercomparison and comparing the lognormal fits instead. Given lognormal fits were used, all data was included in the averaging (no minimum threshold like with the DMSs). The large error bars  $<10\ nm$  and  $>100\ nm$  represent the tails of the lognormally fitted size distributions and therefore have larger uncertainties.

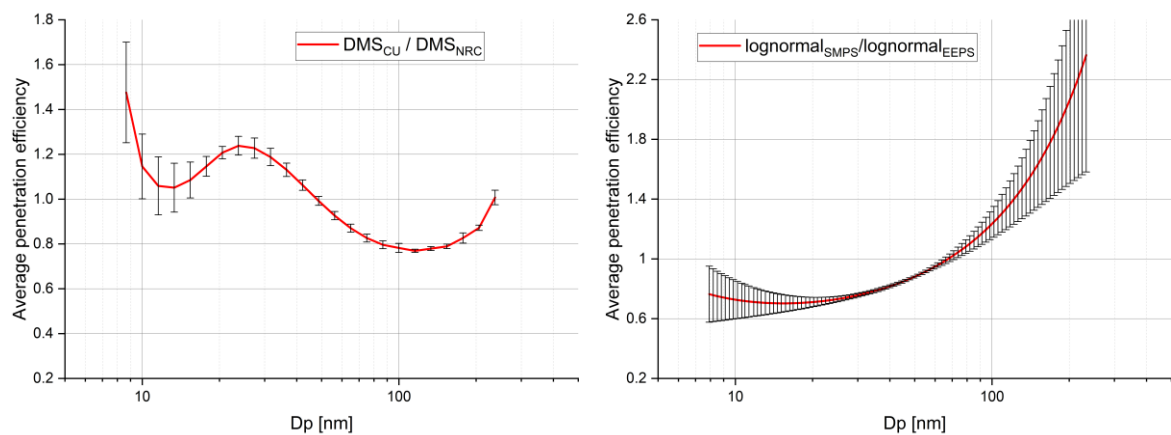


Figure 62: Correction functions between the CU DMS and the NRC DMS (left) and the SMPS and the EEPS (right) using the pre-test size intercomparison data

#### 5.4.1.2 Results measured Vs predicted: Full sampling system

During a subset of RQL 2 test points (TP 1-19 - measured GMD range 26-41 nm), the NRC DMS was located near the sampling probe on an undiluted segment. The measured and modelled losses were calculated as per the equations below:

$$measured\ loss = \frac{DMS_{CU} \times DF_1}{DMS_{NRC} \times correction_{function}(DMS\ CU\ Vs\ NRC)}$$

$$modelled\ loss = \frac{UTRC_{DMS_{CU}\ to\ common\ point} \times cyclone_{loss}}{UTRC_{DMS_{NRC}\ to\ common\ point}}$$

The “measured loss” in the full sampling system were calculated by dividing size distributions measured by the CU DMS located in parallel with the EUR nvPM number and mass to that measured by the NRC DMS located near the probe. The correction function discussed above as well as  $DF_1$  correction of the “measured” loss were required to permit direct comparison with the UTRC predicted loss.

The “modelled” loss correspond to the predicted loss in the sampling system between the two size analysers (including the cyclone).

The results are presented in **Figure 63**, in which it can be seen that the measured and modelled loss agree within the error bars of the measurement between 10 – 100 nm, further validating the use of the UTRC



## Work Package 4: Deliverables Report

model for predicting losses in a regulatory compliant sampling system. The deviations observed < 10 nm and > 100 nm can be attributed to the uncertainty associated with the “measured” loss. Indeed, in this experiment, the total size distributions were divided by each other and therefore the uncertainty is larger near the tails of the measured modes, particularly given fast-spectrometer were used. A more precise measurement of the losses could be achieved by measuring losses at individual sizes using size-selection with a DMA, however the flowrate is too high at the inlet of a regulatory compliant system to afford the use of a DMA.

It is noted that in **Figure 63**, the error bars represent the average of up to nineteen test points if the minimum concentration threshold ( $1E4 \text{ \#/cm}^3$ ) is met. Therefore, error bars can be misleading at > 100 nm where the minimum threshold is generally only met for a couple of test points, making the error bars appear smaller than for other data points where more data is used in the average.

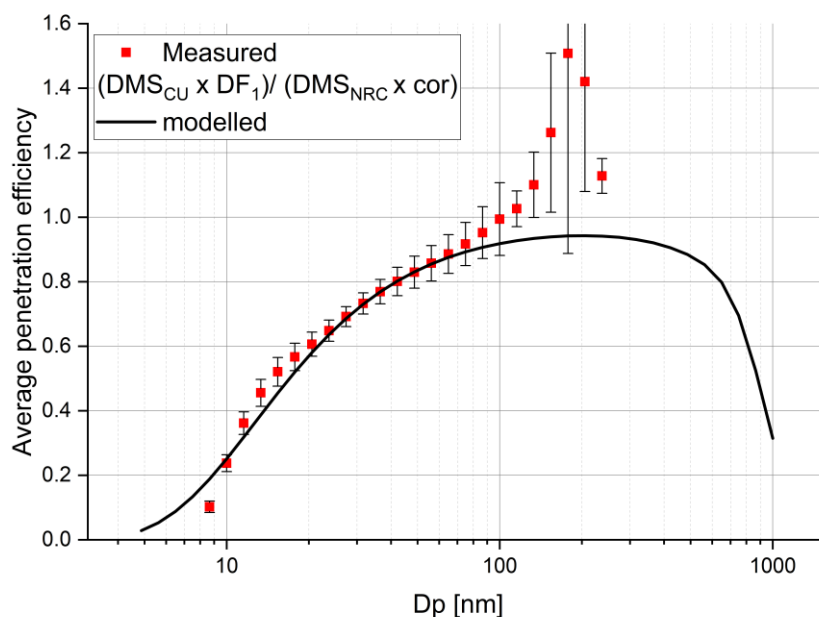


Figure 63: Comparison of the “measured” (DMS CU Vs DMS NRC) and “modelled” (UTRC) losses in a regulatory compliant sampling system

#### 5.4.1.3 Results measured Vs predicted: 25 m line

During limited RQL 2 tests, the SMPS and NRC DMS were moved to measure from the diluter vent of the Swiss and EUR systems retrospectively (TP27 – TP33 for the SMPS and TP27 – 40 for DMS NRC), with comparisons to the EEPS and CU DMS used to calculate “measured” loss in the respective 25 m nvPM lines. The losses were calculated as described in section 5.4.1.2, with the exception of  $DF_1$  which was not required in this case as both instruments were measuring diluted sample. The comparison between the losses “measured” by the size instruments and “modelled” by the UTRC model can be found in **Figure 64**.

It can be seen that the modelled loss generally underpredict the measured loss by ~5 to 20% in the 10 – 100 nm region. The measured loss by the EEPS/SMPS and DMS NRC/DMS CU agree well with each other although the DMSs measured penetration fluctuates above and below that of the EEPS/SMPS on the 08/12 (TP27 – 33), where it was later found that the CU DMS had significant noise around 10-20 nm. It is hypothesised that the underprediction of modelled loss compared with measured loss in the 25m line is



## Work Package 4: Deliverables Report

due to the size measurement being located in the vent, with may not be sampling a representative aerosol and may be experienced slightly different dilution and diluter losses than the sample to the nvPM analysers. It is noted that underprediction of modelled penetration when compared to losses measured in the vent has already been reported in the literature for a regulatory compliant sampling system at high thrust condition for particles > 50 nm [7].

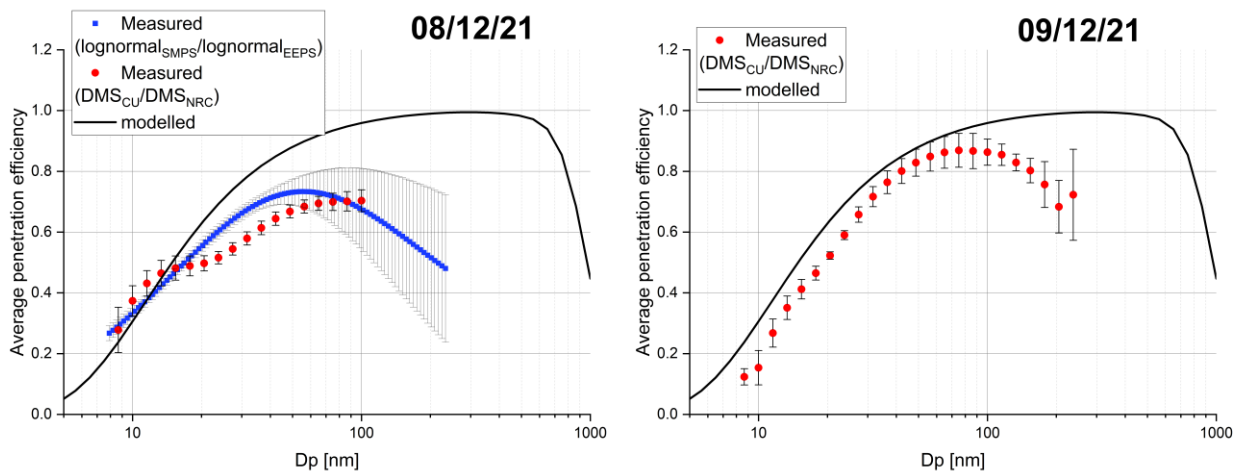


Figure 64: Comparison of the “measured” (DMS CU Vs DMS NRC & SMPS Vs EEPS) and “modelled” (UTRC) losses in the 25m line of a regulatory compliant sampling system (the 08/12/21 corresponds to TP 27-33 and the 09/12/21 corresponds to TP 34-40)

### 5.4.2 Comparison of size distribution properties (GMD, GSD) at the combustor-exit RQL 2 test

As previously discussed, a total of four size analysers were simultaneously located at different points along the sampling systems (i.e., near Swiss or EUR nvPM number/mass, in diluter vent, near inlet probe). To compare the different size analysers and assess their suitability for system loss correction, the measured size distributions were all corrected to the combustor-exit using the UTRC model.

The combustor-exit GMD for the different instruments is plotted in **Figure 65 (a)** against the average GMD. It can be seen that the combustor-exit GMD predicted by the different analysers all agree closely with each other (within  $\pm 3$  nm of the average), with the SMPS generally predicting the largest GMD, and EUR DMS predicting the smallest up to 35nm.

Additionally the combustor-exit GMD predicted by the SAE ARP 6481 is compared to the average GMD from the size instruments in **Figure 65 (b)**. It can be seen the ARP 6481 method, which uses the measured nvPM number and mass to predict a combustor-exit GMD, generally underpredicts the measured-derived average GMD by  $\sim 5$  nm and that < 25 nm, it sometimes predicts highly different GMDs, likely due to the high uncertainty associated with nvPM mass measurement near LOD.

The combustor-exit GSD for the different instruments is presented in **Figure 66** against the average GSD. It is seen that the GSDs generally agree within  $\pm 0.05$  of the average, with the EEPS generally predicting the smallest GSD and the DMS NRC predicting the largest.



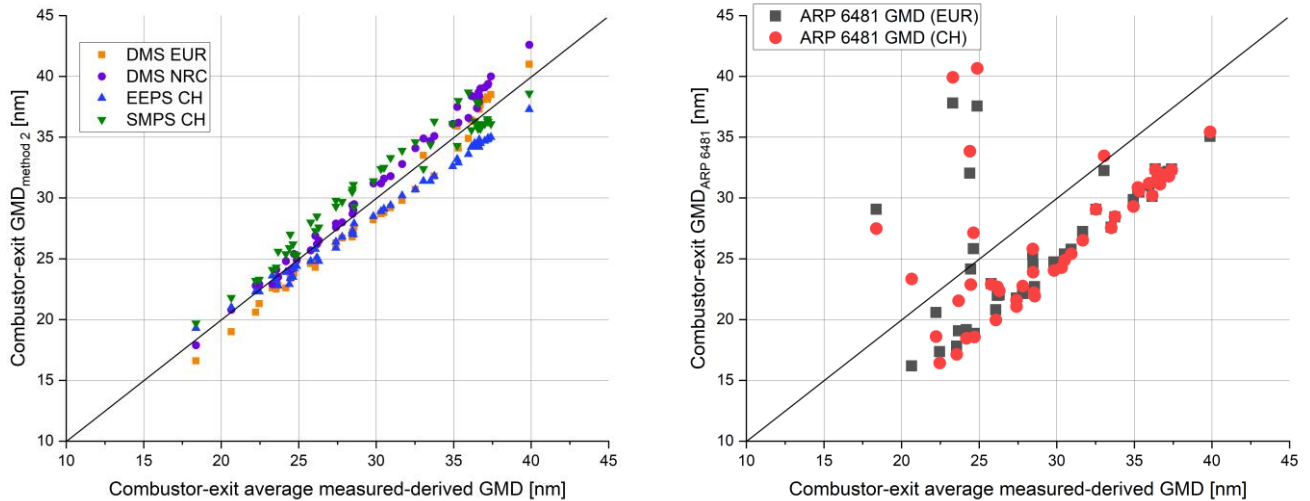


Figure 65: Combustor-exit GMD measured by the four size instruments Vs their average (left) and Combustor-exit GMD predicted by the ARP 6481 loss correction methodology Vs the measured-average (right)

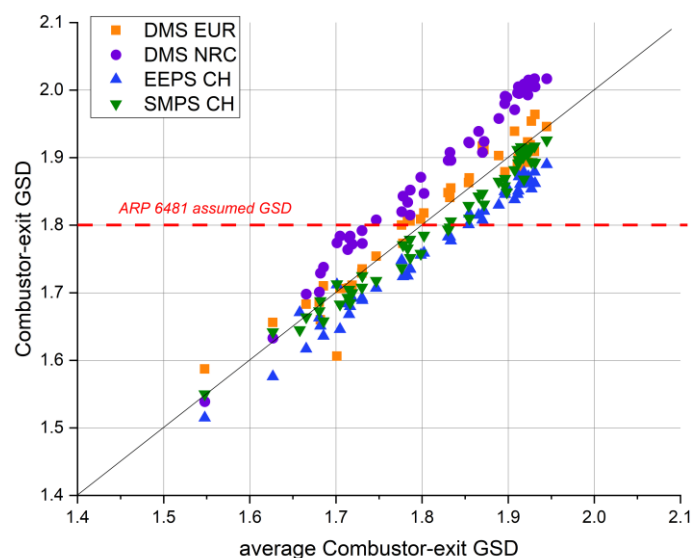


Figure 66: Combustor-exit GSD measured by the four size instruments Vs their average

### 5.4.3 Number correction factor (Ksl num) RQL 2 test

Number correction factors calculated using both the regulatory loss method (ARP 6481 – method 0) and measured particle size method (bin-by-bin – method 2) are presented in **Figure 67** against the measured GMD. It is noted that  $ksl\_num$  was calculated for  $D_p > 10$  nm at the combustor-exit for both methods, following ARP 6481 methodology.

Firstly in **Figure 67 (a)** for method 0, it can be seen that the  $ksl\_num$  from the Swiss system is on average 5% higher than  $ksl\_num$  from the EUR. This difference can be attributed to the slightly higher nvPM mass measured by the Swiss system (i.e., ~3% higher EI mass on average – section 4.2.2) and the slightly different system and instrument losses between the two compliant systems. Overall, method 0  $ksl\_num$  is seen to



## Work Package 4: Deliverables Report

correlate with the measured GMD > 25 nm, but not < 25 nm, systematic of the higher nvPM mass measurement uncertainty near LOD.

Secondly in **Figure 67 (b)** for method 2 using size distributions measured by four analysers at different locations, it can be seen that  $ksl\_num$  follows the same trends with  $ksl\_num$  increasing with decreasing GMD corresponding to higher diffusional losses. At any given test point,  $ksl\_num$  generally varies by 0.3 (or 10%) between the minimum  $ksl\_num$  (generally SMPS) and the maximum  $ksl\_num$  (generally EEPS). This can be explained by the fact that the SMPS generally measured the largest size distribution while the EEPS measured the smallest. It is noted that the instrument location (near nvPM number/mass, in diluter vent, near probe) doesn't seem to have a meaningful impact as the trends for the SMPS and NRC DMS are the same regardless of their positions.

The  $ksl\_num$  predicted by method 0 and method 2 (as displayed in **Figure 67**) were subsequently averaged to further assess the difference between the two loss correction methodologies. The results are presented in **Figure 68**, where it is observed that method 0 generally overpredicts method 2 by ~5% > 27 nm but can significantly underpredict  $ksl\_num$  < 27 nm when compared with method 2.

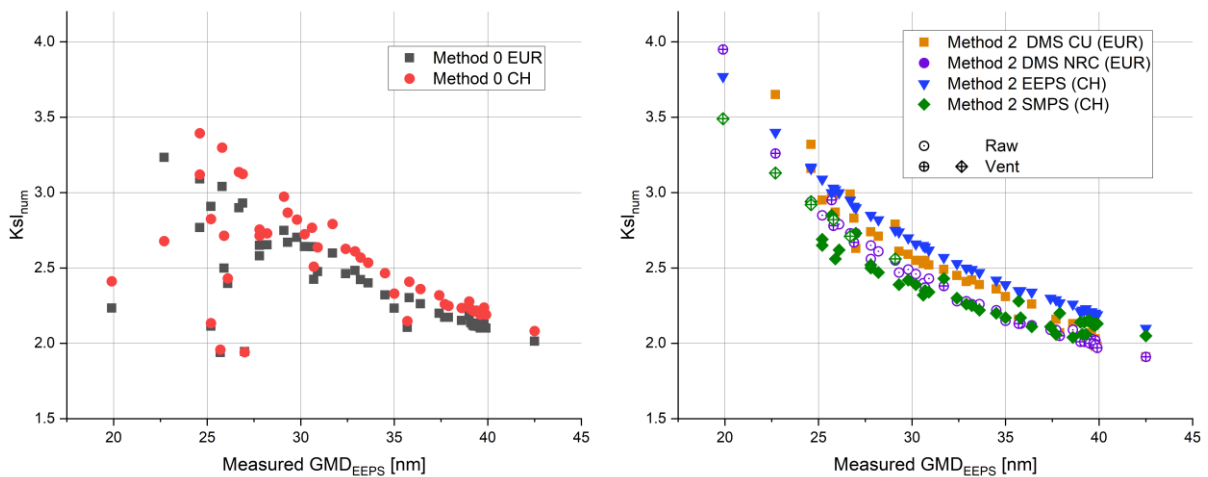


Figure 67: Number loss correction factor ( $ksl\_num$ ) calculated using the ARP 6481 method 0 (left) and the bin-by-bin method 2 (right) plotted against the measured GMD



## Work Package 4: Deliverables Report

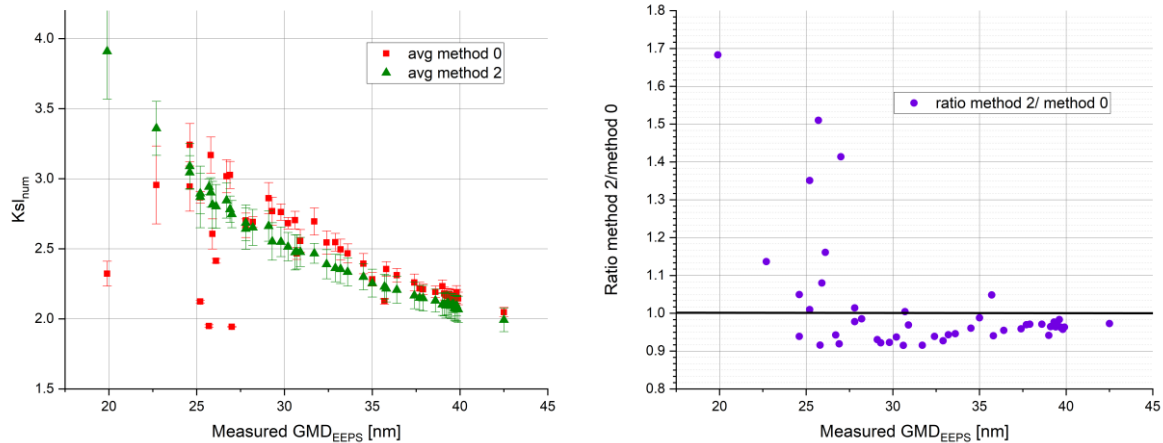


Figure 68 : Average number loss correction factor ( $ksl_{num}$ ) plotted against the measured GMD for method 0 and method 2 (left) and ratio of the two methods Vs the measured GMD (right) - error bars represent  $\pm 1$  standard deviation of the average (i.e., average of 2 data points for method 0 and average of 4 data points for method 2)

#### 5.4.4 Mass correction factor ( $ksl_{mass}$ ) RQL 2 test

Mass correction factors calculated using both the regulatory loss method (ARP 6481 – method 0) and measured particle size method (bin-by-bin – method 2) are presented in **Figure 69** against the measured GMD. It is noted that for method 2,  $ksl_{mass}$  was calculated for  $D_p < 240$  nm for the DMS-500s and the EEPS as both of these analysers measured a larger size spectrum than the SMPS, which was previously found to impact  $ksl_{mass}$  (see section 5.3.2).

In **Figure 69 (a)**,  $ksl_{mass}$  derived from method 0 for the EUR and Swiss systems agrees within 0.7% on average. Similarly to  $ksl_{num}$  (**Figure 67 (a)**),  $ksl_{mass}$  follows a trend  $> 27$  nm GMD with large scatter  $< 27$  nm, thought to originate from the higher nvPM mass measurement uncertainty near LOD.

In **Figure 69 (b)**,  $ksl_{mass}$  estimated using the different size instruments (method 2) was found to vary by 0.03 (or 2%) on average between the minimum  $ksl_{mass}$  (generally DMS NRC) and the maximum  $ksl_{mass}$  (generally EEPS).

The  $ksl_{mass}$  predicted by method 0 and method 2 (as displayed in **Figure 69**) were subsequently averaged to further assess the difference between the two loss correction methodologies. The results are presented in **Figure 70**, where it is observed that method 0 generally overpredicts method 2 by  $\sim 3\%$  at sizes  $> 27$  nm but can also significantly underpredict  $ksl_{mass} < 27$  nm when compared with method 2.



## Work Package 4: Deliverables Report

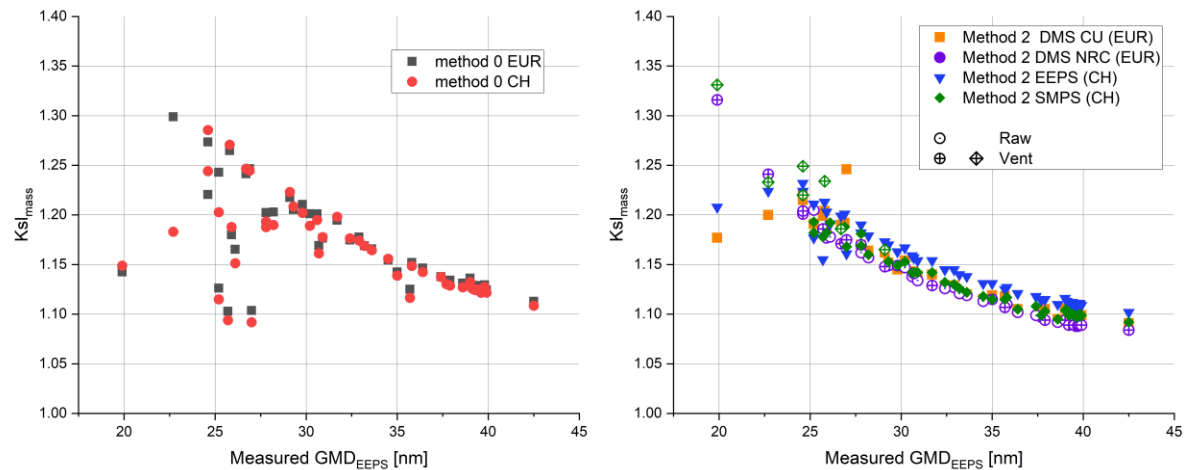


Figure 69: Mass loss correction factor ( $ksl\_mass$ ) calculated using the ARP 6481 method 0 (left) and the bin-by-bin method 2 (right) plotted against the measured GMD

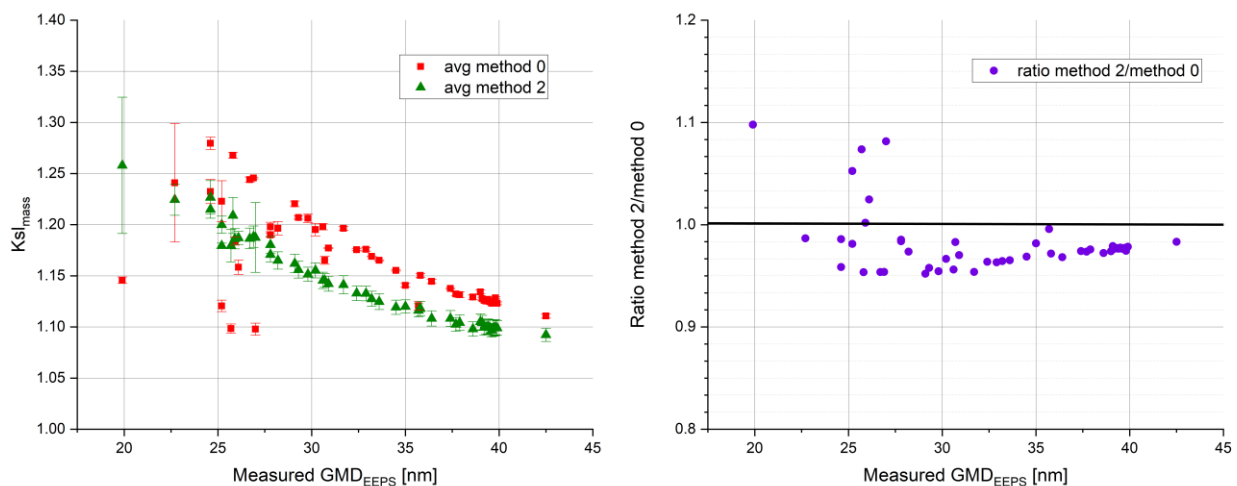


Figure 70: Average mass loss correction factor ( $ksl\_mass$ ) plotted against the measured GMD for method 0 and method 2 (left) and ratio of the two methods Vs the measured GMD (right) - error bars represent  $\pm 1$  standard deviation of the average (i.e., average of 2 data points for method 0 and average of 4 data points for method 2)

### 5.4.5 Particle loss correction discussion RQL 2 test

In agreement with findings of RQL 1 test, results of RQL 2 testing highlight that the regulatory loss correction method (based on a ratio of measured mass and number, with limiting assumptions) can significantly underpredict the system loss witnessed when the measured GMD is  $< 25$  nm (i.e., near nvPM mass LOD), particularly for nvPM number correction. It was found that the penetration efficiency modelled by the UTRC model (used in the regulatory method) compared well with measured-derived penetration efficiency. However, under prediction of penetrations from measurements in diluter vent may indicate non uniform dilution of different particle sizes, hence requires more understanding.

It was also observed that when setting similar upper and lower size boundaries (10-240 nm for RQL 2 data analysis), the bin-by-bin (i.e., method 2) number and mass correction factors offered general agreement



for the different size analysers tested, regardless of instrument type and location (~10% uncertainty for  $ksl\_num$  and ~2% for  $ksl\_mass$ ).

## 5.5 Impact of fuel composition on nvPM emissions

### 5.5.1 Small-scale Laboratory Testing

To quantify the impact of fuel composition on nvPM emissions as part of the RAPTOR programme a small-scale assessment of fuel variation was performed by ONERA using their bespoke liquid fuel CAST burner (M4.3). Full details of the testing and results are presented in **Appendix 8.3**. However, in summary four different fuels with different sulfur and aromatic contents within the limits of ASTM certification were tested. Two different CAST set points were tested for each fuel. Both points kept the same kerosene flow ( $Q_k = 105 \mu\text{L}/\text{min}$ ) and changed propane and air flows, being  $Q_p = 30 \text{ mL}/\text{min}$ ;  $Q_{air} = 2.0 \text{ L}/\text{min}$  for first point and  $Q_p = 20 \text{ mL}/\text{min}$ ;  $Q_{air} = 1.5 \text{ L}/\text{min}$  for the second. BC mass concentration, nvPM number concentration and particle size distributions were measured for each point and each fuel. Overall the results were as expected, with a reduction of mass and number emissions observed when reducing the concentration of aromatic compounds in the fuel. Particle diameter also decreased when the aromatic content of the fuel decreased. The only exception to this trend was observed for the first set point and fuels containing 4 ppm of Sulphur. In this case the observed reduction on emissions was smaller than the uncertainty associated to the measure, so it cannot be concluded that there is an impact on emissions linked to aromatic content. The reason behind this is not clear. It was observed that the condition selected for the first point was stable for all other fuels, with the exception of the fuel containing 4 ppm of Sulphur and 16% of aromatic compounds. This might explain the large uncertainty associated to this measure. In any case, the trends observed were in general similar to those observed in previous experiments. Thus, the results obtained using a small-scale combustion source do not indicate any potential problem with proposed hydrogen content based fuel correction methodologies.

### 5.5.2 RQL Combustor Rig Testing

The impact of alternative fuels was not a deliverable of the RAPTOR RQL 1 & 2 testing campaigns, however as discussed previously (**Section 2.3**) several fuels were employed in order to ensure a wide range of nvPM number and mass concentration and nvPM size distributions. To ensure the full usefulness of the data was achieved, in conjunction with RAPTOR researchers, additional analysis of the data was performed as part of a PhD thesis by Harper (2022) [11], which highlighted that the best metric to detail nvPM fuel impact was hydrogen content. As seen in **Figure 71**, analysis of the impact of alternative fuels across the different test conditions during RQL 1 testing highlighted that consistent trends of reducing nvPM number and mass were observed at elevated fuel hydrogen content.





Work Package 4: Deliverables Report

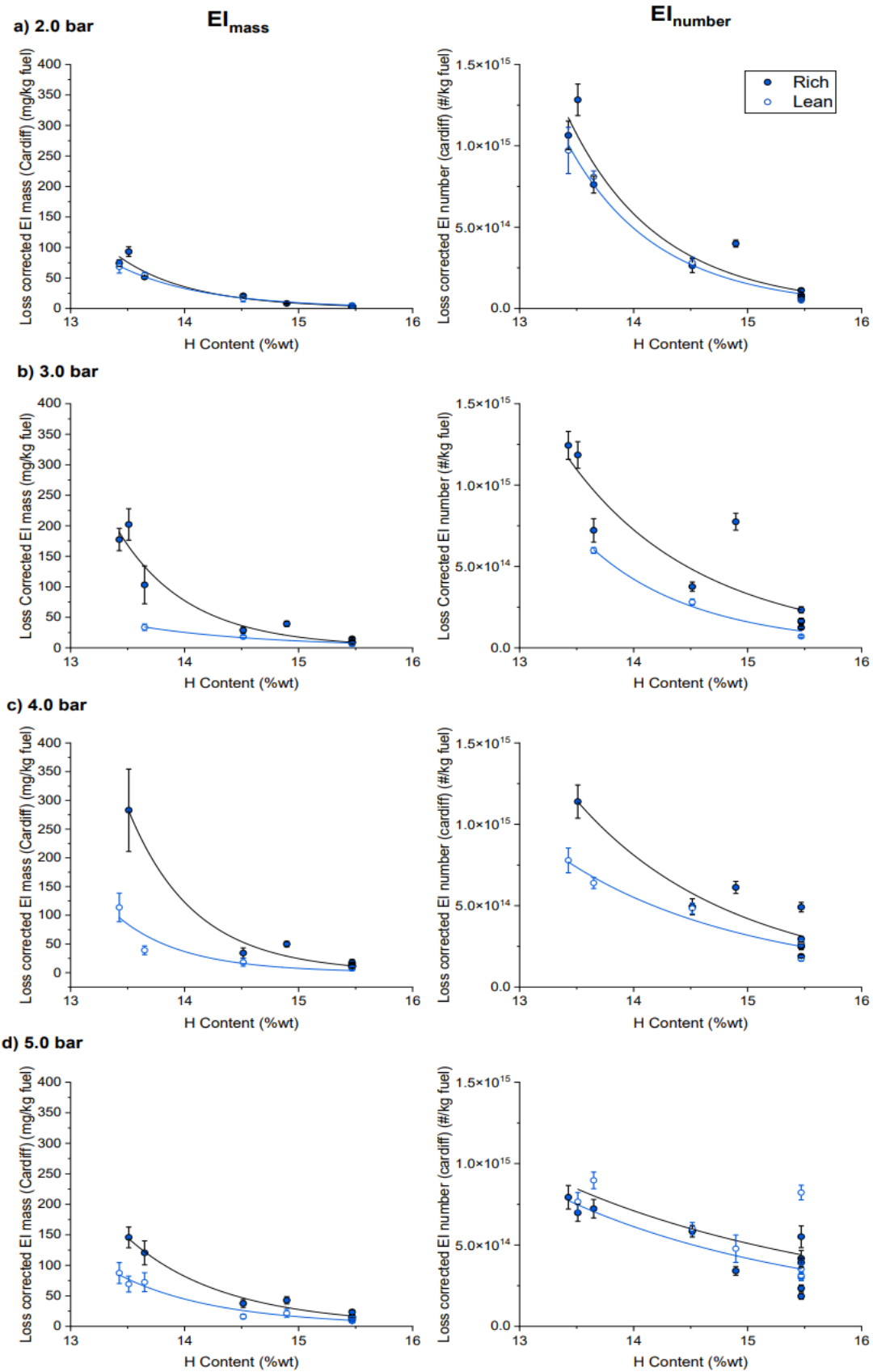


Figure 71 Fuel impact on loss corrected nvPM emissions for alternative fuels in RQL 1 test.



## Work Package 4: Deliverables Report

Towards assessing whether a global hydrogen content nvPM fuel correction methodology is viable, RQL 1 & 2 data was subsequently analysed using the same methodology as outlined for data from a previous Jetscreen programme described by Harper et al. [5]. To afford a global trend independent of power, fuel or combustor variant, each data point was normalised to the corresponding nvPM concentration witnessed for a baseline fuel of 14.5% Hydrogen at the same nominally identical test condition (AFR, T, P, combustor type). All data from three distinct campaigns (Jetscreen, RQL 1 & RQL 2) were then plotted as shown in **Figure 72** to determine trendlines indicating the impact of fuel hydrogen content on nvPM mass, number and size.

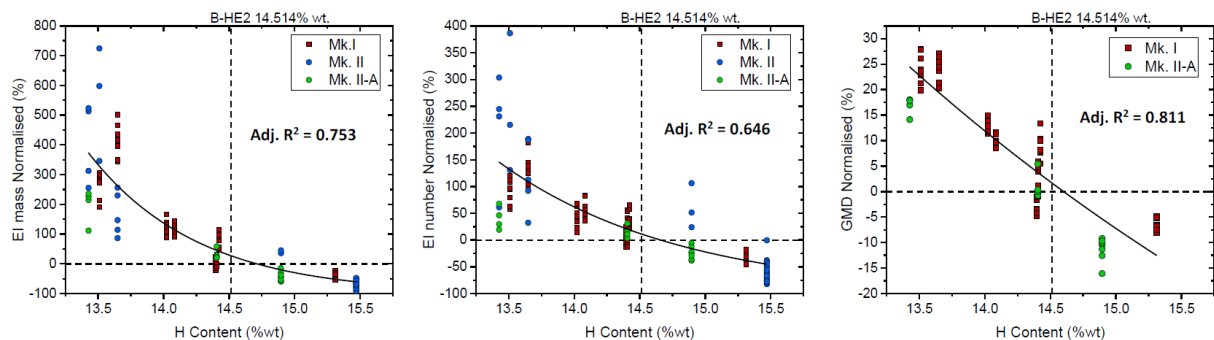


Figure 72: Normalised nvPM emissions dataset (mass left, number middle and GMD right) across the Mk. 1 (Jetscreen), Mk. II (RQL test 1) and Mk. II-A (RQL test 2)

As can be seen, there appear to be general trends which largely fit the data well at hydrogen contents of >13.75% with larger scatter observed at the lowest hydrogen content (dirtiest) fuels. It is thought this scatter is driven by day to day variation and wall sooting of the combustor during these high mass loading tests. However, the global trends highlight there is a definite trend of decreasing nvPM mass, number and size with increasing hydrogen content supporting recent decisions of CAEP/12 to adopt a fuel hydrogen content correction methodology for nvPM, towards reducing uncertainty in the stringency of the standard.

## 5.6 Impact of humidity on nvPM emissions (M4.2 RQL test)

A dedicated humidity experiment was performed as part of RQL 2 test in which water in the form of steam was added to pre-heated primary and secondary air (>100°C), in a similar manner as previously reported in the literature [10]. Up to 5% water by mass was injected either in the primary air, secondary air, or both and the impact on the produced nvPM emissions was quantified. A “dirty” Jet-A fuel was used (fuel 3 in **Table 1**) to ensure a sufficiently high reference nvPM number and mass signal.

The impact of water injection in the primary (1- 5% by mass) and secondary air (1-2% by mass) on measured nvPM number and mass is presented as a timeseries **Figure 73**. It is seen that an increase in humidity in the primary zone is seen to significantly reduce nvPM emissions while increased humidity in the secondary zone increases nvPM emissions. However, it is noted that water injection in the secondary air led to instabilities in the rig and significantly higher nvPM fluctuations when compared with injecting water in the primary air.



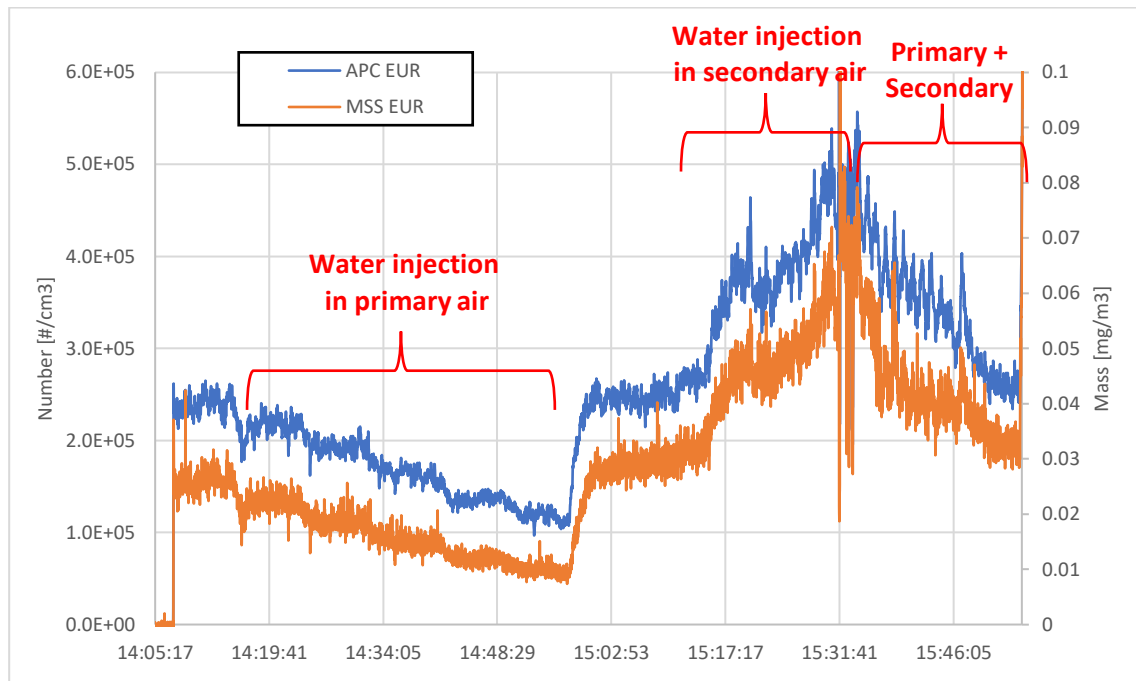


Figure 73: Timeseries of the EUR system nvPM number and mass when injecting water in the primary air and secondary air in the RQL combustor rig

The impact on nvPM emissions associated with increased humidity was subsequently quantified by normalising the “wet” cases (x% water in primary and/or secondary air) to the “dry” case (0% water loading), with the results presented in **Figure 74** for EI mass and in **Figure 75** for EI number. It is found that water injection in the primary air consistently reduced nvPM number and mass emissions, up to ~60% reduction for EI mass and ~50% for EI number at 5% water loading, with particle size also being reduced (GMD reduction of 6 nm at 5% water). Conversely, water injection in the secondary air is seen to increase both nvPM number and mass. These competing factors are thought to arise from a suppression in soot formation, brought about by increased hydrogen and hydrogen intermediates in the primary flame zone and a reduction in soot oxidation caused by reduced local temperature in the secondary zone.

For the limited cases where humidity was increased in both the primary and secondary zones in parallel a rise in nvPM was witnessed, however care is required in interpreting this result given the zero-repeat point was also seen to be 20% higher likely due to changes in local temperature brought about by the water testing from previous tests.

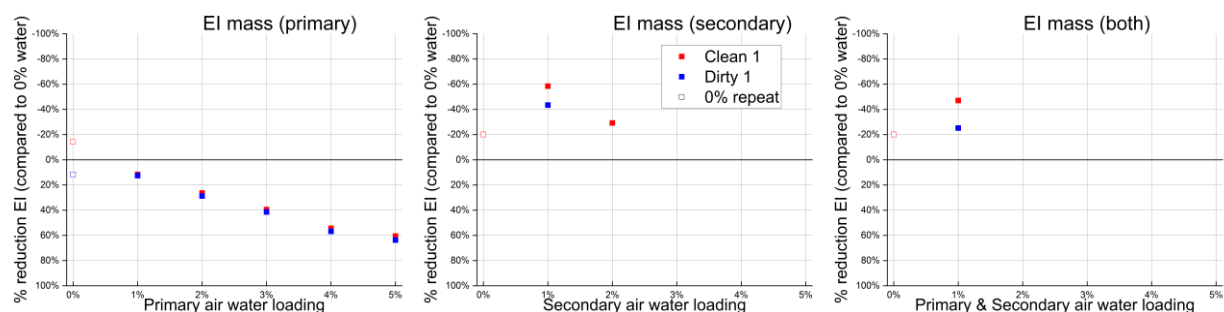


Figure 74: EI mass percentage reduction when adding water (% mass) in the RQL combustor primary air (left), secondary air (centre) and both (right)



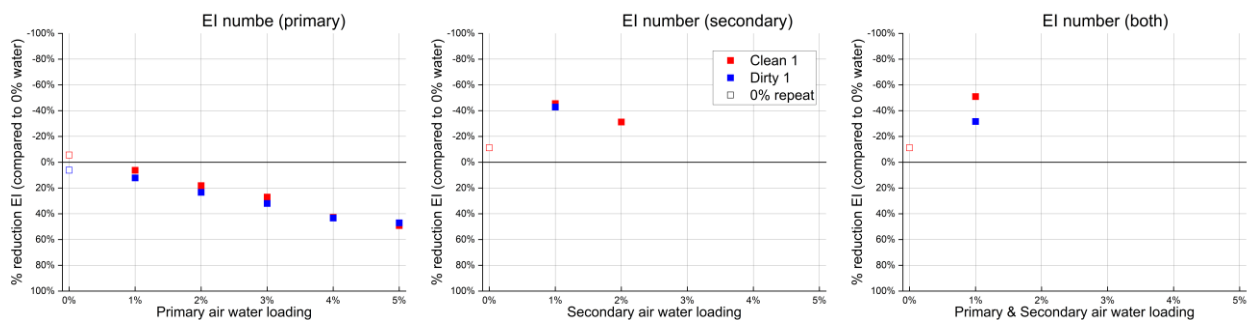


Figure 75: EI number percentage reduction when adding water (% mass) in the RQL combustor primary air (left), secondary air (centre) and both (right)

The testing highlights that increased humidity impacts the formation and oxidation of soot in the combustor with competing effects. As such it appears humidity levels may impact the uncertainty of reported nvPM EI's but this impact will likely be combustion technology dependant hence requires further understanding before a correction could be developed.

## 5.7 Conclusions – Improvements and correction requirements CAEP/12 (WP4.2)

In terms of particle size measurement, it was observed that good correlation could be found across two compliant sampling systems using various sizing technologies with the following findings proposed:

- The Combustion DMS-500, TSI SMPS & TSI EEPS measured similar particle size distributions reporting similar GMD ( $\pm 6\%$  of the mean), GSD ( $\pm 4\%$  of the mean) and shape profiles across a range of sizes and distributions (mono and bi-modal), suggesting that different 'fast' size analysers may be suitable for use in future standards to aid size-based loss correction.
- No difference in SMPS size or total number concentrations were observed with different chargers (X-ray Vs. radioactive source) or using an additional catalytic stripper, after loss correction, demonstrating that radioactive sources which require licenses may not be essential in future standards and that in the case of the RQL combustor rig volatile coatings or nucleated PM did not impact the measured size. However, these findings would also need to be supported on large-scale engines of different technologies before adoption in future standards.
- Size derived number concentrations (EEPS, SMPS and DMS-500) using the relevant loss and size dependant counting efficiency corrections overpredicted the nvPM number concentrations reported by the ICAO compliant number counter systems (AVL APC) by up to 60% after STP correction was applied. The best correlations were achieved by CU DMS-500 during RQL 1 test (2% average difference) and the SMPS during RQL 2 test (16% average difference). It is noted that the 12-month period between the two RQL test significantly impacted the DMS-500 number concentration measurement with the average difference increasing to 26%.
- Size derived mass concentration (EEPS, SMPS and DMS-500) after loss correction overpredicted the measured nvPM mass by approximately a factor 2, highlighting the large uncertainty associated with deriving mass from a particle size measurement, and suggesting the unit density assumption is not applicable to RQL rig soot.



#### Work Package 4: Deliverables Report

In terms of assessment of particle loss correction, using both the regulatory methods offered in ARP 6481 and ICAO Annex 16, Vol II, Appendix 8 and a contemporary method using a bin-by-bin correction of measured size distributions:

- The reported number correction factors obtained using the regulatory method (ARP 6481) diverged significantly from the bin-by-bin size measurement method for GMD < 30 nm, driven largely by the assumption of lognormality and fact that bi-modal distributions were witnessed during RQL 1 test, and by the uncertainty associated with nvPM mass measurement near LOD. This highlights that if the existing ICAO Annex 16, loss methodology is maintained moving forwards that improvements to LOD for mass are likely required. If size-based loss is however adopted this tighter LOD requirement is likely not required.
- The UTRC model was experimentally validated using simultaneous DMS-500 measurements near the sampling probe and by the nvPM analysers. However, particle size measurements performed in diluter 1 vent led to higher measured loss when compared with the UTRC model predictions, suggesting there may be preferential sampling in diluter 1 and/or different loss/dilution.
- Predicted combustor-exit GMD derived from different size instrument technologies (subsequently used to derive ksl\_num and ksl\_mass) was shown to correlate well ( $\pm 3$  nm of the average). Resulting in loss correction factors for both number and mass obtained using particle size measurement (SMPS, EEPS and DMS-500, including at different locations) agreeing well with each other ( $\sim 10\%$  uncertainty for ksl\_num and  $\sim 2\%$  for ksl\_mass) when assessed using the same overall size range.
- Ksl\_num using the bin-by-bin method-2 ranged from 2 – 25 during RQL 1 test when the full-size distribution was used (from  $D_p \sim 5$  nm). Ksl\_num only ranged from 2 – 4 during RQL 2 test when only size distributions >10 nm (at the combustor-exit) was observed. This highlights the requirement for an agreed size range of nvPM for system loss correction, as aerosols with  $D_p < 10$  nm require large ksl\_num factors which when applied to very low measured concentrations at the end of the sampling system, will likely result in high uncertainty.
- Ksl\_mass can also be impacted by the size range selected, with the loss correction factor approximately doubling when including DMS-500 data >240 nm (due to the additional cyclone loss at large sizes).

#### Laboratory and RQL combustor alternative fuel testing highlighted

- Fuels containing higher hydrogen content emit lower nvPM mass and number with reductions of circa 400% for mass and 200% for number predicted across a fuel hydrogen content change of 2% (13.5-15.5%) when normalised to a baseline fuel of 14.5%. Therefore, a Fuel Hydrogen content correlated correction methodology as derived in CAEP/12 is supported for reporting nvPM EI number and mass concentrations. Global correlations highlighted scatter for the RQL combustor tests maybe suggesting correlations may need to consider technology and power variations.

#### Humidity Trials highlighted

- Increased humidity in the primary and secondary zone of the RQL combustor rig displayed competing trends, with reductions of 60% in EI mass and number observed at 5% water by mass in the primary zone and 40% increase in EI mass and number observed at 2% water by mass in the secondary zone. In the case of the RQL test humidity increase in both zones showed an increase in nvPM, but this impact needs to be further assessed given the varying rig temperature.



## 6 Benefits of future technologies and regulation in terms of reducing nvPM impact beyond CAEP/12 (D4.3).

### 6.1 Introduction

Aviation was one of the strongest growing transport sectors before COVID-19 pandemic, with an expected 5% annual growth to 2030 [12], and an expected growth in CO<sub>2</sub> emissions to 3% of global emissions by 2050 [13]. This motivated the aviation industry to invest in developments aimed at reducing their emissions. The COVID 19 pandemic has caused a sharp decline in air traffic volume. There are many hypotheses on how the air traffic will recover in the next years. Gudmundsson et al. [14] forecast that a recovery in passenger volume would most likely take until 2022 or 2023. A more recent forecast by IATA [15] agrees a recovery of traffic levels to the same level of 2019 will occur between 2022 and 2023, but they state that this recovery will be different in different markets, for example, it is predicted the Asia pacific market, will most likely recover earlier due to the large proportion of domestic flights in this region. Boeing forecast [16] estimate that between four and five years are required to recover to air traffic levels of 2019, in a similar way Airbus forecast [17] predict between 2023 and 2025 which is four to six years. Finally, Eurocontrol also predict dates between 2024 and 2025 [18]. Therefore it maybe surmised that the COVID-19 pandemic has only represented a shift of few years in respect previous scenarios, therefore a reduction of emissions must still be a main objective of aviation industry.

Future approaches for emissions reduction include, improved combustion technologies, electric/hybrid solutions, sustainable aviation fuels, hydrogen etc. Hence an assessment of the state of the art of each, and the potential impact in emissions is presented highlighting future scenarios and possible requirements for change in PM certification.

### 6.2 Assessment of nvPM emission characteristics of unregulated engines

Currently, only turbofan and turbojet engines with rated thrust >26.7 kN are certified for gaseous and nvPM emissions. Small turbofan, turbojet, turboprop and turboshaft engines are not emissions-certified. An exception is the smoke number standard which applies to turbojet and turbofan engines of all sizes. Studies of small unregulated engines are lacking in reported nvPM emission characteristics (with actual EIs and particle size distribution data). One of the objectives of RAPTOR was to assess existing data of emissions of unregulated engines with standardised emission measurements. The Swiss nvPM reference system has been utilized in measurements of unregulated engines in on-wing emission tests. Tests of further turboshaft and turboprop engines were foreseen to be performed during the duration of the RAPTOR project, however, due to the COVID-19 pandemic, these tests were postponed to an undefined time frame after project completion. Nevertheless, the tests carried out to date have allowed comparison of nvPM emission characteristics of two unregulated turbofan engines with an ensemble of 21 large conventional cannular and annular turbofan engines, including RQL (TALON and TALON II combustors of large Pratt & Whitney turbofans). The emission tests were performed using SMARTEMIS between 2017 and 2021 in various facilities, providing essential data for the analysis presented below.



## 6.2.1 Particle size distribution properties and nvPM mass and number

The GMD and GSD of the lognormal distribution at the engine exit plane (i.e., corrected for particle losses in the sampling and measurement system) of the large and unregulated engines are shown in Figure 76. The GMD and GSD were determined from the fits of the product of the lognormal distribution and the modelled penetration function (exhaust probe inlet to SMPS inlet). The unregulated engines, shown in red, followed the same trends as the large engines highlighted in grey. As seen the GMD increases with an increasing thrust with maximum values witnessed at take-off. The GMDs ranged between  $\sim 10$  and  $45$  nm, which is inline with data of the large engines in this and other data sets. The GMD trends have a noticeable offset across all power levels, virtually enveloping the data for the large engines. It is noted that GMDs GSDs at  $<30\%$  for one of the unregulated engines could not be determined due to extremely low mass concentrations ( $< 1 \mu\text{g}/\text{m}^3$ ) and the lognormal distribution could not be confidently fitted to the data. The GSDs of the unregulated engines were also found in the range typical for large engines, with most data points between 1.9 and 2.2.

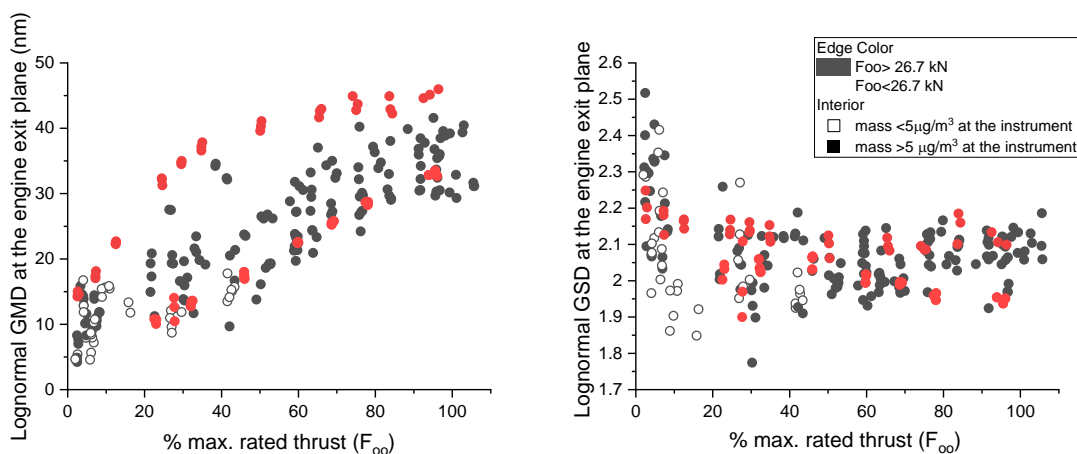


Figure 76: Geometric mean diameter (GMD, left) and geometric standard deviation (GSD, right) as a function of engine thrust. The GMD and GSD were obtained from fits of lognormal distributions and the system penetration function to the SMPS measurement data. The thrust was determined either from direct test cell measurements and correction to standard day or from correlations with the low-pressure shaft speed (N1).

A useful parameter in the analysis of nvPM emissions is the ratio of nvPM number to nvPM mass (N/M, number of particles per mg of nvPM), which varies with GMD, GSD and engine power. The GMD and GSD plotted as a function of N/M are shown in **Figure 61**. The highest N/M corresponds to the smallest GMD, typically found at engine idle. The uncertainty in N/M increases with decreasing mass concentration and is to a great extent affected by the sampling system cleanliness. In this assessment the average effective density was used as a quality control for the validity of the N/M (ratio of nvPM mass to the integrated volume of the SMPS size distributions). The average density is typically in the range from  $\sim 0.5$  to  $\sim 1.2 \text{ g}/\text{cm}^3$ . Densities significantly higher than  $1 \text{ g}/\text{cm}^3$  hint to a system cleanliness problem (e.g., average density of  $6 \text{ g}/\text{cm}^3$  is nonsensical and the data point is an outlier due to failed nvPM mass cleanliness). The GMD and GSD as a function of N/M of the unregulated engines followed the same trends as the large turbfans. The GMD decreased as a function of N/M and the GSD was in a narrow range, independent of N/M (similar to the trends with engine thrust shown above).



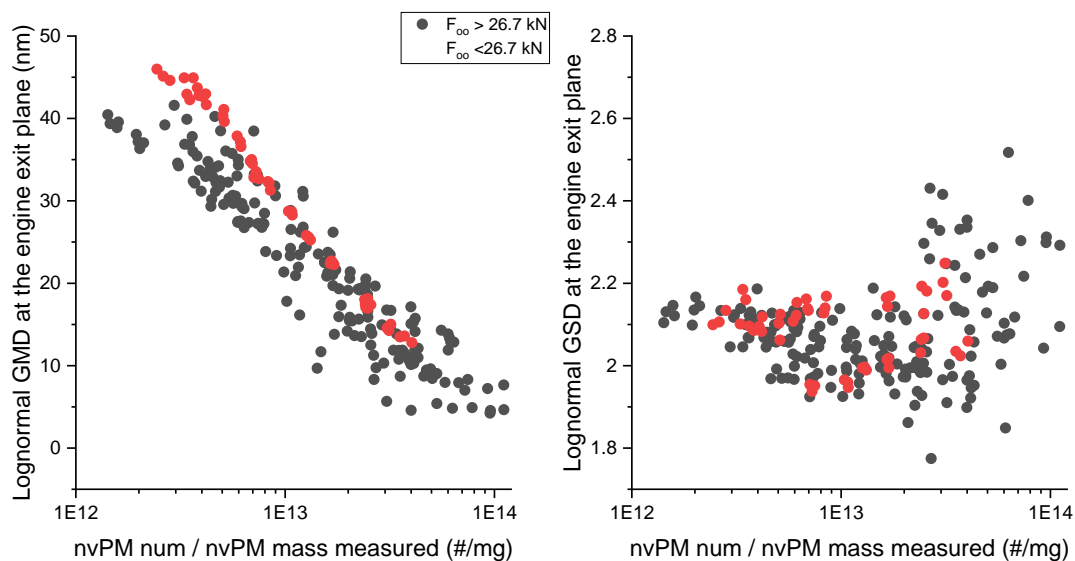


Figure 77: Geometric mean diameter (GMD, left) and geometric standard deviation (GSD, right) as a function of the nvPM number to mass ratio measured (i.e. no system loss correction applied). The GMD and GSD were obtained from fits of lognormal distributions and the system penetration function to the SMPS measurement data.

In terms of the absolute nvPM emission values (without system loss correction), both engines tested were well below the CAEP/11 limits for new and in-production engines (by means of extrapolating the limit lines below 26.7 kN). The nvPM mass emissions were in the range of 300-600 mg/kN and the nvPM number emissions were in the range of  $3E15 - 6E15$  / kN. These results are equivalent to the limit for a new turbofan engine type with a rated thrust of 100 kN (i.e., an engine more than four times the size of the engines tested). Thus, the limited data collected suggest that unregulated engines can achieve fairly low LTO cycle nvPM emissions.

### 6.2.2 nvPM mass – smoke number correlation

Smoke number (SN) has remained an important parameter for estimating nvPM emissions from engines that are not certified for nvPM. A new correlation between nvPM mass SN has been developed from nvPM tests of representative engines. This correlation SCOPE11 [19] is implemented in the latest version of the ICAO Airport Air Quality Manual (ICAO Doc 9889). Figure 78 shows the nvPM mass – smoke number (SN) correlation determined from measurements using SMARTemis on large and unregulated turbofan engines between 2017 and 2021. The engines tested had separate bypass flow and exhaust nozzles as well as mixed flow nozzles (core flow diluted with bypass flow before exhaust sampling). The two unregulated engines had mixed-flow nozzles, which is common for small turbofan engines. The trends of nvPM mass as a function of SN followed the trends found for large engines. Some test conditions produced SN = 0 (no measurable change in reflectance of a filter paper used to collect raw exhaust gas aerosol).





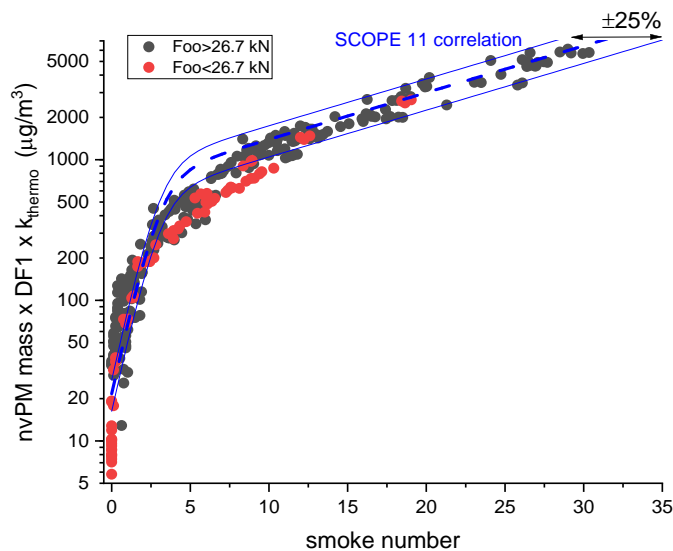


Figure 78: nvPM mass as a function of smoke number for large (grey) and unregulated turbofan engines (red). The blue curve shows the SCOPE11 correlation implemented in FOA 4.0.

In conclusion, the limited dataset for the unregulated engines and a comprehensive dataset for large engines have shown that the unregulated engines tested followed the trends for large turbofans in terms of thrust dependence and magnitude of the nvPM number and mass and PSD characteristics. It is noted that no engines with staged combustors and lean-burn combustors were included. Due to the limitations in engine technology scaling, it is unlikely that lean burn combustion technology will be implemented in small gas turbine engines. The trends in nvPM mass and SN were also in line with the data found for large engines. The absolute values of LTO nvPM emissions indicate that unregulated engines can achieve fairly low LTO cycle nvPM emissions. Future work shall complement these datasets with measurements of common types of turboprop and turboshaft engines. But highlight that prediction of contribution of unregulated engines to total aviation emissions are likely possible by determining total fuel flow from these engines.

### 6.3 Modern low emissions combustion technologies

Over the past 50 years, the aviation industry has improved engine technology to reduce specific fuel consumption and emissions. Until the 1970s the main focus was the development of engines which operated at higher overall pressure ratios (OPR) and turbine entry temperatures (TET). In this way an increase in thermal efficiency resulted in a reduction of fuel consumption. This reduction has resulted in a net reduction in CO<sub>2</sub> emissions proportional to the total amount of burned fuel. However, higher combustor inlet temperatures and pressures lead to an increase in NO<sub>x</sub> emissions [20]. In 1986 the International Civil Aviation Organization (ICAO) started to apply a standard to all in production engines (CAEP 1), since then, this regulation has evolved to an ever more strict standard; up to the next CAEP 13 cycle. The introduction and tightening of successive regulations has motivated the development of low emission combustors towards reduced NO<sub>x</sub> and smoke emissions from aircraft engines. As discussed earlier, It is noted that full regulation is only applied to engines > 26.7kN of sea level static rated thrust [21]. There are a large number



of technologies that have/are being developed to minimise emissions of aircraft engines, which are summarised below covering technologies already at TRL 9 to technologies currently at lower TRLs.

### 6.3.1 Rich-Burn Quick-Quench Lean Burn (RQL)

In RQL the combustion is in first place done in fuel-rich conditions (primary zone). Having a rich combustion helps to enhanced combustion stability and a reduced NO<sub>x</sub> production owing to a relatively low flame temperature and low concentration of oxygen containing species. Conversely, the resulting concentration of CO, Unburned Hydro-Carbons (UHC) and soot in this zone is high [22]. To solve this, dilution airflow is used in a quench section to oxidise soot, CO, hydrogen and hydrocarbon intermediates. This addition, if not correctly controlled, has the drawback that the equivalence ratio can fall to near stoichiometry, resulting in further formation of NO<sub>x</sub>. To avoid this, the mix of dilution air and primary zone exhaust has to be fast, so the switch between the rich and lean burn is quick enough to minimise the formation of thermal NO<sub>x</sub>. This process is then followed by the lean burn section being employed to further consume unburned CO and UHC.

RQL combustors are used in a wide range of engines. Pratt and Whitney developed their RQL combustor family TALON. The first generation (TALON I) was used in PW4098 engine (1999) [23]. The second generation, TALON II, was introduced in the PW6000 engine (2005) and achieved further emissions reduction [23]. The latest version of this combustors, TALON X are used in different PW engines and have demonstrated a NO<sub>x</sub> reduction of 25% compared to TALON II combustors in both engine and rig testing [24]. Rolls-Royce and CFM international have also developed RQL combustors in their respective Trent 1000 and CFM56 series. In terms of NO<sub>x</sub> emissions, RQL technology from different companies produce similar NO<sub>x</sub> EI's respective of their OPR [20]. However, RQL technology has higher soot production compared to lean burn technology, but recent RQL developments by Rolls Royce and Pratt and Whitney sufficiently control the production of soot to regulatory standards. Thus, RQL is still a viable approach for current engines, which with future adoption of SAF could be low in terms of both NO<sub>x</sub> and PM.

### 6.3.2 Double Annular Combustor (DAC)

In double annular combustors, combustion zones are distributed in two concentric rings, this allows a radial staging strategy. At low power settings, the combustion zones used are those in the outer ring, known as the pilot zone. In this way, equivalence ratio rises towards stoichiometric and combustion efficiency increases, reducing CO and UHC. In addition, the locally high combustion equivalence ratio reduces the risk of combustion instability. At higher power settings, the combustion zones in the inner ring are used in addition to the pilot, commonly termed the main zone. The equivalence ratios for both zones are usually kept at 0.614 to have a lean combustion required to control NO<sub>x</sub> and soot production. For intermediate regimes, only a part of the main zone is operative.

CFM international used this technology in CFM56-5B, 5B/P, and 7B engines (1995–1998). General Electric also uses this technology in the GE90 (1995). Normally this type of low emissions combustor is used in engines in medium and large categories with rated thrust in the range of 102.2- 504.9 kN [27]. In general, all the DAC versions yield a similar trend for NO<sub>x</sub> emissions. As engine OPRs increase NO<sub>x</sub> emission levels increase. Overall DAC exhibits lower NO<sub>x</sub> emissions compared to RQL combustors. However, for high OPRs NO<sub>x</sub> emissions produced by DAC start to be close to CAEP/6 limits, the situation is similar for CO, with a good performance in low OPRs but higher emissions for high OPRs [28]. One of the possible reasons behind this observation may be the need of a higher cooling flow to the larger surface area resulting from the



## Work Package 4: Deliverables Report

annular configuration, resulting in less air for lean combustion. The UHC emissions yield similar trends. Regarding soot emissions, these are generally lower than RQL combustors with smoke numbers generally below 6, with a very small variation with OPRs.

### 6.3.3 Axial Staged Combustor (ASC)

The ASC have a similar working principle to the DAC, with the exception that staging is done through the fuel injection zones and placed in the axial direction. In this case the pilot zone is situated upstream of the combustor, while the main is downstream. The equivalence ratios are similar to those employed in DAC for different power conditions. One of the main differences with DAC is that the pilot and main zones have two separate fuel delivery systems.

The first ASC combustors were used in the IAE V2500 engine. Pratt and Whitney developed an ASC combustor in the frame of NASA program ERA to be used on engines with high bypass ratio and higher OPR.

A reduction of around 40% in NO<sub>x</sub> emissions can be achieved by ASC in LTO cycle, and up to 50% reduction in cruise regime. For example, a comparison between a baseline V2500 engine and an axially staged model [29] shows a reduction of 43% for NO<sub>x</sub> emission index for take-off regime. Regarding CO emissions, while the idle CO emissions are reduced 62% compared to the baseline system, for other LTO cycle points the emissions can be up to a factor of 10 higher than those produced by the baseline engine. A test comparing a Pratt and Whitney ACS and TALON X combustor performed at NASA Advanced Subsonic Combustion Rig (ASCR) [30] shows very low NO<sub>x</sub> emissions for the LTO cycle from ACS compared to TALON X, being 88% less than CAEP/6 limits. Furthermore, UHC and soot emissions were also well below those produced by TALON X. The only drawback was CO emissions that, overall, were higher than those produced by the TALON X combustor.

### 6.3.4 Twin Annular Premixing Swirler combustor (TAPS)

The TAPS configuration is similar to the conventional single annular combustor (SAC). The main difference is the fuel injector heads in a TAPS engine afford an internally staged partially premixed technology, utilising pilot and main stages which are concentrically mounted. The pilot uses a simplex atomiser to spray the fuel in an air-blast mode between two axial air streams. The fuel spray interacts with the surrounding co-rotating or counter rotating swirl to generate a pilot recirculation zone which stabilizes the pilot flame. The pilot only mode maintains sufficiently high combustion efficiency and stability at low power (from ignition to idle). At higher power, the main is turned on and the main flame is stabilized in the mixing layer between the pilot and main. The small recirculation zone produced is key to stabilisation of the main flame as it stores radicals from the pilot combustion [31].

General Electric and NASA started the development of the TAPS in 1996 [32], the early development efforts involved the technology demonstration in General Electric DAC engines. Then, in the early 2000's, the development focus was shifted to the SAC versions of TAPS. The SAC TAPS was tested in a CFM56 7-B engine and then transitioned to the GEnx series of engines. It entered into service in 2010 and was used in the Boeing 747-8F and 787 [33]. The first emissions certification data for GEnx TAPS including 13 models was published in 2009. After the successful integration of TAPS combustors to larger engines, General Electric and the Federal Aviation Administration (FAA) launched a program for scaling TAPS technology, namely TAPS II, for narrow body applications. TAPS II is implemented as a part of LEAP engine for powering the



#### Work Package 4: Deliverables Report

COMAC 919, Airbus A320 NEO and Boeing 737 Max [34]. TAPS has also been applied to power different classes of thrust and OPR engines including the GE-Passport, powering Bombardier Global 7000/8000 business jets.

The TAPS II combustors achieve remarkable NO<sub>x</sub> emission reduction levels [27]. The margin from the CAEP/6 standard ranges between 40% and 60% depending on the OPR. Regarding soot emissions, TAPS II presents a peak of emissions at 30% LTO regime, with a smoke number of 4.2, but above this point, smoke number was not measurable.

### 6.3.5 Lean Direct Injector (LDI)

In LDI combustors, the fuel is directly injected into the chamber and quickly mixes with a large fraction of air. In this way the peak flame temperature at medium/high power can be reduced if fuel and air are mixed before the reaction is completed [35]. Like TAPS, LDI combustors present an internally staged singular annular configuration. Pilot and main are mounted concentrically. The pilot and main flow fields are separated by a splitter, causing a bifurcated flow field, leading to the separation of pilot and main flames. At low power, only the pilot is used and the flame is stabilised in the bifurcated flow field to assure the combustion efficiency and stability. As power increases, the main fuel is injected into the main bifurcated flow field, leading to rapid fuel evaporation and low residence time to produce low NO<sub>x</sub> emissions. As power is increased, the fuel flow is transferred from pilot to main. At powers from cruise to full power, approximately 10% of the fuel enters into the pilot and 90% goes to main [36].

Rolls Royce is using the LDI concept in the development of ALECSys engine. Limited emissions data is available for this combustor because it is still under development with the current TRL < 9. As such there is no ICAO certified data yet reported. The NEWAC report [37] claims that a 70% reduction of NO<sub>x</sub> emissions relative to CAEP/2 is attained by this technology. Indeed, the engine testing for the E3E core that fits LDI combustor indicated NO<sub>x</sub> levels in the region of 35% - 45%, relative to CAEP/6, which shows a 30% - 35% reduction compared to rich burn [38]. ALECSys launch is planned in 2025.

### 6.3.6 Lean Premixed Pre-vaporised (LPP)

In LPP technology the fuel is first vaporised and then mixed with the air flow to create a homogeneous mixture before entering the combustion zone. NO<sub>x</sub> emissions are drastically decreased due to the low flame temperature and the elimination of hot spots from the combustion zone. LPP combustors consist of three regions, whereby the first is dedicated to fuel injection, vaporization, and fuel-air mixing; the second is dedicated to combustion, where the flame is stabilized in the recirculation zones and the third that is dedicated to dilution.

The concept of LPP started to be developed in the early 1970s under the NASA Experimental Clean Combustor Program (ECCP) program. One of the first concepts for LPP was proposed by General Electric and consisted of a radial/axial staged combustor with a premixing main stage. Later, General Electrics and Pratt and Whitney continued to develop the concept of LPP under NASA HSCT program in the 1990s, resulting in two LPP concepts: the LPP Stepped Dome (SD) concept and LPP Multi-stage Radial/Axial (MRA) concept. Both employ fuel staging architecture with cyclonic pilots and premixing tubes. The major difference between them is the layout of the staging zones: in the stepped dome arrangement at least one of the annular sections of the dome is recessed in respect to the other. This helps to isolate the pilot from



the other injectors to decrease CO and UHC emissions that are problematic at low powers. LPP MRA was selected for the final development considering the advantages over SD with respect to fuel nozzle manufacturability, reliability, cost and weight, etc. [39]. More recently, the LPP concept has been developed by Turbomeca (Safran Helicopter Engines) under the European New Aero Engine Core Concepts (NEWAC) program. Limited information is available regarding emissions for LPP combustors developed in the NEWAC program, but a NO<sub>x</sub> reduction of 57% versus CAEP/2 limit has been validated on a full annular combustor test at LTO cycles [39].

### 6.3.7 Variable Geometry Combustor (VGC)

The overall approach of VGC is to control the combustion stoichiometry in the primary zone by regulating the air flow through a variable geometry control system. The air flow splitter is driven by a hydraulic system and moves forward and backwards to vary the air flow ratio into the primary zone. At lower power conditions, the degree of opening of the splitter increases the quantity of air diverted backwards to create a high primary fuel to air ratio (FAR) whilst reducing flow velocity for high combustion efficiency and improved stability. As power is increased, the splitter opens, introducing more air into the primary zone to achieve lean combustion, reducing NO<sub>x</sub> and soot emissions.

The variable geometry concept has not been matured and therefore has not been currently applied for aero engines. This is mainly due to the high cost and weight of variable geometry systems.

## 6.4 Sustainable Aviation Fuels (SAFs)

### 6.4.1 Drop-in SAFs

To complement technological improvements of combustors, the aviation industry seeks carbon neutral synthetic aviation fuels that help to meet long term net-zero emissions goals [40]. Given, Hydrocarbons will always release CO<sub>2</sub> no matter how efficient, this is the only possibility of achieving this goal even when considering step changes in combustor performance. In addition, fossil fuel is a geopolitical resource of great importance, as can be seen in the current conflict on going in Ukraine. Therefore, having the possibility of producing synthetic fuel, independent of foreign fossil fuel sources assists with future security of supply issues. Producing a substitute for standard jet fuel is challenging, not only it has to fulfil a certain number of performance properties such as net heat of combustion, thermal stability, viscosity, distillation curve, freezing point, flash point, smoke point, density, lubricity, aromatic content, sulfur content, etc. [41] but Jet fuel is not only used for combustion in the aircraft. Fuel is used to exchange heat with the oil, to power fuelhydraulic actuators, and to lubricate pumps [42]. In addition, the nitrile seals used in older aircrafts (but still used in the current fleet) are sensitive to fuel composition, and they need a minimum presence of aromatic compounds to avoid shrinkage and fuel leaks [43]. So future synthetic fuels must also satisfy these functionalities. This is the so called drop-in fuel concept, whereby, a given fuel can be used in the current fleet without the requirement to introduce any modification to existing aircraft. So far, the industry has focused on the development of synthesised aviation fuels with maximum blend limit percentages with standard jet fuel to allow their use as a drop-in fuel, and it is noted that not all synthesised fuels which are approved for blending have the potential of being used without blending. The aviation industry is moving toward the use 100% synthesised aviation fuels that also meet sustainability criteria, known as Sustainable Aviation Fuels (SAF) as is illustrated by ongoing test programs which are utilising 100% SAF such as ECLIF (DLR) or VOLCAN (AIRBUS).



## Work Package 4: Deliverables Report

The landscape of synthetic fuels, in aviation, has significantly evolved since approval by the American Society for Testing Materials (ASTM) of synthetic fuels in 2009, namely Fischer-Tropsch Synthetic Paraffinic Kerosene (FT-SPK). FT-SPKs are approved for commercial use in a blending ratio up to 50 % with Jet A-1, in this case the lack of aromatic compounds of FT-SPK mean they cannot be used as a drop-in fuel at 100 %. Hydro processed Esters and Fatty Acids (HEFAs), which produce synthetic paraffinic kerosene from vegetable oils or animal fats, were approved in 2011 and also require blending (up to 50 %) with conventional Jet A-1 and, as in the case of FT-SPK, cannot be used at 100% as a drop-in fuel due to the lack of aromatic compounds. In June 2014, the certification body ASTM also approved the Hydro processed Fermented Sugars Synthetized Iso-Parafins (HFS-SIP) pathway. The process to obtain this fuel uses saccharides (C5 and C6 sugars) originating from different feedstocks for fermentation by yeasts directly creating hydrocarbons. This fermentation product is then converted by a standard chemical process into farnesane which can be blended as a biobased jet fuel component up to 10 % with Jet A-1 fuel. In this case, the fuel not only lacks aromatic compounds, but also the distribution of paraffin is different to those found in Jet-A1, so there is no option of using it as a 100% drop-in fuel. In 2015 a new pathway based on the Fischer-Tropsch process was approved, namely the Fischer-Tropsch Synthetic Kerosene with Aromatics (FT-SKA) route, with blend ratios up to 50% permissible. This is the first synthetic fuel that has the potential of becoming a true drop-in fuel to 100%, since its chemical composition is identical to that of Jet A-1. In 2016, Alcohol-to-Jet Synthetic Paraffinic Kerosene (AtJ-SPK) was approved with blends up to 50%. AtJ-SPK fuels are a blend of hydro processed synthesised paraffinic hydrocarbons wholly derived from iso-butanol processed through dehydration, oligomerization, hydrogenation, and fractionation. As for other SPK fuels, the lack of aromatic compounds and a paraffinic profile differing to that of Jet A-1, means again it does not have the potential of becoming a 100% drop-in. Recently (2020) two more pathways have been approved by ASTM, namely, the Catalytic Hydrothermolysis Jet (CHJ) and Hydro processed Hydrocarbon synthetic Paraffinic Kerosene (HHC-SPK). CHJ uses processed waste oils or energy oils to produce clean free fatty acids which are cracked, isomerised, and cyclised into paraffin, isoparaffin, cycloparaffin, and aromatic compounds. CHJ approved blend ratios of < 50 % are permitted, but it has the potential to become a 100% drop-in fuel, due to its identical composition to Jet-A1. HHC-SPK uses biologically derived hydrocarbons such as algae to produce the synthetic paraffinic kerosene. It currently has an authorised blend ratio of 10% and as other SPKs is not possible to use as a 100% drop-in fuel.

The existing synthesized fuels that are blended to Jet A-1 are not necessarily sustainable, as environmental, social, and economic performance requirements are not part of ASTM qualification. The ICAO Carbon Offsetting and Reduction Scheme for International Aviation (CORSIA) [44] evaluate production, feedstock, land-use, social impact, and life-cycle carbon footprint of various possible paths, and consider relevant environmental, social, and economic risks that fuels certified as sustainable under this process are labelled as SAFs. The synthesized fuels complying with ASTM D7566 can be made according to sustainability criteria to become SAF.

The use of SAF in aviation is rather limited. The first commercial flight using biofuel was performed in 2011 by KLM. The situation from a research point of view is similar; studies dealing with aviation biofuel emissions are scarce. Corporan et al. [45-47] and DeWitt et al. [48] reported a reduction in Particle Matter (PM) emission when FT fuel was used in substitution of standard jet fuel. However, these studies were performed on engines that were not representative of those present in the current commercial fleet. Timko et al. [49] studied the performance of FT fuel in a CFM56 engine, one of the most common in the current commercial fleet, reporting a reduction of PM when using FT fuel especially in low engine regimes. NASA performed a specific measurement campaign to study alternative fuel performance, the Alternative Aviation Fuel Experiment (AAFEX) [50], during which FT and HEFA fuels were tested [51]. The results were similar to those



#### Work Package 4: Deliverables Report

found by Timko et al [49]. In a recent work, Moore et al. [52] reported a reduction of up to 50% on PM emission at cruise conditions, for a 50/50 blend of HEFA fuel and standard jet fuel during the ECLIF program. In all cases, studies were focused on the physical characterization of the PM (size, number and mass) not on their precise chemical characterisation.

If studies of drop-in SAF blends are limited, the studies using 100% SAF are rare. These tests are limited either to use in relatively modern engines where nitrile seals have been replaced with better performing fluorocarbons and fluorosilicone seals affording the use of 100% non-drop-in SAFs can be used or to use FT-SKA or CHJ SAFs. In 2016 ARA reported the first flight of a military aircraft on 100% CHJ [53]. Airbus reported a test flight of an A350 with 100% HEFA SAF in March 2021 [54]. United airlines also performed a commercial flight in December 2021 with one engine using 100% SAF [55]. Rolls Royce have also performed tests with 100% SAF fuel in their newest business aviation engine in development, the Pearl 200 [56]. To the authors knowledge there are no reported emissions for the test flights using 100% SAF, they were performed as a concept demonstration. Nevertheless, trials recently performed as part of the ECLIF and VOLCAN projects measured emissions from engines using 100% SAF. Results are not currently public available, but preliminary results undertaken by RAPTOR researchers during the VOLCAN test on a LEAP engine using 100% HEFA SAF suggest an important reduction in nvPM emissions.

### 6.4.2 Non-drop-in Hydrogen

Nowadays there is growing interest in hydrogen as a solution to decarbonising aviation. Hydrogen has a specific energy that is 2.8 times higher than jet A-1. However, due to its low density, hydrogens volume based energy density is much lower, making that the use of gaseous hydrogen impossible for aviation. When liquified hydrogen has a volumetric energy density only 4.1 times lower than jet fuel, making it an interesting option as fuel. The main drawback is that liquid hydrogen must be kept at temperatures of 20 K, making its use in aviation challenging.

One potential solution to this problem is to use a hydrogen carrier such as ammonia. Ammonia combustion is not a new concept, the first investigations of ammonia combustion date back to the 1950s. Elbaz et al. [65] recently published an extensive review concerning ammonia combustion summarising recent advances in this field. The main conclusion of the review is that the direct use of ammonia as fuel can be reliable but there are many points that need to be solved, like toxicity, high ignition delay time, narrow flammability limits and high NO<sub>x</sub> production.

Hydrogen can also be used in fuel cells, to generate electricity that can be used by an electric engine. This has been called the true zero solution [66], since with the exception of water vapour the emissions would be zero. In the case of using liquid hydrogen combustion, even though CO, CO<sub>2</sub>, UHC and soot emissions would be irradiated, there is still the potential to produce NO<sub>x</sub> and a large quantity along with water, which can produce contrails, diminishing the reduction on impact gained by using hydrogen.

In 2022 airbus launched their ZEROe demonstrator [67] aiming to test hydrogen combustion technology on an A380 multimodal platform by 2025. CFM international will collaborate in the development of this demonstrator. They aim to use not only hydrogen combustion, but also to combine it with hydrogen fuel cells. It is probably too soon to anticipate what will happen in the future with current concept designs of hydrogen aircrafts, but what currently seems apparent is that initially the use of hydrogen will be limited to regional scale. One of the key points for successfully integrating hydrogen combustion in aviation will be the availability of green hydrogen, with a future switch from current production of blue hydrogen to a production based on renewable energies.



## 6.5 Electric powered aircraft

Another approach to reduce aviation emission is the use of electric powered aircrafts. Electric propulsion systems do not generate on-board emissions. However, the specific energy of electrical energy storage sources, such as batteries, is much lower than that of fossil fuel. Without an important breakthrough in energy storage, aircrafts using 100 % electric propulsion systems can and will not achieve similar flight range/endurance as currently offered by combustion powered aircraft in the foreseeable future. This fact is why most current effort in 100% electric aircraft has been focused on personal or small size aircrafts. Among others, one example is Lilium jet a small aircraft that uses multi-distributed electric propulsion. A first test flight of the demonstrator was conducted in 2019 and a new flight test campaign started at the beginning of April 2022 in Spain [57]. As 100% electric aircraft will not likely play a major impact in the near-future intercontinental fleet, further details of this concept are not offered in this report.

Due to limitations of 100% electric aircrafts, the concept of Hybrid Electric Propulsion System (HEPS) have recently gained attention as a solution for, at least, regional scale aircrafts. HEPS integrates an electric powertrain with a conventional combustion engine to provide the propulsion, combining the zero emission properties of electric engines with the extended range of internal combustion engine (ICE). The concept results in decreased fuel burn compared with ICE-powered aircraft, and increased flying range compared with electric aircraft. For these reasons, there is a significant interest in further research into this area by the aviation industry. However, those advantages come at the cost of increased complexity of the system design and hybrid energy management.

An HEPS combines both fuel and battery concepts, there are different configurations available as summarised below.

### 6.5.1 Series configuration

In a series hybrid configuration, the propeller is driven only by the electric motor [58]. The engine power derived from combustion is converted into electrical power via a generator. The electrical power can be used to power the electric engine directly or can be stored in the battery by a charging process. This system is the one most easily extended to distributed electric powertrain, so is the best suited to hybridise multi-rotor aircraft and large-scale airplanes. The advantages of a series hybrid configuration is that the engine is completely decoupled from the propeller and its output power is not related to the power demand of the powertrain. In other words, the engine can run at its optimal operating condition during the different working condition. The series architecture has the additional advantage of flexibility for locating the internal combustion engine owing to the mechanical decoupling. The main disadvantage is power loss in the combustion and electrical energy conversion. Another drawback is the need of three propulsion devices: engine, generator, and electric engine. Finally, series architecture cannot make use of the maximum combined power potential of the internal combustion engine and electric engine, since the internal combustion engine is not mechanically connected to the load.

### 6.5.2 Parallel configuration

In parallel configuration, the internal combustion engine and the electrical engine are both connected mechanically to the propeller, so they can contribute to the propulsion energy either simultaneously or individually [58]. The internal combustion engine can also drive the generator, charging the battery. One advantage over series configuration is the need of only two propulsion devices. This configuration allows the use of a smaller engine for the same performance [59]. The power losses are also reduced compared





#### Work Package 4: Deliverables Report

with the series configuration, since there is no need for a mechanical - electrical energy conversion. One of the problems of this configuration is that the rotational speed of propeller is not always the optimal speed of the engine, so operating at the optimum region of engine cannot be guaranteed. This problem can be solved in two ways, using a Continuously Variable Transmission (CVT) to decouple engine and propeller rotational speeds, or develop an energy management strategy, which optimises the power contribution of the internal combustion engine and the electrical engine.

This configuration can also be classified in function of the position of the electric engine in the drive train [60]. When applied to aircrafts, the two most used architectures [61] are single shaft; when the internal combustion engine is connected to the electric engine but not directly linked to the propeller, and double shaft, when the internal combustion and electric engines are mounted in two separate drive shafts.

### 6.5.3 Series - Parallel configuration

A Series - parallel configuration, is a mixture of the series and parallel configuration. In this case, the propeller, engine, motor and generator are connected to a planetary gear. In this way the power distribution is more flexible and also both engines can work in their most efficient region. Despite these advantages, the need of complicated gearing and energy management, make this configuration the least likely to be included in hybrid aircrafts.

The development of HEPS in aircrafts covers all sizes, from small to large aircrafts. In principle, the category which may most impact the actual fleet is the large-scale hydric airplanes. These aim to replace traditional planes in the regional scale, hence in this report these will be focused on in this category.

Delft University of technology has conducted different theoretical studies linked to the use of hybrid systems in regional planes. They designed a hybrid regional aircraft based on the ATR 72-600 with capacity for 68 passengers. The wing area for the concept regional plane was 18% larger than the reference one. The study assessed a potential reduction in fuel consumption and emissions, but this was highly dependent on the flight range [62]. In 2017 Airbus, Siemens and Rolls Royce started a collaboration to develop a hybrid electric plane, the E-fan X program, the idea was to use a BAe 146 plane, and substitute one of the four turbofans with a Siemens electric engine. Unfortunately, due to the COVID 19 crisis, this program was abandoned in 2020. NASA is also working on their own concept plane the N3-X. This introduces a new concept of HEPS, namely turboelectric distributed propulsion. This consists in a hybridisation of a turboshaft engine and distributed electric power train in a series configuration. Zunum aero, a company backed by Boeing, started the development of their version of a hybrid regional plane, reaching an agreement with Safran Helicopter Engines to use their Ardiden 3 engine as the internal combustion engine. However, in 2018 economic problems forced Zunum aero to stop this development. Despite these problems, hybrid electric planes are still being developed [64]. In any case, the future of hybrid technologies will most likely come in the form of a small internal combustion engine, e.g. an adapted helicopter engines, as planned by Zunum aero. Nowadays engines below 26.7kN of sea level static rated thrust are not included in certification, mainly due to their relatively small contribution with respect to larger engines of the fleet. But if hybrid electric planes become an option for regional flights, their use may increase making the case for the requirement for their certification as discussed previously.



## 6.6 Future Total PM Regulation

Recent EU funded programmes such as AVIATOR are highlighting that regulated nvPM is only a subset of the total-PM witnessed from aircraft engines downwind of the aircraft, resulting from the condensation of volatile precursors as the hot exhaust dilutes and cools and the entrainment of vented lubrication oil. As such as SAF and low emissions engine technologies are more widely adopted, it is perceived nvPM emissions will reduce requiring potentially new PM standards to ensure air quality standards.

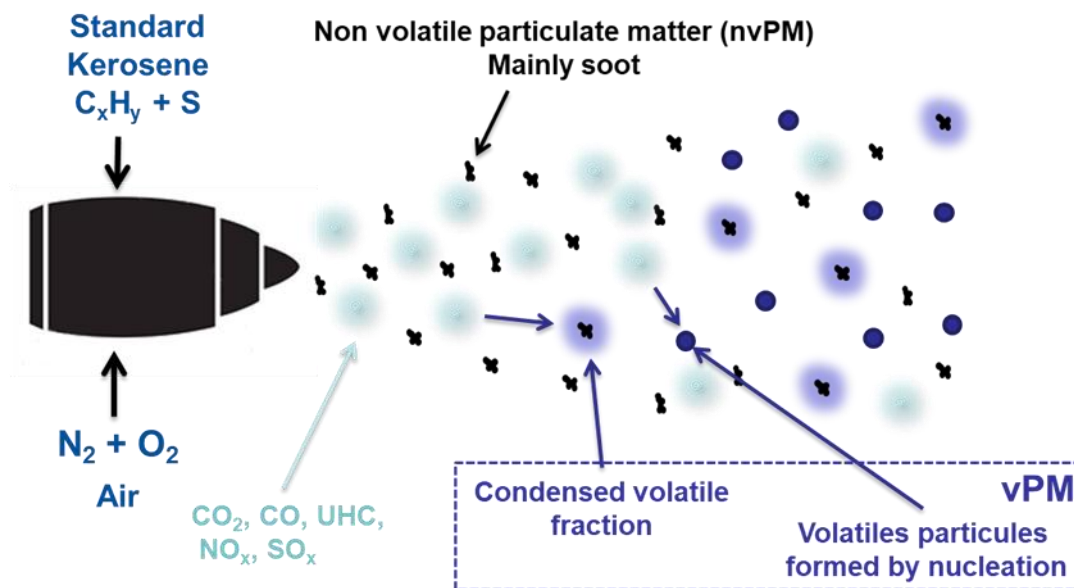


Figure 79 Schematic representation of plume evolution

Total-PM refers to all Particulate Matter resulting from emissions from an engine. As seen in **Figure 79**, this is a combination of the nvPM and the volatile fraction vPM. As the exhaust of the aircraft cools, the gaseous species in the plume cool and condense or nucleate to form the volatile fraction. The vPM can either condense onto the soot (nvPM) mode or nucleate the form new particles in the smallest size range (<20nm). This secondary process, unlike the production of the primary nvPM, is a dynamic one, and one that depends on not only the engine emissions, but also the ambient conditions .

New particle formation will compete with volatile matter condensation on pre-existing aerosol, known as condensational sink. So one key parameter will be emitted nvPM number and how fast the plume is diluted. Another extremely important parameter is temperature, nucleation rates are directly linked with evaporation rate of the first molecular clusters formed by collision of gas molecules [68] this evaporation rate will depend on the stability of these molecular clusters and on temperature. The higher the temperature the higher the evaporation rate, and less likely that the molecular cluster survives to reach the critical size required to become a particle. Thus, the nucleation mechanism found at ground and cruise level might be different.

Sulfuric acid formed in the engine exhaust seems to be linked to the formation of volatile particles by nucleation. However, the amount of sulphur present in the fuel converted to sulfuric acid in the exhaust is too small to explain the number of particles observed [69]. Chemi-ions and organic compounds emitted by the engine are one of the most suitable candidates to explain new particle formation in the engine exhaust



## Work Package 4: Deliverables Report

[70], but the molecular mechanism behind this phenomenon is still unknown. Most likely these mechanisms will be similar to those observed in the atmosphere, like highly oxygenated molecules (HOMs) nucleation [71-72] or nitric acid-ammonia nucleation [73], which can be important especially at cruise conditions.

The secondary material, the total-PM, can become the dominant number and mass in advected plumes. Timko et al., [74-75], estimated that the number concentration of particles increased by one to two orders of magnitude, whilst Stettler et al., [76] estimated that organic carbon (OC) and sulphate (SO<sub>4</sub>) accounts for 53% of the total PM 2.5 mass emitted from airports.

The vPM components from the exhaust plume may not be externally mixed. Wong et al., [77] modelling total-PM from vPM formation at low thrust in the near field, found that the nucleation mode consisted of a sulphate core coated with organics. Similar results were reported by Peck et al., [78]. The percentage mass of SO<sub>4</sub> in the nucleation mode decreased with increasing ambient temperature, whilst conversely, the percentage mass condensed on the soot mode increased. For the organics, the total mass in both modes decreased with increasing ambient temperature. Previous modelling work by Wong et al., [79], suggests that the majority of the organic deposition on the soot mode occurs as the plumes cools, before dilution dominates.

Not all studies agree that the nucleation mode is SO<sub>4</sub> or organic coated SO<sub>4</sub>. Yu et al., [80] found near 100% organic nucleation mode particles, with similar results reported by Timko et al., [74]. It has to be noted that the composition of nucleation particles of the diameter reported by Yu et al. [80] will mostly provide information of which compounds are responsible of the growth of the particles from critical clusters size (around 1.2 nm) to the detected size, but does not necessarily provides information of the compounds responsible of critical cluster formation, on other words, even with a composition close to 100% organics, therefore it cannot be ruled out that that other molecules, for example sulfuric acid, are responsible for the first steps in nucleation.

Combustion by-products are not the only source of vPM formation. The contribution of oil has been well documented. The work Yu and colleagues at Aerodyne Research Inc. have led the field in this research [80 & 81]. Oil can constitute small to 100% of the vPM contribution to the total-PM in advected plumes. Different manufacturers have different approaches to removing vented oil, either ejecting in the core, bypass or overboard. The different modes of venting impact what phase the oil enters and mixes with the exhaust plume.

### 6.6.1 Sampling Methodology

Sampling of PM from aircraft engines involves very complicated sampling systems, with long sample lines and dilution, neither of which are ideal for nucleation mode PM transport. Whilst the ICAO nvPM sampling system was not designed to sample total-PM, several studies have succeeded in using the system [82-84], the authors were able to sample from near engine exit plane distances (~4m) and attribute signatures from different contribution factors to the organic plume. They found contributions from unburnt Jet fuel and, a semi-volatile fraction present at low powers (low engine temperatures). These factors were compared with ambient work of Timko [49] on advected plumes, which showed some similarities, providing evidence that the ICAO system may be suitable for total-PM measurements of the coated soot mode.

The work also sampled the emissions of a developmental combustor rig. The rig had a large quench air system, and this caused a third factor to be detected contributing to the total-PM, a low volatility fraction. This quenched air organic fraction was seen on another prototype combustor using high quench air.



## 6.6.2 Fuel Effects

The effects of fuel hydrogen content and nvPM has become well established [5, 45, 46,47,49 &52]. vPM and fuel properties is highly uncertain. Williams et al., [84], sampling an APU running on alternative fuels at various distances, found at high power, the organics mass spectra all appeared similar. At 10m, differences in the organics were reported for the different fuels, but not related to any fuel property. Recent analysis by Smith [85], sampling 9 different fuels on an open source RQL combustion rig, and using the ICAO nvPM sampling system, was not able to detect any difference between fuel types and measured vPM. This may have been due to sampling at exit plane of the combustor and not an advected plume.

## 6.6.3 Impacts on communities

The effects of total-PM on local communities has been documented. Hudda et al., [86] presented data of elevated levels of ultra-fine particles up to 18km from LAX, peaking in the 10 – 17nm size range. Similar results from Masiol et al., [87] also showed the influence of Heathrow in central London with the presence of <20nm particles. However, few studies have attempted to quantify the chemical composition of these small particles. The convention wisdom has been that these particles are dominated by sulphate nucleation, being too small to be the nvPM emitted by the engines. Ungeheuer et al., [88] using novel filter analysis techniques, determined that all of the ultra-fine particles <50nm measured downwind of Frankfurt airport were from lubrication oil.

## 6.6.4 Road map moving forward

Measurement of vPM in the exhaust of aircraft engines is challenging, especially the vPM coming from nucleation. Condensation and nucleation occurs once the plume is diluted and cooled down, and this process is key for the formation of vPM. Therefore, measuring at the exit plane of the engines, as is done in certification process, is not the best way to study vPM. So the best approach is to measure at a certain distance behind the engine, however this presents different problems. First of all, most test benches available for engine testing are only prepared to measure at engine exit plane, since this is the protocol for engine certification measurements. In the case where the measurement behind the engine is possible, ambient conditions will have an impact of the vPM formation process, so comparison between measurements conducted in different environmental conditions may be not comparable.

One of the potential solutions for this problem is the use of ageing chambers like PAM-OFR or TSAR to simulate the ageing of the plume under controlled conditions. These reactors present two main problems. The first is that they are done to simulate long ageing, so OH exposure rates goes from 1 day to a few weeks. The ageing in the plume occurs in a few minutes. Another limitation is the temperature that can be reached in the reactor, limiting the use to simulate only ground ageing. The ideal ageing reactor for aviation would be able to have shorter exposure times to OH and a temperature control that allows studies at low temperatures to simulate cruise conditions.

Another big challenge has to do with measurement techniques able to deal with nucleated vPM. Critical cluster size is normally in the range of 1.1 -1.3 nm [68], and nucleation mode maximum size is between 1 and 10 nm. This means that particle counters generally used in certification, with a cut off of 10 nm, will most likely not detect most of nucleation mode particles. Particle counters measuring down to 3 nm are relatively accessible, but still will be missing the critical size. Airmodus have developed a specific instrument, the Particle size Magnifier (PSM), that can be used in combination with a traditional CPC to extend the cut of limit down to 1nm, capturing the critical cluster size [91]. A recent collaboration between Airmodus and



#### Work Package 4: Deliverables Report

Grimm has led to the integration of PSM with the Scanning Mobility Particle Spectrometer (SMSP) from GRIMM allowing the measurement of particle size distributions between 1 and 55 nm [92]. These instruments can be integrated in actual measurement chains used in aviation, to gain further insight in vPM formation processes.

If measuring concentration and size distributions down to critical clusters size is challenging, chemical characterisation of this particle sizes is even more challenging. Traditional mass spectrometry technique dedicated to aerosols, like Aerosol Mass Spectrometer (AMS) have a poor transference of small particles, which limits the size of particles that can be analysed to those with a diameter larger than 40 nm. This means that the information provided by this technique is related to the compounds responsible of particle growth but not necessarily to those responsible of nucleation. There is one mass spectrometry technique specially designed to characterize nucleating molecular clusters, the Atmospheric pressure interface Time of flight spectrometer (API-ToF) [93]. This technique is capable of providing the chemical composition of molecular clusters from two molecules clusters up to cluster of around 2 nm of diameter. The main problem with this instrument is that the sampling lines must be as near as possible to the source to minimise the loss of these small particles. In the case of engine testing this is not possible.

### 6.6.5 Summary

Towards future regulation of total-PM/ vPM there are a number of points that will need to be fully considered including:

- A detailed understanding of the chemical composition and formation of the sub 20 and ideally sub 10 nm modes
- Further assessment of the current ICAO sampling system for suitability of sampling and forming organic condensation onto the soot mode (non-nucleation mode vPM)
- Determination of the suitability of engine exit vs stack measurements for representative sampling of vPM.
- Modelling of vPM to total-PM formation and understanding of plume dynamics (dilution vs cooling) and ambient atmospheric effects
- Beyond the fence transformations and modelling to better understand the impacts of local communities
- Development of a standard for vPM and TPM sampling to capture the ultra-fine mode.



## 7 References

1. Simmons, H.C. et al. 1975. *AIR-ATOMIZING FUEL NOZZLE* 3,980,233 [Patent].
2. MAKIDA, M. et al. 2006. PRELIMINARY EXPERIMENTAL RESEARCH TO DEVELOP A COMBUSTOR FOR SMALL CLASS AIRCRAFT ENGINE UTILIZING PRIMARY RICH COMBUSTION APPROACH. *ASME Turbo Expo 2006* , pp. 1–8.
3. GT2019:91624 *Manufacture, characterization and stability limits of an AM Prefilming air-blast atomizer* Andrew P., Crayford Franck Lacan Jon Runyon, Philip J. Bowen, Shrinivas Balwadkar, Joseph Harper, Daniel Pugh
4. SAE Aerospace 2017. ARP6320 Procedure for the Continuous Sampling and Measurement of Non-Volatile Particulate Matter Emissions from Aircraft Turbine Engines.
5. Harper, J. et al. 2022 Influence of alternative fuel properties and combustor operating conditions on the nvPM and gaseous emissions produced by a small-scale RQL combustor. *Fuel*, Volume 315, 123045, ISSN 0016-2361, <https://doi.org/10.1016/j.fuel.2021.123045>.
6. ICAO 2018. Annex 16 - Environmental Protection.
7. Kinsey, John S. et al. 2021, Assessment of a regulatory measurement system for the determination of the non-volatile particulate matter emissions from commercial aircraft engines, *Journal of Aerosol Science*, Volume 154, 105734, ISSN 0021-8502, <https://doi.org/10.1016/j.jaerosci.2020.105734>.
8. Lobo, P. et al. 2020, Comparison of standardized sampling and measurement reference systems for aircraft engine non-volatile particulate matter emissions, *Journal of Aerosol Science*, Volume 145, 105557, ISSN 0021-8502, <https://doi.org/10.1016/j.jaerosci.2020.105557>.
9. Eliot F. Durand, Andrew P. Crayford & Mark Johnson (2020) *Experimental validation of thermophoretic and bend nanoparticle loss for a regulatory prescribed aircraft nvPM sampling system*, *Aerosol Science and Technology*, 54:9, 1019-1033, DOI: [10.1080/02786826.2020.1756212](https://doi.org/10.1080/02786826.2020.1756212).
10. Crayford, A, et al. (2020) "Influence of Humidity and Fuel Hydrogen Content on Ultrafine Non-Volatile Particulate Matter Formation in RQL Gas Turbine Technology." *Proceedings of the ASME Turbo Expo 2020: Turbomachinery Technical Conference and Exposition. Volume 4A: Combustion, Fuels, and Emissions*. Virtual, Online. September 21–25. V04AT04A065. ASME. <https://doi.org/10.1115/GT2020-15168>
11. Harper, J "An Experimental Study of the nvPM Emissions Produced by Alternative Aviation Fuels in a Newly-Developed RQL Research Combustor" PhD – submitted to Cardiff University for examination 31<sup>st</sup> March 2022
12. Lee, D. S., et al. Transport impacts on atmosphere and climate: Aviation, *Atmos. Environ.*, 44, 4678-4734, 2010.
13. European Aviation Environmental Report 2016; doi: 10.2822/385503
14. Gudmundsson, S. et al. Forecasting temporal world recovery in air transport markets in the presence of large economic shocks : The case of COVID-19, *J. Air Transp. Manag.*, 91, 102007, 2021
15. International Air Transport Association (IATA). COVID-19 An almost full recovery of air travel in prospect, IATA: Montreal, QC, Canada, 2021
16. Boeing. Commercial Market Outlook 2021-2040; Boeing, Seattle, WA, USA, 2021
17. Airbus. Airbus ramps up production as it eyes post-COVID recovery. Available on line <https://www.bbc.com/news/business-57267194>



## Work Package 4: Deliverables Report

18. Eurocontrol. Eurocontrol forecast update 2021-2024 European flight movements and service units – three scenarios for recovery from COVID-19, Statfor, May 2021, Eurocontrol: Brussels, Belgium, 2021
19. Agarwal, A., et al. (2019). SCOPE11 Method for Estimating Aircraft Black Carbon Mass and Particle Number Emissions. *Environmental Science and Technology*, 53(3), 1364–1373. <https://doi.org/10.1021/acs.est.8b04060>
20. Mongia, H.C., et al. Low emissions propulsion engine combustor technology evolution : Past, present and future, 24<sup>th</sup> congress of international Council of the aeronautical Sciences, Yokohama, Japan, 2004
21. International Civil Aviation Organization (ICAO), ICAO. Anex 16 to the Convention on International Civil Aviation, Environmental Protection, Volume II, Aircraft Engine Emissions, Technical report, third edition, ICAO, 2008
22. Samuelsen, G.S. et al. Experimental and modeling investigation of the effect of air preheat on the formation of NO<sub>x</sub> in a RQL combustor, *Heat Mass Transf.* 49, 219-231, 2013.
23. Moran, J. Engine Technology Development to address Local Air Quality Concerns, ICAO Colloquium on Aviation Emissions with Exhibition.14-16, 2007
24. McKinney, R., et al. The Pratt & Whitney TALON X low emissions combustor: revolutionary results with evolutionary technology. 45th AIAA aerospace sciences meeting and exhibit. 2007.
25. Mongia, H.C., Future Trends in commercial Aviation Engines Combustion. Novel Combustion concepts for sustainable Energy Development, Springer, 113-176, 2014
26. Lefebvre, A. H. Gas turbine combustion. CRC press, 1998.
27. ICAO, ICAO. Aircraft Engine Emissions Databank. Int. Civ. Aviat. Organ, 2006.
28. Mongia, H.C., N+3 and N+4 generation aeropropulsion engine combustor: PART 2: medium size-rich dome engines and lean-dome, ASME TURBO EXPO, USA, 2013
29. Smith, R. Advanced low emissions subsonic combustor study. No. GRC-E-DAA-TN10123. 1998.
30. Lee, C-M. NASA project develops next generation low-emissions combustor technologies. 51st AIAA aerospace sciences meeting including the new horizons forum and aerospace exposition. 2013.
31. Dhanuka, S.K., et al. Vortex-shedding and mixing layer effects on periodic flashback in a lean premixed pre-vaporized gas turbine combustor, *Proceedings of the combustion Institute*, 32, 2901-2908, 2009
32. Peddie, C. L. and Shaw. R.B. NASA Ultra Efficient Engine Technology Project Overview. *2003 NASA Seal/Secondary Air System Workshop, Volume 1*. 2004.
33. Foust, M., et al. Development of the GE aviation low emissions TAPS combustor for next generation aircraft engines. 50th AIAA aerospace sciences meeting including the new horizons forum and aerospace exposition. 2012.
34. Stickles, R. and Barrett, J. TAPS II combustor final report. Continuous Lower Energy, Emissions and Noise (CLEEN) Technologies Development, Federal Aviation Administration, 2013.
35. Tacina, R., et al. A lean-direct-injection combustor using a 9 point swirl-venturi fuel injector. XVII International Symposium on Air Breathing Engines (ISABE), Munich, Germany, 2005.
36. Lazik, W., et al. Low NO<sub>x</sub> combustor development for the Engine3E core engine demonstrator. XVIII International Symposium on Air Breathing Engines (ISABE), Beijing, China, Sept. 2007.
37. Sieber, J. NEWAC Technologies-Highly Innovative Technologies for Future Aero Engines. URL <http://www.newac.eu> , 2011.
38. Forum-AE Coordination & Support Action, FP7 – 605506. 2014
39. ARTTIC, NEWAC Publishable Final Activity Report, NEWAC – FP6-030876, 2011.
40. ATAG (2021). Waypoint 2050. Air Transport Action Group. Available at: <https://aviationbenefits.org/environmental-efficiency/climate-action/waypoint-2050/>.



## Work Package 4: Deliverables Report

41. Hemighaus, Get al. *Aviation Fuels Technical Review*. San Ramon, CA: Chevron Products Company, 2007.
42. Heyne, J., et al. Sustainable Aviation Fuel Prescreening Tools and Procedures. *Fuel*, 290, 120004, 2021.
43. Graham, J. et al. . Impact of Alternative Jet Fuel and Fuel Blends on Non- Metallic Materials Used in Commercial Aircraft Fuel Systems. Available at: [https://www.faa.gov/about/office\\_org/headquarters\\_offices/apl/research/aircraft\\_technology/clean/reports/media/Boeing\\_Alt\\_Fuels\\_Final.pdf](https://www.faa.gov/about/office_org/headquarters_offices/apl/research/aircraft_technology/clean/reports/media/Boeing_Alt_Fuels_Final.pdf) , 2013 :
44. ICAO (2021a). Carbon Offsetting and Reduction Scheme for International Aviation (CORSIA). Montreal, Quebec, Canada. Available at: <https://www.icao.int/environmental-protection/CORSIA/Pages/default.aspx>.
45. Corporan, E., et al. Emissions characteristics of a turbine engine and research combustor burning a Fischer–Tropsch jet fuel. *Energy Fuels*, 21, 2615–2626, 2007.
46. Corporan, E., et al. Chemical, thermal stability, sealswell and emissions studies of alternative jet fuels. *Energy Fuels*, 25, 955–966, 2011.
47. Corporan, et al. Impacts of biodiesel on pollutant emissions of a JP-8-fueled turbine engine. *J. Air Waste Manage. Assoc.*, 55, 940–949, 2015.
48. DeWitt, et al. Effects of aromatic type and concentration in Fischer–Tropsch fuel on emissions production and material compatibility. *Energy Fuels*, 22, 2411–2418, 2008.
49. Timko, M.T., et al. Combustion Products of Petroleum Jet Fuel, a Fischer–Tropsch Synthetic Fuel, and a Biomass Fatty Acid Methyl Ester Fuel for a Gas Turbine Engine, *Combust. Sci. Technol.*, 183, 1039–1068, 2011.
50. <https://aero-fp.larc.nasa.gov/projects/aafex>
51. Moore, R. H. et al. Influence of jet fuel composition on aircraft engine emissions: a synthesis of aerosol emissions data from the NASA APEX, AAFEX, and ACCESS missions. *Energy Fuels*, 29, 2591–2600, 2015.
52. Moore R.H. et al. Biofuel blending reduced particle emissions from aircraft engines at cruise conditions, *Nature*, 543, 411–415, 2017.
53. <https://www.ara.com/products/readijet/>
54. <https://www.airbus.com/en/newsroom/stories/2021-03-an-a350-fuelled-by-100-saf-just-took-off>
55. <https://www.ge.com/news/reports/united-flies-worlds-first-passenger-flight-on-100-sustainable-aviation-fuel-supplying-one>
56. <https://www.rolls-royce.com/media/press-releases/2021/01-02-2021-business-aviation-rr-conducts-first-tests-of-100-percent-sustainable-aviation-fuel.aspx>
57. <https://lilium.com/newsroom-detail/lilium-begins-flight-testing-in-spain>
58. Chris, M. and Abul Masrur, M., *Hybrid electric vehicles: principles and applications with practical perspectives*. John Wiley & Sons, 2017.
59. Ching Chue, C. The state of the art of electric, hybrid, and fuel cell vehicles, *Proceedings of the IEEE* 95.4, 704–718, 2007.
60. Guzzella, L. and Sciarretta, A. *Vehicle propulsion systems*. Vol. 1. Springer-Verlag Berlin Heidelberg, 2007.
61. Hiserote R. and Harmon, F., Analysis of hybrid-electric propulsion system designs for small unmanned aircraft systems. 8th annual international energy conversion engineering conference; Virginia, USA. Reston: AIAA, 6687–6696. 201
62. Van Bogaert, J., Assessment of potential fuel saving benefits of hybrid-electric regional aircraft. Dissertation accessible in <https://repository.tudelft.nl/islandora/object/uuid%3A0fc7019f-d988-45c1-a7e2-55825f4f90ca> , 2015.
63. <https://www.airbus.com/innovation/future-technology/electric-flight/e-fan-x.html>.
64. <https://www.icao.int/environmental-protection/Pages/electric-aircraft.aspx>





## Work Package 4: Deliverables Report

65. Elbaz A.M., et al. Review on the recent advances on ammonia combustion from the fundamentals to the applications, *Fuel Communications*, 10,100053, 2022
66. <https://www.rolandberger.com/en/Insights/Publications/Hydrogen-A-future-fuel-for-aviation.html>
67. <https://www.airbus.com/en/innovation/zero-emission/hydrogen/zeroe>
68. Kulmala M, et al. Direct observations of atmospheric aerosol nucleation, *Science*,339,943-946.2013
69. Vancassel, X., et al. Volatile particles formation during PartEmis: a modelling study, *Atmos. Chem. Phys.*, 4, 439-447, 2004.
70. Sorokin, A., et al. On volatile particle formation in aircraft exhaust plumes, *Phys. Chem. Earth C*, 26, 557-561, 2001
71. Riccobono, F., et al., Oxidation Products of Biogenic Emissions Contribute to Nucleation of Atmospheric Particles, *Science*, 344, 717-721, 2014.
72. Kirkby, J., et al. Ion-induced nucleation of pure biogenic particles, *Nature*, 533, 521-526, 2016.
73. Wang, M., K., et al. Rapid growth of new atmospheric particles by nitric acid and ammonia condensation. *Nature*, 581, 184–189 (2020).
74. Timko, M. T., et al. Gas turbine engine emissions—part II: Chemical properties of particulate matter, *Journal of Engineering for Gas Turbines and Power*, 132, 1–15, 2010
75. Timko, M.T., et al. Atmospheric measurements of the physical evolution of aircraft exhaust plumes. *Environ. Sci. & Technol.* 47, 3513-3520, 2013.
76. Stettler, M. E., et al.: Air quality and public health impacts of UK airports. Part I: Emissions, *Atmospheric Environment*, 45, 5415–5424, 2011.
77. Wong, H.-W., et al. Roles of organic emissions in the formation of near field aircraft-emitted volatile particulate matter: a kinetic microphysical modeling study. *Journal of Engineering for Gas Turbines and Power*, 137, 072606-1-072606-10,2015.
78. Peck, J., et al. A volatile particle microphysical simulation model for the evolution of surrogate organic emissions in an aircraft exhaust plume. TAC-4 Proceedings June 22nd to 25th, 21-26,2015.
79. Wong, H.-W., et al., Detailed microphysical modeling of the formation of organic and sulfuric coatings on aircraft emitted soot particles in the near field. *Aerosol Science and Technology* 48, 981-995, 2014.
80. Yu, Z., et al., Mode-specific, semi-volatile chemical composition of particulate matter emission from a commercial gas turbine aircraft engine. *Atmospheric Environment* 218, 116974-1-116974-8, 2015
81. Yu, Z., et al. Identification of Lubrication Oil in the Particulate Matter Emissions from Engine Exhaust of In-Service Commercial Aircraft. *Environ. Sci. Technol.* 2012, 46, 17, 9630–9637, 2012.
82. Lobo, P., et al. PM emissions measurements of in943 service commercial aircraft engines during the Delta-Atlanta Hartsfield Study, *Atmos. Environ.*, 104, 237–245, 2015.
83. Smith, L. D. et al Examining chemical composition of gas turbine-emitted organic aerosol using positive matrix factorization (PMF). *Journal of Aerosol Science*. Elsevier Ltd, 159, p. 105869. 2022.
84. Williams, P. I., Allan, J. D., Lobo, P., Coe, H., Christie, S., Wilson, C., Hagen, D., Whitefield, P., Raper, D., and Rye, L. (2012): Impact of alternative fuels on emissions characteristics of a gas turbine engine - Part 2: Volatile and semivolatile particulate matter emissions, *Environmental Science and Technology*, doi: 10.1021/es301899s
85. Smith, L – PhD Thesis – Submission to University of Manchester 2022
86. Hudda N. and Fruin, S. A. International Airport Impacts to Air Quality: Size and Related Properties of Large Increases in Ultrafine Particle Number Concentrations, *Environmental Science & Technology*, 50, 3362-3370, 2016.
87. Masiol, M., et al. Sources of sub-micrometre particles near a major international airport, *Atmos. Chem. Phys.*, 17, 12379–12403, 2017.



## Work Package 4: Deliverables Report

88. Ungeheuer, F., et al. Identification and source attribution of organic compounds in ultrafine particles near Frankfurt International Airport. *Atmos. Chem. Phys.*, 21, 3763–3775, 2021.
89. E. Kang, et al. Introducing the concept of Potential Aerosol Mass (PAM), *Atmos. Chem. Phys.*, 7, 5727–5744, 2007
90. Simonen, P., et al. new oxidation flow reactor for measuring secondary aerosol formation of rapidly changing emission sources, *Atmos. Meas. Tech.*, 10, 1519–1537, 2017.
91. Vanhanen, J., et al. Particle size magnifier for nano-CN detection, *Aerosol Sci. Tech.*, 45, 533–542, 2011.
92. Steiner, G., et al. Monitoring ambient aerosol size distributions from 1 - 55 nm with the GRIMM-AIRMODUS PSMPS, the 23rd EGU General Assembly, held online 19-30 April, 2021.
93. Junninen, et al., A high-resolution mass spectrometer to measure atmospheric ion composition, *Atmos. Meas. Tech.*, 3, 1039–1053, 2010.



## 8 Appendix

## 8.1 EUR APC CPC/VPR cal certs



## AVL 489 Particle Counter Aviation Calibration Certificate

Date:	30-Sep-2020
Device:	GH0965
Chopper Diluter	460

Makro	XF0339	V1.30
-------	--------	-------

Measured Inlet Flows of Instruments		
Device	Vol. Flow	Normalization Cond.
APC Chopper Dil. low	4791 ml/min	25°C; 1013.25mbar
Master CPC	1021 ml/min	ambient conditions

Used Instruments		Type	Serial No.
DMA	TSI 3080		71124079
Master CPC	TSI TSI 3772		3772121004
Mass Flow Meter	Vögtlin GCR-B5SA-BA25		141570
Calibration aerosol: APG combustion soot			

Zero Concentration with HEPA-Filter	
APC	0.29 #/cm <sup>3</sup> at pcrf=10*10=100
Master CPC	0.000 #/cm <sup>3</sup>

Nr	values set			Flows		Measured Penetrations		
	Diluter 1 low/high	Diluter 1	Diluter 2	Dilution Factor		100nm (>70%)	50nm (>65%)	15nm (>30%)
1	low	10	10	73		76.3%	72.9%	51.4%
2	low	25	10	187		77.6%	76.3%	50.4%
3	low	50	10	376		79.0%	77.0%	50.6%
4	low	100	10	762		81.2%	78.5%	49.9%
5	low	150	10	1153		84.0%	77.5%	47.2%

\*Only calibrated at Stages 1-5. One of those stages MUST be used for ICAO Annex 16: Environmental Protection, Vol. II, Appendix 7 compliant measurements.

Volatile Particle Removal Efficiency for Tetraoctane 30nm: **99.76%**

AVL List GmbH does hereby certify that the above described instrument conforms to the original manufacturer's specifications and has been calibrated using standards whose accuracies are traceable to national standards or have been derived from accepted values of natural physical constants or have been derived by the ration type of self calibration techniques. This report may not be reproduced, except in full, unless permission for the publication of an approved abstract is obtained in writing from the calibration organization issuing this report.

Signature  
(Armin Sejdic)

## Work Package 4: Deliverables Report

PN_1888
<b>ÖKD 39</b>
25-Sep-2020

Seite 5/5 zum Kalibrierschein vom 25-Sep-2020  
Page 5/5 of calibration certificate dated 25-Sep-2020



Kalibrierung - Zähleffizienz - **außerhalb des akkreditierten Partikelgrößenbereichs**  
*Calibration - Counting efficiency - not within the accredited particle size range*

Partikelgröße* <i>Particle size*</i>	Nom. Konzentration <i>Nom. concentration</i>	Gem. Konzentration <i>Meas. Concentration</i>	Referenzkonz. <i>Reference conc.</i>	Zähleffizienz <i>Counting eff.</i>	rel. Messunsicherheit <i>rel. meas. uncertainty</i>
[nm]	[#/cm <sup>3</sup> ]	[#/cm <sup>3</sup> ]	[#/cm <sup>3</sup> ]	[]	[]
15	7000	6318	7034	0.898	5.9%
10	3000	2395	3192	0.750	7.9%

\* Die Messunsicherheit für die Partikelgröße beträgt 4% laut Kalibrierung des DEMC bei einem Nationalen Metrologischen Institut.

\* *The measurement uncertainty for the particle size is 4% according to the calibration of the DEMC at a National Metrological Institute.*

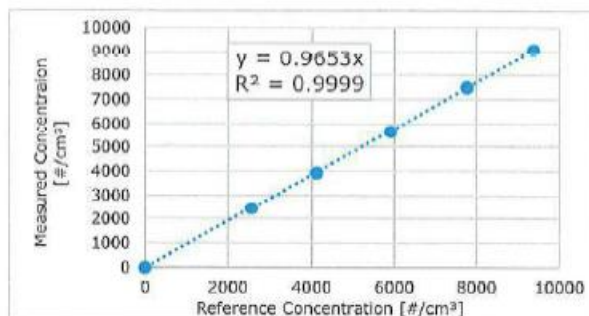
Evaluierung\* der Limits entsprechend UN/ECE GRPE-PMP Sub23nm draft  
*Limit evaluation\* according UN/ECE GRPE-PMP Sub23nm draft*

Kalibrierung - Linearität  
*Calibration - Linearity*

Nr. <i>No.</i>	Nom. Konz. <i>Nom. Conc.</i>	Ref. Konz. <i>Ref. Conc.</i>	Gem. Konz. <i>Meas. Conc.</i>	Zähleffizienz <i>Counting eff.</i>	Limit <i>Limit</i>	Status <i>Status</i>	Residuum abw. <i>Residual dev.</i>
	[#/cm <sup>3</sup> ]	[#/cm <sup>3</sup> ]	[#/cm <sup>3</sup> ]	[]	[]	[]	[%]
1	10000	9375	9081	0.969	0.9-1.1	passed	0.3%
2	8000	7765	7504	0.966	0.9-1.1	passed	0.1%
3	6000	5907	5663	0.959	0.9-1.1	passed	-0.7%
4	4000	4117	3954	0.960	0.9-1.1	passed	-0.5%
5	2500	2569	2462	0.958	0.9-1.1	passed	-0.7%
6	0	0	0	-	<0.5#/cm <sup>3</sup>	passed	-

Berechnung des k-Faktors bei 55nm  
*k-factor calculation at 55nm*

	Wert <i>Value</i>	Limit <i>Limit</i>
Steigung/Slope	0.965	0.9-1.1
R <sup>2</sup>	1.000	>0.97
k-Faktor	1.036	-



Zähleffizienz bei 10nm und 15nm mit angewandtem k-Faktor  
*Counting efficiency at 10nm and 15nm with k-factor applied*

Partikelgröße <i>Particle size</i>	Zähleffizienz <i>Counting eff.</i>	Limit <i>Limit</i>	Status <i>Status</i>
[nm]	[]	[]	[]
10	0.777	0.5-0.8	passed
15	0.930	≥0.9	passed



## 8.2 SWISS APC CPC/VPR cal certs



### AVL 489 Particle Counter Aviation Calibration Certificate

Date:	29-Sep-2020
Device:	GH0672
Chopper Diluter	409 507

Makro	XF0339	V1.30
-------	--------	-------

Measured Inlet Flows of Instruments		
Device	Vol. Flow	Normalization Cond.
APC Chopper Dil. low	4376 ml/min	25°C; 1013.25mbar
Master CPC	1010 ml/min	ambient conditions

Used Instruments		
Type	Serial No.	
DMA	TSI 3080	71124079
Master CPC	TSI TSI 3772	3772121004
Mass Flow Meter	Vögtlin GCR-B5SA-BA25	141570
Calibration aerosol: APG combustion soot		

Zero Concentration with HEPA-Filter	
APC	0.04 #/cm <sup>3</sup> at pcrf=10*10=100
Master CPC	0.000 #/cm <sup>3</sup>

Nr	values set			Dilution Factor	Measured Penetrations		
	Diluter 1 low/high	Diluter 1	Diluter 2		100nm (>70%)	50nm (>65%)	15nm (>30%)
1	low	10	10	71	72.4%	67.7%	48.4%
2	low	25	10	179	76.2%	67.3%	47.0%
3	low	50	10	363	76.6%	67.7%	47.0%
4	low	100	10	705	75.3%	65.8%	44.2%
5	low	150	10	1051	73.5%	64.0%	41.7%

\*Only calibrated at Stages 1-5. One of those stages MUST be used for ICAO Annex 16: Environmental Protection, Vol. II, Appendix 7 compliant measurements.

Volatile Particle Removal Efficiency for Tetraoctane 30nm:	99.99%
--	--------

AVL List GmbH does hereby certify that the above described instrument conforms to the original manufacturer's specifications and has been calibrated using standards whose accuracies are traceable to national standards or have been derived from accepted values of natural physical constants or have been derived by the ration type of self calibration techniques. This report may not be reproduced, except in full, unless permission for the publication of an approved abstract is obtained in writing from the calibration organization issuing this report.

Signature  
  
 (Armin Sejdin)



PN_1891
<b>ÖKD 39</b>
28-Sep-2020

Seite 5/5 zum Kalibrierschein vom 28-Sep-2020  
Page 5/5 of calibration certificate dated 28-Sep-2020



Kalibrierung - Zähleffizienz - **außerhalb des akkreditierten Partikelgrößenbereichs**  
*Calibration - Counting efficiency - not within the accredited particle size range*

Partikelgröße* Particle size* [nm]	Nom. Konzentration Nom. concentration [#/cm <sup>3</sup> ]	Gem. Konzentration Meas. Concentration [#/cm <sup>3</sup> ]	Referenzkonz. Reference conc. [#/cm <sup>3</sup> ]	Zähleffizienz Counting eff. []	rel. Messunsicherheit rel. meas. uncertainty []
15	7000	5585	6188	0.902	5.9%
10	3000	2284	3029	0.754	7.9%

\* Die Messunsicherheit für die Partikelgröße beträgt 4% laut Kalibrierung des DEMC bei einem Nationalen Metrologischen Institut.  
\* The measurement uncertainty for the particle size is 4% according to the calibration of the DEMC at a National Metrological Institute.

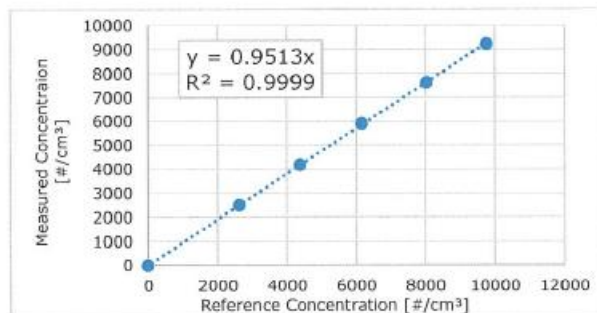
Evaluierung\* der Limits entsprechend UN/ECE GRPE-PMP Sub23nm draft  
*Limit evaluation\* according UN/ECE GRPE-PMP Sub23nm draft*

Kalibrierung - Linearität  
*Calibration - Linearity*

Nr. No.	Nom. Konz. Nom. Conc. [#/cm <sup>3</sup> ]	Ref. Konz. Ref. Conc [#/cm <sup>3</sup> ]	Gem. Konz. Meas. Conc. [#/cm <sup>3</sup> ]	Zähleffizienz Counting eff. []	Limit Limit []	Status Status []	Residuum abw. Residual dev. [%]
1	10000	9759	9241	0.947	0.9-1.1	passed	-0.5%
2	8000	8035	7637	0.950	0.9-1.1	passed	-0.1%
3	6000	6159	5916	0.961	0.9-1.1	passed	1.0%
4	4000	4377	4185	0.956	0.9-1.1	passed	0.5%
5	2500	2621	2507	0.957	0.9-1.1	passed	0.6%
6	0	0	0	-	<0.5#/cm <sup>3</sup>	passed	-

Berechnung des k-Faktors bei 55nm  
*k-factor calculation at 55nm*

	Wert Value	Limit Limit
Steigung/Slope	0.951	0.9-1.1
R <sup>2</sup>	1.000	>0.97
k-Faktor	1.051	-



Zähleffizienz bei 10nm und 15nm mit angewandtem k-Faktor  
*Counting efficiency at 10nm and 15nm with k-factor applied*

Partikelgröße Particle size [nm]	Zähleffizienz Counting eff. []	Limit Limit []	Status Status []
10	0.792	0.5-0.8	passed
15	0.949	≥0.9	passed



## 8.3 ONERA mini-CAST report

### TABLE DES MATIÈRES

EXECUTIVE SUMMARY .....	3
List of figures .....	7
List of tables .....	12
1 Introduction .....	13
2 Experimental Setup .....	14
2.1 GTRC’s High Pressure Combustor Rig Design .....	14
2.1.1 High Pressure Optical Chamber (HPOC) .....	14
2.1.2 Rich Quench Lean (RQL) combustor rig .....	15
2.2 Particulate and gaseous sampling and measurement .....	16
2.3 Fuels .....	19
3 Operation and Data processing .....	20
3.1 Rig operating conditions .....	20
3.2 Test matrix .....	20
3.3 Data reporting and processing .....	21
3.4 Particle loss correction .....	21
4 Uncertainty in current CAEP10/11 nvPM regulatory practices (D4.1) .....	22
4.1 nvPM Mass measurement uncertainty RQL 1 test (M4.1) .....	22
4.1.1 EI Mass Intercomparison RQL 1 test (Swiss Vs. EUR) .....	22
4.1.2 EI Mass Intra-comparisons RQL 1 test .....	23
4.1.3 RQL 1: Mass measurement uncertainty discussion .....	25
4.2 nvPM Mass measurement uncertainty RQL 2 test (M4.2) .....	25
4.2.1 Pre-test mass instrument intercomparison RQL 2 test .....	25
4.2.2 EI mass intercomparison RQL 2 test (Swiss Vs. EUR) .....	27
4.2.3 EI mass intra-comparisons RQL 2 test .....	28
4.2.4 nvPM mass calibration uncertainty RQL 2 test (NIOSH 5040) .....	30
4.2.5 Mass measurement uncertainty discussion .....	34
4.3 nvPM Number measurement uncertainty M4.1 RQL 1 test .....	34
4.3.1 EI Number Intercomparison RQL 1 test .....	34
4.3.2 EI Number Intra-comparison RQL 1 test .....	36
4.3.3 RQL 1: Number measurement uncertainty discussion .....	37



## Work Package 4: Deliverables Report

4.4	nvPM Number measurement uncertainty M4.2 RQL 2 test .....	37
4.4.1	EI Number intercomparison RQL 2 test .....	38
4.4.2	Number measurement uncertainty discussion .....	38
4.5	Line cleanliness, shedding and LOD of mass measurement M4.1 RQL test.....	39
4.5.1	Cleanliness checks RQL 1 (Cyclone cleaning).....	39
4.5.2	Measured Size derived Volume over time RQL 1 .....	40
4.5.3	Comparison nvPM mass raw/diluted near LOD RQL 1 .....	41
4.6	Line cleanliness, shedding and LOD of mass measurement RQL 2 test .....	42
4.6.1	Cleanliness checks RQL 2 (Cyclone cleaning).....	42
4.6.2	Comparison nvPM mass raw/diluted near LOD RQL 2 .....	44
4.6.3	Discussion on line cleanliness, shedding and LOD of mass measurement .....	45
4.7	VPR uncertainty.....	46
4.7.1	VPR penetration efficiency measurement (M4.1 RQL test).....	46
4.7.2	VPR penetration MC uncertainty analysis (RQL 2) .....	49
4.8	System-to-System MC uncertainty analysis .....	55
4.9	Conclusions – CAEP/11 uncertainties (D4.1) .....	56
5	Corrections to be considered towards reduced uncertainty in CAEP/12 (D4.2) .....	58
5.1	nvPM Size measurements RQL 1 test .....	58
5.1.1	Sizing Instrument Intercomparison RQL 1 test .....	58
5.1.2	SMPS Hardware impact RQL 1 test .....	59
5.1.3	Size derived number concentrations RQL 1 test .....	62
5.1.4	Size measurement uncertainty discussion RQL 1 test .....	63
5.2	nvPM size measurements RQL 2 test .....	65
5.2.1	Pre-test size instrument intercomparison RQL 2 test.....	65
5.2.2	Size-derived number and mass concentrations RQL 2 test .....	67
5.2.3	Size measurement uncertainty discussion RQL 2 test .....	69
5.3	Particle loss correction RQL 1 test.....	69
5.3.1	Number correction factor ( $K_{sl_{num}}$ ) RQL 1 test.....	70
5.3.2	Mass correction factor ( $K_{sl_{mass}}$ ) RQL 1 test .....	70
5.3.3	Loss correction discussion RQL 1 test.....	72
5.4	Particle loss correction RQL 2 test.....	72
5.4.1	Measured Vs predicted loss RQL 2 test .....	72
5.4.2	Comparison of size distribution properties (GMD, GSD) at the combustor-exit	
RQL 2 test	75	
5.4.3	Number correction factor ( $K_{sl_{num}}$ ) RQL 2 test .....	76





## Work Package 4: Deliverables Report

5.4.4	Mass correction factor (Ksl mass) RQL 2 test .....	78
5.4.5	Particle loss correction discussion RQL 2 test .....	79
5.5	Impact of fuel composition on nvPM emissions.....	80
5.5.1	Small-scale Laboratory Testing.....	80
5.5.2	RQL Combustor Rig Testing .....	80
5.6	Impact of humidity on nvPM emissions (M4.2 RQL test) .....	82
5.7	Conclusions – Improvements and correction requirements CAEP/12 (WP4.2)	84
6	Benefits of future technologies and regulation in terms of reducing nvPM impact beyond CAEP/12 (D4.3). .....	86
6.1	Introduction .....	86
6.2	Assessment of nvPM emission characteristics of unregulated engines .....	86
6.2.1	Particle size distribution properties and nvPM mass and number .....	87
6.2.2	nvPM mass – smoke number correlation.....	88
6.3	Modern low emissions combustion technologies .....	89
6.3.1	Rich-Burn Quick-Quench Lean Burn (RQL) .....	90
6.3.2	Double Annular Combustor (DAC).....	90
6.3.3	Axial Staged Combustor (ASC).....	91
6.3.4	Twin Annular Premixing Swirler combustor (TAPS).....	91
6.3.5	Lean Direct Injector (LDI).....	92
6.3.6	Lean Premixed Pre-vaporised (LPP).....	92
6.3.7	Variable Geometry Combustor (VGC) .....	93
6.4	Sustainable Aviation Fuels (SAFs).....	93
6.4.1	Drop-in SAFs.....	93
6.4.2	Non-drop-in Hydrogen .....	95
6.5	Electric powered aircraft.....	96
6.5.1	Series configuration .....	96
6.5.2	Parallel configuration .....	96
6.5.3	Series - Parallel configuration.....	97
6.6	Future Total PM Regulation .....	98
6.6.1	Sampling Methodology .....	99
6.6.2	Fuel Effects.....	100
6.6.3	Impacts on communities .....	100
6.6.4	Road map moving forward.....	100
6.6.5	Summary .....	101
7	References.....	102



## Work Package 4: Deliverables Report

8	Appendix .....	107
8.1	EUR APC CPC/VPR cal certs .....	107
8.2	SWISS APC CPC/VPR cal certs .....	109
8.3	ONERA mini-CAST report .....	111
	Glossary.....	115
	Introduction .....	116
8.3.1	CAMPAIGN description .....	116
8.3.2	Experimental set up .....	118
8.3.3	Results.....	122
8.3.4	Conclusions .....	131



## Glossary

ASTM: American Society for Testing and Materials

BC: Black carbon

CPC: Condensation Particle Counter

CS: Catalytic Stripper

DEED: Dekati® Engine Exhaust Diluter

DMA: Differential Mobility Analyzer

GMD: Geometric Mean Diameter

GSD: Geometric Standard Deviation

LII: Laser Induced Incandescence

nvPM: non-volatile Particulate Matter

SMPS: Scanning Mobility Particle Sizer

EASA: European Aviation Safety Agency



## Introduction

Particulate Matter (PM) emissions from aircraft engines adversely affect air quality in and around airports, contributing to public health concerns for airport workers and within neighbouring communities. In order to better understand and mitigate aircraft PM emissions, the International Civil Aviation Organization (ICAO) has adopted new regulatory standards for the measurement and reporting of aircraft engine non-volatile Particle Matter (nvPM) mass and number emissions from 1st January 2020 for in-production turbofan and turbojet engines with rated thrust greater than 26.7 kN.

However, there remains unquantified uncertainty in the reported nvPM Emission Indices concerned with the impact of both fuel composition and ambient conditions, in addition to calibration and particle loss uncertainties introduced by the sampling and measurement system itself. Furthermore, the nvPM regulation does not address all the effects on the global atmosphere, currently excluding cruise conditions and the contribution of smaller engines and engines rated on shaft speed.

These factors, along with the potential impact of emerging technologies, need to be considered for a future European roadmap for improving current nvPM methodologies and future nvPM measurement technologies and regulation beyond CAEP/11.

This report presents the work done to assess the impact of ICAO Annex 16 compliant fuel composition specifications in terms of nvPM. For this we have used the Combustion Aerosol Standard (CAST) Generator available at ONERA especially designed to work with aeronautic fuel. In addition we have deployed a dedicated set of instrument to monitor particulate matter for different fuels (Fig 1). This measurement campaign was performed in the frame of RAPTOR project between 12 and 21 of February 2019.



*Figure 1 - Instruments deployed during the measurement campaign*

### 8.3.1 CAMPAIGN description

In this section we will describe precisely the different fuels used, the source of particles, the measurement line and all the instruments used to characterize emissions.



### 8.3.1.1 Fuel matrix

The aim of the campaign was to evaluate the potential impact of fuel composition on emissions and how this can impact certification measurements. For this we make a selection of fuels covering the limits of the American Society for Testing and Materials (ASTM) requirements for certification in terms of sulfur content and aromatic content.

We selected as reference a Jet A-1 with low content of aromatics (16 % including 0.5 % of naphthalene) and sulfur (4 ppm), from now on we will refer to this fuel as Jet A-1<sup>ref</sup>. Using this fuel as base, we made other 3 blends:

- reference fuel plus an aromatic blend, to set the total aromatic content to 23 % (including 3 % of naphthalene), we will refer to this fuel as Jet A-1<sup>aro</sup> ;
- reference fuel plus sulfur to set the total sulfur content to 3000 ppm, we will refer to this fuel as Jet A-1<sup>sul</sup> ;
- reference fuel plus aromatic and sulfur added to set the total aromatic content to 23 % (including 3 % of naphthalene) and the total sulfur content to 3000 ppm, being these the higher limits set by ASTM for both parameters. We will refer to this fuel as Jet A-1<sup>lim</sup>.

### 8.3.1.2 Source

To study emissions produced by these fuels we used a CAST generator modified to be used with aeronautics fuel. This generator is based on the design of mini-CAST, a well-known standard source of soot. In liquid CAST (Fig. 2) a propane flame is used to heat the liquid fuel that is then vaporized to generate the flame. The emissions at the tip of the flame are quenched by a flow of 7 L/min of nitrogen. After this, emissions are diluted by a flow of 20 L/min of filtered and dried compress air. The main advantage of the CAST generator is the low fuel consumption (between 50 and 105  $\mu\text{L}/\text{min}$ ).

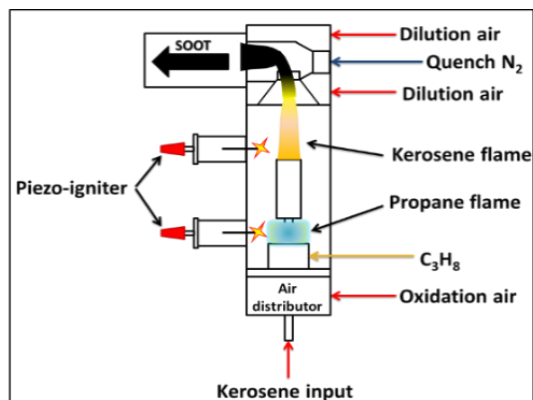


Figure 2 - Schematic representation of CAST generator

In the first stage for the campaign, several set points for CAST were tested, where the propane flow ( $Q_p$ ), kerosene flow ( $Q_k$ ) and air flow ( $Q_{air}$ ) were varied. The aim was to select two working points to do the systematic study on emissions. We selected two working point leading to emissions with different properties. As the aim of the study was to compare different fuel, the choice of set point was limited to set point stable for all fuels. For example, while air flows of 1.2 L/min was stable for high aromatic content fuels; the lowest air flow stable for low aromatic fuels was 1.5 L/min. Finally the to set point selected were



## Work Package 4: Deliverables Report

105  $\mu\text{L}/\text{min}$  kerosene flow, 30 mL/min propane flow and 2 L/min of air flow for the first point and 105  $\mu\text{L}/\text{m}$  kerosene flow, 20 mL/min propane flow and 1.5 L/min of air flow for the second point.

### 8.3.2 Experimental set up

#### 8.3.2.1 Sample conditioning

We have used a combination of a catalytic stripper and a Dekati<sup>®</sup> Engine Exhaust Diluter (DEED) (Fig. 3) to remove the volatile particle that might be present in the sample flow. DEED meets the AIR6241 requirements for measurement of aeronautical emissions for the Volatile Particle Remover (VPR) system (This system firstly employs a catalytic bed heated to 450 °C, with the purpose of destroying volatile organic compounds. The sample is then double diluted, first hot (150 °C) and then at room temperature. The dilution air is compressed air, filtered and dried. At the end of this process, the final sample contains only soot at a temperature of 23 °C.

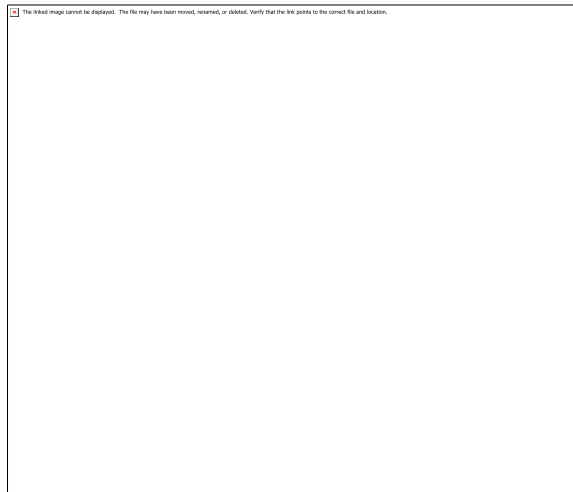


Figure 3 - Schematic representation of DEED

#### 8.3.2.2 Particle measurement

During the campaign we used different instruments to measure particle number, mass and size distribution:

- Laser Induced Incandescence

Laser Induced Incandescence (LII) (ARTIUM 300) measures the thermal emission emitted from soot particles heated by the fundamental mode of a Nd:YAG pulsed laser (usually 1064 nm) to temperatures in the 2500 K to 4500 K range. The laser fluence is set to a value which heats the soot particles below their sublimation threshold values (4000 K for black carbon). The emission signal is recorded at an angle of 90 ° for two specific wavelengths (Fig. 4). Emission recorded from LII signals can be used for determinate the mass concentration, volume concentration, active surface area and primary particle diameter of soot particles emissions. LII can measure at a rate of 10 Hz. This is one of the instruments accepted in the engine certification procedure. ONERA LII is compliant to European Aviation Safety Agency (EASA) requirements for non-volatile Particulate Matter (nvPM) mass concentration measurement.



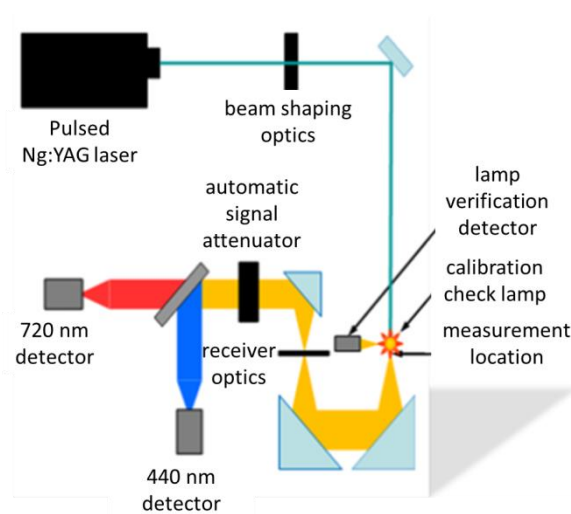


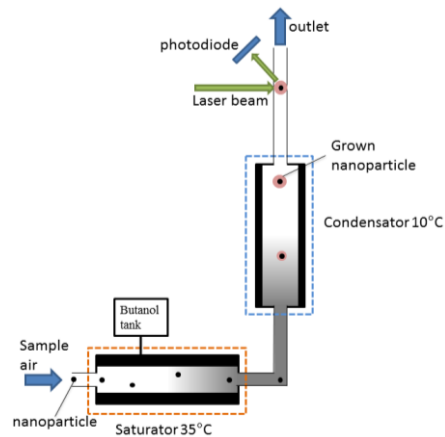
Figure 4 - LII scheme

- Condensational Particle Counter

In Condensation Particle Counters (CPC), particles are detected and counted by laser scattering in a very similar way to a standard optical particle counter, but in a CPC particles are first grown by condensation to a size of 10-12  $\mu\text{m}$ , allowing the detection of nanoparticles.

The CPC (GRIMM 5403) used in the essays uses the diffusional thermal cooling method to grow particles to detectable sizes (Fig. 5). First the sample flow goes through a saturator at 35 °C, where the sample flow is saturated with butanol vapor. After this, the sample is driven through a condensation chamber at 10 °C, where the aerosol particles are grown by condensation of butanol on their surface. In this way, we will be able to measure particles above 5 nm. Due to the temperature requirement for the saturation on butanol, the sample flow temperature should be below the saturator temperature, no avoid the over heat of the saturator, which will lead to a higher supersaturation of butanol, and to the formation of particles from homogeneous nucleation, resulting in an overestimation of particle number. In addition, the optical counter has a limit of detection in single particle mode of 40000 particles per cubic centimeters. Therefore, the sample flow must be diluted to achieve concentrations on that limit. The measurement rate of CPC is 1 Hz. ONERA CPC isn't fully compliant to EASA requirements because it has a cut-off of measurement of 5 nm instead of 10 nm. On the other hand, it is compliant to the 50 % and 90 % cut-off values required





Figur 5 -. CPC schematic

- Scanning Mobility Particle Spectrometer

The Scanning Mobility Particle Spectrometer (SMPS) is based on the principle of the mobility of a charged particle in an electric field. Particles entering the system are neutralized and then charged with X-ray such that they have a Fuchs equilibrium charge distribution. Then, they enter a Differential Mobility Analyzer (DMA) where the aerosol is classified according to electrical mobility, with only particles of a narrow range of mobility exiting through the output slit. The DMA (Fig. 6) consists of a cylinder, with a negatively charged rod at the center; the main flow through the DMA is a particle free laminar 'sheath' air. The particle flow is injected at the outside edge of the DMA. Particles with a positive charge move across the sheath flow towards the central rod, at a rate determined by their electrical mobility. Particles of a given mobility exit through the sample slit at the top of the DMA, while all other particles exit with the exhaust flow. The size of particles exiting through the slit is determined by the charge, central rod voltage, and flow within the DMA. By exponentially scanning the voltage on the central rod, a full particle size distribution is built up. The monodisperse distribution coming out from the DMA then is driven to a CPC to determine the particle number of the given size.

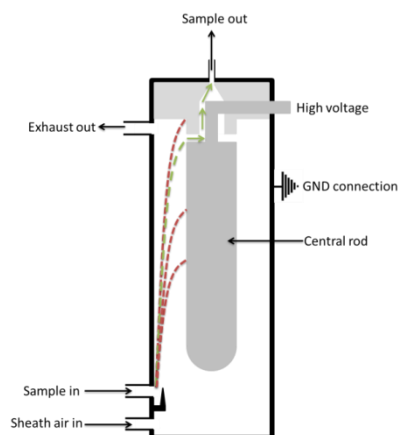


Figure 6 - Schematic representation of a DMA





## Work Package 4: Deliverables Report

## 8.3.2.3 Filter sampling

In addition to the on line characterization techniques, different filters were collected to perform off-line analysis on oxidative potential of emissions, planned in WP 5. The filter were collected before the sample treatment, thus it correspond to the raw emissions. Two different types of filters were used, filters in quartz and filters in PTFE (Fig. 7). Samples were collected at 5 L/min during 10 seconds.



Figure 7 - Filters obtained during the campaign

## 8.3.2.4 Measurement line deployment

A schematic representation of the line is presented in figure 8.

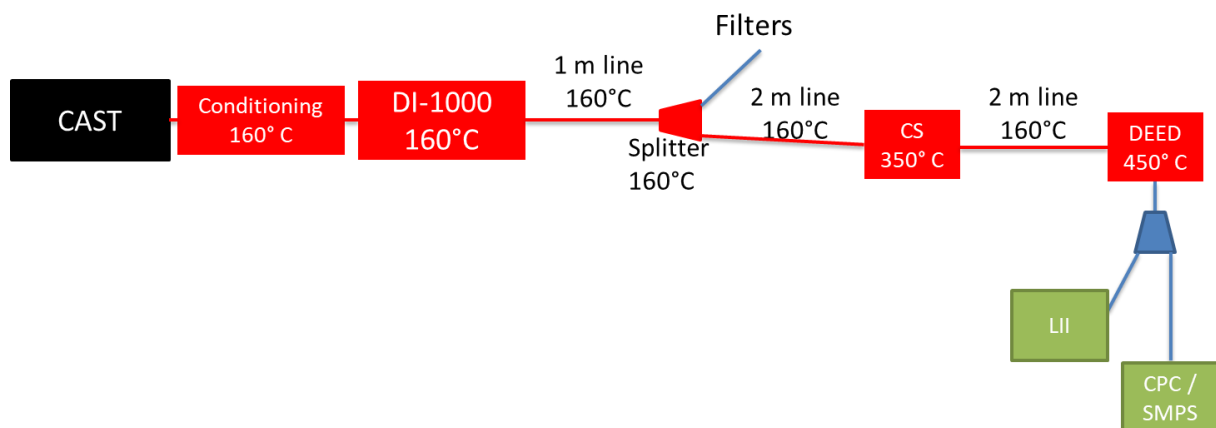


Figure 8 - Schematic representation of the measurement line

The exhaust from CAST generator was diluted using an ejector dilutor (DI-1000, Dekati). The dilutor was kept at 160 °C and the dilution was done with filtered compress air at 160 °C as well to avoid condensation. After the dilution, the sample was driven to a stainless steel splitter through a 1 meter line heated to 160 °C. The splitter was as well heated to 160 °C. Filter sample was taken in this point. After the splitter, the sample was driven to a catalytic stripper heated to 350 °C (catalytic instruments) through a 2 meters line heated to 160 °C. The Catalytic stripper was connected to a DEED through another 2 meters line heated as well to 160



°C. After DEED the sample flow was analyzed using a LII to determine the soot mass concentration and by a SMPS to determine particle size distribution. In addition, the CPC from the SMSP was used alternatively to determine the particle number concentration. We consider as source the combination of CAST and DI-1000, so only correction for DEED dilution is applied to the data (dilution factor = 55.84).

### 8.3.3 Results

The productive RAPTOR tests were done 14, 17 and 18 of February 2020. Nevertheless, the chosen set points were also studied on other tests. Both results will be included in the results analysis, though it must be kept on mind that the conditions for the non-productive test were different to those for productive test.

#### 8.3.3.1 Black carbon mass concentration

##### 8.3.3.1.1 CAST set point 1 ( $Q_k = 105 \mu\text{L}/\text{min}$ ; $Q_p = 30 \text{ mL}/\text{min}$ ; $Q_{\text{air}} = 2.0 \text{ L}/\text{min}$ )

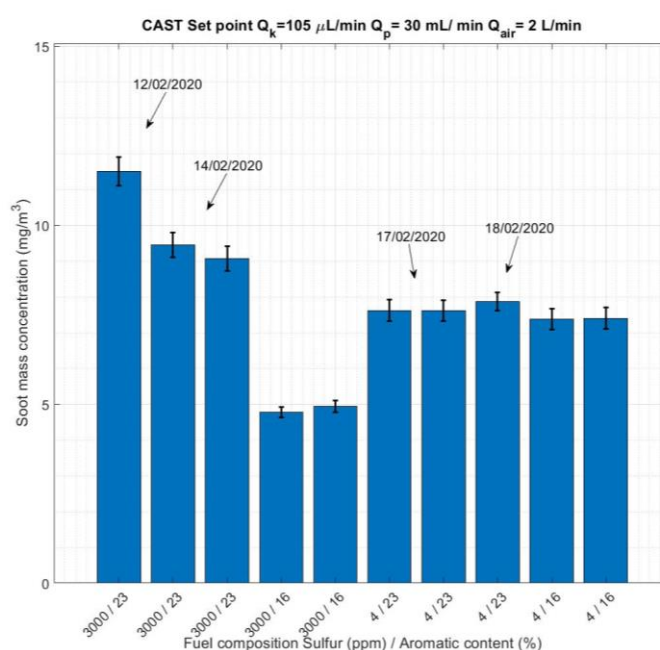


Figure 9 - Black carbon mass concentration measured by LII for different fuels

Fig. 9 depicts black carbon (BC) mass measured by LII for fuels with different composition. As can be seen, there are different measurements for each fuel. During productive essays LII was continuously measuring, while SMPS and CPC were used alternatively, so we decided to average LII measurements done during SMPS measurements (8 minutes) and during CPC measurements (3 minutes). In addition, data for two non-productive tests are added to the plot, one performed 12/02 and other one performed 18/02. The variability of two measures done during the same essay is between 0.1 % and 4 %. BC mass produced during 12/02 essay, was 18 % higher than the one produced during the test done on 14/02 with the same fuel and same set point. On the other hand, the test done on 18/02 produced a similar amount of BC to the one done on 17/02 with the same fuel and set point. Table 1 summarizes LII results for CAST set point 1.

Table 1 - BC mass concentration measured by LII during different tests

Date	Sulfur content	Aromatic content	Black carbon mass	Standard
------	----------------	------------------	-------------------	----------



## Work Package 4: Deliverables Report

	(ppm)	(%)	(mg/m <sup>3</sup> )	deviation
12/02/2020	3000	23	11.503	0.396
14/02/2020	3000	23	9.442	0.346
14/02/2020	3000	23	9.068	0.341
17/02/2020	3000	16	4.780	0.145
17/02/2020	3000	16	4.942	0.167
17/02/2020	4	23	7.617	0.302
17/02/2020	4	23	7.605	0.290
18/02/2020	4	23	7.868	0.257
18/02/2020	4	16	7.376	0.296
18/02/2020	4	16	7.398	0.301

Highest emissions were produced by the Jet A-1<sup>lim</sup> fuel and lowered by Jet A-1<sup>sul</sup> fuel. For fuels with 4 ppm of sulfur emissions, they were similar for both aromatic contents, being slightly higher for Jet A-1<sup>aro</sup> fuel. While the results for fuels containing 3000 ppm is expected, the ones for fuels containing 4 ppm of sulfur are quite surprising. A similar behavior on BC emissions with respect to aromatic content was expected independently to sulfur content. The reason behind this behavior is not clear.

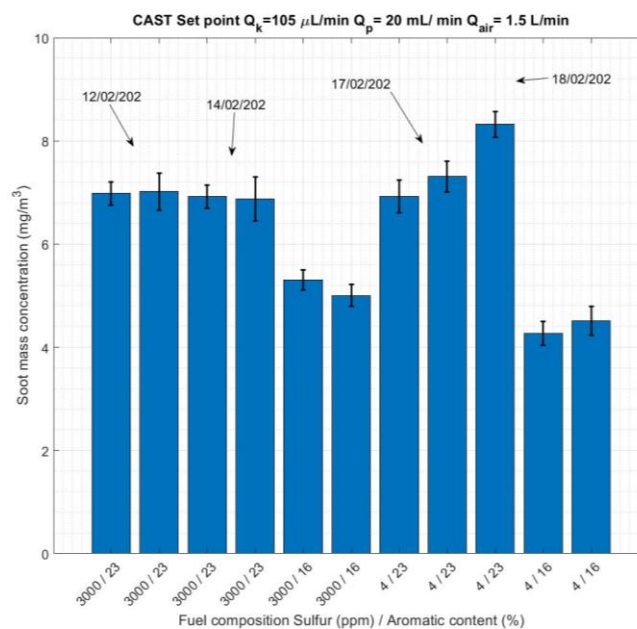
8.3.3.1.2 CAST set point 2 ( $Q_k = 105 \mu\text{L}/\text{min}$  ;  $Q_p = 20 \text{ mL}/\text{min}$  ;  $Q_{\text{air}} = 1.5 \text{ L}/\text{min}$ )

Figure 10 - Black carbon mass concentration measured by LII for different fuels

The tests done for CAST set point 2 were the same that those for set point 1. For this set point, variability for measures done the same day was between 0.6 % and 5 %. In this case, the measures done in different days have an opposite behavior that the one observed for set point 1. The measures done on 12/02 are



## Work Package 4: Deliverables Report

similar to those done on 14/02 for the same fuel and set point, while the ones done on 18/02 are 14 % higher than those done on 17/02 for the same fuel and set point. Table 2 summarize LII results for CAST set point 2.

Table 2 - BC mass concentration measured by LII during different tests

Date	Sulfur content (ppm)	Aromatic content (%)	Black carbon mass (mg/m <sup>3</sup> )	Standard deviation
12/02/2020	3000	23	6.980	0.223
12/02/2020	3000	23	7.019	0.357
14/02/2020	3000	23	6.919	0.223
14/02/2020	3000	23	6.874	0.424
17/02/2020	3000	16	5.299	0.195
17/02/2020	3000	16	5.003	0.212
17/02/2020	4	23	6.924	0.313
17/02/2020	4	23	7.315	0.296
18/02/2020	4	23	8.320	0.251
18/02/2020	4	16	4.266	0.229
18/02/2020	4	16	4.517	0.279

In the case of set point 2 results are as expected. Highest emissions are obtained for both fuels with 23 % aromatic content with similar soot mass emitted for the fuels with 3000 ppm and 4 ppm of sulfur. Although it has to be pointed out that the results for the fuel with 4 ppm of sulfur are more dispersed than those for the fuel with 3000 ppm of sulfur. Lowest emissions are found for fuel with 16 % aromatic content. In this case the emissions for the fuel containing 3000 ppm of sulfur are slightly higher than those for the fuel containing 4 ppm of sulfur.



## Work Package 4: Deliverables Report

## 8.3.3.2 Particle Number

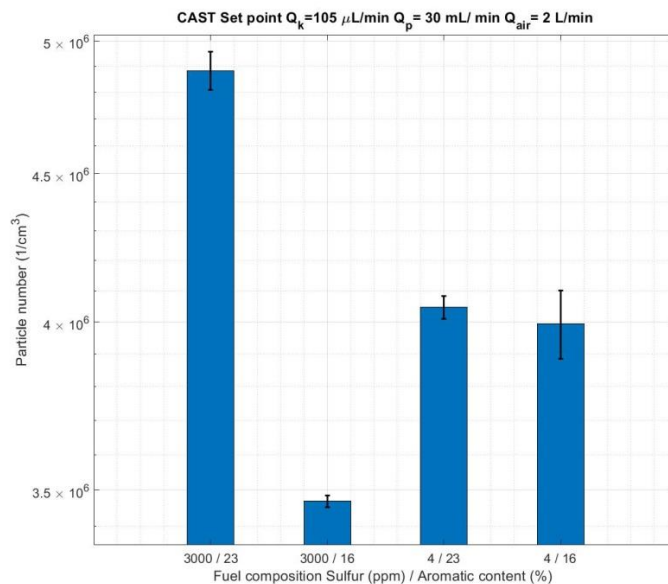
8.3.3.2.1 CAST set point 1 ( $Q_k = 105 \mu\text{L}/\text{min}$  ;  $Q_p = 30 \text{ mL}/\text{min}$  ;  $Q_{\text{air}} = 2.0 \text{ L}/\text{min}$ )

Figure 11 - Particle number measured for CAST set point 1

Figure 11 depicts the particle number measured for different fuels and CAST set point 1. The trend observed is similar to the one observed for BC mass concentration. Highest emissions are observed for the Jet A-1<sup>lim</sup> fuel, lowest by Jet A-1<sup>sul</sup> and similar emissions produced by fuels with 4 ppm of sulfur. Table 3 summarizes particle numbers measured for different fuels and CAST set point 1

Table 3 - Particle number measured during different tests

Date	Sulfur content (ppm)	Aromatic content (%)	Particle number (1/cm <sup>3</sup> )	Standard deviation
14/02/2020	3000	23	4.88 · 10 <sup>6</sup>	0.07 · 10 <sup>6</sup>
17/02/2020	3000	16	3.47 · 10 <sup>6</sup>	0.02 · 10 <sup>6</sup>
17/02/2020	4	23	4.05 · 10 <sup>6</sup>	0.04 · 10 <sup>6</sup>
18/02/2020	4	16	3.99 · 10 <sup>6</sup>	0.11 · 10 <sup>6</sup>

8.3.3.2.2 CAST set point 2 ( $Q_k = 105 \mu\text{L}/\text{min}$  ;  $Q_p = 20 \text{ mL}/\text{min}$  ;  $Q_{\text{air}} = 1.5 \text{ L}/\text{min}$ )

As for CAST set point 1, particle numbers for CAST set point 2 follow the same trends that BC mass concentration (Fig. 12). In this case, the difference between fuel Jet A-1<sup>lim</sup> and Jet A-1<sup>sul</sup> is not as marked as for BC mass concentration.



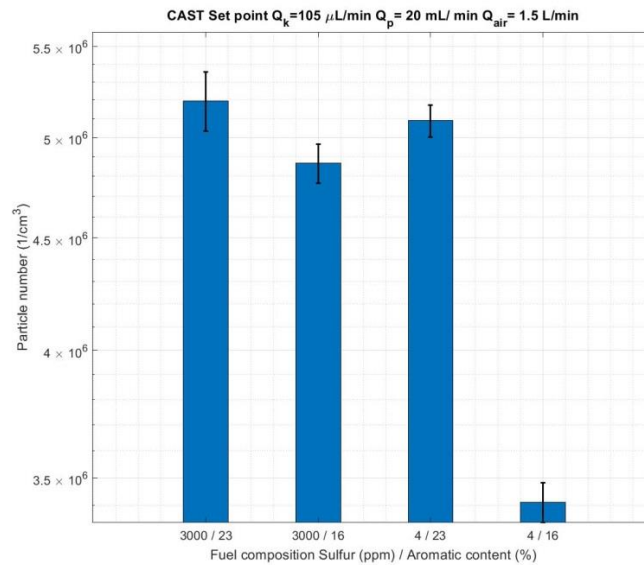


Figure 12 - Particle number measured for CAST set point 1

As for CAST set point 1, particle numbers for CAST set point 2 follow the same trends that BC mass concentration (Fig. 12). In this case, the difference between fuel Jet A-1<sup>lim</sup> and Jet A-1<sup>sul</sup> is not as marked as for BC mass concentration. As for BC mass concentration, the fuel presenting higher emissions in particle number is Jet A-1<sup>lim</sup> and the one presenting lower emissions is Jet A-1<sup>ref</sup>.

Table 4 - Particle number measured during different tests

Date	Sulfur content (ppm)	Aromatic content (%)	Particle number (1/cm <sup>3</sup> )	Standard deviation
14/02/2020	3000	23	5.19 · 10 <sup>6</sup>	0.16 · 10 <sup>6</sup>
17/02/2020	3000	16	4.86 · 10 <sup>6</sup>	0.10 · 10 <sup>6</sup>
17/02/2020	4	23	5.09 · 10 <sup>6</sup>	0.08 · 10 <sup>6</sup>
18/02/2020	4	16	3.41 · 10 <sup>6</sup>	0.07 · 10 <sup>6</sup>

### 8.3.3.3 Particle size

#### 8.3.3.3.1 CAST set point 1 ( $Q_k = 105 \mu\text{L}/\text{min}$ ; $Q_p = 30 \text{ mL}/\text{min}$ ; $Q_{\text{air}} = 2.0 \text{ L}/\text{min}$ )

SMPS measurements were done in series with CPC measurements. For each set point, at least 2 size distributions were recorded. The only exception was the measures done 18/02 for Jet A-1<sup>aro</sup>, since this was a non-productive test. Figure 13 depicts the size distributions obtained for each fuel for CAST set point 1.



Work Package 4: Deliverables Report

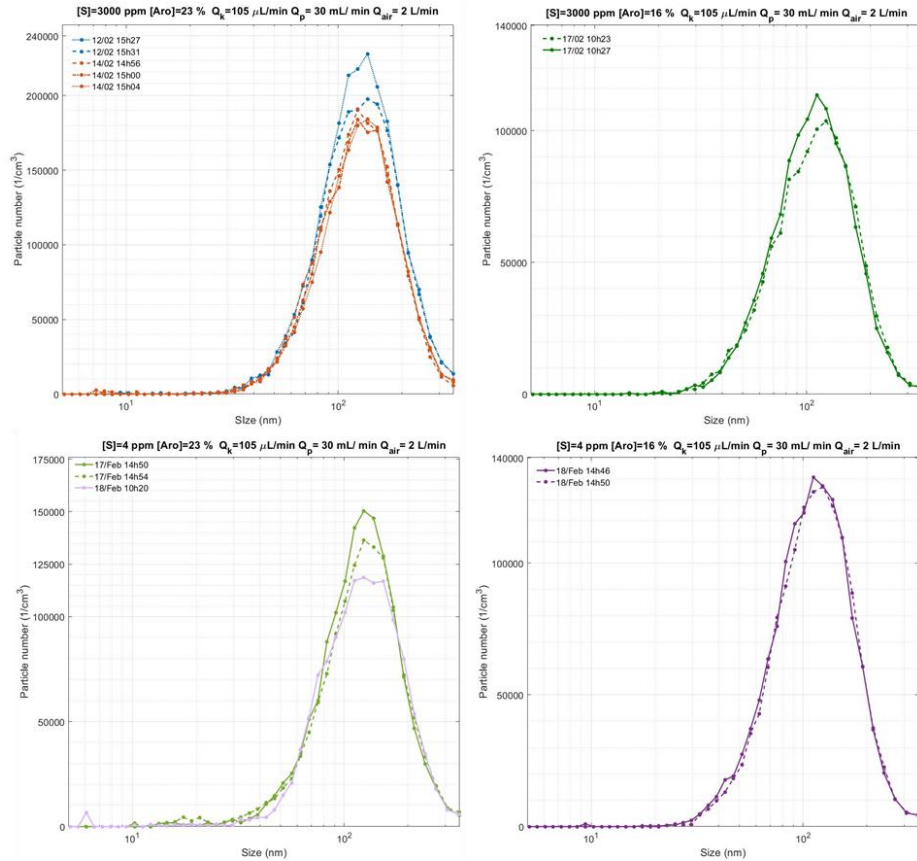
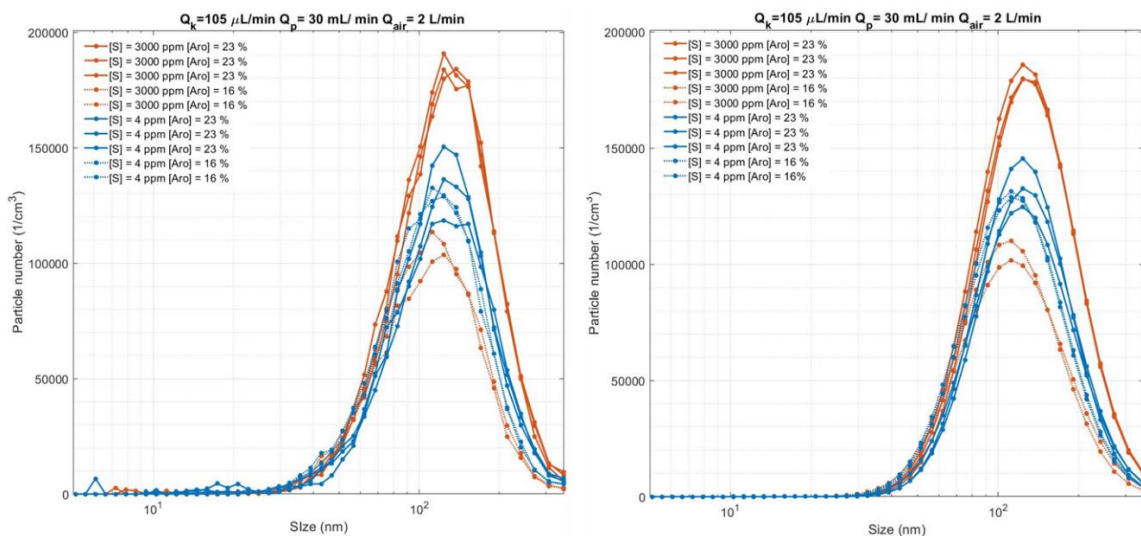


Figure 13 - Size distributions measured for CAST set point 1

In general, the size distributions were reproducible, only size distribution taken in different days for same fuel, presented some difference, but eventually in total number, not in shape.

Figure 14 shows a comparison of size distribution for different fuels (right panel). We have fitted the size distributions to a lognormal function (left panel) and average results for the fit for each fuel are given in Table 5.



## Work Package 4: Deliverables Report

Figure 15 - Size distributions comparison for different fuels, measured (right panel) and fitted to a log normal function (left panel)

Table 5 - Size distribution fit parameters for each fuel for CAST set point 1

Date	Sulfur content (ppm)	Aromatic content (%)	Particle number (1/cm <sup>3</sup> )	GMD (nm)	GSD
12/02/2020	3000	23	$2.15 \pm 0.09 \cdot 10^6$	$124.4 \pm 0.4$	$1.50 \pm 0.01$
14/02/2020	3000	23	$1.83 \pm 0.05 \cdot 10^6$	$123.1 \pm 1.8$	$1.50 \pm 0.01$
17/02/2020	3000	16	$1.14 \pm 0.03 \cdot 10^6$	$107.5 \pm 2.0$	$1.53 \pm 0.02$
17/02/2020	4	23	$1.32 \pm 0.05 \cdot 10^6$	$119.9 \pm 2.0$	$1.49 \pm 0.02$
18/02/2020*	4	23	$1.29 \cdot 10^6$	118.0	1.51
18/02/2020	4	16	$1.35 \pm 0.02 \cdot 10^6$	$110.6 \pm 0.1$	$1.51 \pm 0.01$

\* Only one size distribution available

As can be seen in fig. 14, the total number trend observed by SMPS for different fuels is similar to the one observed for particle number measured with CPC. Regarding the size distributions, particle emitted for all fuels present a monomodal distribution, Geometrical Mean Diameter (GMD) is smaller for the fuels with an aromatic content of 16 % (Figure 15).

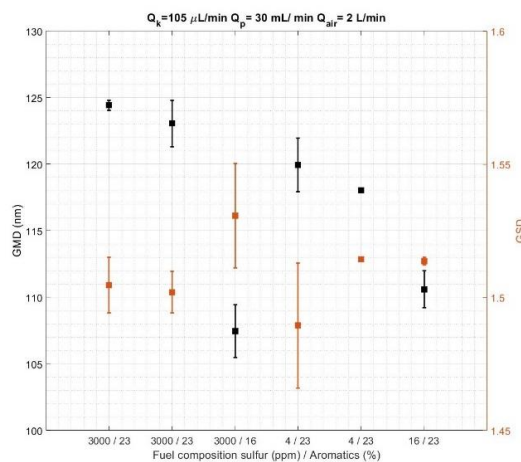


Figure 16 - Geometrical mean diameter and geometric standard deviation of fitted size distributions for different fuels

### 8.3.3.3.2 CAST set point 2 ( $Q_k = 105 \mu\text{L}/\text{min}$ ; $Q_p = 20 \text{ mL}/\text{min}$ ; $Q_{\text{air}} = 1.5 \text{ L}/\text{min}$ )

Figure 16 depicts the size distribution obtained for CAST set point 2 for each fuel. As can be seen, all fuels except Jet A-1<sup>ref</sup>, present a bimodal size distribution. In addition, we found that the size distribution obtained 17/02 for Jet A-1<sup>pro</sup> fuel is different to the one obtained during 18/02 test. The main difference is found in the mode observed around 30 nm. We have not found any reason for this discrepancy. During the CAST characterization study, we observed that this CAST set point is really sensible to the air flow, a small change in 0.05 Lpm lead to a shift in the position of the mode at 30 nm and to a change on its intensity. This maybe one of the reasons of the discrepancies observed.





## Work Package 4: Deliverables Report

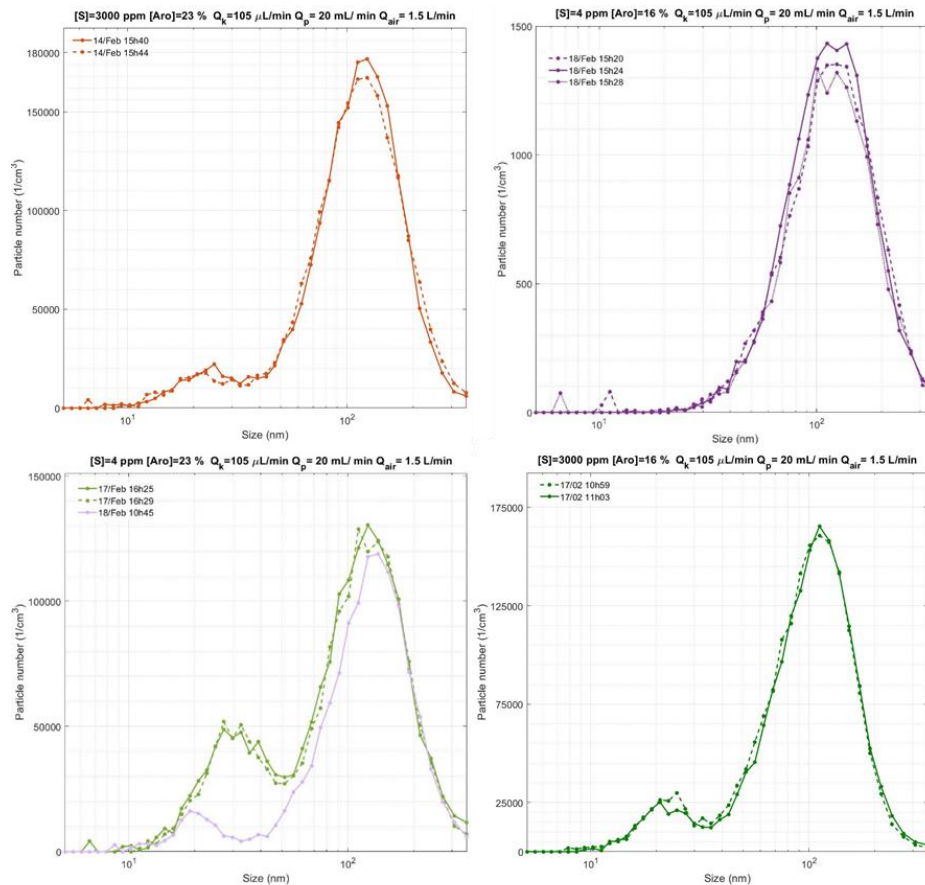


Figure 17 - Size distributions measured for CAST set point 1

As for the size distributions obtained for CAST set point 1, we have fit the size distributions, this time using two lognormal functions (except for Jet A-1<sup>ref</sup> fuel). Figure 18 compares the measured size distributions for different fuels and Figure 19 compares fitted size distributions.



## Work Package 4: Deliverables Report

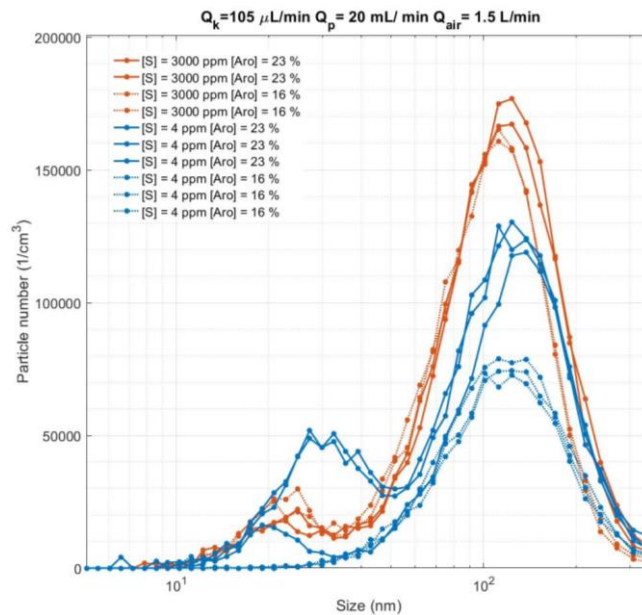


Figure 1 - Measured size distributions comparison for different fuels

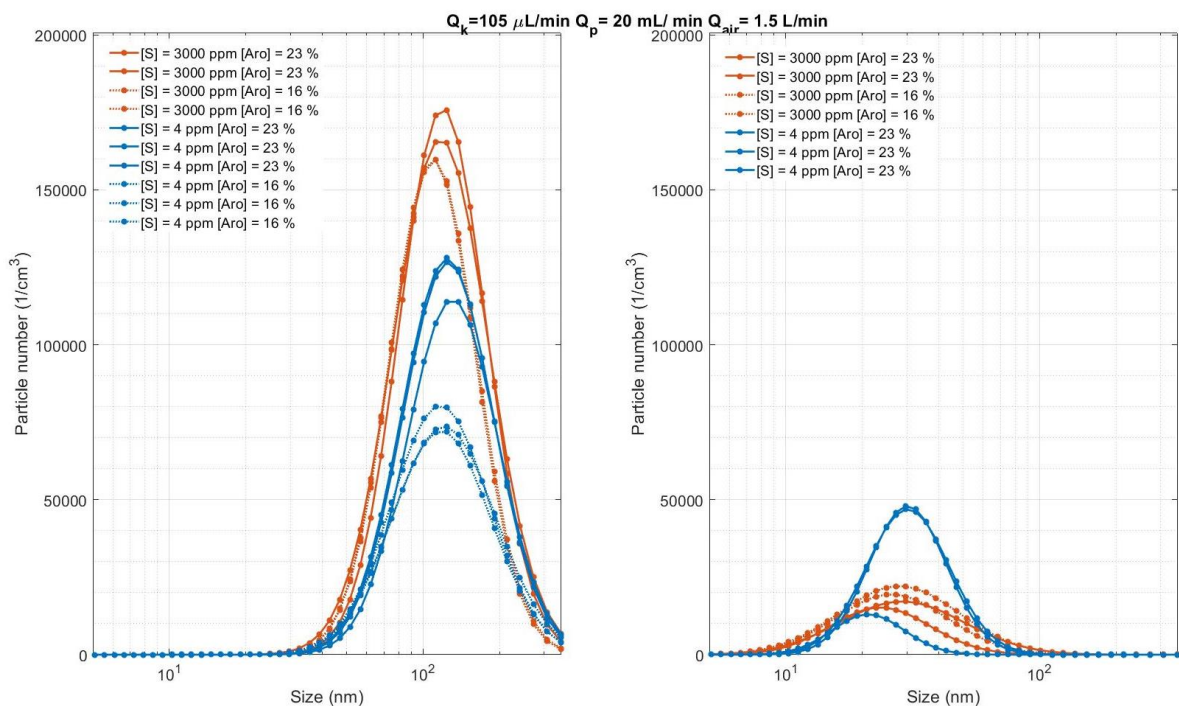


Figure 19 - Fitted size distributions comparison for different fuels

The fitted data clearly show that the main difference between the size distributions measured on 17/02 and 18/02 for Jet A-1<sup>aro</sup> fuel is found in the mode around 30 nm. Taking into account the results for other fuels, the size distribution obtained on 18/02 seem to be more coherent with other results than the one obtained on 17/02.



## Work Package 4: Deliverables Report

Table 6 summarizes the fit results for different fuels.

Table 6 - Size distribution fit parameters for each fuel for CAST set point 2

Date	Sulfur content (ppm)	Aromatic content (%)	Mode 1			Mode 2		
			Particle number	GMD	GSD	Particle number	GMD	GSD
			(1/cm <sup>3</sup> )	(nm)		(1/cm <sup>3</sup> )	(nm)	
14/02/2020	3000	23	1.73±0.05·10 <sup>6</sup>	114.7±2.1	1.50±0.04	2.33±0.54·10 <sup>5</sup>	25.8±3.5	1.65±0.12
17/02/2020	3000	16	1.54±0.01·10 <sup>6</sup>	107.0±0.8	1.47±0.01	3.09±0.42·10 <sup>5</sup>	26.7±1.3	1.68±0.04
17/02/2020	4	23	1.28±0.02·10 <sup>6</sup>	120.9±0.7	1.50±0.01	4.85±0.15·10 <sup>5</sup>	30.0±0.1	1.44±0.02
18/02/2020*	4	23	1.14·10 <sup>6</sup>	126.1	1.50	1.21·10 <sup>5</sup>	21.0	1.38
18/02/2020	4	16	0.83±0.04·10 <sup>6</sup>	114.0±1.5	1.55±0.01	0	0	0

\* Only one size distribution available

The results obtained for the mode at 110-120 nm are similar to those obtained for the mono-modal distribution of CAST point 1 (Fig. 20). GMD is smaller for the fuels with an aromatic content of 16 % and the same amount of sulfur. On the other hand, GMD for Jet A-1<sup>lim</sup> and Jet A-1<sup>ref</sup> are similar. In the case of the second mode, there is no difference in GMD between the fuels with 3000 ppm of sulfur. Regarding the fuels with 4 ppm of sulfur, while mode 2 is present for Jet A-1<sup>aro</sup>, it is not present in Jet A-1<sup>ref</sup> fuel. It is hard to find a reason for this observation, since the GMD and area of the mode for the tests done on 17/02 and 18/02 are really different.

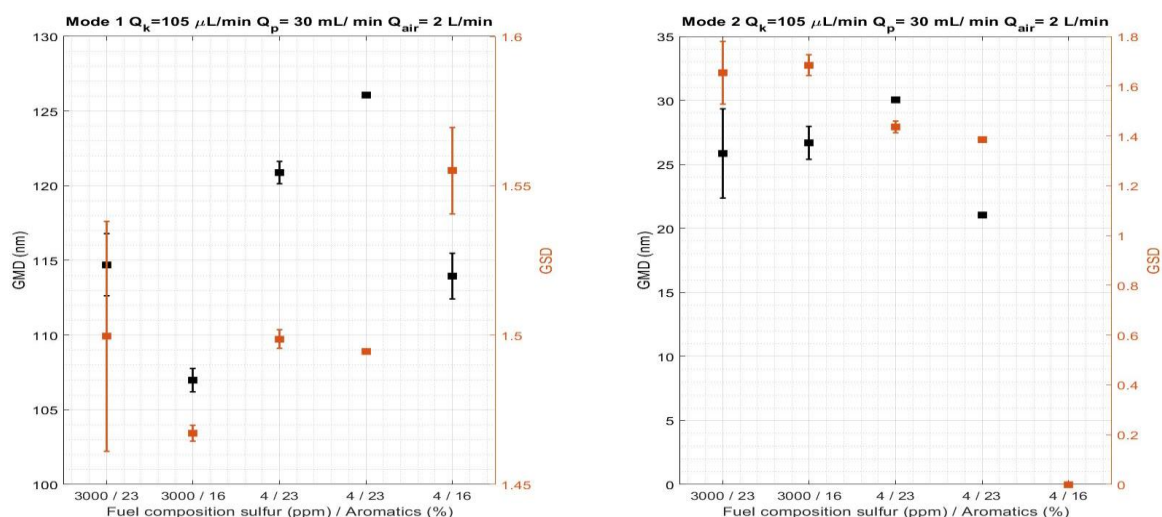


Figure 20 - Geometrical mean diameter and geometric standard deviation of fitted size distributions for different fuels for mode 1(left) and mode 2 (right)

### 8.3.4 Conclusions

We have tested four different fuels with different sulfur content and aromatic content always in the limit of ASTM certification. Two different CAST set points were tested for each fuel. Results for the first CAST set point tested ( $Q_k = 105 \mu\text{L}/\text{min}$  ;  $Q_p = 30 \text{ mL}/\text{min}$  ;  $Q_{\text{air}} = 2.0 \text{ L}/\text{min}$ ), for the fuels containing 3000 ppm of



## Work Package 4: Deliverables Report

sulfur, showed a reduction on BC mass concentration of 51 % when the aromatic content was reduced from 23 % (including 3 % of naphthalene) to 16 % (including 0.5 % of naphthalene). Particle number follows the same trend with a reduction of 29 %. In terms of size, the GMD was reduced by 13 %. In the case of fuels containing 4 ppm of sulfur, BC mass concentration showed a reduction of 4 % when the aromatic content was reduced, as this falls into the variability measured for BC mass concentration, we cannot say the aromatic content reduction have any effect in BC mass concentration for this set point for fuels with 4 ppm of sulfur. Particle number presents as well a negligible reduction with the reduction of aromatic content. GMD present also a modest reduction of 7 % with the reduction of aromatic content from 23 % to 16 %.

For the second CAST set point tested ( $Q_k = 105 \mu\text{L}/\text{min}$  ;  $Q_p = 20 \text{ mL}/\text{min}$  ;  $Q_{\text{air}} = 1.5 \text{ L}/\text{min}$ ), fuels with 3000 ppm and 4 ppm of sulfur presents a similar trend for BC mas concentration and particle number when the aromatic content is reduced from 23% to 16 %. BC mass concentration is reduced by 26 % for the fuel containing 3000 ppm of sulfur and 42 % for the one with 4 ppm of sulfur when the aromatic content is reduced from 23 % to 16 %. In a similar way, particle number is reduced by 6 % for the fuel with 3000 ppm of sulfur and 33 % for the on with 4 ppm of sulfur. Regarding the size, all fuels except the reference one, presents a bimodal distribution. The first mode is similar to the one found for CAST set point 1, and its GMD present a reduction of 7 % when reducing the aromatic content for both fuels (with 3000 and 4 ppm of sulfur). The second mode GMD does not seem to have any change with the aromatic content for the fuels with 3000 ppm of sulfur. In the case of fuels with 4 ppm of sulfur, the mode completely disappears when reducing the aromatic content from 21 % to 16%.

